Euler-Lagrange Simulation of Flow Structure Formation and Evolution in Dense Gas-Solid Flows

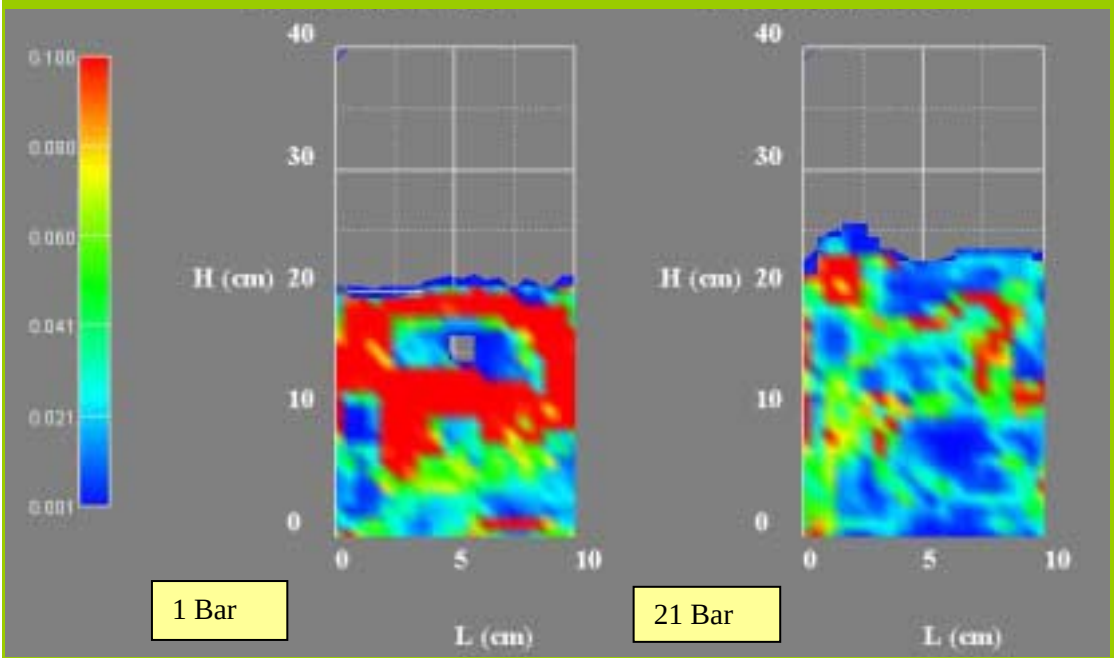

Jie Li

EULER-LAGRANGE SIMULATION
OF
FLOW STRUCTURE FORMATION AND EVOLUTION
IN
DENSE GAS-SOLID FLOWS

The research reported in this thesis was financially supported by Dutch Natural Science Foundation (***NWO***) and Twente University. It was part of research program of the J. M. Burgers Center for Fluid Dynamics, the Dutch research school for process technology (**OSPT**) and Process technology Institute Twente (**PIT**).

Promotion committee:

Prof. dr. C. Hoede (dean)	University of Twente
Prof. dr. ir. J. A. M. Kuipers (promotor)	University of Twente
Prof. dr. ir. W. P. M. van Swaaij	University of Twente
Prof. dr. ir. G. F. Versteeg	University of Twente
Prof. L. Tadrist	University of Aix-Marseille I
Prof. dr. ir. J. Schouten	Eindhoven University of Technology
Prof. dr. ir. H. E. A. van den Akker	Delft University of Technology
Prof. J.-H. Li	Chinese Academy of Sciences

PrintPartners Ipskamp B. V.

Publisher: PrintPartner Ipskamp, P. O. Box 333, 7500 AH Enschede, the Netherlands, www.ppi.nl

ISBN: 90 36518601

EULER-LAGRANGE SIMULATION
OF
FLOW STRUCTURE FORMATION AND EVOLUTION
IN
DENSE GAS-SOLID FLOWS

PROEFSCHRIFT

ter verkrijging van
de graad van doctor aan de Universiteit Twente,
op gezag van de rector magnificus,
prof. dr. F. A. van Vught,
volgens besluit van het College voor Promoties
in het openbaar te verdedigen
op vrijdag 28 maart 2003 om 16:45 uur

door

Jie Li
geboren op 4 september 1964
te Shaanxi, P. R. China

Dit proefschrift is goedgekeurd door de promotor

Prof. dr. ir. J. A. M. Kuipers

To my parents
To Hua
To all on whose work
I have been able to build

CONTENTS

CHAPTER 3

Effect of Competition between Particle-Particle and Gas-Particle Interactions on Flow Patterns in Dense Gas-Fluidized Beds

CHAPTER 6

Flow Structure Formation in Circulating Gas-Fluidized Beds

Summary

Gas-solid two-phase flow is a ubiquitous phenomenon in nature and also widely applied in process industries. One of the basic properties, the large density difference, makes its fluid dynamics quite different from that prevailing in liquid-solid systems because particles in a gas phase possess a relatively long relaxation time. This property decisively determines the extraordinary complexity of particle laden flows, namely inherently unsteady and dominated by phenomena with strong nonlinearity, such as gas-particle interaction, and intensive energy dissipation due to inter-particle collisions. As a consequence, these flows are characterized by extremely complicated dynamic behaviors, displaying a variety of flow structures with widely varying time and length scales. It is for this reason that many important aspects of (fluid) dynamics of gas-fluidized bed are still poorly understood though a lot of efforts have been devoted during the last few decades.

Due to the complex nature of gas-solid flows, it is a formidable challenge to attempt to describe the fluid dynamics in a gas-fluidized bed by a "general" model. We therefore concluded that a **multi-scale strategy** in CFD simulation employing different computational methods is the most appropriate way to study these flows: 1) Lattice-Boltzmann method for precisely quantifying the drag at the micro-scale, 2) discrete particle method for taking into account both particle-particle collision and gas-solid interaction at the meso-scale, and 3) "two-fluid" model, by representing the particles as a continuous medium at the macro-scale. The discrete particle method offers the advantage that of both particle-fluid and particle-particle interaction on the scale of single particles can be taken into account while a sufficiently large enough amount of particles can be studied.

This work aims at exploring the fundamental phenomena prevailing in dense particle laden flows, including the flow structure formation, regime transition, pressure influence and so on, by employing the discrete particle method.

Besides the above-mentioned basic tool, it is essential to develop a scheme to identify the contribution of each factor in order to obtain insight in the system behavior. With regard to this aspect, we adopted the idea of "**process decomposition**". With this methodology the separate effects of sub-processes on the global system behavior can be studied. In the context of gas-solid two-phase flow, two approaches have been followed in this study, which include 1) the decomposition of gas-solid interaction, or drag, and particle dissipative collision and 2) the quantification of each basic process via energy budget analysis. Using the first method, it

was possible to identify the impact of particle collisional dissipation on the flow structure formation. Through the analysis of various processes in an “ideal” collisional system the impact of fluid-particle interaction on the instability in gas-fluidization could be identified. Particle energy, drawn from the gas phase, is consumed during various processes such as particle collision, displacement, rotation, translating and random motion. All these quantities can be precisely calculated by the discrete particle model. Using a simple energy budget analysis, it was possible to connect these basic processes to the flow structure formation and evolution on macro-scale and therefore develop the criteria to predict the flow structure formation and its evolution. Our results obtained demonstrate that this methodology is very promising.

Competition between particle collision and gas-solid interaction

Extensive simulations have been carried out on flow structure formation and its evolution with particular focus on particle–particle interaction and particle-fluid interaction in dense gas-fluidized beds. It has been demonstrated that **the competition between particle-particle non-ideal collision and fluid-particle interaction fully dominates the flow pattern formation and evolution**.

As the gas-solid interaction is intensified, the flow regime may span from the fixed bed regime to the turbulent regime where the flow regime transition is actually the expression of the altering role of particle-particle interaction and fluid-particle interaction. The uniform expansion regime prevailing after the onset of fluidization results from dominant gas-particle interaction. Very strong non-ideal particle collisional interaction results in the bubbling regime. Two less ordered regimes, the turbulent and fast regime, originate from a compromise between these two interactions where particle-particle interaction gradually gives way to gas-particle interaction. It has been shown that there exists a pseudo-equilibrium point between these two regimes where the flow structure is relatively uniform at the meso-scale with a stable system state. On the contrary, intensification of particle-particle and particle-wall collisions is demonstrated to increase the energy dissipation and leads to a heterogeneous flow structure.

Drag influence

The effect of fluid-particle drag on flow structure has been overlooked in previous research due to lack of theoretical tools and experimental difficulties. In this study it has been shown that it plays a very important role to trigger the non-homogeneous flow structure formation, or instability of gas fluidization and consequently provides a fundamental mechanism to produce bubbly flow.

It has been demonstrated in this work that the heterogeneous flow structure does exist in systems with both non-ideal particles collisions and ideal particles collisions. The heterogeneous structure in systems with ideal particles is purely caused by non-linearity of the drag: the stronger the dependence of drag on voidage, the more heterogeneous flow structures prevail and the shorter (in terms of the range of gas velocities) the homogeneous flow regime. It is found that **the non-linear drag force has the "phase separation" function by means of accelerating the particles in the dense phase and decelerating the particles in the dilute phase thereby triggering non-homogeneous flow structure formation**. Particle collisional dissipation further prevents the formation of a homogeneous flow structure. Additionally, by quantitatively comparing flow structures computed from the discrete particle method (DPM) by using various drag correlations reported in literature the most appropriate drag correlation is identified.

It is also elucidated that the force balance for the particles (gravity and drag force) decisively ensures a homogeneous flow structure for ideal particle systems. However, for non-ideal particles an extra condition (energy balance) is required to guarantee the formation of the homogenous flow structure. It is deduced that only those gas-solid systems, with 1) particles suspended in an equilibrium state and 2) limited particle collisional dissipation, display homogeneous flow structures.

Contribution of particle collision

Following the study of the effect of drag on flow structure, the impact of particle-particle interaction on flow instability and bubble formation in dense gas-fluidized beds was studied. The factors determining bubble formation have been debated for a long time, nevertheless the precise role of particle-particle interaction is still unclear.

In this study it has been shown that **the occurrence of regular patterns (bubble, jet) results from the strong particle–particle collisional dissipation after breakage of the system equilibrium. The bubble and jet(s) formed feed back a stronger particle-particle collisional interaction** and it is this enhanced interaction that dissipates most of the particle energy and consequently promotes the formation of the dense emulsion phase. Any factor, such as elevated pressure, which tends to reduce the particle collisional interaction, leads to the bubble instability: size reduction and breakup. It has been demonstrated in addition that the bubbling point is caused by the changing role of the gas from particle suspension to particle collisional dissipation.

Pattern formation in circulating fluidized beds

Finally, the spatial-temporal pattern formation in high velocity gas-solid flows and the transition to dilute transportation (abrupt change to homogeneous flow) were studied.

It has been found that heterogeneous flow structures in circulating fluidized beds are induced by two kinds of mechanisms: non-linearity of gas drag force and particle collisional dissipation. These two factors determine the internal local flow structure of the system.

For the simulated CFB system, a smaller group effect in the drag correlation produces a more pronounced heterogeneous flow pattern (in other words, cluster formation results from weak gas-particle interaction) where the inter-particle collisional dissipation consumes the particle energy, drawn from the gas phase, up to 20%. Of these two mechanisms, the non-linear drag force or gas-solid interaction is the key one to initialize the heterogeneous flow structure formation. Particle group effect has two opposite functions in circulating fluidized beds: 1) suppressing the otherwise accelerated individual particles in dense regions, and 2) promoting the otherwise decelerated individual particles in dilute regions. When both the non-linear drag and non-ideal particle collision take effect, a denser cluster/dilute flow structure is formed.

If the gas velocity exceeds a critical value, the fluid-particle interaction dominates the particle collisional dissipation and as a consequence the second homogeneous flow regime is formed.

To summarize, the discrete particle method provides a powerful tool to explore the heterogeneous flow structure formation and evolution. Using the methodology adopted, we are able to qualitatively understand the instability mechanism of gas fluidization. Apparently, there is still a lot of work to be done to realize the final prediction of gas fluidization hydrodynamics, such as the quantification of flow region transition from the first principle, influences of the inter-particle cohesive force, particle morphology, gas drag, etc. Among them, a more elaborate gas drag correlation, is urgently required.

Samenvatting

Gas-vast tweefasenstroming komt veelvuldig voor in de natuur en wordt veelvuldig toegepast in de procesindustrie. Een fundamentele eigenschap, namelijk het grote dichtheidsverschil, veroorzaakt dat de dynamica sterk verschilt van die in vloeistof-vast systemen omdat de deeltjes in een gasfase een relatief grote relaxatietijd bezitten. Deze eigenschap bepaalt in doorslaggevende zin de uitzonderlijke complexiteit van de stroming van een gas beladen met deeltjes, zoals het inherente dynamische gedrag en dominantie door verschijnselen als sterke niet-lineaire gas-deeltjes interactie en intensieve energiedissipatie tengevolge van onderlinge deeltjesbotsingen. Dienten-gevolge, worden deze stromingen gekarakteriseerd door een extreem complex dynamisch gedrag met een grote verscheidenheid aan structuren en een groot bereik aan tijdschalen en lengteschalen. Dit vormt de onderliggende oorzaak van het gebrek aan begrip van vele belangrijke aspecten van de (fluid) dynamica van wervelbedden ondanks de aanzienlijke gewijde inspanningen gedurende de laatste decaden.

Tengevolge van de complexe aard van gas-vast stromingen, vormt de beschrijving van de (fluid) dynamica van wervelbedden met een “algemeen” model een formidabele uitdaging. Derhalve vormt een multi-schaal strategie voor CFD modellering, waarbij gebruik wordt gemaakt van verschillende simulatiemethoden, de meest geschikte aanpak om deze stromingen te bestuderen: 1) Lattice-Boltzmann methode voor het precies kwantificeren van de gas-deeltjes wrijving op microschaal, 2) discrete deeltjes methode voor het verdisconteren van zowel deeltjes-deeltjes botsingen als gas-deeltjes interactie op mesoschaal, en 3) “two-fluid” model waarbij de deeltjes als een continue medium worden gerepresenteerd. Discrete deeltjes modellering, biedt als voordeel dat zowel deeltjes-deeltjes interactie op de schaal van enkelvoudige deeltjes meegenomen kan worden terwijl een voldoende groot aantal deeltjes bestudeerd kan worden.

Dit werk heeft als doel de fundamentele verschijnselen, optredend in dichte met deeltjes beladen gasstromingen, middels discrete deeltjes simulatie te bestuderen zoals structuurvorming, regime transitie, drukeffecten, etc.

Naast de bovengenoemde basis tool, is het essentieel om een methodiek te ontwikkelen waarmee de bijdrage van elke factor geidentificeerd kan worden teneinde inzicht te verkrijgen in het systeemgedrag. Met betrekking tot dit aspect is “procesdecompositie” toegepast. Met deze methodologie kan het effect van afzonderlijke sub-processen op het

globale systeemgedrag bestudeerd worden. Binnen de context van gas-vast tweefasenstroming zijn er twee werkwijzen gevolgd in deze studie, welke bestaan uit 1) decompositie van de gas-vast interactie of gas-vast wrijving en dissipatie tengevolge van deeltjesbotsingen 2) kwantificering van alle basisprocessen middels energiebudget analyse. Middels de eerste methode bleek het mogelijk om het effect van dissipatie tengevolge van deeltjesbotsingen op structuurvorming in kaart te brengen. Middels de analyse van de verschillende processen voor systemen met ideale botsingen kon het effect van gas-deeltjes interactie op instabiliteiten bij gas-fluidisatie geidentificeerd worden. De energie van deeltjes, verkregen uit de gasfase, wordt geconsumeerd gedurende verschillende processen zoals botsingen, rotatie, translatie en random beweging van deeltjes. Met behulp van het discrete deeltjesmodel kunnen al deze grootheden nauwkeurig worden berekend. Op basis van een eenvoudige energiebudget analyse bleek het mogelijk om deze basisprocessen in verband te brengen met de vorming van structuren in de stroming en de evolutie op macroschaal en tevens criteria te ontwikkelen waarmee de vorming van structuren in de stroming en haar evolutie voorspeld kan worden. De verkregen resultaten geven aan dat deze methodologie veelbelovend is.

Competitie tussen deeltjesbotsingen en gas-deeltjes interactie

Er zijn uitgebreide simulaties uitgevoerd m.b.t. de vorming en evolutie van structuren in de stroming met focus op deeltjes-deeltjes interactie en gas-deeltjes interactie in dichte gas-gefluidiseerde bedden. Er is aangetoond dat de vorming en evolutie van stromingspatronen volledig wordt bepaald door de competitie tussen niet-ideale deeltjes-deeltjes botsingen en fluidum-deeltjes interactie.

Indien de gas-deeltjes interactie wordt geintensifeerd kan het stromingsregime varieren van het vast bed regime tot het turbulente regime waarbij de stromingsregime transitie de wijzigende rol reflecteert van deeltjes-deeltjes interactie en gas-deeltjes interactie. Het regime met uniforme expansie, optredend na aanvang van fluidisatie, is het gevolg van dominante gas-deeltjes interactie. Twee minder geordende regimes, het turbulente en het snelle fluidisatie regime, ontstaan als gevolg van een compromis tussen deze twee typen interacties waarbij gas-deeltjes interactie geleidelijk de rol van deeltjes-deeltjes interactie overneemt. Er is aangetoond dat er een pseudo-evenwichtspunt bestaat tussen deze twee regimes waarbij de structuur in de stroming relatief uniform is op mesoschaal met een stabiele systeemtoestand. In tegenstelling tot het voorgaande leidt intensificatie van de deeltjes-deeltjes en deeltjes-wand botsingen tot een verhoogde energiedissipatie en een heterogene structuur in de stroming.

Invloed van wrijving tussen gas en deeltjes

Het effect van gas-deeltjes wrijving op structuurvorming in de stroming is onderbelicht gebleven in eerdere studies vanwege het ontbreken van geschikte theoretische tools en experimentele beperkingen. In deze studie is aangetoond dat gas-deeltjes wrijving een zeer belangrijke rol speelt bij het initieren van de vorming van niet-homogene structuren in de stroming, of instabiliteit bij gas-fluidisatie en derhalve een fundamenteel mechanisme vormt bij heterogene fluidisatie.

Tevens is in deze studie aangetoond dat de heterogene structuur in de stroming bestaat in systemen met ideale deeltjesbotsingen maar ook in systemen met niet-ideale deeltjesbotsingen. De heterogene structuur in systemen met ideale deeltjesbotsingen wordt uitsluitend veroorzaakt door de niet-lineaire gas-deeltjes wrijving: des te sterker de afhankelijkheid van de porositeit, des te meer heterogene structuren er bestaan en des te korter (in termen van het bereik van de gassnelheid) het homogene stromingsregime. Er is gevonden dat de niet-lineaire gas-deeltjes wrijvingskracht een fase-separatie effect bezit middels het versnellen van deeltjes in de dichte fase en het vertragen van deeltjes in de verdunde fase waarbij de vorming van niet-homogene structuren in de stroming wordt veroorzaakt. Verder wordt de vorming van homogene structuren voorkomen tengevolge van dissipatie tengevolge van deeltjesbotsingen. Daarnaast is middels een kwantitatieve vergelijking van de structuren berekend middels discrete deeltjes simulaties, waarbij gebruik is gemaakt van verschillende in de literatuur gerapporteerde correlaties voor gas-deeltjes wrijving, de meest geschikte correlatie geidentificeerd.

Tevens is gevonden dat de krachtenbalans voor de deeltjes (gravitatie en wrijving) in beslissende zin het bestaan van een homogene structuur waarborgt voor ideale deeltjes. Echter, voor niet-ideale deeltjes is een additionele conditie (energiebalans) vereist teneinde de vorming van een homogene structuur te garanderen. Hieruit is afgeleid dat alleen gas-vast systemen met 1) deeltjes gesuspendeerd in een evenwichtstoestand en 2) beperkte dissipatie tengevolge van deeltjesbotsingen, een homogene structuur bezitten.

Bijdrage van deeltjesbotsingen

In vervolg op de studie van het effect van gas-deeltjes wrijving op de structuurvorming, is het effect van deeltjes-deeltjes interactie op de stromingsinstabiliteit en belvorming in dichte gas-gefluidiseerde bedden bestudeerd. De factoren welke belvorming bepalen zijn gedurende enkele decaden onderwerp van debat geweest, niettemin is de exacte rol van deeltjes-deeltjes interactie nog steeds onduidelijk.

In deze studie is aangetoond dat de vorming van regelmatige patronen (bel, jet) het gevolg is van sterke dissipatie tengevolge van deeltjes-deeltjes botsingen nadat het systeemevenwicht

is verstoord. De gevormde bel/jets koppelen in versterkte mate de interactie tengevolge van de deeltjes-deeltjes botsingen terug en deze versterkte interactie leidt tot dissipatie van het grootste deel van de deeltjesenergie en bevordert dientengevolge de vorming van een dichte emulsiefase. Elke factor, zoals verhoogde druk, welke energiedissipatie tengevolge van deeltjesbotsingen neigt te onderdrukken, leidt to instabiliteit van bellen met reductie van belgrootte en belsplijting als gevolg. Er is tevens aangetoond dat het punt van belvorming wordt veroorzaakt door de wijzigende rol van het gas: van medium voor deeltjessuspensie naar medium dat de dissipatie tengevolge van deeltjesbotsingen veroorzaakt.

Patroonvorming in circulerende wervelbedden

Tenslotte, zijn de patroonvorming in ruimte en tijd voor hoge-snelheid gas-fluidisatie en de transitie naar verdund vertikaal transport (abrupte overgang naar homogene stroming) bestudeerd.

Er is gebleken dat heterogene structuren in circulerende bedden geinduceerd worden door twee typen mechanismen: niet-lineariteit van de gas-deeltjes wrijvingskracht (groepeffect) en dissipatie tengevolge van deeltjesbotsingen. Deze twee factoren bepalen de interne structuur van de stroming in het systeem.

Voor het gesimuleerde CFB systeem produceert een kleiner groepeffect in de correlatie voor de gas-deeltjes wrijving een meer geprononceerd heterogeen stromingspatroon (met andere woorden: clustervorming resulteert vanwege zwakke gas-deeltjes interactie) waarbij de dissipatie tengevolge van onderlinge deeltjesbotsingen circa 20% van de deeltjesenergie consumeert verkregen vanuit de gasfase. Van de twee genoemde mechanismen is de niet-lineaire gas-deeltjes wrijving of gas-deeltjes interactie de kern welke de heterogene structuur in de stroming initieert. Het groepeffect in de correlatie voor gas-deeltjes wrijving speelt twee tegengestelde rollen in circulerende wervelbedden: 1) onderdrukking van de overigens versnellende individuele deeltjes in dichte zones, en 2) beinvloeding van de overigens vertragende individuele deeltjes in verdunde zones. Indien zowel niet-lineaire gas-deeltjes wrijving als ook niet-ideale deeltjesbotsingen optreden dan worden dichte clusters en verdunde zones gevormd in de stroming.

Indien de gassnelheid een kritische snelheid overschrijdt, domineert de fluidum-deeltjes interactie de dissipatie tengevolge van deeltjesbotsingen en dientengevolge wordt een tweede homogene stromingsregime gevormd.

Samenvattend, de discrete deeltjes methode is een krachtige tool waarmee de vorming en evolutie van heterogene structuren in de stroming bestudeerd kan worden. Middels de gevolgde methodologie is in kwalitatieve zin inzicht verkregen in het mechanisme van instabiliteit voor gas-fluidisatie. Er dient evenwel nog veel werk verricht te worden teneinde

de hydrodynamica van gas-fluidisatie volledig te kunnen voorspellen, zoals het kwantificeren van de transitie van flowregimes op basis van fundamentele principes en effecten van cohesive krachten tussen deeltjes, morfologie van deeltjes, effect van gas-deeltjes wrijving, etc. In dit verband is de beschikbaarheid van een meer verfijnde correlatie voor gas-deeltjes wrijving dringend vereist.

Chapter 1

GENERAL INTRODUCTION

Abstract

In this chapter, a brief introduction to the nature of pattern formation in dense particulate laden flow is presented. Poor understanding of pattern formation in particulate flows, including both granular flows and particle-fluid two-phase flows, seriously renders the design, control and optimization of powder processing and production processes. To completely understand these systems, gas-solid-solid interactions should be taken into account at various length scales. Approaches and results available up to date to characterize, both experimentally and theoretically, the flow structures and their evolutions are critically reviewed. Particular attention is paid to the various treatments of the internal interactions in the solids phase, such as bed elasticity, particle pressure, etc., and their capabilities in capturing flow structures and regime transitions. With respect to the peculiar nature of non-equilibrium flows, it is believed that the continuum assumption of the solids phase contains its natural weakness for precisely predicting the flow behaviors. On the contrary, the discrete particle approach is more suitable to explore the fundamentals of pattern formation and evolution due to its more precise descriptions of both particle-fluid interaction and particle-particle interaction. Accordingly, a methodology based on the discrete particle approach is adopted and three basic supporting techniques are employed in this thesis to explore the mechanisms underlying the flow behaviors, which are discrete particle simulation, process decomposition and non-linear theory. Finally, the outline of this thesis is presented.

1. Pattern formation

Pattern formation in complex systems is a ubiquitous phenomenon in nature, society and process equipment. An increasing number of disciplines including physics, chemistry, biology, engineering, economics and sociology have to deal with them. Gas fluidization is one of these disciplines. Complex systems are composed of many parts and these parts interact with other parts in a more or less complicated manner to form specific spatial, temporal and functional structures. A striking character of the patterns is that they are formed spontaneously and meanwhile are closely connected with dissipation. Therefore, sometimes it is also entitled “self-organization phenomenon” and/or “dissipative structure”. Many of these structures are found in nature and engineering fields. Examples include coherent oscillations of laser light, spiral structures formed by fluids and chemical transformations, regular patterns composed by a vibrating granule. Interestingly, these phenomena are also encountered in biology and sociology, for example, during regeneration of the cut hydra, growth processes of mushrooms, as well as cooperation and/or competition between social groups.

Although the examples may come from different disciplines, they do share some **common features**. The typical features are summarized as follows: 1) *composed of a number of sub-systems*. In case the system is composed of a single component with identical properties, the system should be uniform and no complicated structure is formed at all. 2) *structure-rich expressing modes (patterns) and multiple state (regimes) in macro-scale*. From one state to another normally abrupt changes or qualitative changes occur. 3) *non-linear internal controlling mechanism*. Non-linear interaction, being a key feature, plays a very essential role to promote the pattern formation and regime transition, which is materialized by its “dramatically up-down” capacity. This is especially the case when the system approaches a critical transition point. Without this peculiar feature, the linear type of interaction can only cause quantitative accumulation, but is unable to trigger the qualitative phase change. 4) *non-equilibrium state*. The non-equilibrium state of the system is the necessary pre-condition to construct a complicated structure, which seems to fully result from the system properties themselves. Combined with the non-linear interactions between the sub-systems, it produces another very important feature of this system, which is: 5) *strong system dissipation*. Consequently, continuously new materials and/or energy has to be supplied to the system to sustain its existence. Therefore, sometimes pattern formation is associated with “dissipative structure”.

Due to developments in non-linear theory the connecting themes of these complicated systems are now better understood and have led to new approaches. For instance, the discovery of coherent oscillations of laser light has resulted in the invention of new powerful techniques. Therefore, it attracts great interests of scientists and engineers from many disciplines to be involved in this fascinating research field. As one of the complex systems, fluidization has many common features as described above, such as self-organized patterns

(bubble, cluster), multiple regimes, dissipative processes etc. Hence, there should be some common laws underlying the pattern formation in gas-fluidized beds. Before we go to this specific field, to which this thesis is devoted to, let us firstly take a look at two examples, which bear resemblance to dense particulate flows. The first example is on flow structure in fluids, the famous Rayleigh-Benard convection cells. The second example is on flow pattern

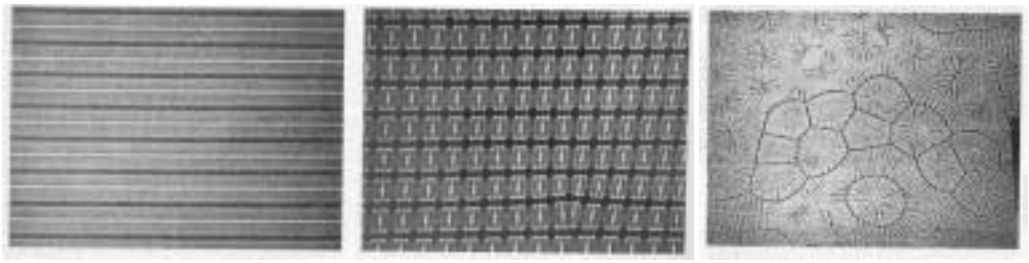

a) Rolls b) Squares c) Turbulence

Figure 1.1: Variation of convection flow patterns with increase of the driving force of temperature difference between top and bottom plate in Benard-Rayleigh convection (adopted from Tritton, 1988).

formation in vibrated fluidized beds. When a temperature difference is imposed on a shallow layer of fluid a density difference develops in the fluid: the hot fluid near the bottom becomes less dense and rises due to the buoyancy force, whereas the upper dense layer tends to sink. As the temperature difference between bottom and top increases, the flow pattern shows different structures: uniform, convection roll cells rotating in opposite directions to each other, square cells (bimodal flows) and irregular patterns changing with time (convection induced turbulence). Figure 1.1 shows these structures. Interestingly, the flow pattern nearby the onset of convection displays either as *polygonal* cells (square, triangle and hexagon) by means of combining two or more rolls at a certain angle, or as *circular* patterns of spiral convection rolls and target rolls (concentric) by means of twisting and fragmenting the rolls (Ball, 1999). Depending on the system composition and fluid depth, the pattern appears as a single type mode or a combination of two or more types of these modes. Particularly, the pattern adapts itself to the container by repositioning the rolls vertically against the wall (wall effect), which twists the previous parallel rolls. The transition to the convection pattern does not occur, as soon as the temperature gradient is imposed. Rather, a certain threshold in temperature difference should be reached to trigger the pattern formation. During this period the system maintains a uniform structure (resembling the uniform regime of fluidization of A powder).

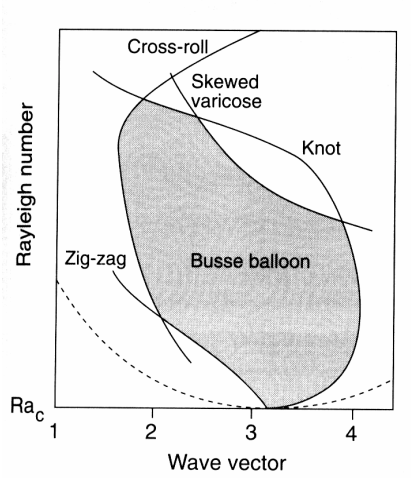

Figure 1.2: Stability diagram for parallel rolls against various deformations.

It has been shown that this pattern formation results from the competition between enhancement of convection (due to buoyancy) and retardation of convection (due to internal friction and thermal diffusion). Rayleigh proposed two dimensionless numbers: the Rayleigh number (defined as follows) and the ratio of cell width to fluid depth, to quantitatively express the transition form one pattern to another.

$$R_a = \frac{\alpha g \Delta T d^3}{\nu k} \qquad (1.1)$$

where α represents the fluid volumetric expansion coefficient, ν the kinematic viscosity and k the thermal diffusivity. Rayleigh established the stability diagram shown below (1708 is the minimum Ra value to trigger rolls). Busse further extended his work by analyzing another instability and making a detailed stability diagram called "Busse balloon" as shown in Figure 1.2. Also, it has been found that the system chooses its pattern by switching the balance between momentum and heat diffusion effects (see Ball, 1999).

Clearly, this system is a nonlinear system. When the imposed temperature difference leads to local heterogeneity, the formed sub-systems consist of light and dense fluid parcels. At this stage, the system exists in a non-equilibrium state and system dissipation increases. When fluid friction can not balance the buoyancy force introduced by the temperature difference, a new flow structure consisting of roll cells is formed, which is associated with enhanced energy dissipation. A further increase of temperature gradient leads to the formation of turbulence.

Similar phenomena have also been observed in granular flows such as vibrated fluidized beds. When a layer of particles is "fluidized" by a periodically vibrated plate inside a container, the granular layer shows a variety of regular patterns. With increasing vibration amplitude and frequency, regimes with following structure are observed: 1) flat; 2) square; 3) stripe; 4) hexagon and 5) disordered, as shown in Figure 1.3 and Figure 1.4.

Figure 1.3: Flow patterns in vibrated fluidized beds. (from: Umbanhowar et al., 1997)

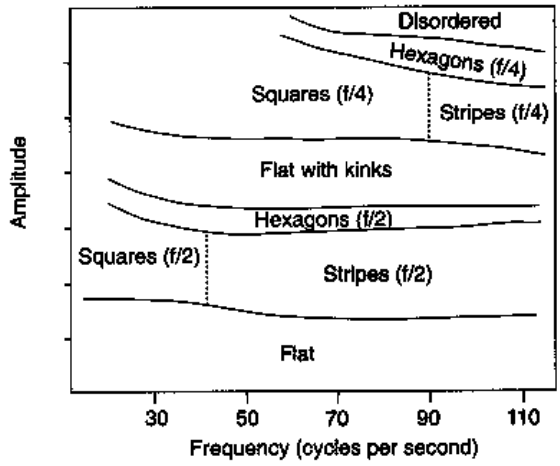

Figure 1.4: Transition of flow patterns for a vibrated granular layer (from: Umbanhowar et al., 1997)

The sub-systems are composed of isolated "packets" where peaks are followed by crater-like depressions as shown in Figure 1.5.

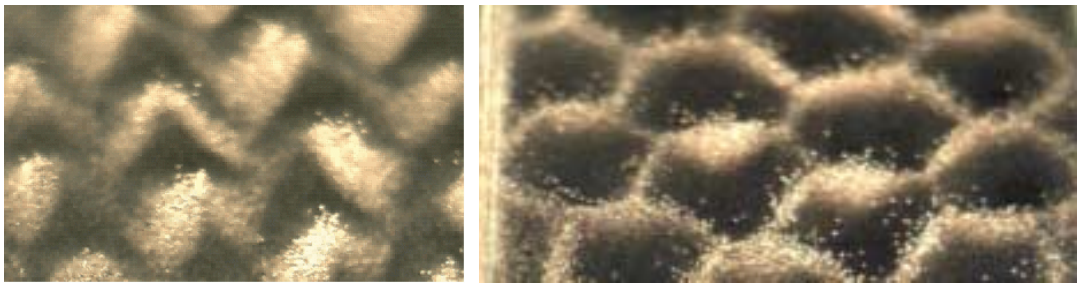

Figure 1.5: Two basic elements of motion pattern in vibrated fluidized beds: peak (left) and crater (right) (courtesy of Aranson, ANL.)

By using discrete particle simulation and taking account only impact and non-ideal collision, Shinbrot (1997) reproduced most of these patterns and predicted that there would be more structures available. He concluded that "… it may on the one hand seem surprising that an exceedingly simplified model, containing little more than a combination of periodic randomization and dissipation, and entirely neglecting gravity, can produce an apparent wealth of spontaneously organized and highly structured patterns. On the other hand, at a fundamental level there is little difference between this construction and well-known reaction–diffusion models. There, too, randomization (in the form of diffusion) competes with dissipation (in the form of reactions) to produce a rich tapestry of regular and irregular patterns".

Clearly, as the vibration amplitude and frequency are altered, the roles of the two types of actions, randomization and dissipation, are changing. Randomization firstly dominates the system when vibration is moderate, and a homogenous flow pattern results. As the vibration is

intensified, dissipative collision is also enhanced. Due to the non-equilibrium nature of particle motion, the pattern is formed. In such a way, randomization gradually gives way to the dissipation and meanwhile a series of patterns is produced. One would expect that certain (undiscovered) laws precisely govern such a very regular structure formation and evolution. Unfortunately, a detailed theoretical prediction of the various structures and transitions has not been achieved up to date. However, one point is definitely clear: **dissipative collision plays an important role in pattern formation**.

In case granular matter is not “fluidized” by a vibration wall but by a gas, what will happen then? It has been established clearly that the system also displays a variety of flow structures: packed, uniform, bubbling, turbulent, fast and dilute transportation. Once again, the system evolutes from uniform, to chaos and finally arrives at a uniform structure. It is unclear how and why the structures are formed and what promotes the transition from one regime to another. This issue is not only interesting from an academic perspective but also is essential to the performance of industrial units since it decisively controls the quality of the contact between the two phases. Now, let us move to the flow pattern formation in fluidization.

2. Fluidization

Fluidization has found many applications in industrial processes since the German engineer Winkler invented the first fluidized bed - a gasification reactor in 1921. Currently fluidized systems find a widespread application in the metallurgical, petroleum, chemical, food, energy and environmental industries. Fluidized systems offer the advantage of good fluid-solid contacting and excellent heat and mass transfer characteristics. Also, the fluid-like property is often extremely convenient, for processes including solids mixing, drying, granulation, to mention just a few. Unfortunately, when the gas velocity is greater than a certain threshold value, the minimum fluidization velocity, a variety of heterogeneous flow patterns appear, which severely prevents the intense gas-solid contact.

2.1 Phenomena

From the macro scale point of view, the general principle of fluidization seems very simple, no more complicated than transforming solids into fluid-like matter and endowing solids with fluid properties. Actually, fluidized solids differ from a normal fluid in many aspects. The

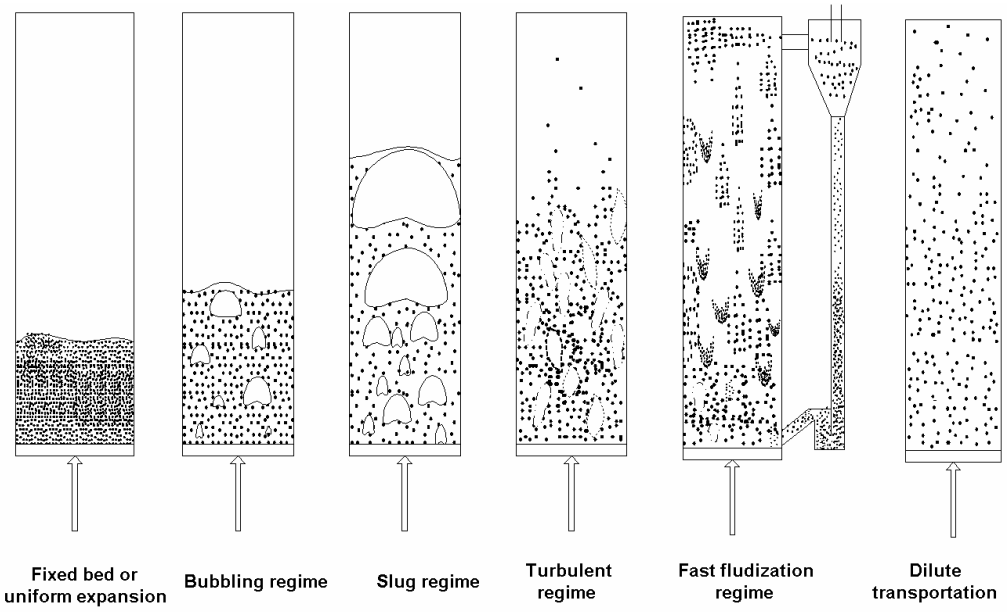

Figure 1.6: Flow structures and evolution in gas-fluidized beds with gas velocity increasing from left to right.

most important one is given by the fact that there exist a variety of heterogeneous flow structures in fluidized solids. Figure 1.6 schematically shows the typical flow regimes encountered in dense gas-fluidized beds. With increasing gas velocity the system experiences a packed state, uniform expansion (depending particle properties), bubbling, slug flow (if the bed diameter is small), turbulent fluidization, fast fluidization and dilute conveying. Amongst

these flow structures, three typical ones namely bubbles, slugs and clusters, can be identified (see Figure 1.7).

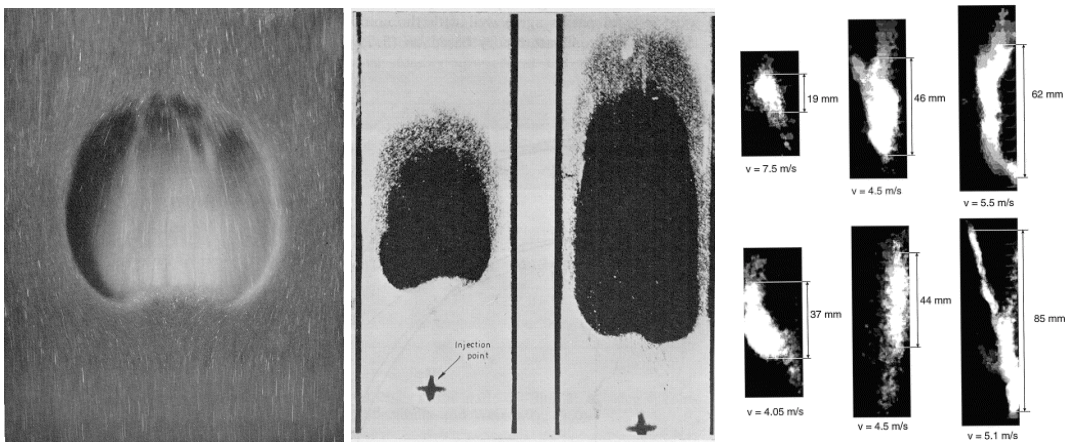

(a) bubble (b) slugs (c) clusters

Figure 1.7: Three typical heterogeneous flow structures observed in dense gas-fluidized beds with gas velocity increasing from left to right. (Adopted from: Rowe, 1971 for bubble; Davidson, 1971 for slug and Lackermeier et al., 2001 for clusters).

The flow pattern depends heavily on **system properties** such as particle density, size and surface roughness and gas phase density, In 1970's Geldart and his coworkers presented his famous powder classification diagram for air fluidization (Geldart, 1973) on basis of distinguishing the particles with respect to their fluidization behaviors, as shown in Figure 1.8. Group A powder, having a small mean size and/or a low particle density, exhibits considerably homogeneous expansion regime and good fluidization properties with a stable maximum size of the bubbles. Group B powder, in the mean size and density range of 40~500

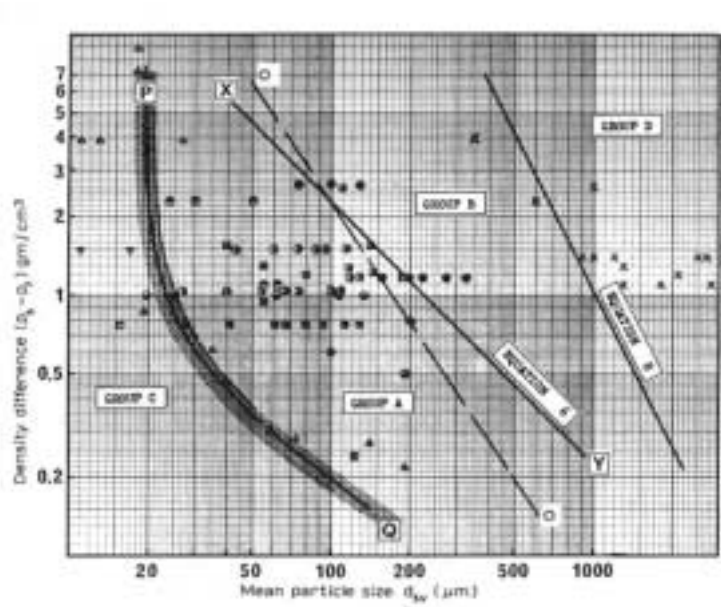

Figure 1.8: Geldart's powder classification diagram for fluidization by air.
(Adopted from: Geldart, 1973)

μm, 1400~4000 kg/m^3, displays a bubbling flow at or only slightly above minimum fluidization and exhibits virtually no homogeneous expansion of the bed. Group D and C are two extremes of the powder, which are difficult to fluidize. Group D powder, in the mean size and density range of greater than 500 micrometer and 4000 kg/m^3, displays explosive bubble growth. On the contrary, group C powder consisting of fine cohesive particles, where the inter-particle force dominates, is very difficult to fluidize. The Geldart classification clearly distinguishes the differences induced by particle properties. Particularly, the parameters used by Geldart to classify the particles, i.e. particle diameter and gas-solid density difference, actually represent two very important quantities in characterizing the flow structure. Because they indirectly reflect two essential aspects of these systems: particle-particle interaction (particle diameter) and particle-fluid interaction (density difference, closely related to system equilibrium). However, the fundamentals behind these phenomena are not clearly understood.

Since there many fluidization regimes, **a map of regimes** is required. Much work has been done in this area, which can be classified into three categories: the first one is a map in which

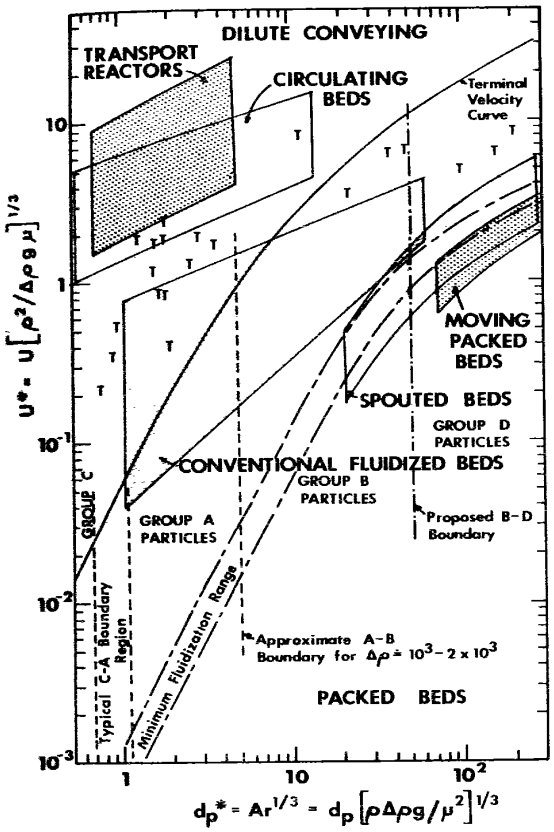

Figure 1.9: Flow regime map for gas-solids upward flows (dimensionless gas velocity vs. dimensionless particle diameter, T's indicates onset of turbulent fluidization. Adopted from: Grace, 1986)

voidage is plotted against superficial gas velocity, as done by Yerushalmi (1976, 1978), Li and Kwauk (1980), Squires (1985) and Rhodes (1989). These flow regime maps do not include the material properties. In the second type the gas velocity is plotted against solid flux as done by Leung (1980) and Klinzing (1981). The third type, the so-called "united regime

map", which was initialized by Reh. (1971) and further developed by Grace and his coworkers (Grace, 1986; Bi et al., 1995a, 1995b), plots the dimensionless superficial velocity versus Archimedes number. This type of regime mapping takes both system properties and hydrodynamics into account. Figure 1.9 shows the unified regime map due to Grace (1986).

Apparently, fluidization is a very complex operation, especially for systems involving Geldart A and B type powder. From Figure 1.8 and 1.9 it is clearly demonstrated that the influence of particle properties is pronounced which implies that **any methodology which inappropriately accounts for particle effects (properties and interaction) would be of very limited use.**

2.2 Present understanding

In order to understand and improve the design of such a complex system, great efforts have been made to understand and quantify the flow structures and flow regime transitions. Two types of methodologies can be identified:

2.3.1 PHENOMENA BASED CHARACTRIZATION

Wilhelm and Kwauk (1948) pioneered the pattern formation research in fluidization and firstly introduced the concept of agglomerate/particulate fluidization. A dimensionless Froude number, defined as $Fr = U_{mf}^2/g.d_p$, was proposed to quantify the flow structure. Based on experimental results, they proposed $Fr = 1$ as a criterion to distinguish between the two types of flows (>1 for agglomerate fluidization). Their work sparked the idea that competition between particle-particle interaction and particle-fluid interaction determines the flow structure. Unfortunately, their criterion is incapable to distinguish the flow structures within a specific system operating in different regimes.

Similar work has been published by others. Richardson and Zaki (1954) used the Pi theorem to obtain the relationship between the ratio of the superficial velocity to the particle terminal velocity as a function of bed voidage, Reynolds number and the ratio of bed diameter to particle size. Zenz (1960) presented an empirical graph of bed voidage against ρ_s/ρ_f with particle size as a parameter, indicating that bubbling flow and slug flow is less pronounced as ρ_s/ρ_f decreases. Zabrodsky (1966) has employed the Archimedes number to correlate a wide array of phenomena. Seven years later, Geldart (1973) presented his well-known diagram to distinguish the flow patterns induced by particle properties and finally Grace (1986) worked out the unified gas-solid flow regime map as shown previously. From these studies, it has become clear that *fluid-particle interactions play an important role in flow pattern formation and regime transition. Particle-particle interaction also constitutes an important factor.*

Romero and Johanson (1962) initialized a different approach to obtain dimensionless groups by non-dimensionalizing the governing equations. They obtained the following set of groups:

$$\frac{\rho_s-\rho_f}{\rho_f},\quad \frac{u_{mf}^2}{gd_p},\quad \frac{d_p u_{mf}\rho_f}{\mu},\quad \frac{H}{D}$$

Broadhust and Becker (1973) proposed a similar set by employing the Pi theorem. In their set the superficial velocity replaces the minimum fluidization velocity. Glicksman and coworkers (1984, 1993, 1994) worked out an even longer list of non-dimensionless groups stating from the two-fluid model formulated by Jackson (1963). In their list, the minimum fluidization velocity in the Froude number (gravity influence) was also replaced by the superficial gas velocity. Unfortunately, particle-particle interactions were not taken into account in these studies. Below the complete set of dimentionless groups proposed by Glicksman and coworkers is listed:

$$\frac{u_0^2}{gL};\quad \frac{\rho_s}{\rho_f},\quad \frac{\rho_s d_p u_0}{\mu},\quad \frac{G_s}{\rho_s u_0};\quad \frac{\rho_f d_p u_0}{\mu};\quad \phi,\quad PSD;\quad \text{bed geometry}$$

2.3.2 THEORETICAL PREDICTION

Davidson and Harrison (1961) initialized a more fundamental hydrodynamic approach although the detailed formulation based on full constitution equations was attributed to Jackson (1963) and his coworker Anderson (1967, 1968 and1969). He proposed the volume-averaged two-fluid model for particulate flows by which it is possible to carry out the instability analysis and characterize the flow structure and regime transition. Even though Jackson's model captured the fact that the growth rate of a disturbance in a gas-fluidized bed is faster than that in a liquid-fluidized bed, it unfortunately showed that a fluidized suspension is always in an unstable state after the gas velocity passes the minimum fluidization point. This conclusion is obviously in contradiction with observations. On the same base, Pigford (1965) and Murray (1965) also arrived at similar results denying the existence of stable homogeneous fluidization.

Recognizing that there must exist a kind of **elastic feedback in the solid phase** to suppress disturbances in a fluidized bed, Wallis (1969) firstly introduced a stress tensor in the solid phase momentum equation to keep the system stable. Since then, great efforts have been made to further develop this type of analysis. However, due to a variety of different assumptions on the origin of the bed elasticity, controversy has arisen and intensive dispute on this issue has been enduring for many years. Broadly, there are two schools of thoughts. One is based on the assumption that bed elasticity is maintained by the inter-particle force, as exemplified by extensive studies by Rietema and his coworkers (1973, 1990, 1993). In this type of model, an elastic modulus E multiplied by the voidage gradient is contained in the solid phase momentum equation, leading to the following instability criterion:

$$\frac{\rho_p^3 d_p^4 g^2}{\mu^2 E} \le \left[\frac{150(1-\varepsilon)}{\varepsilon^2(3-2\varepsilon)}\right]^2$$

The bed elastic modulus E is determined by inter-particle forces (Rietema, 1993) and can be obtained experimentally. The other school is based on the assumption that hydrodynamic forces in the fluid phase dominate the bed stability as advocated by many researchers (Wallis, 1969; Verloop and Heertjes, 1970; Foscolo and Gibilaro, 1984, 1988; Clift, 1992; Anderson et al., 1995). In Gibilaro's model, the bed elasticity is expressed by the compression wave from fluid phase with the propagation velocity of: $V_d = (\partial p/\partial \rho)^{0.5}$. This hydrodynamic force is imparted to the particulate phase proportional to the concentration gradient and the following criterion has been proposed:

$$\frac{gd_p^2}{u_t}\left(\frac{\rho_s - \rho_f}{\rho_s}\right) \geq 0.56n(1-\varepsilon)^{0.5}\varepsilon^{n-1}$$

Where n represents the voidage exponent in the Richardson and Zaki (R & Z) equation. Recently, they extended their analysis to two-dimensions (Chen, et al., 1999) and, meanwhile, included the concept of shock waves extended from a non-linear instability analysis (Brandani and Foscolo, 1994, 1996; Sergeev et al., 1998). Since these types of theories only concern hydrodynamic forces, the stability criterion can be expressed as follows:

$$Ar = \frac{(\rho_s - \rho_g)\rho_s g d_p^3}{\mu^2} < f(\varepsilon)$$

The first theory is able to account for many experimental observations as reported by Yates (1996). It has also been demonstrated that particle collision should be included in the quantification of the heterogeneous flow structure formation and transition. However, the fluid bed elastic modulus, an important parameter in the continuum model, is a parameter which is difficult to predict a priori. This greatly limits the application of this theory. The second theory does provide the framework within which the behaviors at and nearby the bubbling point can be predicted. Unfortunately, since the particle phase is treated as a continuous medium the precise account for the influence of particle-particle interaction is extremely difficult, This effect would be especially important for fine powders where inter-particle forces, such as van der Waals forces and electrostatic forces, become dominant (Pollock et al., 1995).

Since the one-dimensional linear stability analysis can only indicate the existence of a bubble according to the developing velocity of the growing wave, it is unable to predict the final fate of the bubble. Further work in this direction has led to application of non-linear instability analysis method and/or adopting a different source of solid stress tensor to understand how and under what circumstances a bubble is formed. Along this way, an important step towards an understanding of the bubble formation is the discovery of the fact that a one-dimensional wave is unstable to two-dimensional perturbations both from experiments and theoretical simulations (El_Kaissy and Homsy, 1976; Didwania and Homsy, 1982; Needham and Merkin, 1983, 1984 and 1986; Batchelor and Nitsche, 1991; Batchelor, 1988, 1993; Anderson

et al. 1995; Glasser, 1996). It is the instability, induced by multi-dimensional disturbances, which leads to the bubble formation. In recent years, the bifurcation theory has also been employed to explore the association of the solution structure with flow instability in various directions and amplitudes (Dankworth and Sundaresan, 1991; Goz, 1992~1995; Glasser et al., 1996, 1997). It has been shown that (Glasser, 1997) that a one-dimensional traveling wave emerges through a Hopf bifurcation of the uniform state and that a two-dimensional traveling wave originates out of these one- dimensional waves. Unfortunately, both homogeneous and heterogeneous flow structures have *identical* bifurcation structure and the *same* bubble-like shape of the high-amplitude 2-D traveling wave solution. The only difference is the appearance of a fully developed solution in a numerical analysis in which the particle experiences an intermediate stage of deceleration and re-acceleration. Such a subtle difference lays a hard base for deriving a mechanism-based criterion. According to the model equations they presented a dimensionless group, defined as:

$$\Omega = \left(\frac{\rho_s u_t^3}{A \cdot g}\right)^{1/2} > \sim 30 \quad \text{bubbling flow}$$

to characterize the flow pattern. Where A is the viscosity of the particulate phase with a recommended scale of $\rho_s u_t d_p$, where u_t is the terminal velocity. Eventually, it goes back to Kwauk's definition except that the minimum fluidization velocity is replaced by the particle terminal velocity. This formulation would be a promising one to characterize the system structure since it includes the particle-particle interaction (A) and the particle-fluid interaction (g, u_t).

Particularly, it is interesting to note that very recently Koch et al. (1999) tackled the instability problem by taking both particle-particle collision and fluid-particle interaction into account. In their work, kinetic theory of granular flow, accounting for particle-particle interaction, has been employed to model the solid phase pressure whereas a drag correlation obtained from Lattice-Boltzmann simulations (Ladd, 1990) was employed to describe the fluid-particle interaction. Their approach shows very promising results in pattern identification, they concluded that the dependence of drag on voidage plays a crucial role in the development of the instability.

Collectively, all these contributions are helpful to understand the mechanism underlying the pattern formation in dense particle laden flows. However, to achieve a thorough quantification of such flows still substantial research efforts are required. With retrospect to previous work in this direction, one immediately recognizes that all studies conducted in the past were based on continuum approach. Hence, the "wave" is the most frequently used term in the papers and then most troublesome questions arise from here. What is the proper way to determine a series of parameters for this special type of "fluid"? It is during the parameter quantification process that a great number of uncertainties and controversies arise. Then, is there an alternative to "continuum" theory and account for the discrete nature of the particulate phase?

The answer is confirmative! The discrete particle approach offers significant perspective to explore the fundamentals underlying the flow structure formation and evolution since it is based on a natural, easy and direct way to account for the particle-particle and particle-fluid interactions. This thesis is devoted to initializing the exploration in this direction and preliminarily establishing such a framework.

2.3 Analysis methodology of this work

To fully predict the hydrodynamics of fluidized bed chemical reactors, we should resort to a multi-scale model framework, as clarified by Kuipers and van Swaaij (1997). As a part of this framework, this research aims at understanding pattern formation and evolution in dense gas-fluidized beds by employing the intermediate-scale simulation technique: the discrete particle method. To achieve this goal, we require to quantify particle-particle interaction, to determine gas-solid interaction and to know exactly how these sub-systems interact with each other to produce observed flow patterns and furthermore how regime transition takes place. The methodologies, which will be applied to in this study, will be discussed below.

2.3.1 NON-LINEAR THEORY

Compared to Benard convection flow, the vibrated powder layer, the crack developing in solid maters and other non-linear phenomena, fluidization shares many similarities in its appearance. 1) sub-systems of particle-particle, particle-fluid exist; 2) multiple regimes are possible and abrupt regime transitions exist; 3) heterogeneous flow structures; 4) self-organized patterns exist (bubble, slug, cluster) and 5) strong dissipative processes can take place. Hence, it is expected that there should exist non-linear laws behind these phenomena which govern pattern formation and evolution. Accordingly, some ideas from non-linear science will be adopted in this research. Particular attention will be paid to the understanding of 1) how the pattern formation is associated with the system equilibrium; 2) how the sub-systems interact with each other to constitute the pattern and 3) how the non-linear interaction plays a role in the pattern formation.

2.3.2 DISCRETE PARTICLE SIMULATION

As indicated earlier, continuum theory has its shortcomings to explore pattern formation in particulate flows. In this research, the discrete particle method will be adopted. By taking into account both particle-particle interaction and particle-fluid interaction, the effect of these two interactions on flow structure formation and evolution can be studied. Another important advantage of this method is given by its ability to precisely calculate the collisional energy dissipation, which allows for a quantitative understanding of the connection between collisional dissipation and pattern formation. In the model, the motion of each individual particle is directly calculated from the Newtonian equation of motion while accounting for the

interactions with other particles and confining walls. The flow field of the gas phase is described with the volume-averaged Navier-Stokes equations.

2.3.3 PROCESS DECOMPOSITION

To study complicated system in depth, it is usually beneficial to decompose the system into a series of simpler sub-systems (Li and Kwauk, 2003). By means of examining these subsystems in detail the role of each component with respect to macroscopic flow phenomena can be studied. For instance, the real system could be decomposed into two sub-systems: one is the ideal collision system where no dissipation occurs and the other is the non-ideal system with intensive particle-fluid interaction. By analyzing the former, we can understand how drag affects the flow pattern. Meanwhile, analysis of the latter provides knowledge on which factor (collisions or drag) initializes the heterogeneous flow structure. In contrast with other work reported in literature, this research uses process decomposition approach to arrive at the fundamental aspects of detailed understanding of particulate flows.

2.3.4 ENERGY ANALYSIS

For non-equilibrium systems, the approach, based on mass and momentum balance principles only, is not sufficient to fully understand the system behavior. In order to fully understand such systems, energy budget analysis has proven to constitute a powerful tool. Any efforts to formulate this system, which neglect the dissipation effect, would result in incorrect dynamics. For instance, it has been proved that introduction of the kinetic theory of granular mater into the two-fluid model to account for particle collision dissipation improves the model prediction capacity (Nieuwland, 1995).

3. Outline of the thesis

The objective of this work is to understand flow structure formation and evolution in dense particle laden flows. In Chapters 2 the theoretical framework of the Euler-Lagrange simulation method and analysis methodology will be presented. In the next four chapters: chapters 3, 4, 5 and 6, computed flow structures in various fluidization regimes will be discussed.

Chapter 1 briefly introduces the pattern formation in general with respect to its generic features, controlling mechanisms and the various flow patterns observed in dense gas-fluidized beds. A critical review is presented to summarize previous efforts to understand and characterize these flow patterns and regime transitions both experimentally and theoretically. In this chapter also the three main strategies employed in this work are discussed to explore the mechanisms underlying the flow behaviors: discrete particle simulation, process decomposition and non-linear theory.

In **Chapter 2**, a critical review is presented on the discrete particle simulation methods available up to date, including Molecular Dynamics based discrete particle method (DPM), discrete element method (DEM). Particular attention is paid to the discrete particle methods and their potential applications for particular flows. This is followed by the detailed formulation of the discrete particle method. Also, the extensions and improvements of the codes developed originally by Hoomans (1996, 2000) will be discussed.

In **Chapter 3** results of extensive simulations will be presented on flow structure and its evolution with particular focus on particle–particle interaction and particle-fluid interaction in dense gas-fluidized beds. Detailed energy analysis was carried out to understand how particle-particle collisions and particle-fluid interaction interact and compete with each other to produce such a rich set of flow patterns.

It will be demonstrated in this chapter that **the competition between particle-particle non-ideal collision and fluid-particle interaction fully dominates the above mentioned flow pattern formation and evolution**. As the gas-solid interaction intensified, flow regime may span from the fixed bed regime to the turbulent regime (fast fluidization regime and dilute particle transportation will be presented in Chapter 6) and the flow regime transition is actually the expression of the change in role of particle-particle interaction and fluid-particle interaction. The uniform expansion regime after the onset of fluidization (as well as the homogeneous dilute particle transportation regime) results from dominant gas-particle interaction. Very strong non-ideal particle collision results in the bubbling regime. Two less ordered regimes, turbulent and fast regimes, originate from a compromise between these two interactions where particle-particle interaction gradually gives way to the gas-particle interaction to dominate the systems. It is shown that there exists a pseudo-equilibrium point

between these two regimes where flow structure is relatively uniform with respect to meso-scale and system is in a stable state. On the contrary, intensification of particle-particle and particle-wall collisions is demonstrated to increase the energy dissipation and leads to a heterogeneous flow structure.

Thereby this chapter also intends to appease the controversy on bubble formation theories in gas-fluidized beds. Our results indicate that the instability results from the collapse of fluid-phase controlling or gas-particle interaction controlling, which not only depends on inter-particle force but also is closely related to gas-particle interaction forces.

Chapter 4 aims at understanding the influence of the non-linear drag, fluid-particle interaction, on two-phase flow structure formation in dense particle laden flows. Drag force effect on flow structure has been overlooked somehow in the previous research due to lack of theoretical tools and experimental difficulties. However, as will be highlighted in this chapter, it plays a very important role to trigger the non-homogeneous flow structure formation as it provides a fundamental mechanism to trigger bubbly flow.

It will be demonstrated that the heterogeneous flow structure does exist in systems with both non-ideal particles collisions and ideal particles collisions. The heterogeneous structure in systems with ideal particles is purely caused by non-linearity of the effective drag: the stronger the dependence of drag on voidage, the more heterogeneous flow structures and the shorter the homogeneous flow regime. It is found that **non-linear drag force has the "phase separation" function by means of accelerating the particles in dense phase and decelerating the particle in dilute phase to trigger the non-homogeneous flow structure formation**. Particle collisional dissipation further presents the formation of a homogeneous flow structure. Additionally, by quantitatively comparing flow structures computed from the DPM by using various drag correlations reported in literature the most appropriate drag correlation is identified. On this base, a gas-particle synergism theory for pattern formation and regime transition in particulate flows was proposed.

At the end of this chapter, it is elucidated that the force balance for the particles (gravity and drag force) decisively ensures a homogeneous flow structure for ideal particle systems. Any deviation from this equilibrium state leads to heterogeneous flow structures. However, for non-ideal particle system this force balance condition could not guarantee the formation of the homogenous flow structure. It is deduced that only those systems, with 1) equilibrium suspended particles and 2) limited particle collisional dissipation, display homogeneous flow structures.

Chapter 5 focuses on the effect of particle-particle interaction on flow instability and bubble formation in dense gas-fluidized beds. Bubble behaviors with respect to shapes, rise velocity, maximum size and conjunction, as well as break-up, are well understood. However, the way how a bubble is formed has been always debated for a long time. It would be helpful if we

know how particle interaction affects the bubble formation, bubble growth and particularly its stability and vice versa. This chapter provides the evidences showing that such **regular patterns (bubble, jet) result from strong particle–particle collisional dissipation after breaking the system equilibrium**. The bubble and jet(s) formed feedbacks the system with a stronger particle-particle collision and it is this stronger collision that dissipates most of the particle energy and consequently promotes the formation of the dense emulsion phase. This strong particle collisional interaction, featured with a high "viscosity", could mountain bubbles stable. Any factor, such as elevated pressure, which tends to reduce the particle collision, leads to bubble instability: size reduction and breakup. It is demonstrated that the bubbling point is closely connected to the altered role of gas induced particle suspension to particle collisional dissipation.

Chapter 6 intends to highlight the spatial-temporal pattern formation in high velocity gas-solid flows, including both the cluster structure at meso-scale and the core-annular structure at macro-scale, and the transition to dilute transportation or the abrupt change to homogeneous flow. Once again, it will be shown that gas drag plays a very important role at the micro-scale in non-homogeneous flows. Particle collisional dissipation promotes cluster formation. Particularly, it is shown that cluster formation results from weak gas-particle interaction. The core-annular structure is initialized by the non-uniform distribution of the fluid flow in gas-fluidized beds and is intensified by particle collisional dissipation. As gas velocity passes a critical value, the fluid-particle interaction dominates the particle collisional dissipation and as a consequence the second homogeneous flow regime is formed.

References

Anderson, K. G., Sundaresan, S. and Jackson, R. 1995 Instabilities and the formation of bubbles in Fluidized beds. *J. Fluid Mech*., **303**, 327-366.

Anderson, T. B. and Jackson, R. 1967 Fluid mechanical description of fluidized beds: Equations of motion. *Ind. Eng. Chem. Fund*., **6**, 527-539.

Anderson, T. B and Jackson, R. 1968 Fluid mechanical description of fluidized beds: Stability of the state of uniform Fluidization. *Ind. Eng. Chem. Fund*., **7**, 12-21.

Anderson, T. B and Jackson, R. 1969 Fluid mechanical description of fluidized beds: Comparison of theory and experiment. *Ind. Eng. Chem. Fund*., **8**, 137-144.

Ball, P. 1999 The Self-Make Tapestry: *Pattern Formation in Nature,* Oxford University Press.

Batchelor, G. K. 1988 A new theory of the instability of a uniform fluidized bed. *J. Fluid Mech*., **193**, 75-110.

Batchelor, G. K. and Nitsche, J. M. 1991 Instability of stationary unbounded stratified fluid. *J. Fluid Mech*., **227**, 357-391.

Batchelor, G. K. 1993 Secondary instability of a gas-fluidized bed. *J. Fluid Mech*., **257**, 359-371.

Bi, H. T., Grace, J. R. and Zhu, J. X. 1995a Regime transitions affecting gas-solids suspensions and fluidized beds. *Chem. Eng. Res. Des.*, **73**, 154-161.

Bi, H. T. and Grace, J. R. 1995b Flow regime diagrams for gas-solid fluidization and upward transport. *Int. J. of Multiphase Flows*, **21**, 1229-1236.

Brandani S. and Foscolo P.U. 1994 Analysis of discontinuities arising from the one-dimensional equations of change for fluidization, *Chem. Eng Sci*., **49**, 611-619.

Brandani, S., Rapagna, S., Foscolo, P. U. & Gibilaro, L. G. 1996 Jump conditions for one-dimensional two-phase shock waves in fluidized beds: The effect of the jump in fluid pressure. *Chem. Eng. Sci*., **51**, 4639-4647.

Broadhust and Becker 1973, see reference in Glicksman, L. R., Hyre M. R. and Farrell P. A. 1994.

Chen, Z., Gibilaro, L. G. and Foscolo, P. U. 1999 Two-dimensional voidage waves in fluidized beds. *Ind. Eng. Chem. Res.*, **38**, 610-620.

Clift, R. 1992 On the formulation of hydrodynamic stability criteria in fluidized beds. *Powder Tech*., **72**, 199.

Dankworth, D. C. and Sundaresan, S. 1991 Time-dependent flow patterns arising from the instability of uniform Fluidization. *J. Fluid Mech*., **236**, 477-495.

Davidson, J. F. and Harrison, D. 1961 *Trans. Inst. Chem. Eng*., **39**, 230.

Davidson, J. F. and Harrison, D. 1971 Fluidization, Academic Press, UK.

Didwania, A. K. and Homsy, G. M. 1982 Resonant side-band instabilities in wave propagation in fluidized beds. *J. Fluid Mech*., **122**, 433-438.

El-Kaissy, M. M. and Homsy, G. M. 1976 Instability waves and the origin of bubbles in fluidized beds. I: Experiments. *Int. J. Multiphase Flow*, **2**, 379-395.

Foscolo, P. U. and Gibilaro, L. G. 1984 A fully predictable criterion for the transition between particulate and aggregate fluidization. *Chem. Eng. Sci*., **39**, 1667-1675.

Geldart, D. 1973 Types of gas fluidization. *Powder Technology*, **7**, 285.

Gibilaro, L. G., di Flice, R. and Foscolo, P. U. 1988 On the minimum bubbling voidage and the Geldart classification for gas-fluidized beds. *Powder Tech*., **56**, 21-29.

Glasser, B. J., Kevrekidis, I. G. and Sundaresan, S. 1997 Fully developed traveling wave solutions and bubble formation in fluidized beds. *J. Fluid Mech*., **334**, 157-188.

Glasser, B. J., Kevrekidis, I. G. and Sundaresan, S. 1996 One- and two-dimensional traveling wave solutions in gas-fluidized beds. *J. Fluid Mech*., **306**, 183-221.

Glicksman, L. R. Hyre M. and Woloshun, K. 1993 Simplified scaling relationships for fluidized-beds. *Powder Tech*., **77**, 177-199.

Glicksman, L. R. 1984 Scaling relationship for fluidized beds. *Chem. Eng. Sci*., **39**, 1373-1379.

Glicksman, L. R., Hyre M. R. and Farrell P. A. 1994 Dynamic similarity in fluidization. *Int. J. of Multiphase flow*, **20**, 331-386.

Goz, M. F. 1992 On the origin of wave patterns in fluidized beds. *J. Fluid Mech*., **240**, 379-404.

Goz, M. F. 1993 Bifurcation of plane voidage waves in fluidized beds. *Physica D* **65**, 319-351.

Goz, M. F. 1995 Transverse instability of plane wave trains in gas-fluidized beds. *J. Fluid Mech*., **303**, 55-82.

Grace, J. R. 1986 Contacting modes and behavior classification of gas-solid and other two-phase suspensions. *Can. J. Chem. Eng*. **64**, 353-363.

Hoomans, B. P. B., Kuipers, J. A. M., Briels, W. J. and van Swaaij, W. P. M. 1996Discrete particle simulation of bubble and slug formation in a two-dimensional gas-fluidised bed: a hard-sphere approach. *Chem. Eng. Sci*., **51**, 99-118.

Hoomans, B. P. B. 2000 *Granular Dynamics of Gas-Solid Two-Phase Flows*. Ph.D. dissertation, Twente University.

Li Y. and Kwauk, M. 1980 The dynamics of fluidization. In: Fluidization III", edited by Grace, J. R. and Matsen, J. M., Pergamon Press, 537-544.

Jackson, R. 1963 The mechanics of Fluidized beds. I: The stability of the state of uniform Fluidization. *Trans. Inst. Chem. Eng*., **41**, 13-21.

Koch, D. L. and Sangani, A. S. 1999 Particle pressure and marginal stability limits for a homogeneous monodisperse gas-fluidized bed: kinetic theory and numerical simulations. *J. Fluid Mech*., **400**, 229-263.

Klinzing, G. E. 1981 *Gas Solid Transport*. McGraw-Hill, New York.

Kuipers, J. A. M. and van Swaaij, W. P. M. 1997 Application of computational fluid dynamics to chemical reaction engineering. *Rev. Chem. Eng*., 13, 1-118.

Lackermeier, U., Rudnick, C., Werther, J., Bredebusch, A. and Burkharddt, H. 2001 Visualization of flow structures inside a circulating fluidized bed by means of laser sheet and image processing, *Powder Tech.*, **114**, 71-83.

Ladd, A. J. C. 1990 Hydrodynamic transport coefficients of random dispersions of hard spheres. *J. Chem. Phys.*, **93**, 3484.

Leung, L. S. 1980 Vertical pneumatic conveying: a flow regime diagram and a review of choking versus non-choking systems. *Powder Tech*., **25**, 185-190.

Li, J. and Kwauk, M. 2003 Exploring complex systems in chemical engineering -the multi-scale Methology. *Chem. Eng. Sci.*, **58**, 521-535.

Murray, J. D. 1965 On the mathematics of fluidization. I. Fundamental equations and wave propagation. *J. Fluid Mech.* **21**, 465.

Murray, J. D. 1965 On the mathematics of fluidization. II. Steady motion of fully developed bubbles. *J. Fluid Mech.* **22**, 57.

Needham, D. J. and Merkin, J. H. 1983 The propagation of a voidage disturbance in a uniform Fluidized bed. *J. Fluid Mech*., **131**, 427-454.

Needham, D. J. and Merkin, J. H. 1984 The evolution of a two–dimensional small-amplitude voidage disturbance in a uniform fluidized bed. *J. Fluid Mech*., **131**, 427-454.

Needham, D. J. and Merkin, J. H. 1986 The existence and stability of quasi-steady periodic voidage waves in a Fluidized beds. *Z. angew Math. Phys*., **37**, 322-339.

Nieuwland, J. J. 1995 *Hydrodynamic Modeling of Gas-Solid Two-Phase Flows,* Ph. D dissertation, Twente University, The Netherlands.

Pigford, R. L. and Baron, T. 1965 Hydrodynamic stability of a fluidized bed. *Ind. Eng. Chem. Fund*., **4**, 81-87.

Pollock, H. M., Burnham, N. A. and Colton, R. J. 1995 Attractive forces between micro-sized particles: A patch charge model. *J. Adhesion*, **51**, 71.

Richardson, J F. and Zaki W. N. 1954 Sendimentation and fluidization: Part 1. *Trans. Instn. Chem. Engrs*. **32**, 35-53.

Reh, L. 1971 Fluid bed processing. *Chem. Eng. Prog*., **67**, 58-63.

Rhodes, M. J. 1989 The upward flow of gas/solid suspensions. Part 2: a practical quantitative flow regime diagram for the upward flow of gas/solid suspensions. *Chem. Eng. Res. Des*., **67**, 30-37.

Rietema, K. and H. W. Piepers 1990 The effect of interparticle forces on the stability of gas-fluidized beds – I. Experimental evidence. *Chem. Eng. Sci*., **45**, 1627-1639.

Rietema, K., 1973 The effect of interparticle forces on the expansion of a homogeneous gas-fluidized beds. *Chem. Eng. Sci*., **28**, 1493.

Rietema, K., Cottaar, E. J. E and Piepers, H. W. 1993 The effect of interparticle forces on the stability of gas-fluidized beds – II. Theoretical derivation of bed elasticity on the basis of van der Waals forces between powder particles: Experimental evidence. *Chem. Eng. Sci*., **48**, 1687-1697.

Romero and Johanson 1962, see reference in Glicksman, L. R., Hyre M. R. and Farrell P. A. 1994.

Rowe, P. N. 1971 In: "*Fluidization*", edited by Davidson, J. F. and Harrison D., Academic Press, 121.

Sergeev, Y. A., Gibilaro, L. G., Foscolo, P. U. and Brandani, S. 1998 The speed, direction and stability of concentration shocks in a fluidised bed. *Chem. Eng. Sci*., **53**, 1233-1238.

Shinbrot, T. 1997 Granular Patterns: A competition between randomizing shakes and inelastic collisions? *Nature*, **389,** 574-6.

Squires, A. M., Kwauk, M. and Avidan, A. A. 1985 Fluid beds: at last, challenging two entrenched practices. *Science*, **230**, 1329-1337.

Tritton, D. J. 1988 *Physical Fluid Dynamics*, Oxford University Press.

Umbanhowar, P. B. 1997 Patterns in the Sand, *Nature*, **389**, 541.

Verloop, J. and Heertjes, P. M. 1970 Shock waves as a criterion for the transition from homogeneous to heterogeneous fluidization, *Chem. Eng. Sci.*, **25**, 825-832.

Wallis, G. B. 1969 *One Dimension Two-phase Flow*, McGill-Hill, New York.

Wilhelm, R. H. and Kwauk, M. 1948 Fluidization of solid particles. *Chem. Eng. Progr*., **44**, 201-218.

Yates, J. G. 1996 Effects of temperature and pressure on gas-solid fluidization. *Chem. Eng. Sci*., **51**, 167-205.

Yerushalmi, J., Cankurt, N. T., Geldart, D. and Liss, B. 1978 Flow regimes in vertical gas-solid contact systems. *AIChE Symp. Ser.*, **174**, 1-12.

Yerushalmi, J., Turner, D. H. and Squires, A. M. 1976 The fast fluidized bed. *Chem. Proc. Des. Dev*., **15**, 47-51.

Zabrodsky, S. S. 1966 Hydrodynamics and heat transfer in fluidized beds. MIT Press, Cambridge MA.

Zenz, F. A. and D. F. Othmer 1960 Fluidization and Fluid Particle Systems, Reinhold Publishing Corp., New York.

Chapter 2

THEORETICAL FOUNDATION OF EULER-LAGRANGE SIMULATION

Abstract

In this chapter, a brief review is presented on two popular discrete simulation techniques available in the literature, with particular emphasis on their application to simulation of dense particulate flows. The hard-sphere model is believed to be the most suitable tool for exploring the flow structure formation due to its specific advantages of accounting for particle-particle interaction.

In the hard-sphere model the motion of each individual particle is directly calculated from the Newtonian equation of motion while accounting for the interactions with other particles and confining walls. The fluid phase is described by the volume-averaged Navier-Stokes equations for dispersed two-phase flow and solved on a scale larger than the particle size. This requires empirical closure laws for the drag force exerted on the particles by the gas phase. The numerical solution technique, the applied boundary conditions and two-way coupling between the motion of the particles and the motion of the gas-phase are briefly outlined. A description of the calculation of the void fraction from the 2-D granular dynamics model is presented as well.

Extensions of the model which allows for the quantification of particle-particle interaction, particle-fluid interaction and flow structures are also described in this chapter. In addition, a simple method to monitor the system equilibrium is proposed. Finally, the detailed energy budget analysis methodology applied to gas-fluidized beds is presented.

1. Introduction

The history of the discrete particle approach could go back to as early as two centuries ago since Daniel Bernoulli in 1738 advanced the idea that gases are formed of elastic molecules moving at large speeds, colliding and rebounding according to the laws of elementary mechanics. This great idea in fact forms the basis of current models of fluidized beds which treat the particles in a discrete manner. Due to the rapid development of computer hardware, the discrete particle method has been successfully applied to study the behavior of fluidized beds on a fundamental basis. Many phenomena, which had perplexed the fluidization community for a long time, now can be understood in great depth, such as standing waves in vibrated beds, segregation, clustering and inelastic collapse, to name a few. The discovery of the clustering nature of a dense dissipative gas is considered as an important break through in physics as commented by Jaeger *et al*. (1996). The discrete particle method has proven a valuable tool for understanding the behavior of granular material during the past two decades (Campbell, 1985) and for fluidized beds in the past decade (Tsuji, 1993; Hoomans, 1996).

In this work, the focus will be on the granular dynamics of gas-solid two-phase flow. The modeling approaches adopted in Granular Dynamics can be roughly divided into two groups: soft particle and hard particle approaches. Before one of the approaches adopted in this work (hard-sphere) will be described, a short review of the different approaches that are available in the literature will be presented with emphasis on their application to gas-fluidized beds. These approaches can be divided into two types: hard-particle approaches and soft-particle approaches.

1.1 Hard-particle approaches

The hard-sphere simulation technique was first presented by Alder and Wainwright (1957) to study phase transitions in molecular systems by means of numerical simulations. In hard-sphere simulations, the particles are assumed to interact through instantaneous, binary collisions. A sequence of collisions is processed, one collision at a time, in order of occurrence. For this purpose, a list of future collisions is compiled and updated when necessary. A comprehensive introduction to this type of simulation was given by Allen and Tildesley (1990) and the further development and optimization were discussed by Marin et al. (1993). Hoomans (2000) also presented an overview on various hard sphere techniques, such as the Direct Simulation Monte Carlo (DSMC) technique due to Bird (1976), taking inter-particle interaction into account without detecting and processing every single collision that occurs in the system; the time-driven hard-sphere technique due to Hopkins et al. (1991) and so on. Recently Wassen and Frank (2001) summarized the methods available for Lagrangian type of dispersed phase simulation and

applied DSMC to examine the effect of inter-particle collision on cluster formation. These surveys, therefore, will not be repeated here, instead the attention is completely focused on recent developments of this technique in the context of fluidized bed modeling.

Hoomans et al. (1996) were the first to apply a hard-sphere type of simulation technique to gas-fluidized beds. In their two-dimensional model, a sequence of collisions is processed proceeding from one collision to the next by using a collision list that is compiled and updated in a highly efficient manner. In the following section, this technique will be explained briefly. Later on, this model has been extended to a three-dimensional model with respects to discrete part of the model.

By using this model, it has been demonstrated that particle-particle interaction has great impact on bubble formation (Hoomans, et al. 1996), which partially discovers the law underlying pattern formation in gas-fluidized beds. The segregation phenomenon induced by particle size differences and density differences can be correctly predicted from this hard-sphere model as well (Hoomans, et al. 1998). It has also been found that the assumption of an isotropic and Maxwellian particle velocity distribution adopted in kinetic theory of granular dynamics is only valid under circumstances of (nearly) ideal particle collisions with negligible energy dissipation (Goldschmidt et al., 2001). Otherwise, an anisotropic velocity distribution is obtained which becomes more pronounced when the degree of inelasticity increases. In addition, the improvement of fluidization quality at elevated pressure, a well-known phenomenon in high pressure fluidization has also been elucidated by analyzing particle-particle interaction and particle-fluid interaction (Li and Kuipers, 2001). It is clearly shown that the elevated pressure, through enhancing gas-solid interaction and reducing the dissipative collisions, efficiently elongates the regime of uniform fluidization and suppresses the formation of large bubbles.

After slightly modifying the discrete particle model with respect to the entrance and exit conditions (Hoomans, 1999), it has been successfully applied to predict the hydrodynamics of high-velocity circulating fluidized beds. The model captured the typical flow structures of cluster/dilute at meso-scale and the core/annulus structure at macro scale and the “S” shaped solids fraction distribution along the bed axis. It is demonstrated that this heterogeneous structure is closely related to the particle collisional dissipation, which preliminarily unveils the law underlying the formation of the heterogeneous flow structure in high-velocity gas-solid flows.

Similar simulations have been carried out in other groups. Ouyang and Li (1999) developed a slightly different version of this model. Xu and Yu (1997) presented a hybrid simulation technique that features elements from both hard-sphere and soft-sphere techniques. Helland and Tadrist (1999, 2000) employed the sub-grid technique and time-

driven scheme (employed by the soft-sphere model) to locate the collisional particle pair and meanwhile took into account the influence of turbulence. It is interesting to note, from the work of Helland et al. (1999, 2000), that the inter-particle force plays an important role with respect to the axial solids distribution in cohesive powder fluidized beds whereas turbulent viscosity has little impact on the flow structure. Particularly, the instability of circulating fluidized beds is strongly linked to the non-linear drag function due to the group effect of particles in a cloud whereas the collisional parameters have an important influence on the cluster structure. These studies have shed light on the mechanisms, which drive the heterogeneous flow patterns in gas-fluidized beds. Ouyang and Li (1999, 2001) also confirmed the essential role of particle collisional dissipation in the bubble and cluster flow structure formation in dense particulate flows.

Lun and Liu (1997) presented a three-dimensional hard sphere model for the horizontal dilute gas-solid flow (Lun, 1996). Recently, Lun (2000) extended his simulation to turbulent regime by including a multi-scale k-ε model.

Fan and his coworkers (Li et al., 2001; Zhang et al., 2000; Li et al. 2000) employed the hard sphere model to deal with inter-particle collision in gas-liquid-solid three-phase fluidized beds by adding the virtual mass force and the Basset history force acting on the particles. Meanwhile, they accounted for the interstitial effect of liquid between the particles when they approach each other. A so-called “close-distance interaction” model, based on their lattice Boltzmann simulation of dynamics of two spheres approaching in viscous flows (Zhang et al., 1999) was proposed. Their results concerning the bubble behaviors at atmospheric and elevated pressures seem reasonable.

1.2 Soft-particle approaches

The Distinct Element Method (DEM) is the most popular applied method in granular simulation. This method originally developed by Cundall and Strack (1979) was the first granular dynamics simulation technique published in the open literature. They used a two-dimensional soft particle model where the particles were allowed to overlap slightly. The contact forces were subsequently calculated from the deformation history of the contact using a linear spring/dash-pot model. This method allows for multiple particle overlap although the net contact force was obtained from pair-wise interactions. Soft-particle approaches differ in the choice of force scheme used to calculate the inter-particle forces. A review of various popular schemes for repulsive inter-particle forces is presented by Schäfer et al. (1996). Hoomans (2000) distinguished two force schemes using double spring constants due to Walton and Braun (1986) and a continuous potential of an exponential form containing two unknown parameters, the stiffness of the interaction and an interaction constant due to Langston et al. (1994, 1995). In addition, he summarized the previous applications of DEM to simulation of fluidized beds. Here a

brief introduction is given with more focus on recent progress in the context of fluidization.

The application of the soft-sphere approach to gas-fluidized beds was pioneered by Tsuji et al. (1993). They first developed a discrete particle simulation of a two-dimensional bed. Schwarzer (1995) extended this approach to the simulation a two-dimensional liquid-fluidized bed. Apart from the inter-particle forces, lubrication forces were taken into account, which play an important role in liquid-fluidized beds. In addition, a particle size distribution was taken into account.

Xu and Yu (1997) presented a two-dimensional model of a gas-fluidized bed based on the model developed by Tsuji et al. (1993). However, in their simulations a collision detection algorithm that is normally found in hard-sphere simulations was used to determine the first instant of contact precisely. Unfortunately, no comparison was reported that could show the importance of the new detection algorithm with respect to the overall simulation results.

A series of studies has been conducted in Horio's group by employing the DEM method. Mikami et al. (1998) extended the model developed by Tsuji et al. (1993) by incorporating liquid bridge forces to simulate cohesive particle fluidization. The particles used in their simulations are still Geldart D particles but due to the liquid bridge forces, the fluidization behavior resembles the behavior of Geldart C particles strongly. Iwadate and Horio (1998) extended their SAFIRE code further to include van der Waals forces. Kuwagi et al. (2000) investigated fluidized beds with solid bridging iron particles using SAFIRE taking into account metallic sintering. In addition, the effect of tangential lubrication was examined recently (Kuwagi et al., 2000). It seems that increase of particle elasticity and lubrication tends to promote particulate fluidization whereas enhancement of the inter-particle force leads to flow pattern with agglomerates. The group of Horio also extended their models to fluidized beds with internals (Rong et al., 1999) and gas-phase olefin polymerization (Kaneko et al., 1999) where energy balances and chemical reaction rates were taken into account.

A three-dimensional version of the fluidized bed model with respect to the particle phase was presented by Kawaguchi et al. (1998) and recently (Kawaguchi et al. 2000) extended to a quasi-three-dimensional model for cylindrical geometry. Mikami (1998) first presented full 3-D simulations (also with respect to the gas-phase) where no less than 500,000 particles were used.

To understand the fundamentals of flow regime transition, Rhodes and his coworkers (2000, 2001) employed the DEM, developed by Mikami et al. (1998), by replacing the liquid bridge force by an inter-particle force where this forces was expressed as a factor K of the buoyant weight of a single particle. Their results showed that the uniform

expansion regime extends with increasing inter-particle force and as a consequence the minimum bubbling point shifts to high gas velocity (behavior shift from Group B to A then to C). This is plausible because the enhancement of inter-particle force could establish the local force balance and suppress the collisional dissipation, which maintain the system in equilibrium state. A further increase of inter-particle force (to C) would destroy the already established equilibrium and lead to agglomerate formation. Their result indicates that transition of behavior from Group B to A takes place as the inter-particle force is approximately equal to the single particle buoyant weight actually signifies an important fact: apparently the system goes from non-equilibrium state to equilibrium state as clarified in chapter 5. Unfortunately, their simulation always showed the existence of a homogeneous flow regime even if the inter-particle force is zero for B powder, which is in contradiction with reality.

It is also interesting to note that DEM-soft sphere has been applied to gas-particle heat transfer by Li and Mason (2000), who obtained reasonable results. This opens a new way to resolve difficult problems in an mass and heat transport in fluidized suspensions.

Recently, Patankar and Joseph (2001a, 2001b) proposed a 3-D Euler-Lagrange model, which is based on the Multiphase Particle-In-Cell (MPIC) model proposed by Andraw and O'Rourke (1996). In these models, the particle is considered both as continuous and as a discrete phase. On the Eulerian grid, the continuum derivative terms that treat the particle as a fluid are readily evaluated and then mapped back to individual particles. Particle motion is described by the Newtonian equation of motion accounting for drag, gravity, pressure gradient, buoyancy and particle-particle collisions. The last term, for preventing solids volume fraction exceeding the close packing limit, is treated by DEM based approach where a computational particle (or parcel) is composed of a certain mount of individual particles with same properties. Despite saving some CPU time, this model is unable to accurately predict the hydrodynamics in gas-fluidized beds where intensive particle collision prevails.

1.3 Comparison between hard-sphere and soft-sphere model

Hard-particle simulations use an event driven scheme because the interaction times are (assumed to be) small compared to the free flight time of particles. In event driven simulations the progression in physical time depends on the number of collisions that occur. It implies that the simulation proceeds fast in case of few collisions occur but show as the number of collision increases. This approach also does not allow for the existence of the static zones and therefore is only suitable for the simulation of rapid granular flows. Its distinct advantage lies in the precise quantification of the collisional dynamics, with respects to the correct location of collisional pair, various types of energies involved and work done during free flight phase. Therefore, *it is a most suitable tool to understand the fundamentals of fluidized beds operating in regime above minimum fluidization*

conditions. Soft-particle simulations use time driven schemes because the interaction times are large compared to free flight times. In time driven simulations, a constant time step is used to progress through the dynamics of the system. Very small time steps (smaller than 10^{-7} s) can result in a precisely quantification of particle collision according to the Hertz elastic theory but is not attainable by the contemporary computer capacity. Large time step and the linear approximation of the compression process cannot guarantee the precise description of the collision process, for instance, it is relatively difficult to maintain exactly the energy conservation. However, the advantage to allow for multi-particle collisions at the same instant makes it a good candidate to simulate granular flows at relatively low fluidization velocity. In this research, we employ the hard-sphere model.

2. Hard-Sphere approach

In the hard sphere model, the particles are assumed to interact through binary, quasi-instantaneous collisions where contact occurs at a point. The particles are perfect, homogeneous spheres and the interaction forces are impulsive. Between collisions, the particles are in free flight. First, the collision model will be presented and then the computational strategy and some optimization techniques will be described.

2.1 Collision model

In the collision model, it is assumed that the interaction forces are impulsive and therefore all other finite forces are negligible during the collision process. The coordinate systems used in our model are defined in Figure 2.1. Consider the two colliding spheres *a* and *b* shown in Figure 2.1 with respective position vectors $\mathbf{r}_a$ and $\mathbf{r}_b$. The normal unit vector is defined as:

$$\mathbf{n} = \frac{\mathbf{r}_a - \mathbf{r}_b}{|\mathbf{r}_a - \mathbf{r}_b|} \tag{2.1}$$

Hence the normal unit vector points in the direction from the centre of particle *b* to the centre of particle *a*. The point of origin is the contact point. Prior to collision, the spheres with radii R_a and R_b and masses m_a and m_b have translation velocity vectors $\mathbf{v}_a$ and $\mathbf{v}_b$ and rotational velocity vectors ω_a and ω_b (clockwise rotation is negative). Velocities prior-to-collision are indicated by the subscript $_0$.

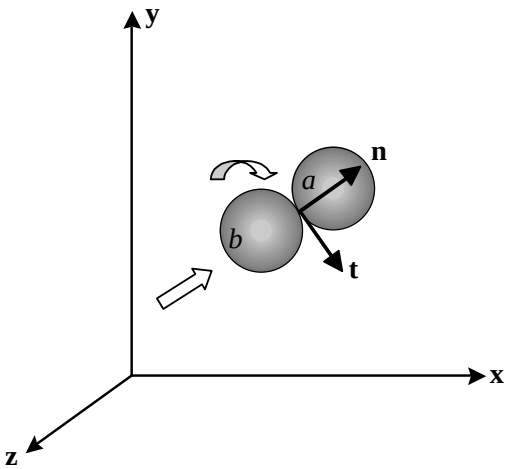

Figure 2.1: *Definition of the coordinate systems.*

For a binary collision of these spheres the following equations can be derived by applying impulse theorems and momentum conservation laws:

$$m_a(\mathbf{v}_a - \mathbf{v}_{a,0}) = \mathbf{J} \tag{2.2}$$

$$m_b(\mathbf{v}_b - \mathbf{v}_{b,0}) = -\mathbf{J} \tag{2.3}$$

$$I_a(\omega_a - \omega_{a,0}) = -(R_a\mathbf{n})\times\mathbf{J} \tag{2.4}$$

$$I_b(\omega_b - \omega_{b,0}) = R_b\mathbf{n}\times(-\mathbf{J}) \tag{2.5}$$

$$m_a(\mathbf{v}_a - \mathbf{v}_{a,0}) = -m_b(\mathbf{v}_b - \mathbf{v}_{b,0}) = \mathbf{J} \tag{2.6}$$

$$\frac{I_a}{R_a}(\omega_a - \omega_{a,0}) = \frac{I_b}{R_b}(\omega_b - \omega_{b,0}) = -\mathbf{n}\times\mathbf{J} \tag{2.7}$$

$$I = \frac{2}{5}mR^2. \tag{2.8}$$

The impulse vector **J** is defined as follows:

$$\mathbf{J} = \int_{t=0}^{t=t_c} \mathbf{F}_{ab}\,dt\,, \tag{2.9}$$

where t_c stands for the contact time (*i.e.* the duration of the contact).

From equations 2.6 and 2.7, the post-collision velocities of both particles can be calculated when the impulse vector **J** is known. If the force $\mathbf{F}_{ab}$ in equation 2.9 were known as a function of all the parameters involved, the impulse **J** could be calculated directly.

To construct the constitutive relations, first the relative velocity at the contact point ($\mathbf{v}_{ab}$) has to be defined:

$$\mathbf{v}_{ab} \equiv (\mathbf{v}_{a,c} - \mathbf{v}_{b,c})\ . \tag{2.10}$$

$$\mathbf{v}_{ab} = (\mathbf{v}_a - \omega_a \times R_a\mathbf{n}) - (\mathbf{v}_b + \omega_b \times R_b\mathbf{n}). \tag{2.11}$$

$$\mathbf{v}_{ab} = (\mathbf{v}_a - \mathbf{v}_b) - (R_a\omega_a + R_b\omega_b)\times\mathbf{n}\,. \tag{2.12}$$

From this relative velocity, the tangential unit vector can be obtained since the normal unit vector is already defined in equation 2.1:

$$\mathbf{t} = \frac{\mathbf{v}_{ab,0} - \mathbf{n}(\mathbf{v}_{ab,0}\cdot\mathbf{n})}{\left|\mathbf{v}_{ab,0} - \mathbf{n}(\mathbf{v}_{ab,0}\cdot\mathbf{n})\right|}\ . \tag{2.13}$$

Equations 2.6 and 2.7 can now be rearranged using $(\mathbf{n}\times\mathbf{J})\times\mathbf{n} = \mathbf{J} - \mathbf{n}(\mathbf{J}\cdot\mathbf{n})$ and equation 2.12 to obtain:

$$\mathbf{v}_{ab} - \mathbf{v}_{ab,0} = B_1\mathbf{J} - (B_1 - B_2)\mathbf{n}(\mathbf{J}\cdot\mathbf{n}) \ , \tag{2.14}$$

where

$$B_1 = \frac{7}{2}\left(\frac{1}{m_a} + \frac{1}{m_b}\right) \tag{2.15}$$

and

$$B_2 = \frac{1}{m_a} + \frac{1}{m_b}. \tag{2.16}$$

Then, constitutive relations are required to close the set of equations. Through these constitutive relations, three parameters enter the model to account for the inelastic dissipation and frictional energy loss. The first parameter is the coefficient of (normal) restitution, $(0 \le e \le 1)$:

$$\mathbf{v}_{ab}\cdot\mathbf{n} = -e(\mathbf{v}_{ab,0}\cdot\mathbf{n}) \ . \tag{2.17}$$

The second parameter is the coefficient of (dynamic) friction, $(\mu \ge 0)$:

$$|\mathbf{n}\times\mathbf{J}| = -\mu(\mathbf{n}\cdot\mathbf{J}) \ . \tag{2.18}$$

The third parameter is the coefficient of tangential restitution, $(0 \le \beta_0 \le 1)$:

$$\mathbf{n}\times\mathbf{v}_{ab} = -\beta_0(\mathbf{n}\times\mathbf{v}_{ab,0}) \ . \tag{2.19}$$

Although it is accepted that these coefficients depend on particle size and impact velocity this is not taken into account in this model. The only exception is made for the coefficient of normal restitution where collisions occurring at a normal impact velocity less than a threshold value '*MINC0*' (typically 10^{-4} m/s) are assumed to be perfectly elastic (e = 1.0).

Combining equations 2.14 and 2.17 yields the following expression for the normal component of the impulse vector:

$$J_n = -(1+e)\frac{\mathbf{v}_{ab,0}\cdot\mathbf{n}}{B_2} \tag{2.20}$$

For the tangential component two types of collisions can be distinguished that are called *sticking* and *sliding*. If the tangential component of the relative velocity is sufficiently high in comparison to the coefficients of friction and tangential restitution, that gross sliding occurs throughout the whole duration of the contact. The collision is of the *sliding* type. The non-sliding collisions are of the *sticking* type. When β_0 is equal to zero the tangential component of the relative velocity becomes zero during a *sticking* collision. When β_0 is greater than zero in such a collision, reversal of the tangential component of the relative velocity will occur. The criterion to determine the type of collision is as follows:

$$\mu < \frac{(1+\beta_0)\mathbf{v}_{ab,0} \cdot \mathbf{t}}{J_n B_1} \qquad \textit{sliding} \qquad (2.21)$$

$$\mu \geq \frac{(1+\beta_0)\mathbf{v}_{ab,0} \cdot \mathbf{t}}{J_n B_1} \qquad \textit{sticking} \qquad (2.22)$$

For collisions of the *sticking* type, the tangential impulse is given by:

$$J_t = -(1+\beta_0)\frac{|\mathbf{n}\times\mathbf{v}_{ab,0}|}{B_1} = -(1+\beta_0)\frac{\mathbf{v}_{ab,0} \cdot \mathbf{t}}{B_1} \qquad (2.\ 23)$$

For collisions of the *sliding* type, the tangential impulse is given by:

$$J_t = -\mu\ J_n\ . \qquad (2.\ 24)$$

The total impulse vector is then simply obtained by addition:

$$\mathbf{J} = J_n \mathbf{n} + J_t \mathbf{t}\ . \qquad (2.25)$$

The post-collision velocities can now be calculated from equations 2.6 and 2.7. For particle-wall collisions the mass of particle *b* (*i.e.* the wall) is assumed infinitely large which makes terms containing $1/m_b$ equal to zero.

The amount of energy dissipated during a collision can be obtained by solving the following integral over the duration of the collision:

$$E_{dsp,tot} = \int v_{ab,n}\, dJ_n + \int v_{ab,t}\, dJ_t\ . \qquad (2.26)$$

The amount of energy dissipated by the normal component in a collision is:

$$E_{dsp,n} = \frac{v_{ab,n,0}^2}{2B_2}\left(1 - e^2\right). \tag{2.27}$$

For the energy dissipated by the tangential component, the two types of collisions have to be distinguished again. If the collision is of the *sticking* kind, the amount of dissipated energy is given by:

$$E_{dsp,t} = \frac{v_{ab,t,0}^2}{2B_1}\left(1 - \beta_0^2\right), \tag{2.28}$$

whereas for the collision of the *sliding* type, the amount of dissipated energy is given by:

$$E_{dsp,t} = -\mu \mathrm{J}_n \left(\mathbf{v}_{ab,0} \cdot \mathbf{t} - \frac{1}{2}\mu B_1 \mathrm{J}_n \right). \tag{2.29}$$

The total amount of energy dissipated in a collision is then obtained by adding the tangential and normal contributions:

$$E_{dsp,tot} = E_{dsp,n} + E_{dsp,t}\,. \tag{2.30}$$

2.2 Sequence of collisions

In the hard-sphere model, a constant time step *DT* is used to take the external forces acting on the particles and gas flow into account. Within this time step *DT* the velocities are assumed to change only due to collisions and therefore a sequence of collisions is processed one collision at a time like in a regular hard-sphere simulation in Molecular Dynamics. So a separate MD hard-sphere simulation is performed within each time step.

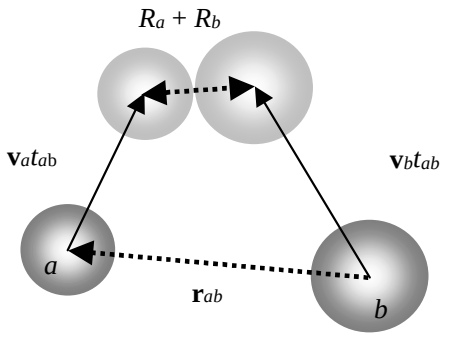

Figure 2.2: *Determination of the collision time t_{ab}.* (from Hoomans, 2000)

To do so it is necessary to determine what pair of particles will collide first which requires the determination of the collision times of all relevant collision pairs. The collision time t_{ab} of a pair of particles (a, b) is defined as the time remaining until these particles will collide. It can be calculated from the initial positions and velocities of both particles.

When particles a and b move from their original position to their new positions where the collision will occur (see Figure **2.2**). A quadratic equation in t_{ab} can be obtained. The smallest solution of this equation corresponds to the collision time (Allen and Tildesley, 1990):

$$t_{ab} = \frac{-\mathbf{r}_{ab} \cdot \mathbf{v}_{ab} - \sqrt{(\mathbf{r}_{ab} \cdot \mathbf{v}_{ab})^2 - v_{ab}^2 \left(r_{ab}^2 - (R_a + R_b)^2\right)}}{v_{ab}^2}, \qquad (2.31)$$

Where $\mathbf{r}_{ab} \equiv \mathbf{r}_a - \mathbf{r}_b$ and $\mathbf{v}_{ab} \equiv \mathbf{v}_a - \mathbf{v}_b$ (in the definition of $\mathbf{v}_{ab}$ here the particle rotation is not taken into account unlike in equation 2.12). Note also that if $\mathbf{r}_{ab} \cdot \mathbf{v}_{ab} > 0$ the particles are moving away from each other and will not collide. In case of a collision with a wall the collision time follows simply from the distance to the wall and the normal velocity component toward that wall which leads for a vertical wall to the following expression:

$$t_{a,wall} = \frac{(|x_{wall}| + R_a) - |\mathbf{r}_{x,a}|}{v_{x,a}} \ . \qquad (2.32)$$

The algorithm used to process a sequence of collisions within a constant time step *DT* is presented in Figure 2.3

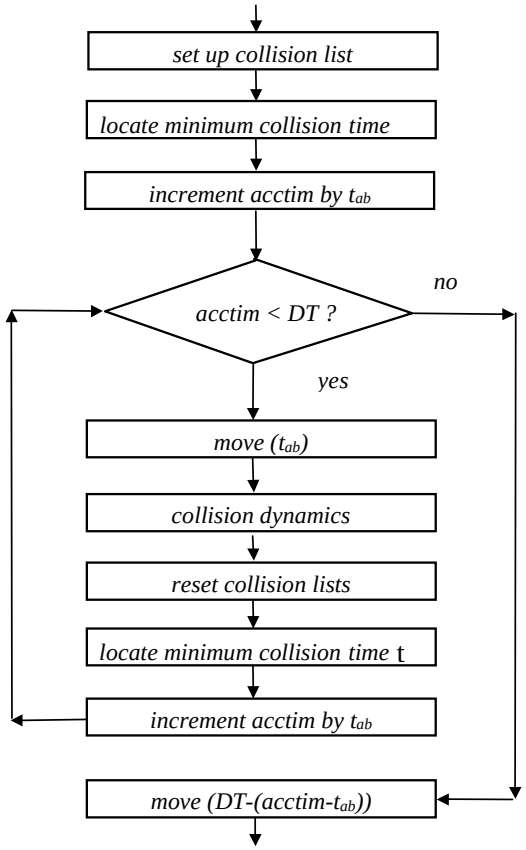

Figure 2.3: *Computational strategy of a hard-sphere simulation within a time step DT.* (from Hoomans, 2000)

First the collision lists are initialized by computing and storing for each particle a collision partner and a corresponding collision time. For each particle, the smallest collision time is determined by scanning all relevant collision partners. The variable *acctim* (accumulated time) keeps track of the time spent since the beginning of the time step. In the routine *move* (t_{ab}) the collision times of all particles are reduced with t_{ab} and the particle positions are updated using a first order explicit integration:

$$\mathbf{r}_a(t + t_{ab}) = \mathbf{r}_a(t) + \mathbf{v}_a t_{ab} \ . \qquad (2.33)$$

The calculation of the collision dynamics involves the collision model presented in the previous paragraph. Subsequently the routine *reset collision lists* is entered where new collision times and partners have to be found for all the particles involved in the collision. This does not only effect the particles *a* and *b* but also the particles that were about to collide with either *a* or *b*. Finally a new collision pair has to be detected and *acctim* can be incremented with the new collision time t_{ab}. As soon as a minimum collision time is found that after addition to *acctim* is greater than the time step *DT*, the loop is finished. After the loop is finished the particles have to be moved forward until *acctim* equals *DT*. During this motion no collision occurs.

2.3 Optimization

To perform simulations of relatively large systems for relatively long times it is essential to optimize the hard-sphere computational strategy. These methodologies have been developed by Hoomans (2000) to speed up the simulation, which include 1) a neighbor list technique to locate the collision pair, 2) the non-colliding particle shifting motion optimization and 3) the fluid-cell-based minimum collisional time location.

When looking for a collision partner for particle *a*, colored black, **only** the particles in its neighbor list within a square of size D_{nblist}, shaded spheres, need to be scanned as shown in Figure 2.4. This neighbor list is also updated at each time step dt_{nblist}. The new neighbor particles are located by scanning the particles **only** in those fluid cells where this particle's center is found and the three nearest adjacent cells for possible neighbors.

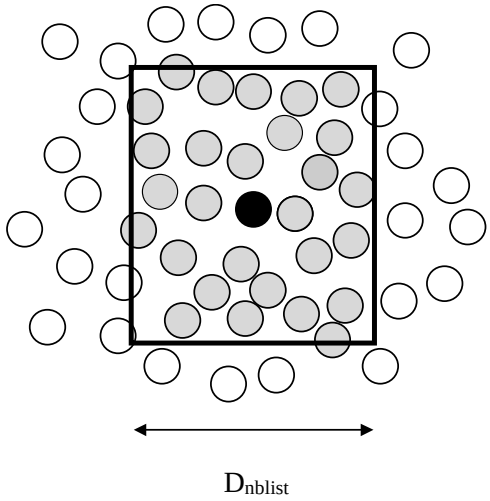

Figure 2.4: *The neighbour list principle: all shaded particles are stored in the neighbour list of the black particle.*

Particle motion update strategy replaces the method that all particles are moved to their new positions before each collision is processed. Instead, **only** the particles that are about to collide are moved but others are not moved to their real position but just "remembered"

by a variable *movetim.* These particles are moved to their new positions until the particles are located as a collisional pair or the loop ends. Although special care must be taken when looking for new collision partners for particles that just collided, since the positions stored in memory for the particles not involved in that collision are not their actual positions, nonetheless the speed gain is substantial, the routine *move*(t_{ab}) went down from 50% to less than 1% of the total amount of CPU time (Hoomans, 2000).

To locate the minimum collisional time, once again it is not necessary to scan all the particles in system. Instead, all the grid cells are scanned only if the smallest collision time is stored in each cell since the total number of grid cells is at least one order of magnitude smaller than the total number of particles. This is much faster. Of course, a new smallest collision time has to be found in the grid cells containing particles that were involved in the last collision but this causes negligible overhead.

After these optimizations, the *main CPU time consumer is the search for possible collisions* even though this search is performed only within the neighbor list! A suitable choice of 1) the size of the neighbor list and 2) the time step for updating the neighbor list is critical. These choices however depend on the sort of system that is simulated. If a neighbor list is chosen to be too small, it is possible that a collision is not detected and overlap between particles can occur. This cannot be tolerated in hard-sphere simulations and if such an overlap is detected the simulation is stopped immediately. On the other hand, if the neighbor list is chosen to be rather large all collisions will be detected but this will go at cost of the computational speed.

A hard-sphere simulation is an *event driven* simulation, which implies that the amount of collisions to be processed per time step depends on the dynamics of the system. The number of collisions to be processed can be considerably higher in a dense region of the bed than in a dilute region. Hence, the CPU time required to progress a time step can vary significantly. It is therefore not straightforward to benefit from parallel computing with a highly optimized *event driven* code.

2.4 External forces

In discrete particle simulation, the particle motion is computed from the Newtonian equation of motion:

$$m_p \frac{d\mathbf{v}_p}{dt} = m_p \mathbf{g} + \frac{V_p \beta}{(1-\varepsilon)}\left(\mathbf{u} - \mathbf{v}_p\right) - V_p \nabla p \qquad (2.34)$$

where m_p represents the mass of a particle, $\mathbf{v}_p$ its velocity, $\mathbf{u}$ the local gas velocity and V_p the volume of a particle. A similar equation of motion was used by Kawaguchi *et al*. (1998). In equation 2.34 the first term on the right hand side is due to gravity. The second term is due to the drag force where β represents an inter-phase momentum exchange coefficient as it usually appears in two-fluid models. For low void fractions ($\varepsilon < 0.80$) β is obtained from the well-known Ergun equation:

$$\beta = 150\frac{(1-\varepsilon)^2}{\varepsilon}\frac{\mu_g}{D_p^2} + 1.75(1-\varepsilon)\frac{\rho_g}{D_p}\left|\mathbf{u} - \mathbf{v}_p\right| \qquad (2.35)$$

where D_p represents the particle diameter, μ_g the viscosity of the gas and ρ_g the density of the gas. For high void fractions, ($\varepsilon \geq 0.80$) the following expression for the inter-phase momentum transfer coefficient has been used which is basically the correlation presented by Wen and Yu (1966) who extended the work of Richardson and Zaki correlation (1954):

$$\beta = \frac{3}{4}C_d \frac{\varepsilon(1-\varepsilon)}{D_p}\rho_g\left|\mathbf{u} - \mathbf{v}_p\right|\varepsilon^{-2.65} \qquad (2.36)$$

The drag coefficient C_d is a function of the particle Reynolds number:

$$C_d = \begin{cases} \dfrac{24}{\mathrm{Re}_p}\left(1 + 0.15\mathrm{Re}_p^{0.687}\right) & \mathrm{Re}_p < 1000 \\ 0.44 & \mathrm{Re}_p \geq 1000 \end{cases} \qquad (2.37)$$

where the particle Reynolds number in this case is defined as:

$$\mathrm{Re}_p = \frac{\varepsilon\rho_g\left|\mathbf{u} - \mathbf{v}_p\right|D_p}{\mu_g} \quad . \qquad (2.38)$$

The pressure gradient in the third term on the right hand side of equation 2.34 accounts for the far-field pressure gradient. Local values of velocities and the pressure gradient are obtained from an area weighted averaging technique using the values of the relevant quantity at the four surrounding grid nodes. The area-weighted averaging technique used to obtain the local averaged value $\overline{Q}$ of a quantity Q(i, j) from the four surrounding computational nodes is shown in Figure 2.5. The local averaged value is calculated as follows:

$$\overline{Q} = \frac{A_{i,j}Q_{i,j} + A_{ii.j}Q_{ii,j} + A_{ii,jj}Q_{ii,jj} + A_{i,jj}Q_{i,jj}}{DXDY} \tag{2.39}$$

where:

$$\begin{aligned} A_{i,j} &= \left(DX - \delta_x\right)\left(DY - \delta_y\right) \\ A_{ii,j} &= \delta_x\left(DY - \delta_y\right) \\ A_{ii,jj} &= \delta_x\delta_y \\ A_{i,jj} &= \left(DX - \delta_x\right)\delta_y \end{aligned} \tag{2.40}$$

The distances δ_x and δ_y, required in this averaging technique, are calculated from the position of the particle in the staggered grid. The integration in time of equation 2.34 was an explicit first order scheme. Other external forces than the ones included in equation 2.34 can be taken into account as well with great flexibility.

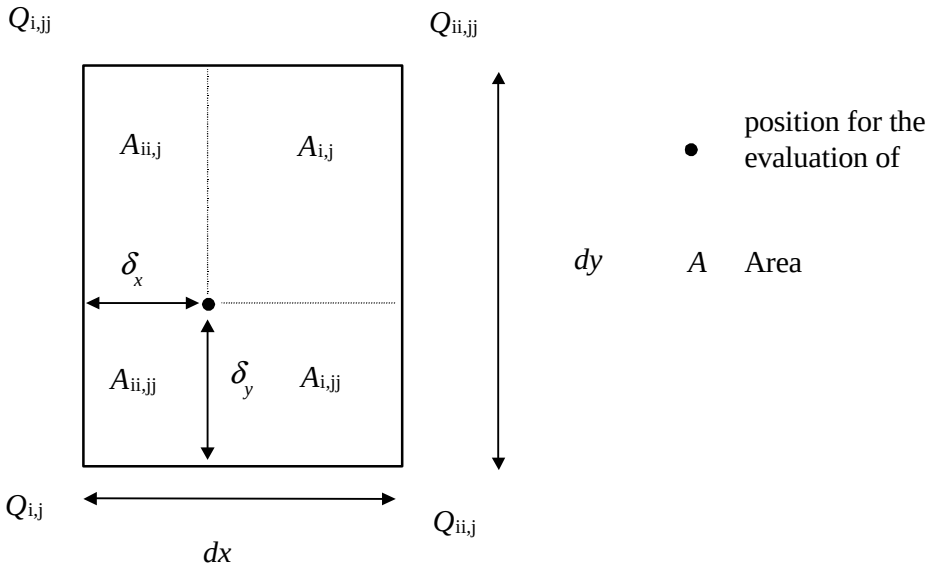

Figure 2.5: *The concept of area weighting* (from Hoomans, 2000).

3. Gas phase hydrodynamics

3.1 Governing equations

The calculation of the gas-phase hydrodynamics mainly follows the lines presented by Kuipers *et al.* (1992). It is based on the numerical solution of the following set of partial differential equations that can be seen as a generalized form of the Navier-Stokes equations for a gas interacting with a solid phase as originally derived by Anderson and Jackson (1967).

Continuity equation of gas phase:

$$\frac{\partial\left(\varepsilon\rho_g\right)}{\partial t}+\left(\nabla\cdot\varepsilon\rho_g\mathbf{u}\right)=0\ . \tag{2.41}$$

Momentum equation of gas phase:

$$\frac{\partial\left(\varepsilon\rho_g\mathbf{u}\right)}{\partial t}+\left(\nabla\cdot\varepsilon\rho_g\mathbf{u}\mathbf{u}\right)=-\varepsilon\nabla p-\mathbf{S}_p-\left(\nabla\cdot\varepsilon\boldsymbol{\tau}_g\right)+\varepsilon\rho_g\mathbf{g}\ . \tag{2.42}$$

In this work isothermal, two-dimensional motion is considered which implies that three basic variables have to be specified. The three basic variables in the model are the pressure (p) and the two velocity components of the gas-phase (u_x and u_y). The void fraction (ε) and the momentum exchange source term ($\mathbf{S}_p$) are obtained from the discrete particle model as will be explained in section 6. All remaining variables have to be specified in terms of the three basic variables and/or the variables obtained from the discrete particle model through constitutive equations.

3.2 Constitutive equations

3.2.1 GAS PHASE DENSITY

The gas phase density (ρ_g) is related to the pressure (p) and the gas phase temperature (T) by the ideal gas law:

$$\rho_g=\frac{M_g}{RT}\,p\ . \tag{2.43}$$

Where, R is the gas constant (8.314 J/(mol K)). The average molecular weight of air (M_g = 28.8 10^{-3} kg/mol) was used and the temperature was set to a constant value of T = 293 K.

3.2.2 GAS PHASE STRESS TENSOR

The viscous stress tensor $\boldsymbol{\tau}_g$ is assumed to depend only on the gas motion. The general form for a Newtonian fluid (Bird *et al*., 1960) has been implemented:

$$\boldsymbol{\tau}_g = -\left[\left(\lambda_g - \frac{2}{3}\mu_g\right)(\nabla\cdot\mathbf{u})\mathbf{I} + \mu_g\left((\nabla\mathbf{u}) + (\nabla\mathbf{u})^T\right)\right]. \qquad (3.44)$$

In the simulations the bulk viscosity of the gas phase λ_g was set equal to zero which is allowed for gases (Bird *et al*., 1960) whereas for the gas phase shear viscosity a constant value of μ_g = 1.8×10^{-5} kg/ms was used. **I** denotes the unit tensor.

Note that no turbulence modeling was taken into account. For bubbling beds this can be justified since the turbulence is damped out in the bed due to the very high volumetric solids fraction.

3.3 Numerical solution

The numerical solution has been described in detail by Kuipers *et al.* (1992, 1993) and will therefore not be discussed here. A finite difference technique, employing a staggered grid to ensure numerical stability, is used to solve the gas-phase conservation equations 2.41 and 2.42. This implies that the scalar variables (p and ε) are defined at the cell centre and that the velocity components are defined at the cell faces as is shown in Figure 2.6.

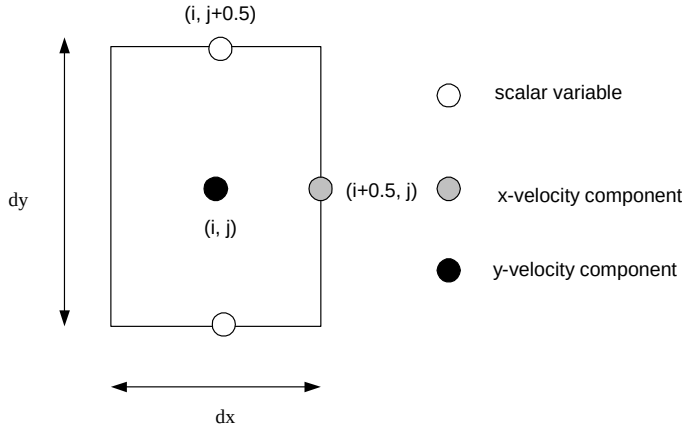

Figure 2.6: *Lay out of the staggered grid.*

A whole-field pressure correction technique is employed to solve the discrete Pressure Poison Equation (PPE). The model is capable of performing transient two-dimensional calculations in a Cartesian or an axi-symmetrical geometry. In the simulations reported in this work only the Cartesian option was used.

3.4 Boundary conditions

For the incorporation of the boundary conditions a flag matrix is used which allows boundary conditions to be specified for each single cell. A variety of boundary conditions can be applied by specification of the value of the cell flag fl(*i*,*j*) which is associated with the relevant boundary condition for that cell(*i*,*j*). The typical set of boundary conditions used in the simulations performed in this study is shown in Figure **2.7**.

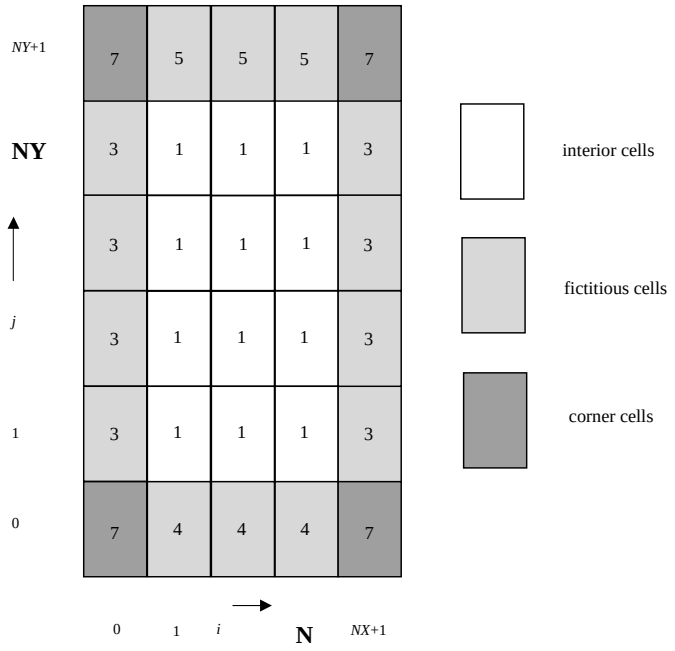

Figure 2.7: *Cell flags for the boundary conditions for the hydrodynamic model.*

The cell flags and the corresponding boundary conditions that are featured in the present code are listed in Table 2.1.

Table 2.1: *Cell flags and corresponding cell types.*

fl(*i*,*j*)	Cell type of cell(*i*,*j*)
1	Interior cell, no boundary conditions have to be specified
2	Impermeable wall, free slip boundaries
3	Impermeable wall, no slip boundaries
4	Influx cell, velocities have to be specified
5	Prescribed pressure cell, free slip boundaries

6	Continuous outflow cell, free slip boundaries
7	Corner cell, no boundary conditions have to be specified

To mimic a distributor plate the void fraction in the inlet cells (fl(i,j) = 4) was set to a constant value of 0.4. Two kinds of conditions have been used for the distributor in this research: a specified normal gas velocity or a prescribed pressure at the inlet. At the inlet always a prescribed pressure was used.

3.5 Two-way coupling

An important issue in granular dynamics simulations of two-phase flow is the two-way coupling which account for feedback effects of the suspended particles to the carried phase. The calculation of the drag force is based on empirical relations that have been fitted to experimental data obtained from three-dimensional beds. Two-way coupling should be incorporated in such a way that the model is capable to predict typical fluidization phenomena such as the pressure drop over the bed at minimum fluidization conditions. This pressure drop, multiplied by the cross sectional area, should balance the force exerted by gravity on the particles. Different approaches have been employed to realize this coupling. Xu and Yu (1997) used a technique similar to the one used by Schwarzer (1995) where the total drag force exerted on a particle was fed back to the gas phase with a minus sign. Hoomans et al. (1998) demonstrated that the pressure drop over the bed at minimum fluidization conditions in the simulations of Xu and Yu (1997) with this technique was over-predicted by a factor 1.5.

This controversy arises partially from the transformation calculation of bed void fraction from 2-D to 3-D. Tsuji *et al.* (1993), Xu and Yu (1997), Kawaguchi *et al*. (1998) and Mikami *et al*. (1998) all calculated the void fraction on the basis of volumes assuming that the system consists of a single layer of particles. Hence, the third dimension equals to the particle diameter. Hoomans (2000) argued that this method yields void fractions that are in general too high, as a results the closest packing can never be obtained, therefore, it is not a correct representation for a three-dimensional system. Keeping in mind that the empirical drag correlations comes from 3-D beds, a transition formulation from 2-D to 3-D based on face-centered cubic was derived, which results in a third dimension of $2\times 3^{-0.75} d_p$, thus slight smaller than the particle diameter. Ouyang and Li (1999) used a transformation similar to Hoomans' correlation. Therefore, special care has to be taken in order to select a two-way coupling technique that ensures that key fluidization features are incorporated correctly.

Two-way coupling is achieved via the calculation of the void fraction and the incorporation of an interaction term in the momentum conservation equation for the gas-phase (equation 2.42). In the following paragraphs, following the lines of Hoomans (2000), the two-way coupling technique used in this study will be presented.

3.5.1 CALCULATION OF THE VOID FRACTION

The solution of equations 2.41 and 2.42 requires specification of the void fraction (ε) which can be obtained from the discrete particle model. As the particle positions are known, the void fraction $\varepsilon(i,j)$ can be calculated based on the area occupied by the particles in that cell i,j. Due to the essentiality of void fraction which considerably influences the motion of the gas phase, a detailed check for overlap is necessary in which

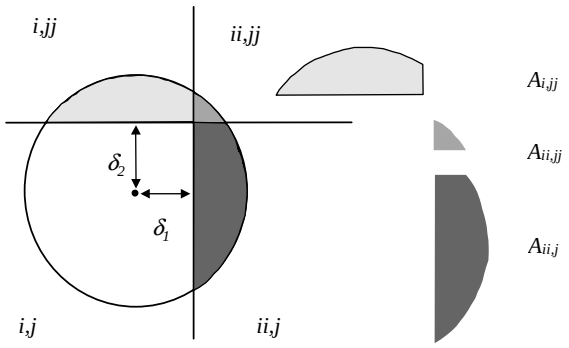

Figure 2.8: *Multiple particle-cell overlap* (from Hoomans, 2000).

multiple cell overlap must be taken into account as illustrated in Figure 2.8. In this figure a case is presented where a particle overlaps four different grid cells. The overlapping area of the particle $A_{ii,jj}$ can be calculated as follows:

$$A_{ii,jj} = \delta_1\delta_2 - \frac{1}{2}R_p\left[\delta_1\sqrt{1-\left(\frac{\delta_1}{R_p}\right)^2} + \delta_2\sqrt{1-\left(\frac{\delta_2}{R_p}\right)^2} - R_p\left(\arccos\left(\frac{\delta_1}{R_p}\right) - \arcsin\left(\frac{\delta_2}{R_p}\right)\right)\right] . \tag{2.45}$$

For the area A_{jj} the following relation can be obtained:

$$A_{jj} = A_{i,jj} + A_{ii,jj} = R_p\left(R_p \arccos\left(\frac{\delta_2}{R_p}\right) - \delta_2\sqrt{1-\left(\frac{\delta_2}{R_p}\right)^2}\right) . \tag{2.46}$$

Keeping in mind that:

$$A_{i,j} + A_{i,jj} + A_{ii,jj} + A_{ii,j} = \pi R_p^2 , \tag{2.47}$$

all four areas can be calculated using basic subtractions. In the case where a particle overlaps with only two cells the area of overlap can simply be obtained from equation 2.46. The void fraction calculated in this way is based on a two-dimensional analysis, which is inconsistent with the applied empiricism in the calculation of the drag force exerted on a particle. To correct for this inconsistency, the void fraction calculated on the basis of area (ε_{2D}) is transformed into a three-dimensional void fraction (ε_{3D}) using the following equation:

$$\varepsilon_{3D} = 1 - \frac{2}{\sqrt{\pi\sqrt{3}}}\left(1-\varepsilon_{2D}\right)^{3/2} . \qquad (2.48)$$

This equation has been derived on the basis of a comparison between a two-dimensional hexagonal lattice and a three-dimensional FCC unit cube assuming equal inter-particle distances. It ensures that the closest packing in the 2-D hexagonal lattice is transformed into the closest packing in the 3-D FCC case. A comparison of two kinds of transitions is shown in Figure 2.9. It can be seen that the single particle layer depth assumption is

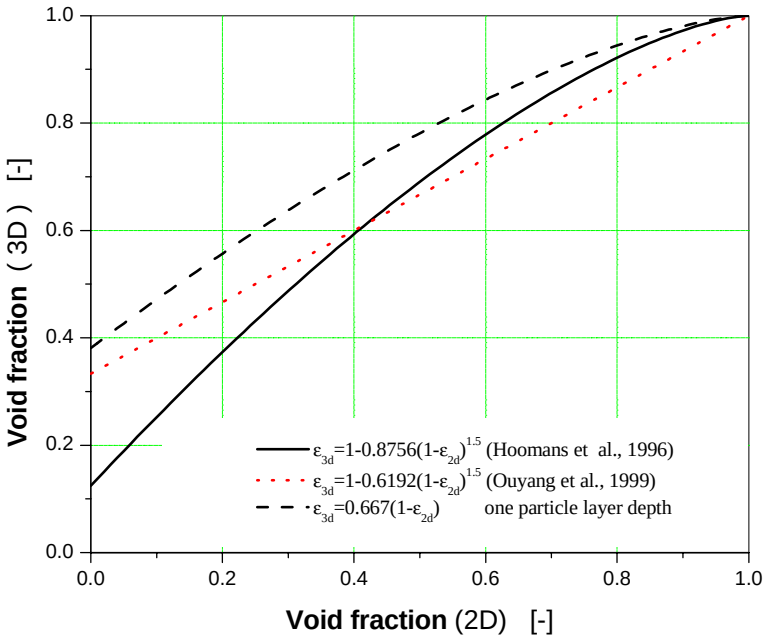

Figure 2.**9:** Comparison among different types of 2-D to 3-D transition.

unable to achieve a dense packed system (void fraction of 0.26 not 0.4, 3-D). However, for a hexagonal packing a more dilute system (3-D) than that for a single particle layer is obtained. Anyway, there remains an uncertainty in the transformation rules. Since most work in this research focus on dense systems, the Hoomans' correlation has been employed.

3.5.2 MOMENTUM TRANSFER

The method used in this work is based on Newton's third law. The reaction force to the drag force exerted on a particle per unit volume is included in the momentum conservation equation 2.2 via a source term $\mathbf{S}_p$ that has the dimension N/m^3:

$$\mathbf{S}_p = -\frac{1}{V}\int \sum_{a=0}^{Npart} \frac{V_p \beta}{(1-\varepsilon)} \quad (\mathbf{u}-\mathbf{v}_a)\delta \quad (\mathbf{r}-\mathbf{r}_a)dV \qquad (2.49)$$

The δ-function ensures that the reaction force acts as a point force at the position of the particle in the system. In the numerical implementation this force-per-volume term is distributed to the four nearest grid nodes using the area weighted averaging technique as described previously in this chapter, where also the expression for the volumetric momentum exchange coefficient β can be found.

Since the source term $\mathbf{S}_p$ has the dimension of force per unit volume the force exerted on the particles has to de divided by the volume of a grid cell. In the 3-D model this is straightforward since the third dimension is determined by the depth of the bed. In the 2-D model a virtual third dimension has to be introduced. This virtual third dimension is estimated based on the same calculation as the conversion from ε_{2D} to ε_{3D}. In the 2-D simulations this leads to the following expression for the volume of a computational cell:

$$V_{cell} = 2DRDZ\,3^{-0.75}D_p, \qquad (2.50)$$

in which the third dimension is slightly less than the particle diameter. Note that this volume depends on the particle size and hence is not a constant in simulations where a particle size distribution is taken into account.

4. Characterization of flow structures

Besides granular dynamics and gas phase hydrodynamics, additional quantification is needed to characterize flow structure and two basic phenomena in particulate systems: particle-particle interaction and fluid-particle interaction.

To portray particle-particle interaction and fluid-particle interaction in particulate flows has proved a difficult task. Although great efforts have been made in the past in this direction, especially on the quantification of fluid-particle interaction, we still are unable to precisely quantify the drag acting on a swarm of particles. Neither can we quantitatively characterize multi-body collisions between particles.

With respect to fluid-solid interaction, most classical methods are based on the assumption that fluidized suspensions are in an equilibrium state. Accordingly, the overall hydrodynamics is thought to be established on basis of the summation of individual particle dynamics. This idea prevails in fluidization research and is exemplified in the well-known Wen and Yu correlation (1966). They originally assumed that a fluidized suspension exists in an equilibrium state and employed single particle hydrodynamics as a starting point for their analysis. However, the experimental data eventually revealed that fluid-solid drag correlated to void fraction in a strong non-linear way. In a recent study employing Lattice-Boltzmann simulation (Hill, 2001) it was confirmed that there exists indeed such a strong non-linear interaction between solids and fluid. These findings suggest that *most fluidization systems are naturally non-equilibrium systems.*

For non-equilibrium and non-linear systems, traditional linear treatments are of limited use. For instance, linear stability analysis, being suitable to describe the transition from uniform to bubbling fluidization, cannot be carried to a stage to predict regime transition particular at higher gas velocities. Material properties, to a great extent, determine the system equilibrium naturally. Therefore, the parameters related to these properties would be definitely useful to delineate the flow structure. Meanwhile, since non-equilibrium is also closely linked to the dynamic behaviors of both phases and therefore controls regime transition, characterization in this respect is also essential (Re, St). Micro-scale simulation (Lattice-Boltzmann, DNS, Dissipative Particle Dynamics) provides a proper base to tackle such problems, but is beyond the scope of this research. Instead in this study generally accepted drag correlations will be examined to assess their effects on flow structures, which will be discussed in more detail in chapter 4.

As far as particle-particle interaction is concerned, fluidization modeling is at an early stage. The most advanced continuum models of gas-fluidized beds which are currently in use are based on the kinetic theory of granular flow which basically is an extension of the kinetic theory of dense gases (Chapman and Cowling, 1970). In this type of model the

granular temperature or the kinetic energy associated with the random granular motion of the particles plays an important role to quantify solid pressure and solid viscosity. In this study DPM is used to directly compute the granular temperature from the velocities of ensembles of particles.

Up to date, there does not exist any systematic approach available to directly quantify the variety of individual interactions in the system and furthermore to link these interactions to the pattern formation and evolution in gas-fluidized bed. As a gas-fluidized bed is a non-equilibrium dissipative system any analysis just based on force considerations is unable to completely capture the real features (Li, 1987). Meanwhile, the fundamental weakness of the methods based on the force descriptions of multiple-body systems lies in the assumption of linearity of these quantities, which make the quantification more complicated and prevent the efficient characterization along this way.

Keeping these factors in mind, a new simple methodology based on energy budget analysis, first presented by Hoomans (2000), is elaborated in this work to allow for thorough understanding of flow structure formation. This includes detailed quantification of the various interactions in terms of work and energy, including gas drag (input), particle suspension (potential energy), motion (translational or rotational) and collisional dissipation (friction and inelastic collision). This method is simple, easy and precise and is able to take all relevant interactions into account, including a particularly difficultly quantity, namely particle collisional dissipation. On this basis, by analyzing the energy budget distribution it is possible to connect various interactions directly to pattern formation. Additionally, this quantification can be conducted not only on a global scale to understand the overall hydrodynamics but also at meso-scale to explore the local interactions and comprehend their spatial distributions. In this research, we focus on the former.

4.1 System equilibrium

Whether a system is in equilibrium or not is an essential issue closely linked to pattern formation. Hence, knowledge on system equilibrium is particularly useful. Microscopically the motion of a single particle is controlled by the local gas flow and particle-particle and particle-wall encounters. When the system is near to linear non-equilibrium, a homogeneous flow structure prevails, particles remain in a steady motion and collisional interaction is limited. Therefore, tracing the behavior of a single particle, with respect its motion, can help us to understand both its microscopic behavior and system equilibrium. Particularly, if the environment of this traced particle (void fraction or coordinate number) is also monitored at the same time, we may know how the particle group effect (non-linear interaction) has its impact on the particle motion and furthermore the *pattern formation.* This can be easily done in DPM and will be explained in detail in chapter 4.

4.2 Quantification of flow structures

4.2.1 CALCULATION OF GRANULAR TEMPERATURE

Single particle behavior reflects particle-particle interaction at micro-scale. However, particle-particle interaction at meso-scale also needs to be quantified, such as collision intensity distribution and its evolution in fluidized beds. Granular temperature, in analogy to temperature in the kinetic theory of gases, represents the intensity of particle collisions and is closely related to the magnitude of the fluctuating velocity of the particles, defined as:

$$\theta = \frac{1}{n}\left\langle C^2 \right\rangle . \tag{2.51}$$

or

$$\theta = \frac{1}{n}\frac{\sum_{1}^{N}(C_k{}^2)}{N} . \tag{2.52}$$

Where $C^2 = \mathbf{C}\cdot\mathbf{C}$, N is particle number in a specified volume. The quantity n denotes the dimensionality of the system (2 for 2-D and 3 for 3-D) and $\boldsymbol{C}_k$ is the fluctuation velocity of the k^{th} particle. The fluctuation velocity is defined as the difference between the velocity of particle k and the local mean particle velocity $\overline{v}_{\mathrm{k}}$ given by:

$$\mathbf{C}_k = v_k - \frac{1}{l}\sum_{l\in D} v_{k,l} \quad . \tag{2.53}$$

For the 2-D case, following formula holds:

$$\theta = \frac{1}{2}(\theta_x + \theta_y) = \frac{1}{2}\left(\frac{\sum_{1}^{N} C_{k,x}^2}{N} + \frac{\sum_{1}^{N} C_{k,y}^2}{N}\right) . \tag{2.54}$$

By sampling the velocity data with respect to space and time, it is possible to quantify the spatial/temporal distribution of particle-particle interaction. As this research intends to characterize the flow patterns in fluidized beds, a single cell is selected as the basic element to calculate the granular temperature. In such a way, the collisions inside and outside of sub-systems such as bubbles and clusters can be distinguished but the cell of course should host enough particles to allow for the correct quantification.

4.2.2 CALCULATION OF MEAN SQUARE SOLID VOLUME FRACTION FLUCTUATION

Flow structure can also be directly delineated by the domain-averaged mean square solid volume fraction fluctuation, defined as follows:

$$< f_s^{'2} >= \frac{1}{NR \times NZ} \sum_{j=1}^{NR \cdot NZ} (f_{s,j} - \overline{f}_s)^2 . \qquad (2.55)$$

Where NR, NZ are the number of computational cells in the radial and axial direction respectively and f_s is the solids volume fraction. The bar represents the domain-averaged value. This domain-averaged mean square solid volume fraction fluctuation equals zero when the system is perfect uniform. This quantity, sensitive to the variation of system void fraction, is mainly employed to characterize flow patterns in dilute gas-solid two flows.

4.2.3 CALCULATION OF STANDARD DEVIATION OF PRESSURE DROP FLUCTUATION

The bed pressure drop is obtained by calculating the pressure difference between the bottom and top portion of the bed. Because of the pressure drop fluctuations, especially in the bubbling fluidization regime, statistical treatment of the data is required to obtain the time-averaged pressure drop. The standard deviation of pressure signal (*s*), defined according to equation 56, is used as a parameter for determining the flow regime transitions. Where, T represents time, P_i the transient pressure-drop and $\overline{P}$ denotes the time-averaged pressure-drop during the period of time T.

$$s = \sqrt{\frac{1}{T} \sum_{i}^{T} (p_i - \overline{p})^2} \qquad (2.56)$$

Note that this type of quantification is only useful when the system operates at low gas velocity since the disturbance that the solids feedback to gas phase is very limited. As for low gas velocity dense beds, both methods above are more or less comparable.

4.3 Energy budget analysis

The hard-sphere model offers a unique advantage to precisely quantify the various contributions to the mechanical energy balance of the system. These quantifications are detailed below.

The instantaneous energies associated with the motion of particles (i.e. the translational kinetic energy and the rotational energy) and the position of particles (i.e. the potential energy) can be calculated from:

$$E_{kin} = \frac{1}{2}\sum_{k}^{Npart} m_k v_k^2 \,, \tag{2. 57}$$

$$E_{rot} = \frac{1}{2}\sum_{k}^{Npart} I_k \omega_k^2 \,, \tag{2. 58}$$

$$E_{pot} = \sum_{k}^{Npart} m_k \left(\mathbf{g}\cdot\mathbf{r}_k\right). \tag{2. 59}$$

where $\mathbf{r}_k$ represents the position vector of particle *k*. The energy that the particles receives from the interaction with the gas phase includes two parts: drag and pressure gradient (buoyancy). These energy sources can be computed from the following expressions:

$$E_{drag} = \sum_{k}^{Npart}\int\left(\frac{V_{p,k}\beta}{(1-\varepsilon)}\left(\mathbf{u}-\mathbf{v}_k\right)\right)\cdot\mathbf{v}_k dt \,. \tag{2. 60}$$

$$E_{buoy} = \sum_{k}^{Npart}\int\left(-V_{p,k}\nabla p\right)\cdot\mathbf{v}_k dt \,. \tag{2. 61}$$

The amount of energy dissipated in collisions due to inelasticity and friction are calculated using equations 2.27 ~ 2.29 given earlier in this chapter. These dissipated energies are taken to be positive by definition.

All the eight different energies mentioned above are calculated independently. Since the dissipated energy is taken to be positive by definition the sum of the potential, kinetic, rotation and dissipated energy should equal the amount of energy that the particles receive from the interaction with the gas phase. According to the energy conservation principle, we have:

$$E_{tot}^0 = E_{pot} + E_{kin} + E_{rot} + E_{dsp} - E_{drag} - E_{buoy} \,. \tag{2. 62}$$

Where, E_{tot}^0 is the initial total energy in the system composed of kinetic, potential and rotational energies as follows:

$$E_{tot}^0 = E_{pot}^0 + E_{kin}^0 + E_{rot}^0 \,. \tag{2. 63}$$

This amount should remain constant during a simulation. Then the fraction of the total energy associated with energy type *i* (*i* = *pot*, *kin*, *rot* and *dsp*) is given by:

$$f_i = \frac{E_i}{E_{tot}^0 + E_{drg} + E_{buoy}} \,. \qquad (2.\ 64)$$

Accordingly, it is possible to establish the precise quantitative connection between various energy types and flow structure formation. Depending on the size of the sampling domain, energy budget analysis can be conducted on both local and global scale. Since energy is a scalar quantity, this method provides great convenience for the characterization. When there exists extra energy input to and/or output from the considered system, as encountered in a circulating fluidized bed, a slight modification of equation 2.62 is required (see chapter 6).

Notation

A	area, m^2
Ar	Archimedes number, [-]
B_1, B_2	collision constants, 1/kg
C_d	drag coefficient, [-]
C	particle fluctuation velocity, [m/s]
D_{nblist}	diameter of neighbour square
D_p	particle diameter, m
DT	time step, s
dt_{nblist}	time step for neighbour list update, s
dx	horizontal computational cell dimension, m
dy	vertical computational cell dimension, m
e	coefficient of restitution, [-]
E	energy, J
$\mathbf{F}$	force, N
$fl(i,j)$	cell flag [-], defined in Table 1
f_s	solids volume fraction, [-]
$\mathbf{g}$	gravitational acceleration, m/s^2
I	moment of inertia, kgm^2
$\mathbf{I}$	unity tensor, [-]
i,j	cell indices, [-]
$\mathbf{J}$	impulse vector, kgm/s
M	molecular weight, kg/mol
m	particle mass, kg
$\mathbf{n}$	normal unit vector, [-]
n_{coll}	total number of collisions, [-]
n_{tot}	total number of particles, [-]
NX	number of computational cells in x-direction, [-]
NY	number of computational cells in y-direction, [-]
p	pressure, Pa
R	gas constant, J/mol K
$\mathbf{r}$	particle position vector, m
R_p	particle radius, m
s	standard deviation of pressure, [pa]
$\mathbf{S}_p$	source term defined in equation 2.49
S_t	Stokes number, [-]
$\mathbf{t}$	tangential unit vector, [-]
T	temperature, K
t	time, s
$\mathbf{T}$	torque, Nm
t_{ab}	collision time, s
$\mathbf{u}$	gas phase velocity, m/s
$\mathbf{v}$	velocity, m/s
V	volume, m^3

Greek symbols

ω	angular velocity, 1/s
ρ	density, kg/m^3
ξ	displacement, m
δ	distance, m
θ	granular temperature, [m^2/s^2]
ε	void fraction, [-]
β	volumetric inter-phase momentum transfer coefficient, kg/(m^{3}s)
β_0	coefficient of tangential restitution, [-]
μ_g	gas shear viscosity, kg/(ms)
λ_g	gas bulk viscosity, kg/(m.s)
μ	friction coefficient, [-]
$\boldsymbol{\tau}$	gas phase stress tensor, kg/ms^2

Subscripts

0	initial condition
a,b	particle indices
av	average
buoy	buoyancy
cp	contact point
drg	drag
dsp	dissipated
g	gas phase
gyr	gyration
i,j	cell indices
kin	kinetic
nblist	neighbour list
p	particle
pot	potential
rot	rotational
w	wall
x	x-component
y	y-component

Superscripts

T	transposed

Reference

Alder, B. J. and Wainwright, T. E. 1957 Phase Transition for a Hard-Sphere System. *J. Chem. Phys*., **27**, 1208.

Allen, M. P. and Tildesley, D. J., *Computer Simulations of Liquids*. Oxford Science Publications, Oxford, UK, 1990.

Anderson, T. B. and Jackson, R. 1967 A fluid mechanical description of fluidized beds (equations of motion). *Ind. Eng. Chem., Fundam.*, **6**, 527.

Andraw M. J. and O'Rourke, P. J. 1996 The multiphase particle-in-cell (MP-PIC) method for dense particulate flows. *Int. J. Multiphase Flow*, **22**, 379.

Bird, G.A. *Molecular Gas Dynamics and Direct Simulation of Gas Flows*. Oxford University Press, Oxford, UK, 1976.

Bird, R. B., Stewart, W. E. and Lightfood, E. N. *Transport phenomena*, John Wiley & Sons, New York, 1960.

Campbell, C. S. and Brennen, C. E. 1985 Computer simulations of granular shear flows. *J. Fluid. Mech*., **151**, 167.

Chapman, S. and Cowling, T. G. 1970 *The Mathematical Theory of Theory of Non-Uniform Gases*, Cambridge University Press, UK.

Cundall, P. A. and Strack, O. D. L. 1979 A discrete numerical model for granular assemblies. *Géotechnique*, **29**, 47.

Goldschmidt, M. 2001 Hydrodynamic modelling of fluidised bed spray granulation. *Ph. D. dissertation*, Twente University, The Netherlands.

Grace, J. R. 1986 Contacting modes and behavior classification of gas-solid and other two-phase suspensions. *Can. J. Chem. Eng*., **64**, 353-363.

Helland E, Occelli R, Tadrist L. 2000 Numerical study of cluster formation in a gas-particle circulating fluidized bed. *Powder Technol*., **110**, 210-221.

Helland, E., Occelli, R. and Tadrist, L. 1999 Numerical study of cohesive powders in a dense fluidized bed. *CR Acad. Sci. II B*, **327,** 1397.

Hill, R. J. 2001 The effects of fluid inertia on flow in porous media. *Ph. D. Dissertation*, Cornell University, USA.

Hoomans, B. P. B. 2000 Granular dynamics in gas-solids two-phase flows. *Ph.D. dissertation*, Twente University, The Netherlands.

Hoomans, B. P. B. and Kuipers, J. A. M. Discrete particle simulation of cluster formation in dense riser flow. *CFB-VI*, Werther J., ed., (1999), DECHMA, Wurzburg, p. 255.

Hoomans, B. P. B., Kuipers, J. A. M., Briels, W. J. and van Swaaij, W. P. M. 1996 Discrete particle simulation of bubble and slug formation in a two-dimensional gas-fluidized bed: a hard-sphere approach. *Chem. Eng. Sci*., **51**, 99.

Hoomans, B. P. B., Kuipers, J. A. M., Briels, W. J. and van Swaaij, W. P. M. 1998 Comments on the paper "Numerical simulation of the gas-solid flow in a fluidized bed by combining discrete particle method with computational fluid dynamics" by B. H. Xu and A. B. Yu. *Chem. Eng. Sci*., **53**, 2645.

Hopkins, M. A. and Louge, M. Y. 1991 Inelastic microstructure in rapid granular flows of smooth disks. *Phys. Fluids* **A 3**(1), 47.

Iwadate, M. and Horio, M., Agglomerating fluidization of wet powders and group c powders: a numerical analysis. *Fluidization IX*, AIChE Engineering Foundation, Durango, L. S. Fan, T. Knowlton Eds., (1998) p.293.

Jaeger, H. M., Nagel, S. R. and Behringer, R. P. 1996 Granular solids, liquids and gases. *Rev. Mod. Phys*., **68**, 1259.

Kaneko, Y., Shiojima, T. and Horio, M. 1999 DEM simulation of fluidized beds for gas-phase olefin polymerization. *Chem. Eng. Sci*., **54**, 5809.

Kawaguchi, T., Sakamoto M., Tanaka, T. and Tsuji, Y. 2000 Quasi-three-dimensional numerical simulation of spouted beds in cylinder. *Powder Technol*., **109**, 3.

Kawaguchi, T., Tanaka, T. and Tsuji, Y. 1998 Numerical simulation of two-dimensional fluidized beds using the discrete element method (comparison between the two- and three-dimensional models). *Powder Technol*., **96**, 129.

Kuipers, J. A. M., van Duin K. J., van Beckum, F. P. H. and van Swaaij, W. P. M. 1992 A numerical model of gas-fluidized beds. *Chem. Eng. Sci*., **47,** 1913.

Kuipers, J. A. M., van Duin K. J., van Beckum, F. P. H. and van Swaaij, W. P. M. 1993 Computer simulation of the hydrodynamics of a two-dimensional gas-fluidized bed. *Comput. Chem. Eng.*, **17**, 839.

Kuwagi K., Takano, K. and Horio, M. 2000 The effect of tangential lubrication by bridge liquid on the behavior of agglomerating fluidized beds. *Powder Technol*., **113**, 287.

Kuwagi, K, T. Mikami, M. and Horio M. 2000 Numerical simulation of metallic solid bridging particles in a fluidised bed at high temperature. *Powder Technol*., **109**, 27.

Langston, P. A., Tüzün U. and Heyes, D. M. 1994 Continuous potential discrete particle simulations of stress and velocity fields in hoppers transition from fluid to granular flow, *Chem. Eng. Sci.,* **49**, 1259.

Langston, P. A., Tüzün, U. and Heyes, D. M. 1995 Discrete element simulation of granular flow in 2D and 3D hoppers: dependence of discharge rate and wall stress on particle interactions. *Chem. Eng. Sci*., **50**, 967.

Li, Y., Yang, G. Q., Zhang, J. P. and Fan, L.-S. 2001 Numerical studies of bubble formation dynamics in gas-liquid-solid fluidization at high pressures. *Powder Technol*., **116**, 246.

Li, J. and Kuipers, J. A. M., Effect of pressure on flow behaviours in dense gas-fluidized beds: A discrete particle simulation study. *Fluidization X*, M. Kwauk, J. Li and W.-C. Yang, Eds., Engineering Foundation, Beijing (2001), p. 389.

Li, J.-H. 1987 Multi-scale Modeling and Method of Energy Minimization for Particle-Fluid Flow. *Ph. D. dissertation*, Institute of Chemical Metallurgy, Academia Sinica, P. R. China.

Li, J. and Mason, D. J. 2000 A computational investigation of transient heat transfer in pneumatic transport of granular particles. *Powder Technol*., **112**, 273.

Li, Y., Zhang, J. P. and Fan, L.-S. 2000 Discrete-phase simulation of single bubble rise behavior at elevated pressures in a bubble column. *Chem. Eng. Sci*., **55**, 4597.

Lun, C. C. K. 1996 Granular dynamics of slightly inelastic spheres in Couette flow. *Phys. Fluids*, **8**, 2868.

Lun, C. C. K., and Liu, H. S. 1997 Numerical simulation of dilute turbulent gas-solid flows in horizontal channels. *Int. J. Multiphase Flow*, **23**, 575.

Lun, C. C. K. 2000 Numerical simulation of dilute turbulent gas-solid flows. *Int. J. Multiphase flow*, **26,** 1707.

Marin, M., Risso, D. and Cordero, P. 1993 Efficient algorithms for many-body hard particle molecular dynamics. *J. Comput. Phys.* **109**, 306.

Mikami, T. 1998 Agglomeration fluidization of liquid/solid bridging particles an its control, *Ph.D Dissertation*, Tokyo University of Agriculture and Technology, Department of Chemical Engineering, Japan.

Mikami, T., Kamiya, H. and Horio, M. 1998 Numerical simulation of cohesive powder behavior in a fluidized bed. *Chem. Eng. Sci*., **53**, 1927.

Ouyang J., Li, J., van der Schaaf and van den Bleek, C. Discrete particle simulations of bubbling fluidization. *Fluidization X*, M. Kwauk, J. Li and W.-C. Yang, Eds., Engineering Foundation, Beijing (2001), p. 285.

Ouyang, J. and Li, J. 1999 Particle-motion-resolved discrete model for simulating gas-solid fluidization. *Chem. Eng. Sci.* **54**, 2077.

Patakar, N. A. and Joseph, D. D. 2001 Modeling and numerical simulation of particulate flows by the Eulerian-Lagrangian approach. *Int. J. Multiphase flow*, **27**, 1659.

Patakar, N. A. and Joseph, D. D. 2001 Lagrangian numerical simulation of particulate flows. *Int. J. Multiphase flow*, **27**, 1685.

Rhodes, M. J., Wang, X. S., Nguyen, M., Stewart, P. and Liffman, K. 2001 Onset of cohesive behavior in gas fluidized beds: a numerical study using DEM simulation. *Chem. Eng. Sci*., **56**, 4433.

Rhodes, M. J., Wang, X. S., Nguyen, M., Stewart, P. and Liffman, K. 2000 Use of discrete element method simulation in studying fluidization characteristics: influence of interparticle force. *Chem. Eng. Sci.*, **56,** 69.

Richardson, J. F. and Zaki, W. N. 1954 Sedimentation and fluidization: part I. *Trans. Inst. Chem. Eng*. **32**, 35.

Rong, D., Mikami, T. and Horio, M. 1999 Particle and bubble movements around tubes immersed in fluidized beds – a numerical study, *Chem. Eng. Sci*., **54**, 5737.

Schäfer, J., Dippel, S. and Wolf, D. E. 1996 Force schemes in simulations of granular materials. *J. Phys. I France*, **6**, 5.

Schwarzer, S. 1995 Sedimentation and flow through porous media: Simulating dynamically coupled discrete and continuum phase. *Phys. Rev. E.*, **52**, 6461.

Tsuji, Y., Kawaguchi, T. and Tanaka, T. 1993 Discrete particle simulation of two dimensional fluidized bed. *Powder Technol*., **77,** 79.

Walton, O. R. and Braun, R. L. 1986 Viscosity and temperature calculations for assemblies of inelastic frictional disks. *Journal of Rheology,* **30**, 949.

Wassen, E. and Frank, T. 2001 Simulation of cluster formation in gas-solid flow induced by particle-particle collisions. *Int. J. Multiphase Flow*, **27**, 437.

Wen, C. Y. and Yu, Y. H. 1966 Mechanics of fluidization. *Chem. Eng. Prog. Symp. Ser*. **62** (62), 100.

Xu, B. H. and Yu, A. B. 1997 Numerical simulation of the gas-solid flow in a fluidized bed by combining discrete particle method with computational fluid dynamics. *Chem. Eng. Sci*. **52**, 2785.

Zhang, J. P., Fan L. S., Zhu, C., Pfeffer, R. and Qi, D. W. 1999 Dynamic behavior of collision of elastic spheres in viscous fluids. *Powder Technol.*, **106**, 98.

Zhang, J. P., Li, Y. and Fan, L.-S. 2000 Discrete phase simulation of gas-liquid-solid fluidization systems: single bubble rising behavior. *Powder Technol*., **113**, 310.

Chapter 3

EFFECT OF COMPETITION BETWEEN PARTICLE-PARTICLE AND GAS-PARTICLE INTERACTIONS ON FLOW PATTERNS IN DENSE GAS-FLUIDIZED BEDS

Abstract

Particle-particle and particle-fluid interactions are two fundamental phenomena in dense particulate flows which interact mutually to compose a variety of flow structures. Discrete particle simulation offers the possibility to compute the energy budgets in dense particulate flows. From energy analysis we can obtain the energy distribution which forms a quantitative basis to understand the various behaviors in gas-particle flows and finally to establish the link between the micro-scale interactions and the macro-scale flow patterns. A simulated full picture of flow pattern formation and its evolution, along with the altering roles of particle–particle collision and particle-fluid interaction in their competition, in dense gas-fluidized beds is presented. Detailed energy analysis is used to explore how particle-particle collision and particle-fluid interaction drives flow pattern formation and transition.

It is shown that the flow structures in various flow regimes, ranging from the fixed to turbulent regimes, can be reproduced from these simulations! Systems with strong collisional dissipation but weak gas-particle interaction display a distinct emulsion-bubble two-phase structure. On the contrary, systems with strong gas-particle interaction but less pronounced collisional dissipation produce uniform structures, which are often observed in the uniform regime just above the incipient fluidization point. If these two interactions are equally important, the system features complex flow patterns (*dissipative structures*) *resembling those displayed in the turbulent fluidization regime.*

Energy analysis demonstrates that the competition between particle-particle collision and particle-fluid interaction determines flow structure formation and its evolution. The flow regime transition is actually the macro-scale expression of the altering of degree of dominance of particle-particle and particle-fluid interactions. It is also found that there exists

a pseudo-equilibrium point between bubbling-like regime and turbulent-like regimes where the flow structure is relatively uniform with respect to meso-scale.

1. Introduction

In gas-solid two-phase flows, particles are dispersed in a carrier gas typically in an inhomogeneous way, involving the presence of voids, bubbles (Rowe, 1971, Gilbertson, 1998) and/or particle clusters (Grace, et al., 1996; Horio, et al. 1994; Lackermeier et al. 2001). However, a complete theory for understanding pattern formation and regime transition is still not available although previous efforts based on continuum have shed some light on this issue (Jackson, 1963; Kuipers et al., 1992; Gidaspow, 1994).

From the micro-scale point of view, the way solids are dispersed in a carrier gas, is affected by three factors: 1) gas-phase flow structure (laminar or turbulent), 2) particle-particle interaction (collisions and inter-particle forces) and 3) gas-solid interaction. Quantitative understanding of these three phenomena in a specific regime, at the transition points and their evolution along the flow regime, would help us to establish a complete theory to predict gas-solid two-phase flow. With the development of discrete particle models, it is now possible to partially achieve this objective (Tsuji, et al., 1993; Hoomans et al., 1996). At low gas velocity, the turbulence influence of the carrier gas can be neglected. Therefore, the competition between particle collisions and particle-fluid interaction determines the flow structure of two-phase flows with respects to their formation and evolution. Promisingly, some recent work (Hoomans et al. 2000) demonstrated that particle-particle collisional properties (restitution and friction coefficient) play an important role in bubble and cluster formation in dense gas-solid flows of relatively large particles.

As a further step towards the goal, this work aims at a quantitative understanding of the way how particle-particle collision and particle-fluid interaction interact with each other to drive pattern-rich flow structures and furthermore promote regime transition.

To arrive at the aforementioned goal, first a two-dimensional flow structure map is produced by using discrete particle simulation. This map is designed as follows: along the horizontal coordinate the particle-fluid interaction is enhanced by increasing operating pressure while particle collisional dissipation gradually increases along the vertical coordinate by lowering the coefficient of restitution and increasing the coefficient of friction. The map gives an overview of what the flow structures look like and how they evolve as a result of the two basic interactions.

Energy budget analysis (Li and Kuipers, 2002), coupled with quantification of the flow structure, will then be performed for all the sub-cases indicated in the map, with particular attention to collisional dissipation and potential energy of the particle assembly. By examining the fractional component of dissipated energy along both coordinate directions, the role of particle-particle collision can be highlighted. With changing gas-solid interaction, the

system experiences regime transition and consequently the effect of the two micro-scale interactions on regime transition emerges as an additional result.

After the role of each type of interaction in the pattern formation processes is clear, it is possible to develop a mechanism-based criterion to distinguish the two types of flow structures: particulate and agglomerate. An attempt has been made to arrive at a suitable criterion as well.

2. Model and simulation

The governing equations and numerical solution procedure used on this study has been reported in chapter 2. The conditions and parameter values used for the simulations are listed in Table 3.1.

Table 3.1: Conditions and parameter values used for simulations on pattern formation in dense gas-fluidized beds.

Bed geometry (2-D)		
width (cm)		10
height (cm)		40 or 80
Particles		
diameter (mm)		0.949
density (k_g/m^3)		1170
number [-]		16,000
incipient fluidization velocity (m/s) and operating pressure (bar)		0.3010 (1 bar), 0.1486 (10), 0.1050 (21), 0.1010 (25), 0.0932 (30), 0.0868 (35), 0.0816 (40), 0.0734 (50).
Simulation		
grid		20×40 (or 80)
simulation time (s)		5 ~10
time step (s)		1×10^{-4}
update nblist (s)		2×10^{-4}
restitution coef.	normal (p-wall & p-p)	1.00 (ideal), 0.95, 0.90, 0.85, 0.80.
	tangential	0
friction coef.	normal (p-wall & p-p)	0.00 (ideal), 0.10, 0.20, 0.30, 0.40.
	tangential	0
Operating conditions		
superficial gas velocity (m/s) and operating pres0073ure (bar)		0.9020 (1 bar), 0.4458 (10), 0.3150 (21), 0.3030 (25), 0.2796 (30), 0.2604 (35), 0.2448 (40), 0.2200 (50)
static bed height (m)		0.15
porosity at incipient fluidization [-]		0.4
pressure (bar)		1, 10, 21, 25, 30, 35, 40, 50.

The properties of gas and solids are selected according to the material properties of ion exchange resin and nitrogen because for this system experimental data has been published (Gilbertson, 1998) However, since it is very time-consuming to simulate the flow behaviors in the real system, a small particle number and resulting bed geometry has been adopted in our study.

The incipient fluidization velocities listed are calculated according to the force balance principle based on Ergun equation. All simulations reported here have been run under the conditions of $3u_{mf}$, where it should be kept in mind that the minimum fluidization velocities vary with system pressure as listed in Table 3.1. This allows for the comparison of flow structures on the same base. Due to the considerable bed expansion in the turbulent regime, a higher bed geometry has also been employed.

3. Results and discussions

3.1 Competition between particle-particle and gas-particle interaction

The simulation results will first be presented in the form of snapshots and are summarized in Figure 3.1. In this map, gas-solid interaction is enhanced by increasing system pressure along the horizontal direction, whereas particle collisional dissipation increases in the vertical direction. The flow structure obtained for the ideal collision case is shown at the bottom. Note that all simulations have been carried out at $3u_{mf.}$

Clearly, increasing heterogeneity of the flow structures is observed in gas-fluidized beds with increasing particle collisional dissipation. Bigger bubbles and a denser emulsion occupy the bed space. However, this strong collision-induced impact on flow structure becomes less pronounced in case the gas-solid interaction is enhanced.

With increasing gas-solid interaction, the heterogeneity is gradually suppressed and a more homogenous flow pattern results. The gas pockets become smaller possessing an irregular shape. There is no clear-cut difference between the void and emulsion phase. Meanwhile, the solids volume fraction in the emulsion phase is smaller compared to the case of weak gas-solid interaction. It is also observed that the dense emulsion phase, constituting a continuous phase at low gas-solid interaction regime, gradually disperses into gas flow and finally becomes the dispersed phase. Particle clusters frequently appear in the bed, which is a typical picture found in turbulent fluidized beds (Bi et al., 2000).

When two systems are compared with different collisional properties (e = 0.9, μ = 0.2 and e = 1.0, μ = 0.0), one readily recognizes that particle collision has significant impact on flow regime transition. Apparently, a less dissipative system possesses a wider range of uniform regimes.

As a result, through adapting particle collisional dissipation and gas-particle interaction we reproduce flow structures, such as bubble/emulsion and cluster/dilute, and flow regime evolution, which have been widely observed in experimental studies. It is demonstrated that particle-particle collision and gas-particle interaction constitute two key issues phenomena determining pattern formation in dense gas-fluidized beds.

However, it is surprisingly found that there still exist heterogeneous flow structures in ideal collisional systems even though they are not so pronounced as those in non-ideal collisional systems. This differs from the finding of Hoomans (2000) that ideal collisional particle yields a perfect homogenous flow structure. Then, what causes such a heterogeneous flow structure?

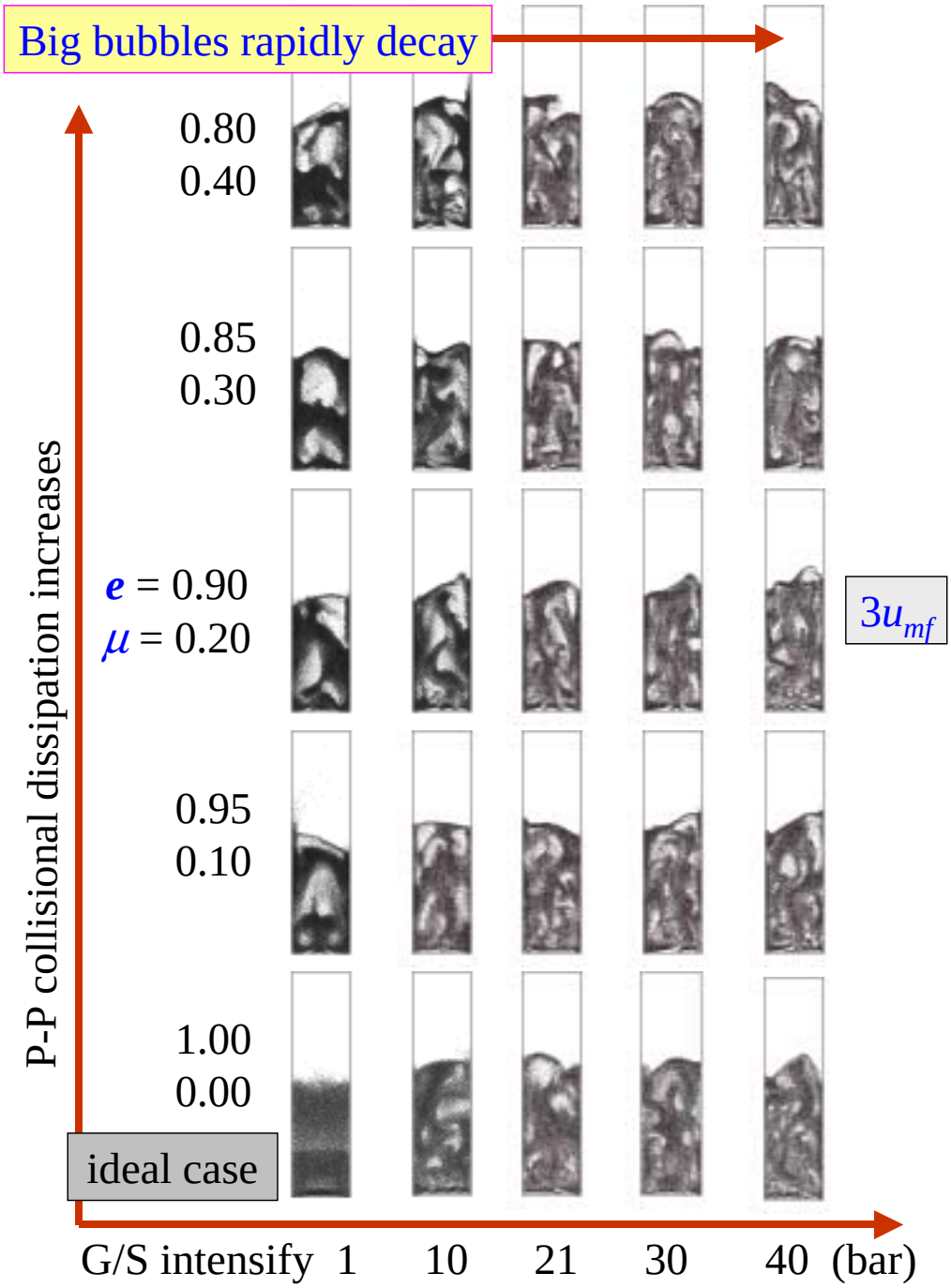

Figure 3.1: Effect of particle-particle collision and gas-particle interaction on flow patterns in dense gas-fluidized beds. *Enhanced collisional dissipation results in more heterogeneous flow structures while homogenous flows are produced with increasing gas-particle interaction.*

It is important to know why the aforementioned phenomena affect the flow structures and how they realize the pattern formation and evolution. Why is collisional dissipation influence stronger at 1 bar than that at 40 bars? To understand these findings, a more detailed analysis is required which will be presented subsequently.

3.2 Particle collisional dissipation induced heterogeneous flow structure

The particle collisional dissipation has a pronounced influence on flow structure and will be discussed in detail in this section with emphasis on flow structure, dynamic behavior and energy budget analysis.

The effect of the particle collisional dissipation on flow structure at 1 bar is shown again in Figure 3.2. From this figure, it can be seen that under otherwise identical conditions, particle collisional dissipation **only** can have such a great difference on flow structure. Especially at atmospheric conditions, the particle collisional dissipation does have an extremely great impact on pattern formation in dense gas-fluidized beds.

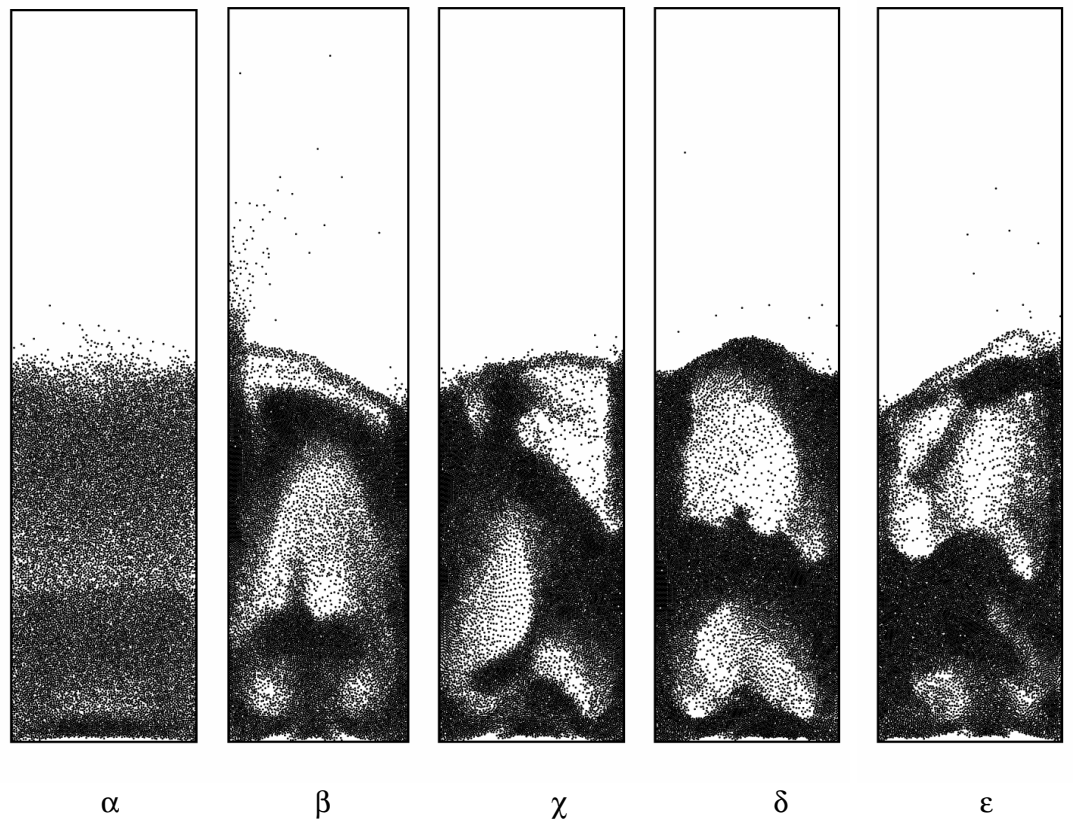

Figure 3.2: Flow patterns in gas-fluidized beds: *effect of particle collisional properties* (for all runs: d_p = 0.949 mm, ρ_p = 1170 kg/m^3; fluid: air, 1 bar, u = 0.903 m/s ($3u_{mf}$). Collisional properties: α: e = 1.00, μ = 0.0; β: e = 0.95, μ = 0.1; χ: e =0.90, μ = 0.2; δ: e = 0.85, μ = 0.3; ε: e = 0.80, μ = 0.4. Where e is restitution coefficient and μ is friction coefficient of the particles.

The pressure drop fluctuations, as shown in Figure 3.3, indicate that stronger particle dissipation leads to higher pressure oscillations occurring at higher frequency. This suggests that the heterogeneity of the system becomes more pronounced in both spatial and time

domains. The averaged pressure drop reasonably agree with particle buoyant weight. A slightly larger value is attributed to the wall friction.

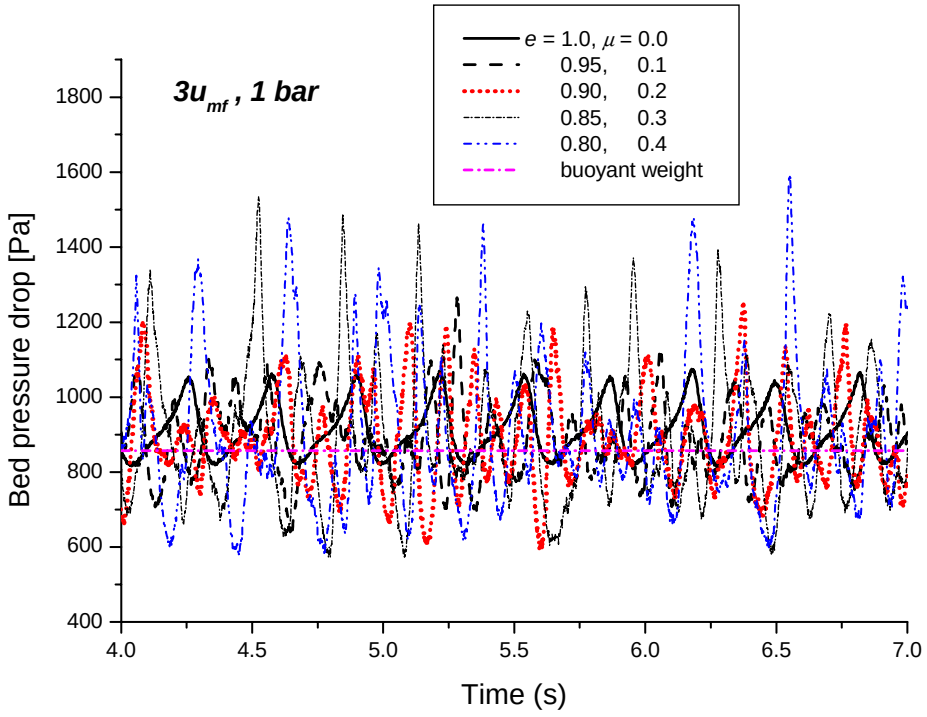

Figure 3.3: Pressure drop fluctuation in gas-fluidized beds at 1 bar: *effects of particle collisional dissipation.*

Figure 3.4 shows the results of energy budget analysis with respect to fractional energy dissipation in gas-fluidized beds. Clearly, once there exist dissipative particle collisions, a

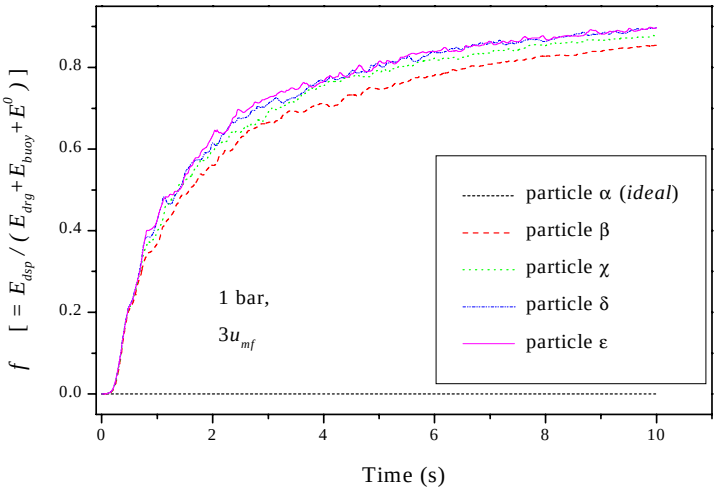

Figure 3.4: Energy budget analysis in gas-fluidized beds: *effect of inelastic and frictional dissipation.*(Collisional properties: α: e = 1.00, μ = 0.0; β: e = 0.95, μ = 0.1; χ: e =0.90, μ = 0.2; δ: e = 0.85, μ = 0.3; ε: e = 0.80, μ = 0.4. E_{dsp}, E_{drg} and E_{buoy} are dissipative energy, work due to drag and buoyancy forces respectively.

large portion of energy is consumed in the collisional process and therefore a limited portion of energy is available for particle suspension. As a result, the particles tend to fall down and heterogeneous flow structures form. The more energy is dissipated in collisions, the more pronounced the heterogeneity of the flow. However, it is interesting to find that this trend just holds for a certain range of collisional parameters (e = 0.85, μ = 0.3). Beyond the upper limit, the amplitude and frequency of pressure drop oscillations do not increase any more but remain constant.

Similar results are obtained for other cases with more pronounced gas-solid interaction (elevated system pressure). The flow structures are shown in Figure 3.1 and the energy analysis results are presented in Figure 3.5, from a to d for operating pressures of 10, 21, 30, 40 bar respectively. Clearly, as the gas-solid interaction is enhanced, the extent of collisional dissipation is significantly reduced. However, the influence still exists.

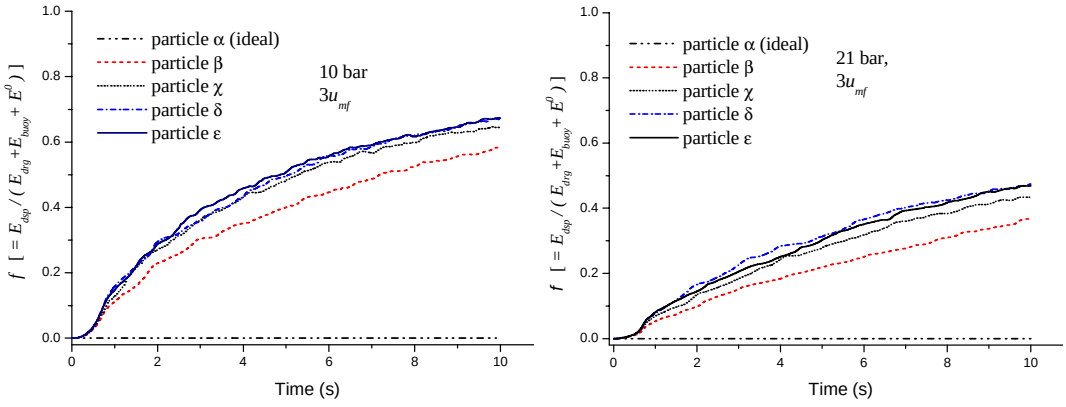

(a) 10 bar (b) 21 bar

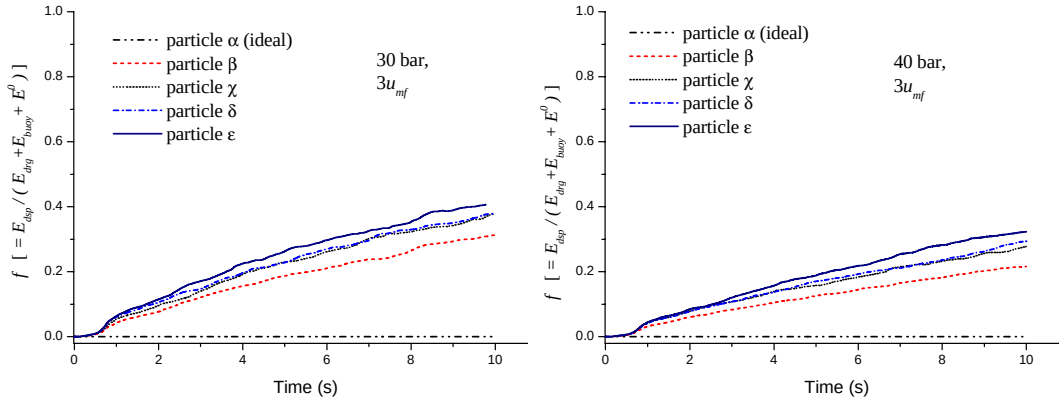

(c) 30 bar (d) 40 bar

Figure 3.5: Energy budget analysis at elevated pressure (i.e. enhanced gas-solid interactions) in dense gas-fluidized beds: *effect due to collisional and frictional dissipation.*

3.3 Particulate flows produced by intensified gas-solid interaction

The effect of gas-solid interaction on pattern formation is relatively complicated and is closely connected to flow regime transition. If systems are composed of particles with different collisional properties, they experience a different flow regime evolution. Therefore, it was decided to analyze these systems separately. In this study, two typical gas-particle systems are selected: an ideal system and a non-ideal system with restitution coefficient of 0.9 and friction coefficient of 0.2. The influence of gas-solid interaction will be studied on base of structure, dynamic behavior and energy analysis.

3.3.1 INFLUENCE OF GAS-SOLID INTERACTION ON PATTERN FORMATION IN NON-IDEAL COLLISION SYSTEM

3.3.1.1 Phenomena and internal structure

Four types of non-ideal collisional particles with same physical properties except the collisional properties, i.e. restitution coefficient and friction coefficient, were employed in the

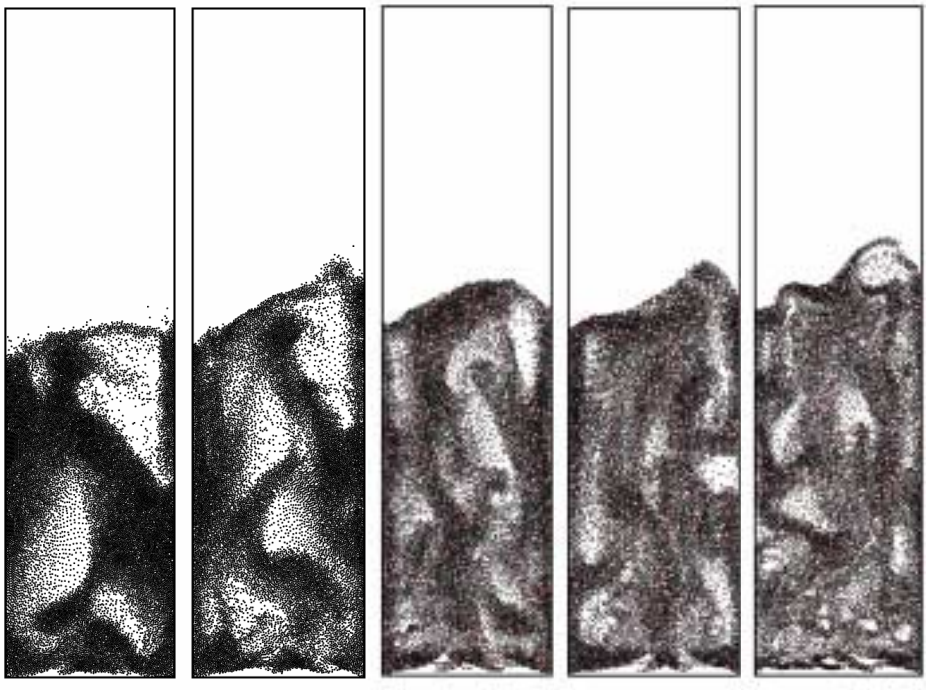

a b c d e

Figure 3.6: Flow patterns in gas-fluidized beds: *intensified gas-solid interaction leads to homogeneous flow structures.* (for all runs: d_p = 0.949 mm, ρ_p = 1170 kg/m^3; e = 0.90, μ = 0.2; fluid: air. Other conditions are for a: 1 bar, u = 0.902 m/s ($3u_{mf}$); for b: 10 bar, u = 0.4458 m/s ($3u_{mf}$); for c: 21 bar, u = 0.315 m/s ($3u_{mf}$); for d: 30 bar, u = 0.2796 m/s ($3u_{mf}$) and for e: 40 bar, u = 0.2448 m/s ($3u_{mf}$).

simulations. Table 3.1 lists all the parameter values. Figure 3.6 shows the snapshots obtained from five simulations using solids with restitution coefficient of 0.9 and friction coefficient of 0.2 operating at five system pressures and $3u_{mf}$.

From the results for non-ideal collision systems, the following phenomena can be discerned:

1) Non-ideal collision systems show a distinct *bubble/emulsion* two-phase structure.
2) Compared to those in the ideal collision systems, there are *less particles inside the bubbles*, whereas the emulsion phase is denser.
3) The more pronounced the non-ideality of the system, the stronger the heterogeneity of the flow.
4) There exist *extreme values* of the collision parameters, after which the heterogeneous flow structure does not significantly change any more.
5) Intensification of gas-solid interaction can remarkably suppress the heterogeneity. When it reaches a certain level, the system resembles the ideal-collision system.

Subsequently, the results of structure and energy analysis will be presented. In this analysis, the contributions from P-P interaction (e,μ) and F-P interaction (pressure) will be especially notified.

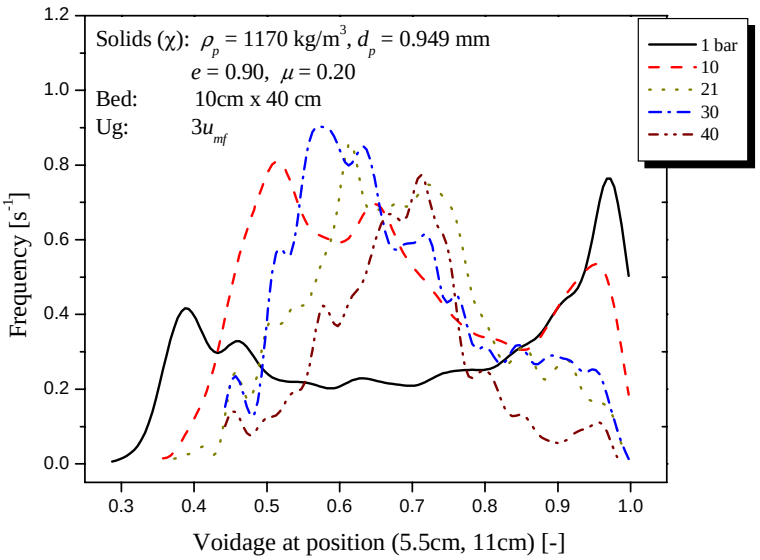

Figure 3.7: Frequency distribution of local void fraction in gas-fluidized beds as a function of system pressure: *Enhanced gas-solid interaction drives two-peak distribution into one peak distribution.*

Figure 3.7 displays the variation of the local voidage signals with system pressure (increasing gas-solid interaction) and Figure 3.8 presents the variation of bed pressure drop in the gas-

fluidized beds. Also, the original pressure-drop signals are shown in Figure 3.9 to highlight the dynamic behaviors in gas-fluidized beds.

At atmospheric conditions, the voidage frequency shows a two-peak distribution: appearing at two extreme ends (0.4, 1). With increasing gas-solid interaction, these two peaks move toward the center and merge to form a single peak distribution with peak shifting to the dilute side.

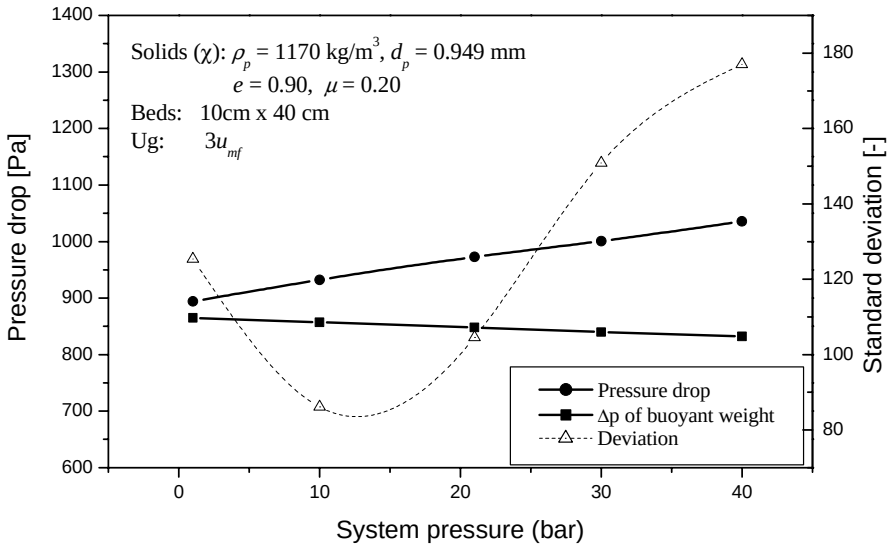

Figure 3.8: Variation of time-averaged pressure-drop and standard variation of pressure drop with system pressure.

Bed pressure drops are slightly larger than pressure drops due to bed buoyant weight and the difference increases with increasing system pressure. This indicates that the entire gas-particle interaction has been enhanced with respects to both gas suspension and drag since buoyant weight decreases, whereas the pressure drop increases. Although pressure drop due to the increasing gas density increases, the total increased quantity should include the contribution made by intensified gas-solids contacting. The traditional concept that bed pressure drop equals to buoyant weight is not applied in these cases anymore.

It is also found that the heterogeneity of the systems on the different scales evolves in an opposite direction. At low gas-solid interaction, the flow pattern displays as strong heterogeneous flow structure at macro-scale, as reflected by high amplitude and low frequency pressure signals in Figure 3.9, but a very homogenous flow structure at meso–scale with low amplitude and low frequency pressure signals (see 1 bar case). On the contrary, the flow pattern at the high gas-solid interaction shows a moderate and/or homogeneous flow structure at macro-scale but a very strong local or meso-scale heterogeneous structure. (see the pressure signals at 40 bar). At intermediate gas-solid interaction, heterogeneous structures exist on both scales (see the pressure signals at 10, 21 bar).

It should be noted here that an increasing standard deviation of the pressure drop does not automatically imply that the systems becomes more heterogeneous. The opposite evolutions of flow structures on the macroscopic and mesoscopic scales in Figure 3.9 could clearly appease this controversy. One should thus be careful, when one employs this type of criterion to evaluate the flow structure.

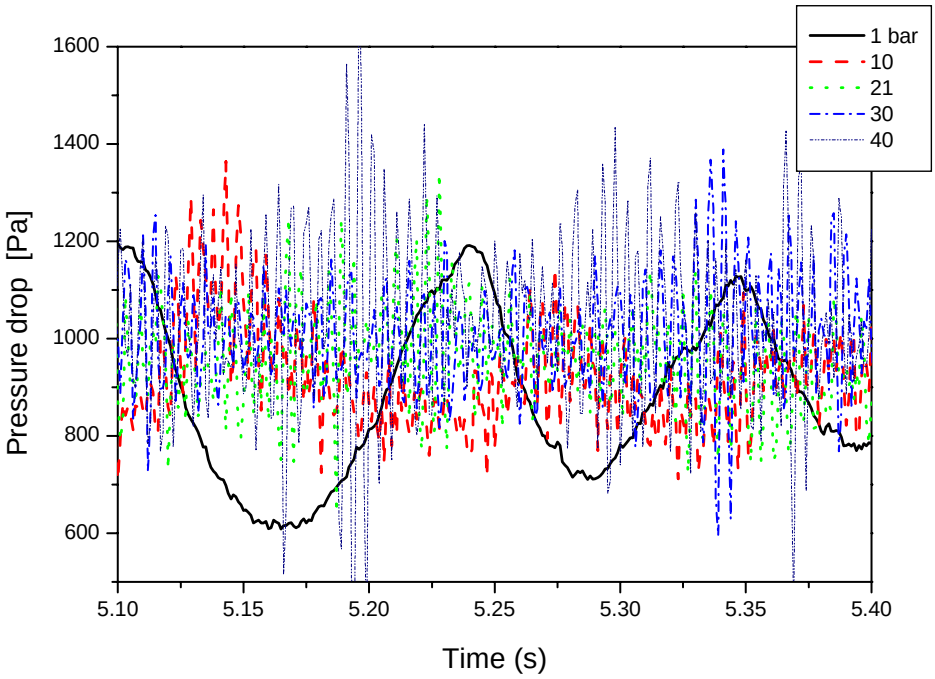

Figure 3.9: Pressure signals from gas-fluidized beds with non-ideal collision operated at $3u_{mf}$ and various system pressures. ($e = 0.90$, $\mu = 0.20$).

With increasing gas-solid interaction, the global heterogeneity is suppressed but local heterogeneity is promoted. Eventually, it leads to particulate fluidization.

3.3.1.2 Energy analysis

Various forms of energy and work performed by the gas are calculated during the simulations and the results are shown in Figure 3.10. The rotational energy is relatively small and is therefore not included. (note: the work due to pressure gradient is already included in the work due to drag force in Figure 3.10a). It can be seen that increasing gas-solid interaction raises the particulate potential energy but reduces the kinetic energy and collisional dissipation.

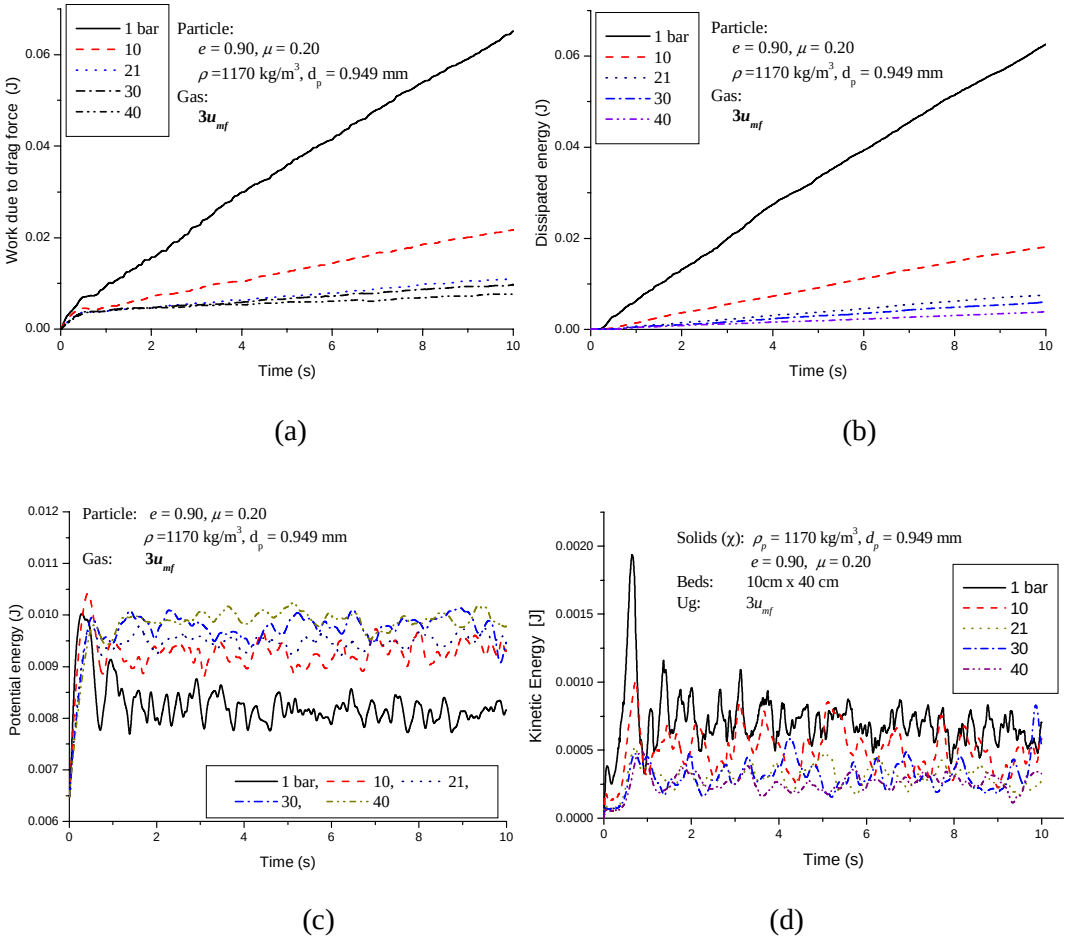

Figure 3.10: Various forms of energy and work performed by the gas: *gas-solid interaction effect.* Rotation energy is relative small and not showed here. *Increasing gas-solid interaction raises potential energy and reduces kinetic and collisional dissipation*.

This can be explained as follows: with increasing gas-solid interaction the average inter-particle distance increases and consequently the number of particle collision reduces. The system kinetic energy is reduced as well. However, the work due to drag is also decreased with increasing gas-solid interaction. To clarify and confirm the role of each action on the flow pattern one has to carry out energy budget analysis.

Figure 3.11 shows the energy budget analysis with respect to particle collisional dissipation. Obviously, a considerable portion of energy, up to eighty percent, is consumed during particle collisions at 1bar. This situation dramatically changes with increasing system pressure or gas-solid interaction. At 40 bar, only 30% of input energy is dissipated during collisions. On the contrary, the portion for energy used in particle suspension, as shown in Figure 3.12, is remarkably increased with increasing gas-solid interaction.

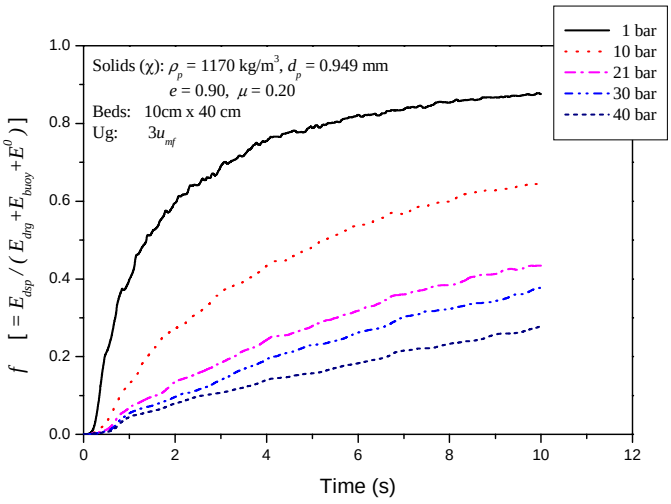

Figure 3.11: Energy budget analysis for collisional dissipation: *increasing gas-solid interaction greatly reduces the collisional dissipation.*

This demonstrates that intensification of gas-solid interaction does greatly suppress the energy dissipation and promotes particle suspension (i.e. increasing the potential energy).

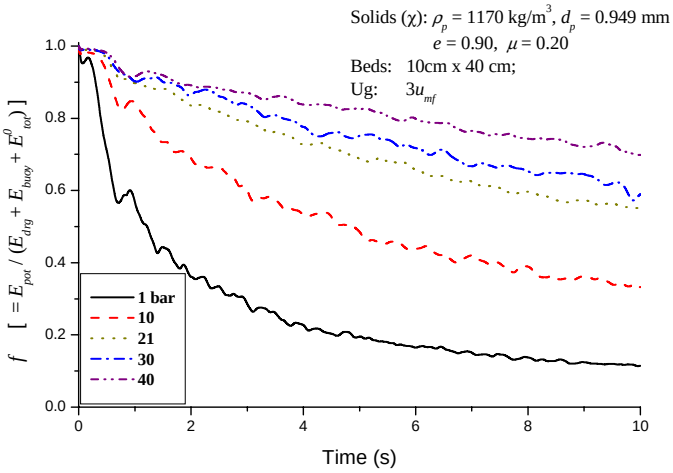

Figure 3.12: Energy budget analysis for particle suspension: *increasing gas-solid interaction efficiently enhances particle suspension.*

3.3.1.3 Regime transition

It is observed that in general kinetic energy tends to decrease with increasing system pressure. However, there exists a sub-extreme point at 21 bar at which kinetic energy is smaller than both 10 bar case and 30 bar case, indicating that the system is relatively stable under this condition. Since particle movement is also closely linked to the granular temperature in the bed, this feature should also be reflected in this quantity. Figure 3.13 shows the global

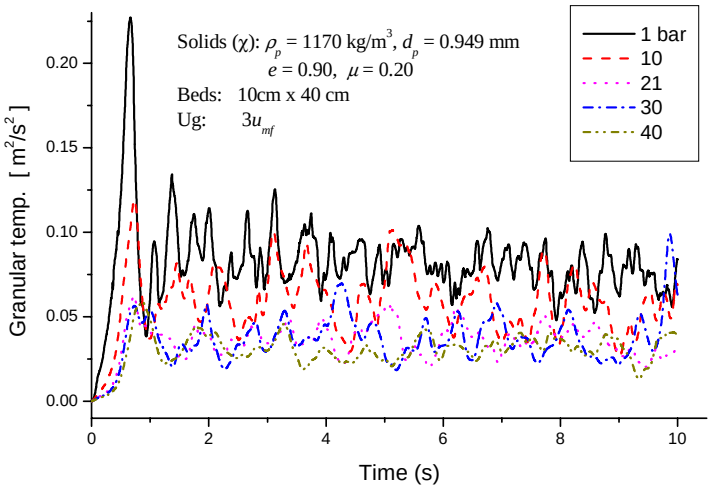

Figure 3.13: Granular temperature in gas-fluidized beds: *increasing gas-solid interaction effect.*

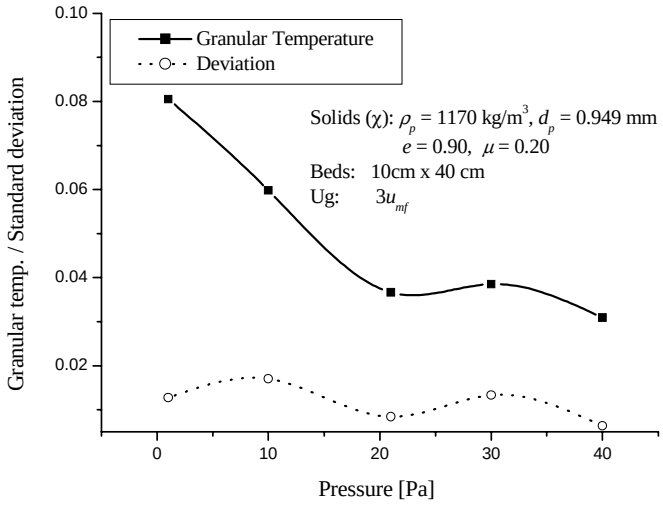

Figure 3.14: Re-plotting of granular temperature in gas-fluidized beds: *increasing gas-solid interaction pressure influence. There exists a transition point at 21 bar.*

granular temperature as a function of time during the simulations. In Figure 3.14 the time-averaged granular temperature is shown as a function of pressure (i. e. increasing gas-particle

interaction). The decrease at 21 bar can be clearly observed. This finding suggests that this point coincides with the transition point from bubbling flow to turbulent flow.

Keeping in mind the opposite trends for macro-scale and meso-scale heterogeneities, as clarified previously, we can explain this transition as follows: increasing gas-solid interaction gradually splits the two-phase macro-scale heterogeneous structure into multiple voids. Although the macro-scale heterogeneity decreases, local heterogeneity in meso-scale, or the cluster scale, is intensified due to the inter-cluster encounters. The competition between these two processes leads to an extreme point, where clusters are small enough to avoid the strong macro-scale interaction. Meanwhile, the cluster interaction is at a moderate level without introducing the strong meso-scale fluctuation.

Figure 3.15 shows the variation of bed mass center with elevated system pressure. Obviously, the enhanced gas-solid interaction leads to an increased bed expansion.

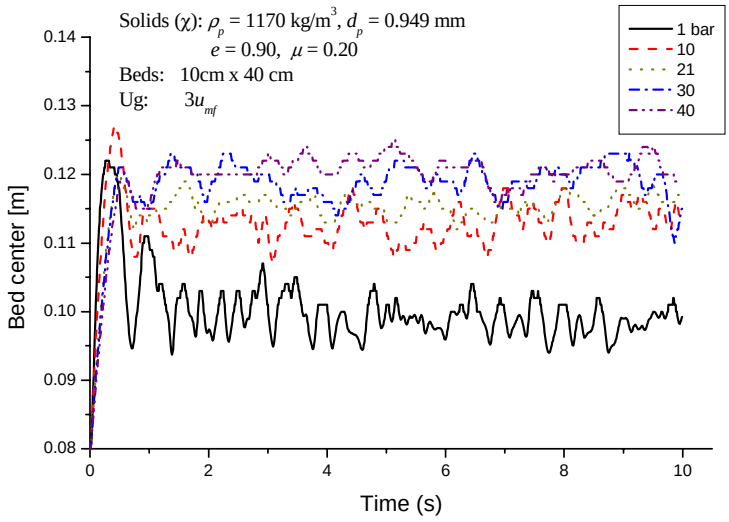

Figure 3.15: Variation of bed center with system pressure: *increasing gas-solid interaction leads to well particle suspension.*

Until now, we have discussed the flow structure formation for one of the non-ideal collisional particles. The detailed energy analyses and characterizations for another three types of non-ideal collisional particles are summarized in Appendix 1. Similar results were obtained for all these cases.

3.3.2 INFLUENCE OF GAS-SOLID INTERACTION ON PATTERN FORMATION IN AN IDEAL COLLISION SYSTEM

When composing the regime map, it is interesting to observe that the non-homogeneous flow structures still exist in ideal-collision systems such as the case of 1 bar in Figure 3.1. This is unexpected behavior because no energy is dissipated during the collision process at all. Then, how is this heterogeneous flow structure formed and what controls this pattern formation? It is therefore definitely interesting to explore the mechanism underlying this pattern formation since it will indicate the fundamental "root", which initializes the heterogeneous flow structure formation. In addition, it guides us to target a correct criterion to predict such a behavior.

3.3.2.1 Observation of the heterogeneous structure formation

Careful observation of the flow structures in a gas-fluidized bed with the ideal collisional particles manifests the following phenomena, with respect to the heterogeneous flow structure formation.

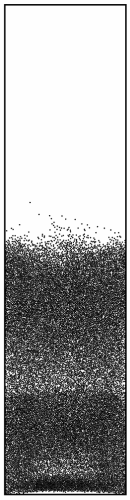

Figure 3.16: Flow structure in a gas-fluidized bed with ideal collisional particles at 1 bar.

I. Voids do not form immediately at the gas distributor but a few centimeters above it. ***Immediately near the distributor there exists a denser layer of particles*** (see Figure 3.16). This behavior always holds during the simulation process.

II. After the void appears, it rises. Meanwhile, the particles pass through the void and fall down onto the dense layer. This phenomenon has been observed in both the plug regime and the bubbling regime. Also this ***particle penetration phenomenon*** has more frequently been found in the fluidized beds with ideal collisions compared to systems with non-ideal collision particles.

III. Compared to the bed structure in the systems with non-ideal particles, more ***loose local structures***, in both the void phase and the emulsion phase, are observed in the gas-fluidized beds with ideal particles.

IV. ***Macro-scale non-uniform structures*** (convection) still exist.

3.3.2.2 Effect on flow structure

The evolution of flow structure with increasing gas-solid interaction for ideal particles is shown in Figure 3.17. A comparison of these flow structures with those for non-ideal particles

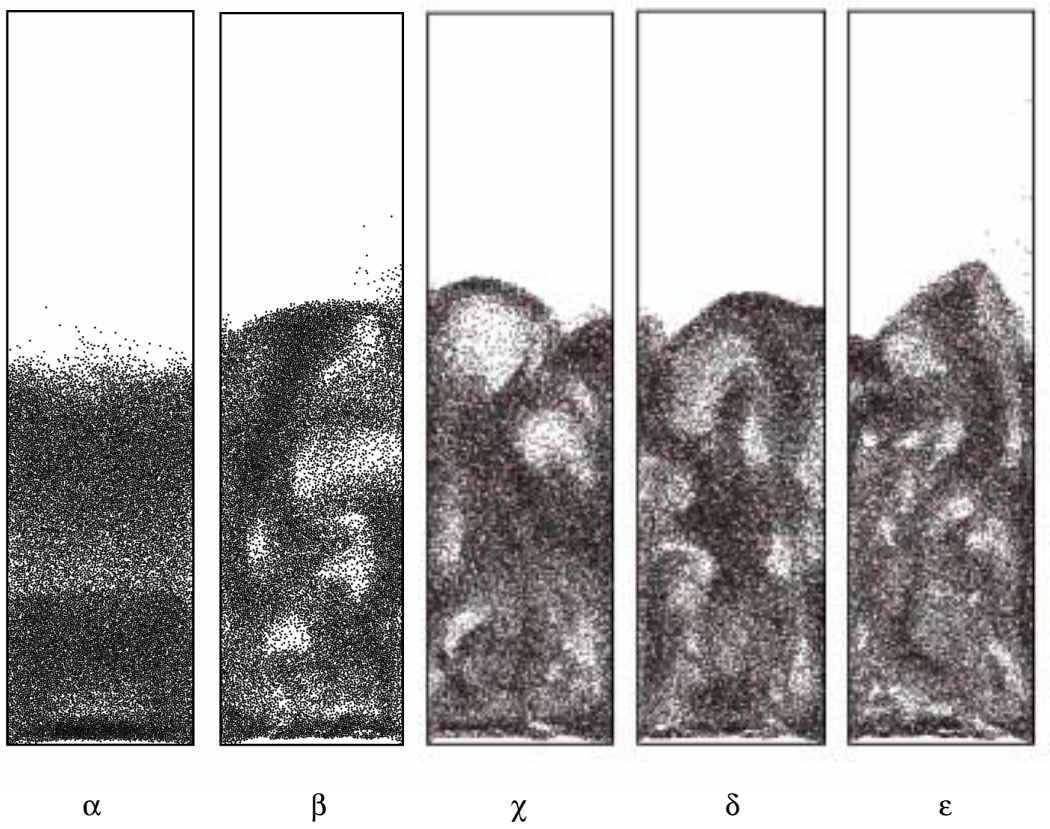

Figure 3.17: Flow patterns in gas-fluidized beds: *effect of elevated pressures* (for all runs: d_p = 0.949 mm, ρ_p = 1170 kg/m^3; e = 1.00, μ = 0.0 (ideal collisions); fluid: air. Where e is restitution coefficient and μ is friction coefficient of the particles. Other conditions are: α: 1 bar, u = 0.902 m/s ($3u_{mf}$); β: 10 bar, u = 0.4458 m/s ($3u_{mf}$); χ: 21 bar, u = 0.315 m/s ($3u_{mf}$); δ: 30 bar, u = 0.2796 m/s ($3u_{mf}$); ε: 40 bar, u = 0.2448 m/s ($3u_{mf}$).

reveals a different trend in evolution, which shows that the heterogeneity first increases and then gradually decreases. However, this conclusion is speculative because the comparison of the flow structure at 1 bar to others indicates that heterogeneity at 1 bar is more serious than that for the elevated pressure cases if it is evaluated from macro-scale point of view. It is interesting to explore this issue since it closely is linked to the controversy concerned with the variation of the bubble size with increasing system pressure. Some studies indicated a continuous decrease in bubble size with (Varada and Grace, 1978) whereas in other studies (Rowe et al., 1984; Hoffman and Yates, 1985; Olowson and Almsteddt, 1990) it is found that the bubble size first increases and then decreases with an increasing system pressure. In order

to fully clarify this structure evolution, detailed quantifications are needed which are described subsequently.

- **Information from global (bed scale) pressure signals**

Dynamic pressure drop signals were calculated during the simulations and the results are shown in Figures 3.18 and 3.19.

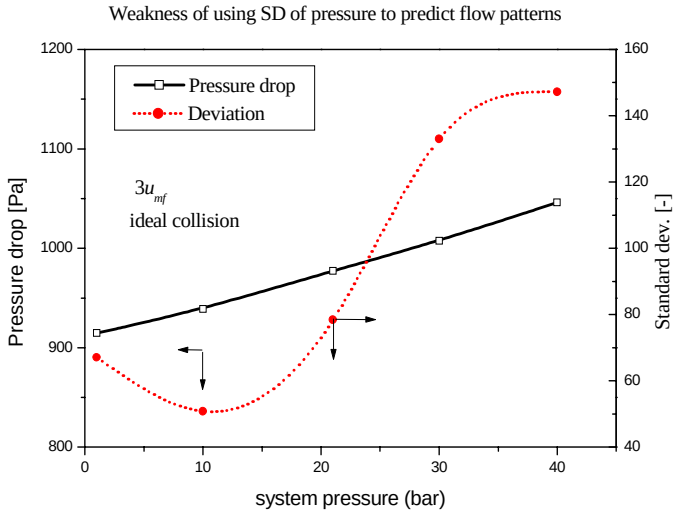

Figure 3.18: Variation of the time-averaged pressure-drop and standard deviations with increasing system pressure.

On **macro-scale**, the amplitude of the pressure oscillation decreases but its frequency increases in the order of 1) 1 bar, 2) 10 bar, 3) 21 bar, 4) 30 bar, and 40 bar. On **micro-scale**,

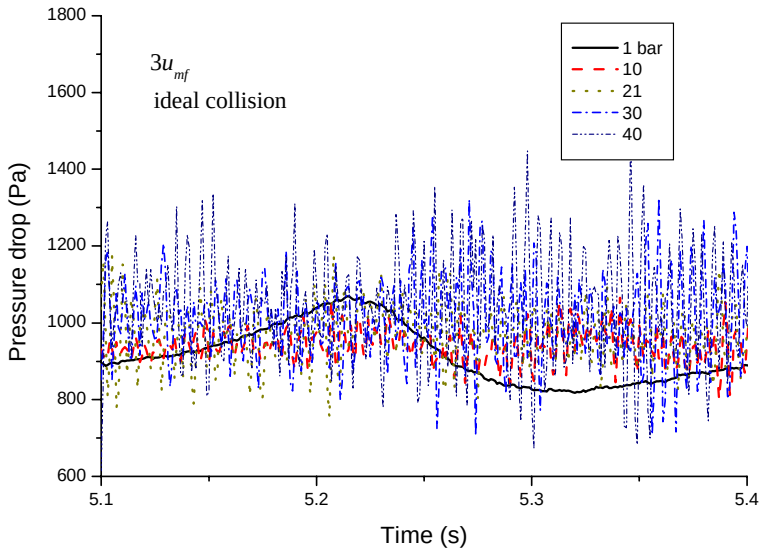

Figure 3.19: Pressure drop signals in gas-fluidized beds operating at increasing system pressure. *Increasing gas-solid interaction suppresses macro-scale heterogeneity but promotes meso-scale heterogeneity.*

the amplitude of the pressure oscillation, on the contrary, increases with increasing system pressure. Also the frequency of the oscillation increases. These findings indicate that the number of local heterogeneous structures increases where each center dissipates more energy. Therefore, elevated pressure suppresses the global heterogeneity in flow structures both in space and time domains leading to global homogeneous flow structure. However, local heterogeneity in the space and time domains increases. As a result of these opposing trends, finally regime transition prevails.

However, it should be noted that the intensity of macro-scale heterogeneity in systems with ideal particles is much less than that for the systems with non-ideal particles.

- **Information from local voidage signals**

Global pressure signals only display overall dynamic properties of the bed. Time series of local voidage however display the local uniformity of the flow structures. Figure 3.20 presents the frequency distribution of local void fraction at a position of 5.5 cm in the horizontal direction and 11 cm in the vertical direction.

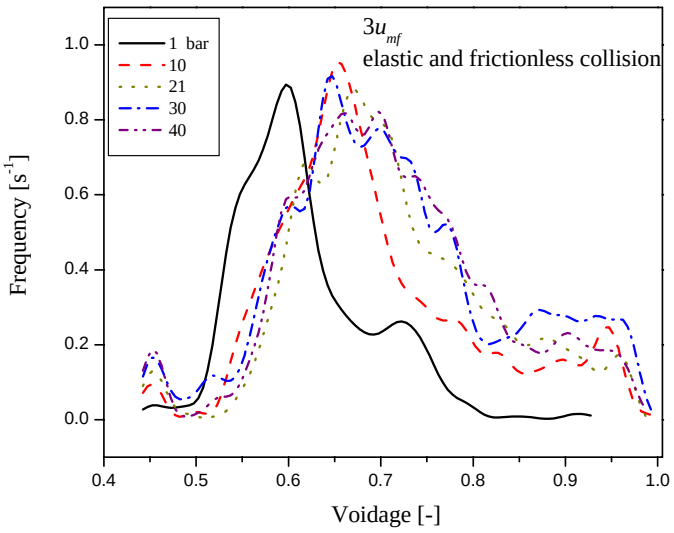

Figure 3.20: Frequency distribution of voidage at position of [5.5 cm, 11 cm] in a gas-fluidized bed with ideal collision particles operating at different system pressures.

Figure 3.20 shows that i) elevated pressure destroys the two-peak distribution and tends to produce globally more uniform systems (peak shifting to the dilute region, half-peak widens). ii) The portions of the two extreme void fractions, however, increase, that is, the occurrence of dense clusters and voids becomes more pronounced. Note that there are virtually no clear voids in the system operating at 1 bar (voidage larger than 0.94). Once again, this demonstrates that increasing gas-solid interaction suppresses global heterogeneity but promotes local heterogeneous flow structure formation.

- **Information from granular temperature**

Granular temperature evolutions are presented in Figure 3.21. The left figure shows the temporal evolution of the granular temperature at a number of system pressures whereas the right figure shows the time-averaged granular temperature as a function of system pressure.

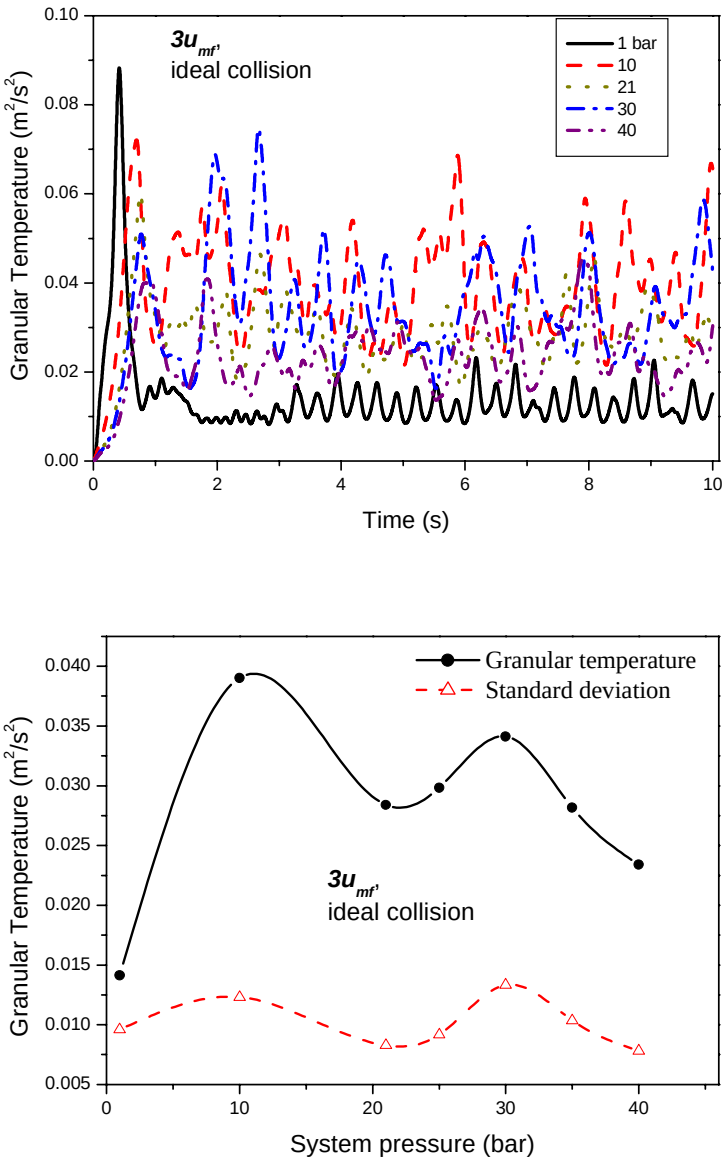

Figure 3.21: Variation of granular temperature with increasing gas-solid interaction in a gas-fluidized bed with ideal collisional particles: (upper) time series, (down) system pressure influence. (in figure b, two more points are added).

According to this characterization, the results indicate that the flow structure at 1 bar is indeed more homogeneous in the sense of the particle collisional interaction even though it is more heterogeneous from macro-scale point of view. Since a local homogeneous structure for ideal

particles avoids occurrence of collisions, it results in a more homogeneous pattern in the sense of spatial particle distribution.

Particularly, it is surprising to observe that there exists a local minimum in the time-averaged granular temperature at 21 bar. This indicates that the system remains in a relative equilibrium state. Taking into account the opposite development of macro- and meso-scale heterogeneities as reflected from the pressure signals, we speculate that this point is the transition point from bubbling flow to turbulent flow.

To fully prove such a speculation, we need to perform energy analysis which will be reported subsequently.

3.3.2.3 Mechanism controlling the pattern evolution

---- Energy budget analysis

From the results presented above, it has become clear that there do exist heterogeneous flow structures in ideal-collisional systems. This heterogeneity develops with increasing gas-solid interaction. During particle collisions energy is not dissipated but re-distributes among the particles. Therefore, other mechanisms cause the pattern formation.

As for the ideal-collision system, there is no rotational energy available because particle friction is absent. The only relevant contributions to the energy balance originate from work done due to drag (including buoyancy) and potential and kinetic energy of the particle assembly. In Figure 3.22 theses contributions are shown as a function of time for different system pressures. Different from the non-ideal collision case, work due to drag increases with enhanced gas-solid interaction. Particle potential energy is increased as well, but not so pronounced. More attention, however, should be paid to the variation of kinetic energy with increasing gas-solid interaction: First, it increases and subsequently it decreases. A similar behavior was found for the granular temperature (see Figure 3.21).

In Figure 3.23 the results of energy budget analysis are presented. At the two extreme pressures (1 bar and 40 bar) the portion of energy distributed to kinetic energy is small indicating that less portion of energy is employed for motion and more for particle suspension. We have already seen that these two extremes correspond to relative uniform flow structures. Therefore, we can conclude that the systems in which a lower portion of energy is attributed to kinetic energy, or strictly speaking the fluctuation movement, tend to produce the homogeneous flow structures. In other words, if a larger portion of energy is employed to raise potential energy, the system more easily forms a homogeneous flow structure.

Very surprisingly, energy budget analysis also manifests a low limit-value point at 21 bar, indicating that a near-equilibrium system (less energy using for motion) exists in this circumstance.

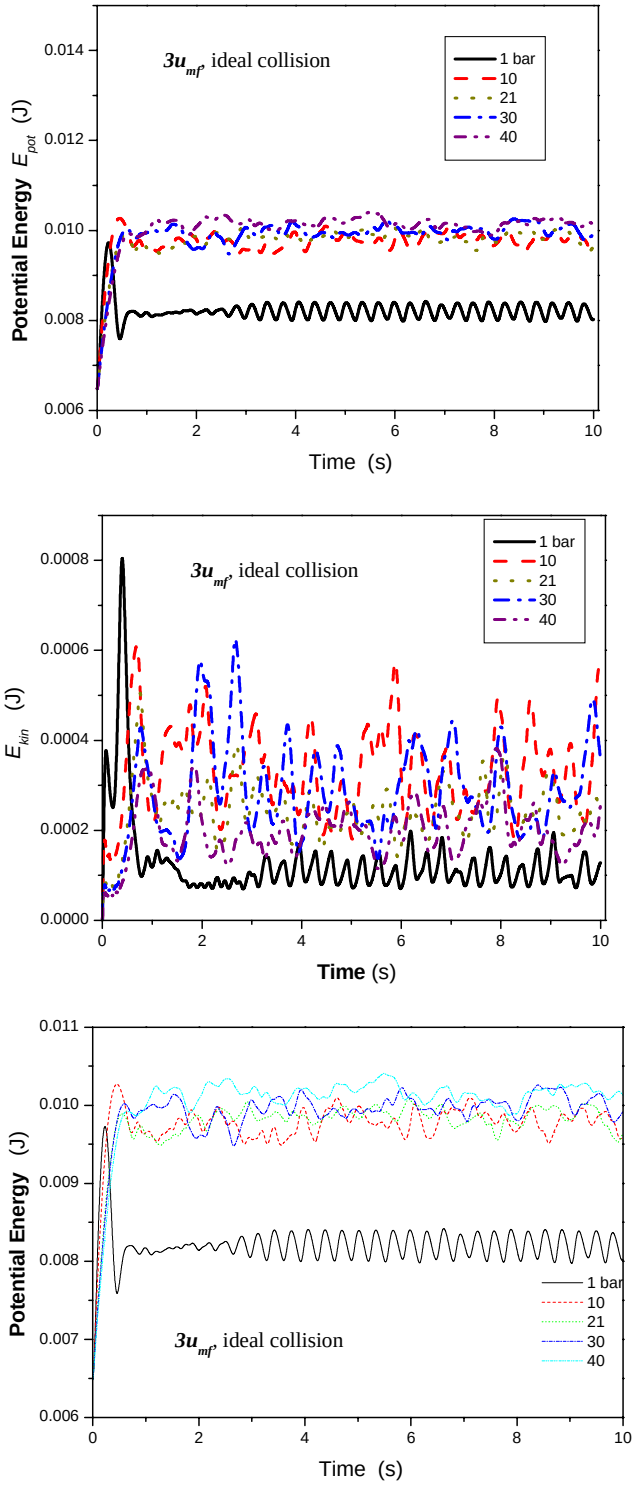

Figure 3.22: Potential (top), kinetic energy (middle), and work due to drag (bottom) in gas-fluidized beds with ideal collisonal particles (no dissipation and rotational energies in ideal collision systems): -*increasing gas-solid interaction effects.*

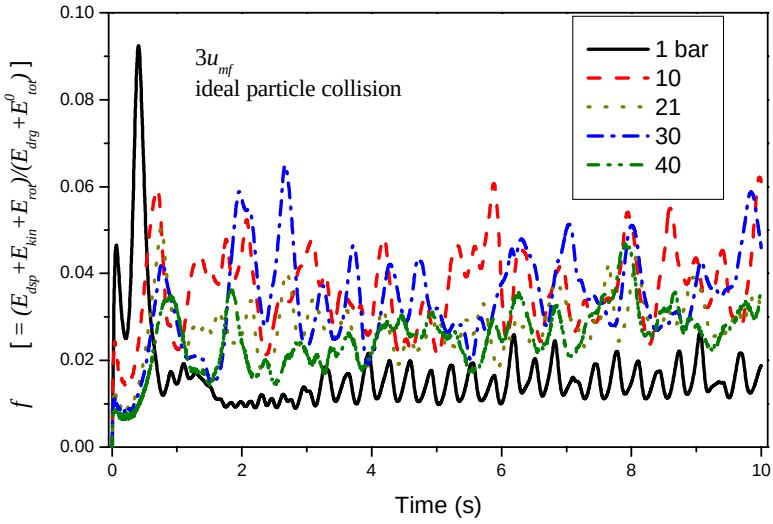

(a)

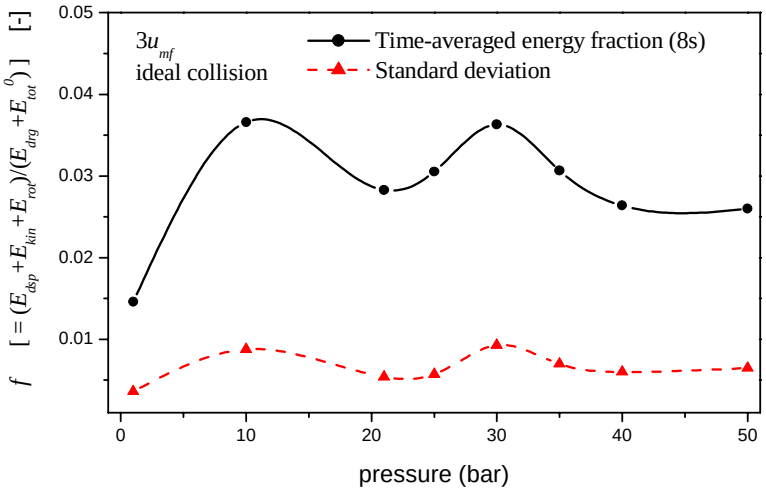

(b)

Figure 3.23: Variation of kinetic energy fraction with increasing gas-solid interaction in gas-fluidized beds of ideal collision particles (here dissipative and rotational energies are zero) (a): time series, (b) time-averaged kinetic energy fraction.

3.3.2.4 Regime transition

To further explore the nature of the regime transition, reconstruction of the computed flow structures has been carried out. The original snapshots of the flow structures were filtered and the results are shown in Figure 3.24.

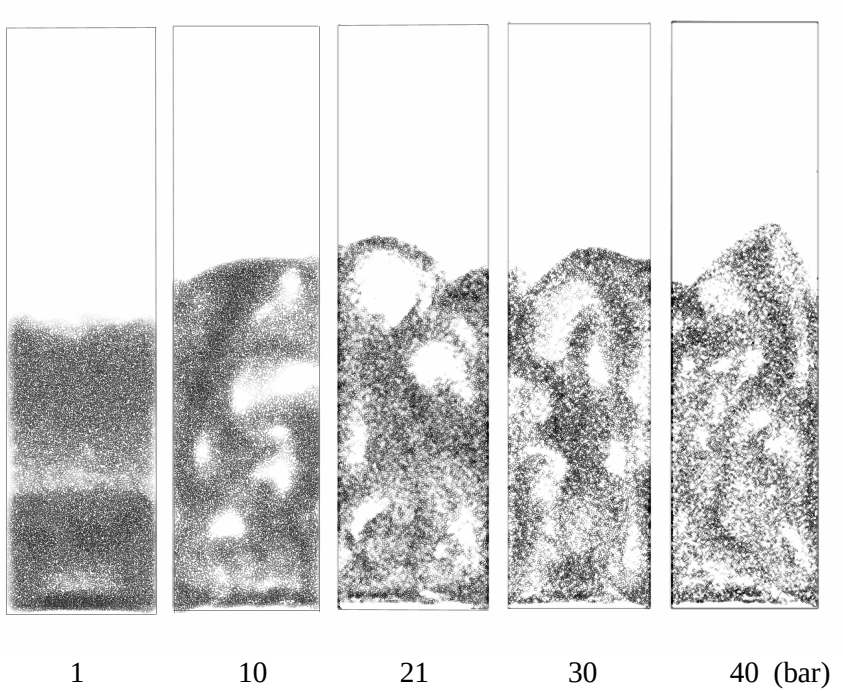

Figure 3.24: Reconstructed flow structures in a gas-fluidized bed with ideal collisional particles, *the increasing gas*-solid *interaction effect* (*smooth: 3 pixels; threshold level: 220*).

By carefully examining the flow structure at 21 bar (the middle one), we can observe that the gas pockets start to connect to each other to form a network. Before the formation of this structure, bubbles are dispersed in the emulsion, thereafter clusters become the dispersed phase. If we view this flow structure from the meso-scale, or in other words, take the cluster as a "macro particle", the system would display also a uniform structure constituting of two components: gas pockets and solid clusters. We might take this structure as a meso-scale uniform structure.

By combing the previous observations with respect to 1) flow structure, 2) dynamic behavior and 3) equilibrium property, we can conclude that this structure represents a "transition state" at which a solid controlling system (particle collision dominant) transfers to a fluid controlling system (gas-solid interaction dominant). Before this point, the dense emulsion phase prevails in the beds and bubbles appear in an isolated manner. At this point dense clusters/voids balances to form an intermediate structure. Thereafter, the dilute phase prevails in the system as a continuous phase and its fraction increases. Particularly, this point corresponds to the transition from the bubbling regime (solid partially control) to turbulent fluidization (fluid partially controlled regime).

3.4 Quantification of flow structures in dense gas-solid flows

By using energy budget analysis we have understood that competition between particle collisional dissipation, coupling the random motion, and particle suspension determines the flow structure formation and evolution. If more energy is distributed to particle random motion and/or dissipation (rotation, inelastic collision), the system tends to form heterogeneous flows. On the contrary, if more portion of energy is distributed to suspending the particles (raising potential energy) a uniform flow structure is easily formed. Accordingly, it should be possible to establish a criterion from energy point of view to distinguish the flow patterns in dense gas-fluidized beds. An attempt will be made along this direction subsequently.

3.4.1 DEFINITION OF THE CRITERION

According to energy budget analysis, the criterion can be defined, in general, as follows:

$$Fr = \frac{E_{dsp} + \Delta E_{kin} + \Delta E_{rot}}{\Delta E_{pot}}. \tag{3.1}$$

Since kinetic energy can be decomposed into two parts: one is for convection and the other is for particle fluctuation motion, that is:

$$E_{kin} = E_{conv} + E_{gran} \ . \tag{3.2}$$

where

$$E_{kin} = \sum_{1}^{Npart} \tfrac{1}{2} m_p v_p^2 . \tag{3.3}$$

$$E_{conv} = \sum_{k}^{Ncell} N_{part,k} \tfrac{1}{2} m_p < \bar{v}_p^2 > . \tag{3.4}$$

$$E_{gran} = \sum_{k}^{Ncell} N_{part,k} \tfrac{3}{2} m_p \theta_k . \tag{3.5}$$

θ_k is the granular temperature in the k^{th} computational cell. Since only the fluctuation portion of motion responds to the flow pattern formation in fluidized beds equation 1 can be simplified as follows:

$$Fr = \frac{E_{dsp} + \Delta E_{gran} + \Delta E_{rot}}{E_{pot} - E_{pot}^0}. \tag{3.6}$$

For ideal collision systems, the dissipative and rotational terms equal zero and can be omitted.

Considering that both particle collisional and rotational energies depend on the particle fluctuating motion, one could characterize the flow structure by simply using Equation (3.7) as follows:

$$Fr = \frac{E_{gran}}{E_{pot}} \equiv \frac{\theta}{g \cdot < h >} . \qquad (3.7)$$

Where, θ is the global granular temperature and <*h*> denotes the bed mass center, which is calculated by:

$$< h >= \frac{\sum_{j=1}^{N_{part}} h_j}{N_{part}} . \qquad (3.8)$$

The physical meaning of this Froude number denotes the ratio of intensities of randomness to order. For the system in which particles are uniformly suspended, fluctuating motion is significantly suppressed and most of energy is used to increase particle potential energy, Froude number approaches to zero. On the contrary, for the systems with strong heterogeneous flow structure, most portion of energy is distributed to fluctuating motion and, thereof the collisional dissipation, and less portion to particle suspension, Froude number increases. The larger *Fr* value the more heterogeneous the flow structure develops.

3.4.2 QUANTIFICATION OF FLOW STRUCTURES

Figure 3.25 shows Froude number, calculated by equation 6, as a function of system pressure (gas-solid interaction) in a gas-fluidized bed with ideal particle collision. The prediction based on equation 7 is shown in Figure 3.26 as well. In these Figures, extra data points obtained from simulations at 25, 35 and 50 bar are included.

By comparing the evolution of flow structures and energy analysis with respect to kinetic energy (Figure 3.23b), we can conclude that above quantifications provide reasonable good predictions for the flow structure.

For systems with non-ideal collisions, quantification of flow structures is presented in Figure 3.27. Once again, it can reasonably well predict the flow structure and its evolution. Figure 3.28 presents a full map to quantitatively characterize the competition between particle collision and gas-solid interaction induced flow patterns.

With reference to the flow structure, Froude number of 0.03 could be a possible criterion to distinguish the agglomerate flow from particulate flow, however, further work is needed to demonstrate the validity of this criterion.

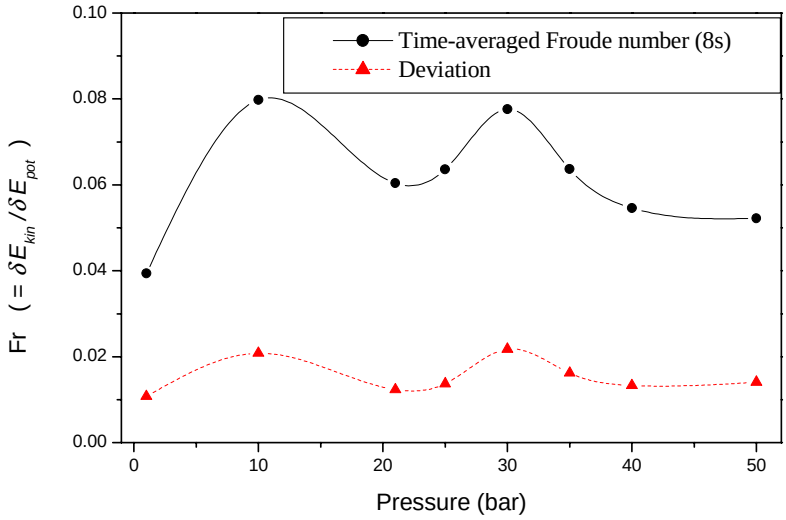

Figure 3.25: Quantification of flow structures in a gas-fluidized bed with ideal collisonal particles by using Froude number defined by equation 6, *effect of increasing gas-solid interaction.*

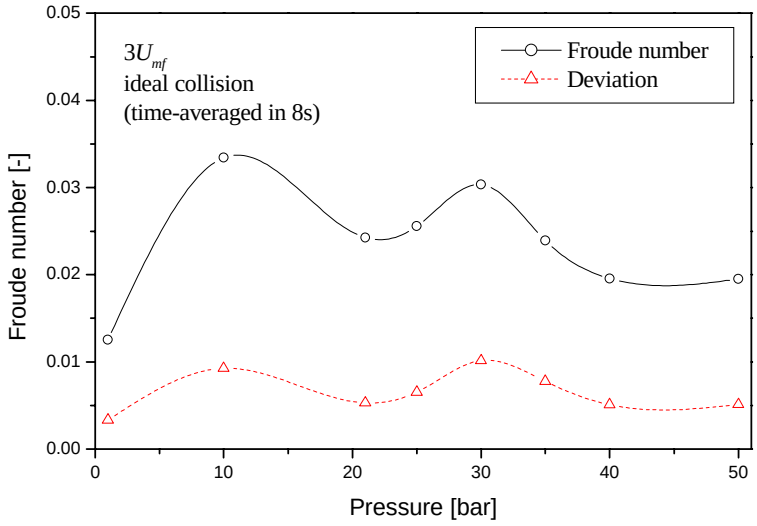

Figure 3.26: Quantification of flow structures in a gas-fluidized bed with ideal collisonal particles by using Froude number defined by equation 7, *effect of increasing gas-solid interaction.*

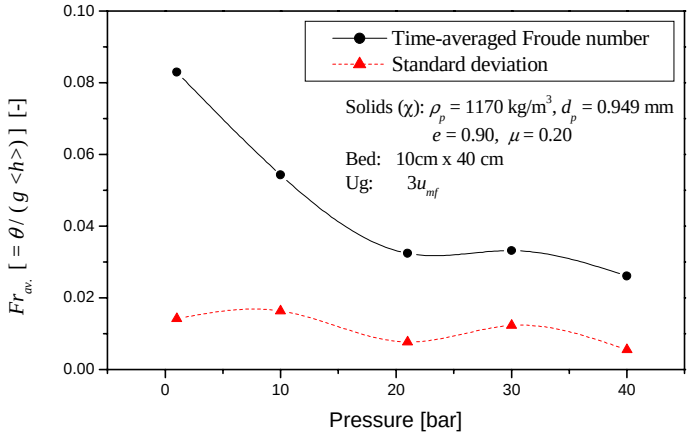

Figure 3.27: Quantification of flow structures in a gas-fluidized bed with non-ideal collisonal particles by using Froude number defined by equation 7, *effect of increasing gas-solid interaction.*

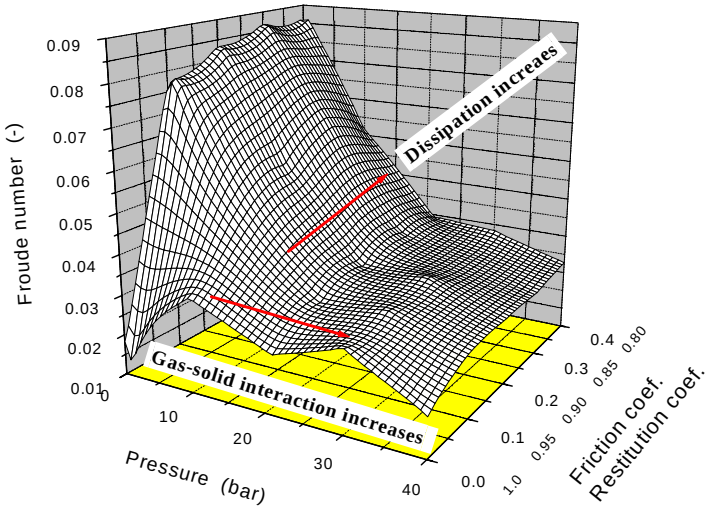

Figure 3.28: Quantification of flow structures: *effects of particle-particle collision and gas-solid interaction.*

4. Conclusions

Using the discrete particle method, the fundamentals underlying flow structure formation and evolution in dense gas-fluidized beds has been studied. The roles of particle-particle collision and gas-solid interaction have been analyzed. The following conclusions can be drawn:

1) Competition between particle-particle collision and gas-solid interaction determines the flow structure formation. Systems dominated by particle dissipative collision tend to form agglomerate flow. On the contrary systems dominated by gas-solid interaction, tend to produce particulate flow.
2) With increasing gas-solid interaction, the heterogeneity of the flow structure evolves in a different way and depends on particle collisional dissipation. For ideal collision systems, it first increases and then decreases. However, it always decreases in non-ideal collision systems;
3) Increasing gas-solid interaction suppresses macro-scale heterogeneity, but intensifies meso-scale heterogeneity. A balance between particle collision and gas suspension results in a pseudo-stable intermediate flow structure where gas pockets connect to each other to form a gas path network. After this point, the gas-solid interaction dominates the system. In the ideal-collision system, there exist not only the homogeneous flow pattern but also the heterogeneous flow pattern. This heterogeneity is closely linked to particle fluctuation motion.
4) It is demonstrated that flow structure is closely related to system energy budget distribution: if more portion energy is distributed to collisional dissipation and/or fluctuation motion, it results in a heterogeneous flow structure. Otherwise, the homogeneous flow structure prevails in the system.

References

Bi, H. T., Ellis, N., Abba, I. A. and Grace, J. R. 2000 A state-of-the-art review of gas-solid turbulent fluidization. *Chem. Eng. Sci*., **55**, 4789.

Gidaspow, D. 1994 *Multiphase flow and fluidization*: continuum and kinetic theory descriptions. Academic Press, Boston.

Gilbertson, M. A. 1998 Observations and measurements of isolated bubbles in a pressurized gas-fluidized bed. *Fluidization IX*, edited by L.-S. Fan and T. M. Knowlton, Engineering Foundation, Durango, p.61.

Grace, J. R., Avidan, A. A., Knowlton, T. M. 1997 *Circulating fluidized beds,* Blackie Academic & Professional, London.

Hoffman, A. C. and Yates, J. G. 1985 Experimental observations of fluidized beds at elevated pressure. *Chem. Eng. Commun*., **41**, 133.

Hoomans, B. P. B., Kuipers, J. A. M., Briels, W. J. and van Swaaij, W. P. M. 1996 Discrete particle simulation of bubble and slug formation in a two-dimensional gas-fluidised bed: a hard-sphere approach. *Chem. Eng. Sci*., **51**, 99.

Hoomans, B. P. B. 2000 *Granular Dynamics of Gas-solid Two-phase Flows*. Ph.D dissertation, Twente University, Enschede, Netherlands.

Horio, M. and Kuroki, H. 1994 Three-dimensional flow visualization of dilutely dispersed solids in bubbling and circulating fluidized beds. *Chem. Eng. Sci*. **49**, 2413.

Jackson, R. 1963 The mechanics of fluidized beds: The motion of fully developed bubbles. *Trans. Inst. Chem. Eng.*, **41**, 22.

Kuipers, J. A. M., van Duin K.J., van Beckum, F. P. H. and van Swaaij, W. P. M. 1992 A numerical model of gas-fluidized beds. *Chem. Eng. Sci*., **47**, 1913.

Lackermeier, U., Rudnick, C., Werther, J., Bredebusch, A. and Burkharddt, H. 2001 Visualization of flow structures inside a circulating fluidized bed by means of laser sheet and image processing. *Powder Tech.*, **114**, 71.

Li J. and Kuipers J. A. M. 2002 Effect of pressure on flow behaviors in a dense gas-fluidized beds: a discrete particle simulation study. Accepted for publication by *Power Technol*.

Olowson, P. A. and Almstedt A. E. 1990 Influence of pressure and fluidization velocity on the gas bubble behavior and gas flow distribution in a fluidized bed. *Chem. Eng. Sci*., **45**, 1733.

Rowe, P. N. 1971 Experimental properties of bubbles. In "*Fluidization*", edited by Davidson, J. F. and Harrison D., Academic Press, UK, p.121.

Rowe, P. N. Foscolo, P. U. Hoffman, A. C. and Yates, J. G. 1984 X-ray observervation of gas fluidized

beds under pressure. In: Fluidization IV, edited by Kunii, D. and Toei, R., Engineering Foundation, p.53-60.

Tsuji, Y., Kawaguchi, T. and Tanaka, T. 1993 Discrete particle simulation of two dimensional fluidized bed. *Powder Technol.*, **77**, 79.

Varadi, T. and Grace, J. R. 1978 High pressure fluidization in a two-dimensional bed, in *Fluidization*, edited by J. F. Davidson and D. L. Keairns, Cambridge Press, Cambridge, UK, p. 55.

Notations

d_p	particle diameter, m
e	restitution coefficient, [-]
E	energy or work, J
f	energy fraction [-]
Fr	Froude number, [-]
g	gravity, m/s2
h	bed height, m
m_p	particle mass, kg
N_{part}	number of particles, [-]
u, U_g	gas superficial gas velocity, m/s
u_{mf}	initial fluidization velocity, m/s
$\boldsymbol{v_p}$	particle velocity, m/s

Greek symbols

ρ_p	particle density, kg/m^3
θ	granular temperature, [m^2/s^2]
ε	void fraction, [-]
μ	friction coefficient, [-]

Subscripts

0	initial condition
av	average
buoy	buoyancy
cell	calculation grid
conv	convection
drg	drag
dsp	dissipated
kin	kinetic
nblist	neighbor list
pot	potential
rot	rotational

Appendix 1

Table A1: Energy budget analysis of particles in dense gas-fluidized beds.

U_g (m/s)	P (bar)	***Input*** W_{drg} ($\times 10^3$ J/s)	***Suspension/movement*** E_{tot} ($\times 10^3$ J)	$\frac{E_{kin}}{E_{tot}}$	$\frac{E_{pot}}{E_{tot}}$	$\frac{E_{rot}}{E_{tot}}$	$\frac{E_{kin}+E_{rot}}{E_{pot}}$	***Dissipation*** W_{dsp} ($\times 10^3$ J/s)	$\frac{W_{dsp,t}}{W_{drg,t}+E^0_{tot}}$	***Quantification*** $\frac{W_{dsp}+E_{kin}+E_{rot}}{E_{pot}-E_{pot.mf}}$	$\frac{E_{kin}+E_{rot}}{E_{pot}-E_{pot.mf}}$	fr [$\times 10^2$] $\frac{<C^2>}{g\cdot<h>}$	$\frac{<C^2>}{g\cdot(<h>-<h_{mf}>)}$
Particles # α, e = 1.0, μ = 0.00 (ideal collision)													
0.902	1	*-0.006*	*8.315*	*1.29%*	*98.71%*	*0*	*1.31%*	*0*	*0*	*2.678*	*3.468%*	*1.25*	*3.37*
0.446	10	*0.0*	*10.116*	*3.25%*	*96.75%*	*0*	*3.363%*	*0*	*0*	*2.160*	*7.049%*	*3.34*	*7.06*
0.315	21	*0.0*	*10.102*	*2.38%*	*97.62%*	*0*	*2.436%*	*0*	*0*	*2.122*	*5.054%*	*2.43*	*5.07*
0.303	25	*0.027*	*10.333*	*2.50%*	*97.50%*	*0*	*2.567%*	*0*	*0*	*2.078*	*6.215%*	*2.56*	*5.24*
0.280	30	*0.026*	*10.275*	*2.95%*	*97.05%*	*0*	*3.046%*	*0*	*0*	*2.110*	*6.265%*	*3.04*	*6.29*
0.260	35	*0.014*	*10.370*	*2.34%*	*97.66%*	*0*	*2.405%*	*0*	*0*	*2.064*	*4.864%*	*2.39*	*4.87*
0.245	40	*0.023*	*10.364*	*1.93%*	*98.07%*	*0*	*1.966%*	*0*	*0*	*2.047*	*3.955%*	*1.96*	*3.97*
0.220	50	*0.001*	*10.365*	*1.928%*	*98.07%*	*0*	*1.969%*	*0*	*0*	*2.0468*	*3.96%*	*1.96*	*3.97*
0.028	800	*0.446*	*11.345*	*0.014%*	*99.99%*	*0*	*0.014%*	*0*	*0*	*1.818*	*0.026%*	*0.0141*	*0.0257*
Particle: # β, e = 0.95, μ = 0.10													
0.902	*1*	*4.839*	*8.838*	*7.40%*	*92.57%*	*0.03%*	*8.05%*	*4.887*	*43.46%*	*4.472*	*0.2155*	*7.95*	*21.5*
0.446	*10*	*1.392*	*9.865*	*4.64%*	*95.34%*	*0.02%*	*4.50%*	*1.357*	*15.92%*	*2.611*	*0.1077*	*4.84*	*10.7*
0.315	*21*	*0.565*	*9.893*	*2.90%*	*97.09%*	*0.01%*	*3.00%*	*0.579*	*7.26%*	*2.326*	*0.0642*	*2.98*	*6.42*
0.280	*30*	*0.482*	*10.168*	*3.09%*	*96.9%*	*0.008%*	*3.20%*	*0.475*	*6.00%*	*2.241*	*0.0666*	*3.18*	*6.66*
0.245	*40*	*0.302*	*10.240*	*2.51%*	*97.48%*	*0.006%*	*2.58%*	*0.273*	*3.91%*	*2.154*	*0.0529*	*2.57*	*5.30*
Particle: # χ, e = 0.90, μ = 0.20													
0.902	*1*	*6.184*	*8.835*	*7.75%*	*92.2%*	*0.05%*	*8.45%*	*6.176*	*48.36%*	*4.942*	*0.2273*	*8.30*	*22.6*
0.446	*10*	*1.831*	*9.786*	*5.16%*	*94.8%*	*0.04%*	*5.49%*	*1.814*	*20.53%*	*2.783*	*0.1228*	*5.43*	*12.2*
0.315	*21*	*0.814*	*9.798*	*3.15%*	*96.8%*	*0.01%*	*3.27%*	*0.763*	*9.70%*	*2.408*	*0.0708*	*3.24*	*7.09*
0.280	*30*	*0.633*	*10.11*	*3.22%*	*96.8%*	*0.02%*	*3.34%*	*0.624*	*7.58%*	*2.295*	*0.0705*	*3.32*	*7.05*
0.245	*40*	*0.383*	*10.19*	*2.56%*	*97.4%*	*0.04%*	*2.63%*	*0.376*	*5.18%*	*2.190*	*0.0543*	*2.61*	*5.43*

Table A1: (continuing): Energy budget analysis of particles in dense gas-fluidized beds.

U_g (m/s)		***Input***	***Suspension/movement***					***Dissipation***		***Quantification***			
	P (bar)	W_{drg} ($\times 10^3$ J/S)	E_{tot} ($\times 10^3$ J)	$\frac{E_{kin}}{E_{tot}}$	$\frac{E_{pot}}{E_{tot}}$	$\frac{E_{rot}}{E_{tot}}$	$\frac{E_{kin}+E_{rot}}{E_{pot}}$	W_{dsp} ($\times 10^3$ J/S)	$\frac{W_{dsp,t}}{W_{drg,t}+E^0_{tot}}$	$\frac{W_{dsp}+E_{kin}+E_{rot}}{E_{pot}-E_{pot.mf}}$	$\frac{E_{kin}+E_{rot}}{E_{pot}-E_{pot.mf}}$	fr [$\times 10^2$]	
												$\frac{<C^2>}{g\cdot<h>}$	$\frac{<C^2>}{g\cdot(<h>-<h_{mf}>)}$
Particle: # **δ**, e = 0.85, μ = 0.30													
0.902	*1*	*7.553*	*9.152*	*8.13%*	*91.85%*	*0.02%*	*8.92%*	*7.593*	*0.5187*	*5.121*	*0.2302*	*8.65*	*22.6*
0.446	*10*	*2.077*	*9.751*	*5.96%*	*94.02%*	*0.02%*	*6.39%*	*2.004*	*0.2149*	*2.902*	*0.1459*	*6.31*	*14.5*
0.315	*21*	*0.931*	*9.797*	*3.44%*	*96.55%*	*0.01%*	*3.59%*	*0.878*	*0.1142*	*2.453*	*0.0782*	*3.55*	*7.81*
0.280	*30*	*0.626*	*10.142*	*3.02%*	*96.97%*	*0.01%*	*3.13%*	*0.624*	*0.0788*	*2.276*	*0.0653*	*3.11*	*6.52*
0.245	*40*	*0.376*	*10.159*	*2.53%*	*97.46%*	*0.01%*	*2.61%*	*0.408*	*0.0533*	*2.203*	*0.0540*	*2.59*	*5.41*
***Particle*: # ε**, e = 0.80, μ = 0.40													
0.902	*1*	*8.223*	*9.213*	*8.145%*	*91.83%*	*0.025%*	*8.97%*	*8.140*	*52.77%*	*5.262*	*23.01%*	*8.62*	*22.4*
0.446	*10*	*2.083*	*9.805*	*5.34%*	*94.64%*	*0.02%*	*5.68%*	*2.040*	*22.22%*	*2.842*	*12.71%*	*5.62*	*12.7*
0.315	*21*	*0.915*	*9.774*	*3.30%*	*96.68%*	*0.02%*	*3.435%*	*0.890*	*10.75%*	*2.454*	*7.47%*	*3.41*	*7.47*
0.280	*30*	*0.727*	*10.106*	*3.25%*	*96.74%*	*0.01%*	*3.384%*	*0.725*	*8.93%*	*2.319*	*7.11%*	*3.34*	*7.07*
0.245	*40*	*0.516*	*10.107*	*2.70%*	*97.29%*	*0.01%*	*2.793%*	*0.492*	*6.21%*	*2.241*	*5.82%*	*2.77*	*5.82*

Chapter 4

GAS-PARTICLE INTERACTIONS IN DENSE GAS-FLUIDIZED BEDS

Abstract

The occurrence of heterogeneous flow structures in gas-particle flows seriously affects gas-solid contacting and transport processes in dense gas-fluidized beds. A computational study, using a discrete particle method based on Molecular Dynamics techniques, has been carried out to explore the mechanisms underlying the formation of heterogeneous flow structures. Based on energy budget analysis and detailed study of particle dynamics, impact of ***non-linear drag force*** *on the flow structure formation in gas-fluidized beds for both ideal collision particles (elastic collision and without inter-particle friction) and non-ideal collision particles has been assessed. Meanwhile, the role of inter-particle inelastic collisions has also been examined.*

*It is demonstrated that heterogeneous flow structures do exist in systems with both non-ideal particle collisions and ideal particle collisions. The heterogeneous structure in an ideal system, featured with looser packing, is purely caused by non-linearity of gas drag: the stronger non-linearity of the gas drag force, the more heterogeneous flow structures develop. A weak dependence of drag on the voidage tends to form homogenous flows. Particularly, it is interesting to see that a non-linear drag force has the "****phase separation****" function by accelerating particles in the dense phase and decelerating particles in the dilute phase to trigger the non-homogeneous flow structure formation. Collisional dissipation dramatically intensifies the formation of heterogeneous flow structures after the system equilibrium breaks. Quantitative comparisons of flow structures obtained by using various drag correlations in literature will also be reported.*

In addition, it will be elucidated that the force balance for the particles decisively ensures the existence of a homogeneous flow structure for ideal collision particle systems. However, for non-ideal collisional particles, both the force balance and energy balance condition are

necessary to guarantee an equilibrium state and therefore permit the existence of a homogeneous flow. It is deduced that only those systems with either equilibrium-suspended particles (force balance) or systems with a limited particle collisional dissipation (energy balance) can maintain a homogeneous flow structure.

1 Introduction

1.1 Flow structure induced by non-linear drag

The occurrence of heterogeneous flow structures in gas-particle flows seriously affects the gas-solid contacting and transport processes in dense gas-fluidized beds. Among the phenomena inducing the heterogeneous flow structure, particle collisional dissipation was indicated as one of the important factors in dense gas-fluidized beds by Hoomans et al. (1996). The finding that dissipative collisions lead to heterogeneous structures is considered as an important discovery in physics (Jaeger et al., 1996). However, the influence of fluid drag, or fluid-particle interaction, on pattern formation in particulate flows has been overlooked in the past due to experimental difficulties and lack of theoretical tools. Actually, this important phenomenon would play an even more fundamental role in triggering the heterogeneous flow structure formation (bubbling flow) in gas-solid two-phase flows since it is characterized by the unique non-linear nature with respect to the particle assembly effect and therefore it would severely affect gas-solid contacting, transfer and reaction processes.

Wylie and Koch (2000) reported that at low Stokes numbers (defined as the ratio of the root-mean-square particle momentum and the momentum loss during particle translation over a distance equal to its radius) the viscous stress in the gas phase can lead to cluster formation by enhancing the hydrodynamic interaction among the particles. Their work was carried out in a simple case of ideal particle collision at low Re number and without considering the gravity acting on the particles. Helland et al. (2000) also observed that non-linear drag has significant impact on flow structure formation in high-velocity circulating gas-fluidized beds. From our previous simulations, we interestingly observed that a heterogeneous flow structure still prevails in dense gas-fluidized beds with *ideal particle collisions* (see chapter 3). Then, the following fundamental questions arise: why does the heterogeneous system exist and how does it originate? From energy analysis, we found that this heterogeneity is closely related to the ratio of kinetic energy and potential energy. In case a large portion of energy is distributed to kinetic part a heterogeneous flow structure prevails. Obviously, the heterogeneous flow structure depends in some way on the local force balance acting on particles, or in other words, the system equilibrium.

For a given system, gravity acting on a particle is constant but gas drag changes dramatically (in a strong non-linear way) with the adjacent particle number density. The presence of other particles restricts fluid space, creates a sharp velocity gradient in the surrounding gas phase and, as a result, yields an increased shear stress on the particle surface. The enhancement of gas drag is closely associated with the particle configuration, gas-solid slip velocity and gas and solids properties. Therefore, the precise quantification of *gas drag acting on a particle in an assembly*

is the key issue for understanding gas-solid interaction in particulate flows. This assembly effect has great impact on gas-solid heat and mass transfer processes (Agarwal, 1988) as well.

Up to date, there are no proper explanations to how and why the non-linear drag produces heterogeneous flow structures. Also we do not know the ways by which gas drag, gravity and particle collision interact with each other to produce various flow structures observed in dense particle-laden flows.

1.2 Drag force acting on a particle in assembly

As far as the drag force is concerned, unfortunately a complete characterization of gas drag acting on a particle in an assembly is not completely clear, even though great efforts have been devoted to this subject. The complexity, induced by mutual interactions between fluid and particle and between particles themselves, seriously hampers the progress. Previous work can be divided into three classes: 1) direct empirical or semi-empirical correlation; 2) determination based on the bed expansion and 3) direct numerical simulation.

Typical examples belonging to the first class are the well-known Wen and Yu (1966) and Ergun correlations (1952). They obtained their correlations by using experimental bed pressure drop data for stationary beds, which limits the applicability of the correlations strictly to equilibrium or near-equilibrium systems. The second method to obtain drag force expressions relies on the correlation between superficial fluid velocity and bed expansion by using Richardson-Zaki (R-Z) type of equation (Richardson, 1971). In the laminar and turbulent regimes, this approach gives identical results compared to those based on pressure drop measurements (voidage exponent 4.65). But in intermediate regimes, the exponent depends on the Reynolds number (see Felice, 1994). For gas-solid systems, the exponent obtained for the R-Z equation is unfortunately extremely scattered, ranging from -3 to 10 (Morgan et al., 1970/1971). This scatter implies that the actual voidage function exponent might deviate significantly from 4.7, the conventional value taken to predict fluid-particle interaction. Particularly, it reflects the ***non-equilibrium*** nature of gas-solid systems: the more difficult the system can be fluidized, the bigger the expansion exponent *n*. Clearly, the correlation obtained in such a way can only predict the two-phase hydrodynamics at macro-scale. The third method, direct numerical simulation, is typified by the micro-scale simulations, such as DNS (Choi and Joseph, 2001), Lattice Boltzmann (Zhang et al. 1999, for liquid-solid system; Hill, 2001, for gas-solid system). Owing to its ability to describe the flow around each particle in great detail, the approach can capture the essential nature of fluid-solid interaction. Unfortunately, this very promising approach is at an early stage.

Obviously, due to the non-equilibrium nature of gas-solid systems, two-phase hydrodynamics is characterized by a **strong non-linearity**. This suggests that the traditional strategies based on

macroscopic balances and assumptions of uniformity (such as capillary, cell models) are too simple to provide a reasonable basis to characterize gas-solid interaction. Only the models, which take into account 1) drag acting on a single particle in infinite flow, 2) adjacent particle effect (voidage, slip velocity) and 3) particle collision effect (dynamic effect), can result in the correct prediction of hydrodynamics of dense gas-solid systems.

This chapter is devoted to understanding the origin of heterogeneous flow structures in dense gas-fluidized beds. The effect of the non-linear gas drag is explored firstly by employing drag correlations with an increasing exponent of the voidage correlation function and the correlations available in literature. Subsequently, the contribution due to collisional dissipation will also be highlighted. Particularly, by monitoring particle motion while keeping track of the particle environment (void fraction) we try to understand how non-linear drag triggers the formation of non-homogeneous flow structures. Finally, the conditions for a full homogeneous flow will be explored.

2 Theoretical background

The discrete particle method is well-suitable to explore the pattern formation in particulate flows owing to its capability of precise description of both particle-particle-wall interaction and fluid-particle interaction. In our model, the motion of each individual particle is directly calculated from the Newtonian equation of motion while accounting for the interactions with other particles, reactor wall and the continuous gas phase. Collisions are assumed to be binary and instantaneous. Key parameters of the collision model are the coefficients of restitution (e) and friction (μ). A sequence of collision is processed using algorithms adopted from Molecular Dynamics (MD) simulation.

The external forces acting on the particles are (Hoomans et al., 1996):

$$\sum \boldsymbol{F} = m_p \boldsymbol{g} + \frac{V_p \beta}{1-\varepsilon}(\boldsymbol{u}-\boldsymbol{V}) - V_p \nabla p \tag{4.1}$$

where β is given by

$$\beta = \tfrac{3}{4} c_d \frac{\varepsilon(1-\varepsilon)}{d_p} \cdot \rho_g \left|\boldsymbol{u}-\boldsymbol{V}\right| \varepsilon^{-\alpha+2} \tag{4.2}$$

The gas-phase hydrodynamics is obtained from the volume-averaged Navier-Stokes equations:

$$\frac{\partial(\varepsilon\rho_g)}{\partial t} + (\nabla \cdot \varepsilon\rho_g \boldsymbol{u}) = 0 \tag{4.3}$$

$$\frac{\partial(\varepsilon\rho_g \boldsymbol{u})}{\partial t} + (\nabla \cdot \varepsilon\rho_g \boldsymbol{u}\boldsymbol{u}) = -\varepsilon\nabla p - \boldsymbol{S}_p - (\nabla \cdot \varepsilon\overline{\boldsymbol{\tau}}_g) + \varepsilon\rho_g \boldsymbol{g} \tag{4.4}$$

$$S_p = \sum_i^{N_{part}} F_{drg,i}\,\delta(x - x_i) \tag{4.5}$$

Where the drag force exerted on the particles enters the momentum equation through a sink term S_p and α denotes the exponent of the drag correlation function. The other formulae used in this study are listed in Table 4.1. Table 4.2 lists the base case conditions used in the simulations. Others will be specified in the discussion section.

Table 4.1: Various drag correlations proposed for particulate flows.

Author(s)	Formulation	Comment
	$F_s = C_d \frac{1}{8}\pi {d_p}^2 \rho_f \left\vert\vec{v}_s\right\vert \vec{v}_s$	Drag force on a single particle in infinite flow
	$F = C_d \cdot \frac{1}{8}\pi d_p^2 \rho_f \cdot \varepsilon^2 \left\vert\vec{u}-\vec{V}\right\vert (\vec{u}-\vec{V}) \cdot f(\varepsilon)$, where $C_d = \begin{cases} \frac{24}{\mathrm{Re}_p}(1+0.15\,\mathrm{Re}_p^{0.687}) & \mathrm{Re}_p < 1000 \\ 0.44 & \mathrm{Re}_p \geq 1000 \end{cases}$ $Re_p = \frac{\varepsilon \rho_g \left\vert \boldsymbol{u}-\boldsymbol{V}\right\vert d_p}{\mu_g}$	Drag force on a particle in assembly. $f(\varepsilon)$ represents the drag correlation function
Wen & Yu (1966)	$f(\varepsilon) = \varepsilon^{-4.7}$	$\alpha = 4.7$
Felice et al. (1994)	$f(\varepsilon) = \varepsilon^{-\alpha}$, $\alpha = 4.7 - 0.65\exp[-\frac{(1.5-\log \mathrm{Re})^2}{2}]$, $2 < Re_t < 500$	Also refer to Jean and Fan (1992)
Happel (1958)	$f(\varepsilon) = \frac{3+2(1-\varepsilon)^{\frac{5}{3}}}{3-4.5(1-\varepsilon)^{\frac{1}{3}}+4.5(1-\varepsilon)^{\frac{5}{3}}-3(1-\varepsilon)^2}$	Cell model.
Koch and Hill (1999, 2001)	$F = F_0(\phi) + F_1(\phi)\,\mathrm{Re}^2$, (Re < 20) $F_0(\phi) = \begin{cases} \frac{1+3(\phi/2)^{1/2}+(135/64)\phi\ln\phi+16.14\phi}{1+0.681\phi-8.48\phi^2+8.16\phi^3} & \phi<0.4 \\ \frac{10\phi}{(1-\phi)^3} & \phi>0.4 \end{cases}$ $F_1(\phi) = 0.110 + 5.10\times10^{-4} e^{11.6\phi}$ $F = F_0(\phi) + F_3(\phi)\,\mathrm{Re}$, (Re > 20) $F_3(\phi) = 0.0673 + 0.212\phi + \frac{0.0232}{(1-\phi)^5}$ where $\mathrm{Re} = \frac{\varepsilon \frac{d_p}{2}(u-v)\rho_f}{\mu}$	Lattice-Boltzmann simulation, ϕ denotes solids fraction.
Ergun (1952)	$\boldsymbol{F} = \frac{V_p \beta}{1-\varepsilon}(\boldsymbol{u}-\boldsymbol{V})$, where $\beta = 150\frac{(1-\varepsilon)^2}{\varepsilon}\frac{\mu_f}{(\phi_s d_p)^2} + 1.75(1-\varepsilon)\frac{\rho_f}{\phi_s d_p}\left\vert\boldsymbol{u}-\boldsymbol{V}\right\vert$	Capillary model, V_p is the particle volume
Rowe (1987)	$\frac{4.7-n}{n-2.35} = 0.175\,\mathrm{Re}_t^{3/4}$	n denotes bed expansion exponent (2.35 ~ 4.7).

Table 4.2: Base case conditions used in the simulations.

Bed geometry	2-D		
Width, cm	10	Height, cm	40, 80
Particles			
Diameter, mm	0.949	Number [-]	16000
Density, k_g/m^3	1170	Incipient fluidization velocity, m/s	0.301
Simulations			
Grid	20×40, 80	Total time, time step, s	10, 1×10^{-4}
Restitution Coefficient		Friction Coefficient	
-Norm. (e, e_w), [-]	1.00 (ideal), 0.90	-Norm. (μ, μ_w), [-]	0.00 (ideal), 0.20
-Shear	0	-Shear	0
Operating conditions			
Superficial gas velocity (u_g), m/s	$3u_{mf}$, $6u_{mf}$ 0.902, 1.8, 2.7, 3.2, 3.6, 4.2	Static bed height, m	0.15
Pressure (bar)	1		

3 Results and discussions

The simulation results demonstrate that gas drag plays a very important role in flow pattern formation in gas-fluidized beds. When altering the voidage functions $f(\varepsilon)$, the flow pattern displays many modes, ranging from perfectly homogeneous particulate flow to extremely heterogeneous flow for both ideal and non-ideal collision systems. The simulation results will be presented first to provide a preliminary impression on the effect of the various drag correlations on the flow structure. Subsequently, analysis of the origin of pattern formation is reported by analyzing the micro-scale particle motion in ideal collisional systems.

3.1 Effect of non-linear drag force

To understand how the voidage function exponent α, a measure of particle "group" effect, affects the flow structure, we carried out a series of simulations by using different values of the exponent, ranging from 0 to 8, keeping other variables the same. Figure 4.1 shows the snapshots of flow structures obtained by using the exponents of 2, 4.7 and 8 respectively for two systems. Clearly, with increasing exponent of voidage function, the bed height increase dramatically.

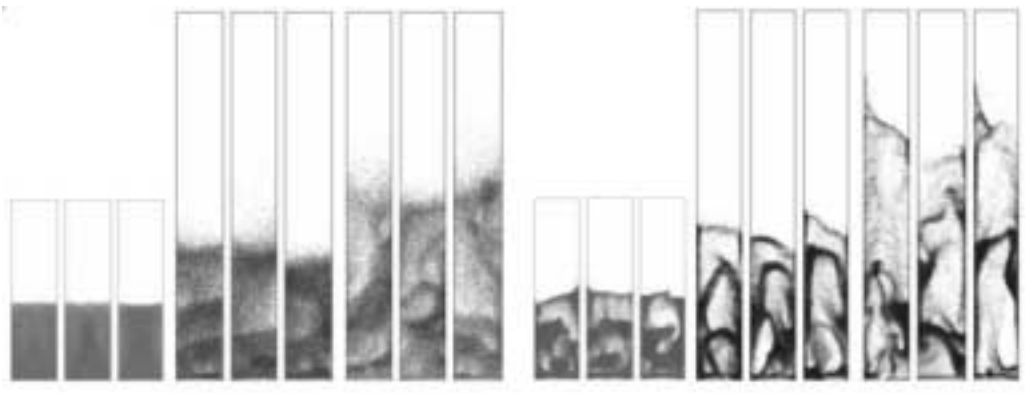

Figure 4.1: Variation of flow structure with voidage function exponent (α). Three sets of snapshots on the left are taken from the simulations at 3, 4 and 5 second under the conditions of α = *2, 4.7, 8* respectively. Except the bed height (40 mm) for the first case, all the other conditions are the same as follows: 2-D bed of 10 mm in width and 80 mm in height, ideal collision, d_p = 0.949 mm, ρ_p = 1170 k_g/m^3, particle number: 16000. Same trend has been found for the non-ideal collision (e = 0.9, μ = 0.2) particle systems on the right.

This is due to the fact that the increase of voidage exponent provides stronger drag force acting on the particles. Particularly, it is surprisingly found that heterogeneous flow structures still exist in ideal systems, which become more pronounced at high voidage exponent. Quantitative

characterization of the heterogeneous flow structure is possible by computing the Froude number given by (see Chapter 3):

$$\mathrm{Fr} = \frac{\theta}{g \cdot \langle h_b \rangle} = \frac{\text{random granular kinetic energy}}{\text{potential energy}} \tag{4.6}$$

where θ represents granular temperature, $\langle h_b \rangle$ the vertical position of the bed mass center and g the gravity constant. A large Fr corresponds to heterogeneous flow structures whereas a small Fr number leads to homogeneous flow structures. This quantification is based on the relationship between energy distribution and flow structure: a system distributing more energy to particle

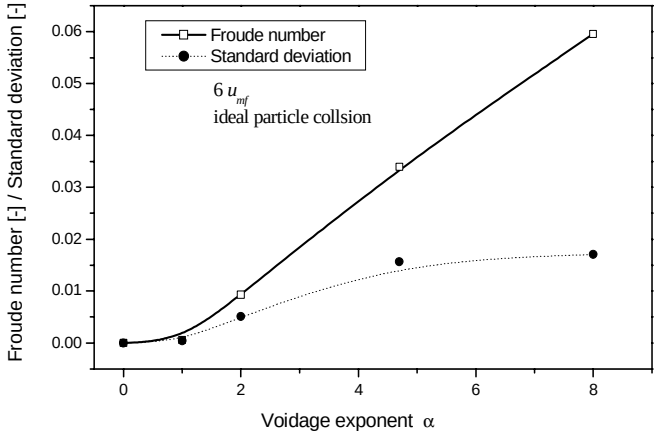

(a)

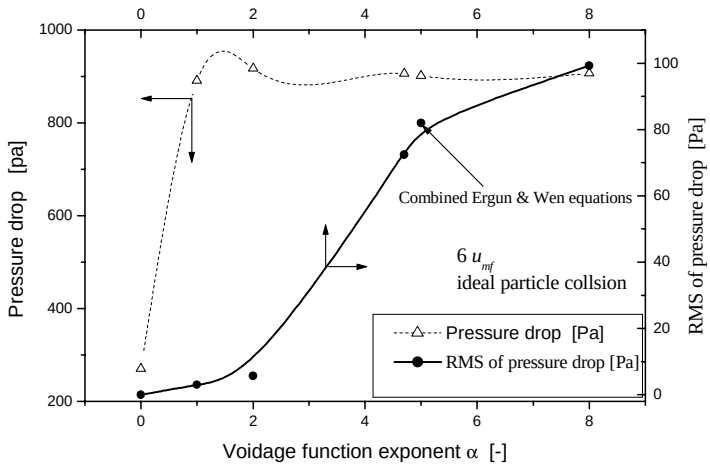

(b)

Figure 4.2: Non-homogeneity of flow structure versus voidage function exponent by a) time-averaged Froude number and b) RMS of pressure drop. *High voidage exponent yields a more pronounced heterogeneous flow structure*. Froude (Fr) is defined as $\theta/(g \cdot \langle h_b \rangle)$, where θ is the granular temperature and $\langle h_b \rangle$ the vertical position of the bed mass center.

suspension tends to form a uniform structure and a system distributing more energy to collisional dissipation inclines to form a heterogeneous flow structure. The detailed energy budget analysis connected to pattern formation in gas-fluidized beds can be found in Chapter 3 and our recent publication (Li and Kuipers, 2001).

The quantitative comparison of the heterogeneity of flow structures is presented in Figure 2. Clearly, the influence of the voidage exponent on flow structure is extremely pronounced. The stronger non-linearity of the gas drag force, the more heterogeneous flow structures develop. A weak dependence of drag on the voidage tends to lead to homogenous flows. Therefore, we can conclude that besides particle collisional dissipation, **non-linearity of gas drag due to the effect of neighboring particles is another, even more fundamental, mechanism underlying pattern formation in dense gas-fluidized beds**. In contrast to particle collisional dissipation, this phenomenon is closely associated with the particle motion: a phenomenon prevailing in non-equilibrium systems.

Simulations have also been conducted for non-ideal systems and the snapshots are shown on the left in Figure 4.1. It displays the same trend as in the ideal system but with an extremely distinguished two-phase structure: clear bubble region coupled with dense emulsion region. The loose packing of particle clusters typically observed in the ideal system is attributed to the fact that no energy is dissipated during the frequent particle-particle encounters. This demonstrates that particle collisional dissipation intensifies the heterogeneity of flow structure and intensifies formation of heterogeneous flow structures. Meanwhile, it suggests that non-linear drag is the fundamental root which triggers the pattern formation. Previously, it has been believed that particle collisional dissipation exclusively leads to the heterogeneous flow structure. Then why and how can the non-linearity of gas drag trigger the formation of such a heterogeneous flow structure in ideal collision systems? If we can answer this question, it is possible to discover the fundamentals that control flow structure formation and its evolution in dense particle laden flows. Since drag has such a great impact on flow structure, it is therefore important to test the various drag correlations proposed in literature.

3.2 Drag correlation versus the induced flow structure

The six voidage functions given in Table 4.1 (also see Figure 4.3) were used to predict the flow structure for the base case conditions summarized in Table 4.2. Felice's equation takes into account the Re number effect on the exponent of the voidage function, especially in the intermediate regime where α is small. Hill's correlation originates from Lattice-Boltzmann simulation (Hill, 2001). From Figure 4.4, it can be seen that Hill's correlation corresponds quite well to Wen and Yu's empirical equation. It would be a good alternative for the combined Wen and Yu and Ergun equations connecting at $\varepsilon = 0.8$. The "modified Happel" equation (equation 7), which is less sensitive to voidage, was also included in our study.

$$f(\varepsilon) = \frac{3 + 25(1-\varepsilon)^{\frac{2}{3}}}{3 - 4.5(1-\varepsilon)^{\frac{1}{3}} + 4.5(1-\varepsilon)^{\frac{2}{3}} - 3(1-\varepsilon)^{2}} . \qquad (4.7)$$

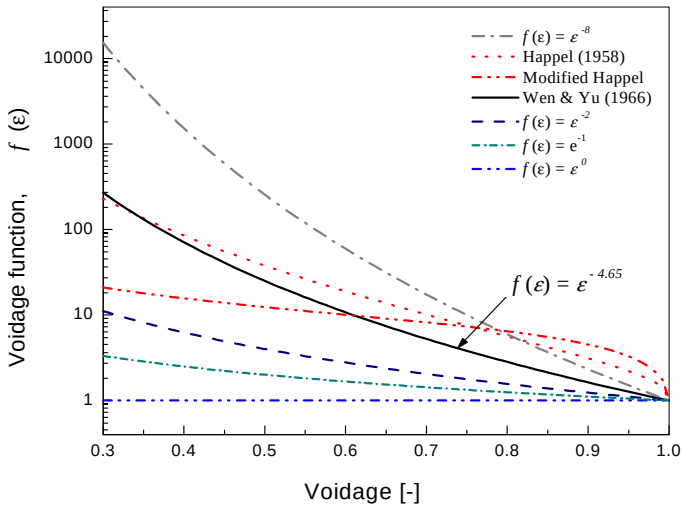

Figure 4.3: The various voidage functions ("group" effect) for dense particulate flows.

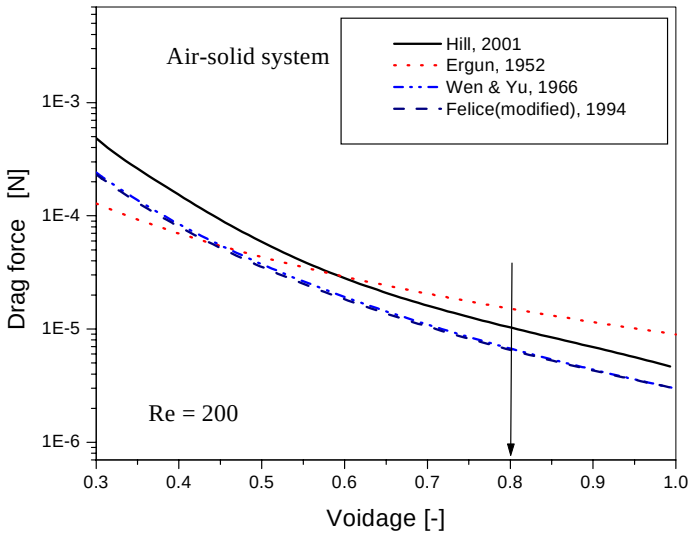

Figure 4.4: Comparison of drag acting on a particle in an assembly calculated from the Ergun equation (semi-empirical formulae), Wen & Yu correlation (experiment) and Hill's correlation (Lattice-Boltzmann simulation).

Figure 4.5 shows the snapshots of the flow structures computed from our model using the different drag correlations. The bed structure analysis has also been carried out by comparing

bed mass center, Froude number, pressure fluctuation (macro-scale). Because of the very small difference between the flow structures obtained using Felice's correlation and those due to Wen and Yu for the ideal collisional system, the corresponding results are therefore omitted (they are only different in case of non-ideal collision systems). Obviously, the computed flow structures resulting from the usage of these different drag correlations are all featured with heterogeneity but with a certain degree of variation. The bed height increases from (a) to (e) (see Figure 4.5) which can be attributed to intensified gas drag as evident from Figure 4.3 and 4.4. Particularly, it is interesting to note that bed height increases dramatically when using the voidage functions of Happel-type despite its small drag produced at low voidage (see Figure 4.3).

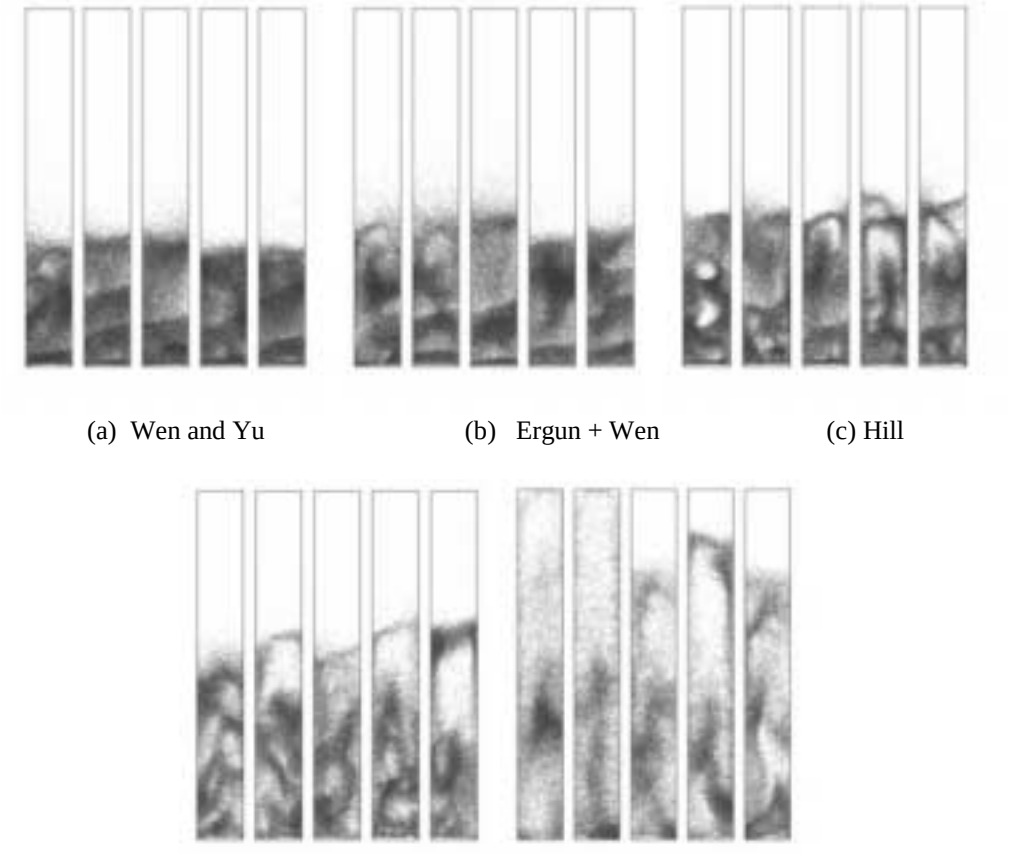

(a) Wen and Yu (b) Ergun + Wen (c) Hill

(d) Happel (e) M-Happel

Figure 4.5: Snapshots of flow patterns at 2, 3, 4, 5 and 6 second respectively under conditions of u_g = 1.8 m/s, ideal particle collision, bed size: 10 mm in width and 80 mm in height, gas drag force on the particles in assembly based on: a) Wen and Yu (1966) correlation; b) the combined Ergun equation (when ε <0.8) and Wen and Yu correlation (when ε >0.8); c) Hill's correlation (Hill, 2001) from Lattice-Boltzmann simulation; d) Happel's "cell" model (1958); e) modified Happel equation, featured with less sharp variation of voidage function with voidage.

In Figure 4.6 and 4.7 the bed pressure drop and the Froude number are shown versus time for the various drag correlations listed in Table 4.1. It can be seen that the evolution of flow structure (in the order as shown in Figure 4.5) follows the same trend as obtained with

intensified gas-solid interaction (see Chapter 3): first relatively uniform (by Wen and Yu), then more heterogeneous (by the combined Ergun and Wen and Yu correlations) followed by more homogeneous flow structures (by Hill, Happel and the modified Happel-type equations). The drag force based on the combined Ergun and Wen and Yu equations yields more heterogeneous flow structures. Hill's drag correlation produces a relatively small pressure fluctuation and low Froude number (see Figure 4.6), implying that it produces a more homogeneous flow structure.

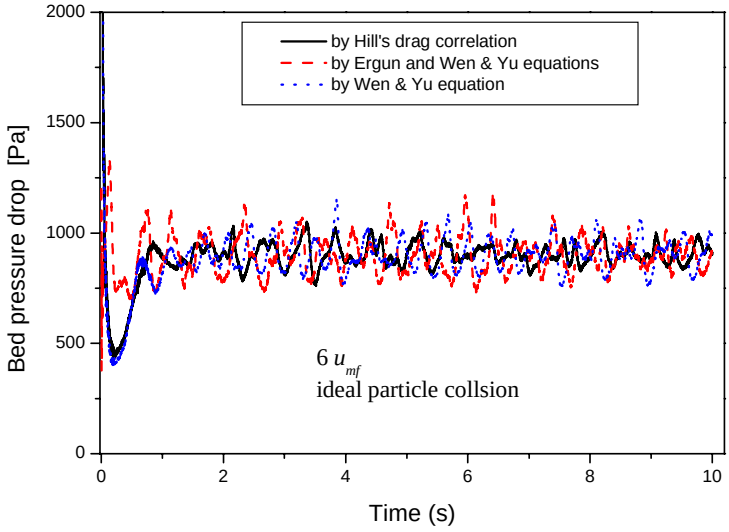

a) Pressure signals

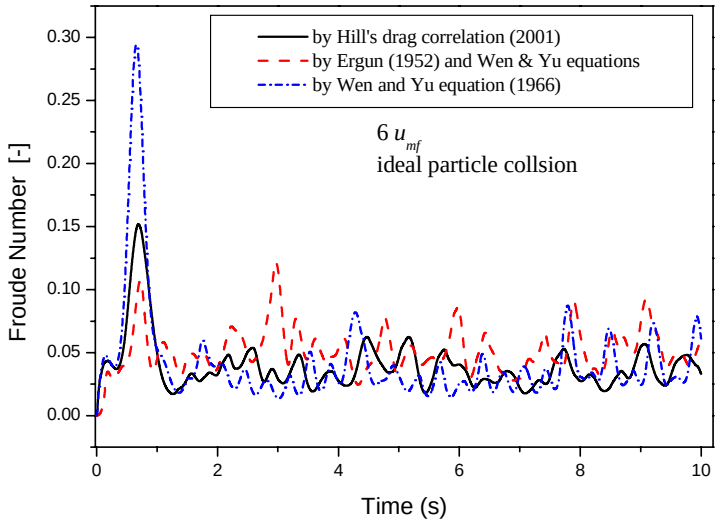

b) Froude number

Figure 4.6: Quantification of flow structure by a) pressure drop fluctuations; b) Froude number computed by using three different correlations.

Happel's correlation produces a more homogeneous flow structure with a huge bed expansion. This becomes more pronounced when drag force increases at high voidage even though the drag force at low voidage is smaller than the corresponding values based on the Wen and Yu correlation (modified Happel). This result demonstrates that there exists a distinct difference of flow behaviors between the particles in the dilute and in the dense regions. Enhancing the gas-solid interaction in the dilute region would efficiently suppress the formation of the heterogeneous flow pattern. Keeping in mind this point for the time being which is closely related to heterogeneous flow structure formation, we will understand such a phenomenon in depth after having observed the particle motion in different regions. Considering that Hill's equation results from pure simulation and still produces the correct gas-solid drag, it could be a good alternative for the Wen and Yu equation to predict gas-particle drag in gas-fluidized beds.

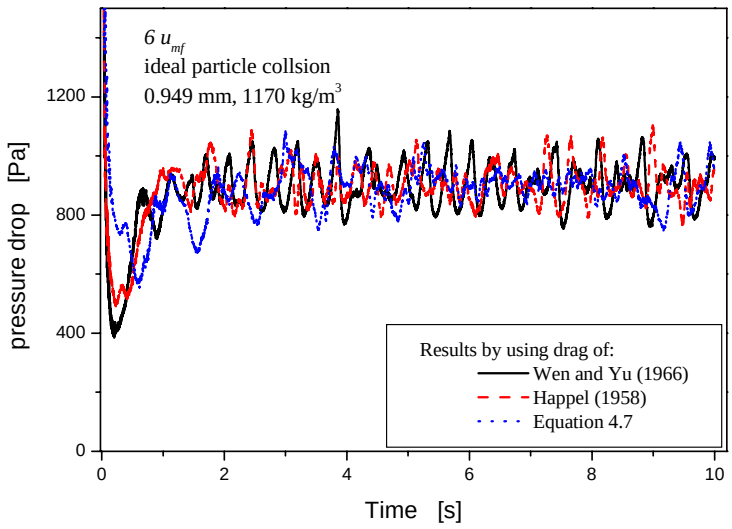

Figure 4.7: Pressure-drop fluctuations in gas-fluidized beds computed by using different drag correlations.

3.3 Non-linear gas drag induced system instability

--- Particle motion analysis

The equilibrium and instability, naturally determined by the system properties, such as density difference, particle size etc, are the key issues in multiphase systems and they directly control the origin and type of flow pattern formation. Particle collision, though dissipating suspension energy, has a great impact on flow pattern as well but only after the system equilibrium is disturbed. If the system is in equilibrium, particles maintain their steady motion. Otherwise the particles will experience unsteady motion with acceleration or deceleration. Therefore, by monitoring particle motion, one can assess system equilibrium state and furthermore understand how the nonlinear gas-solid interaction destroys the system stability.

The velocities, accelerations and adjacent void fractions for labeled particles in gas-fluidized beds with ideal collisional particles has been recorded during the simulations where the combined Ergun equation and Wen and Yu correlation has been employed, both featuring a strong non-linearity dependence of drag force with respect to void fraction. The results for the ideal collisional particles are shown in Figure 4.8.

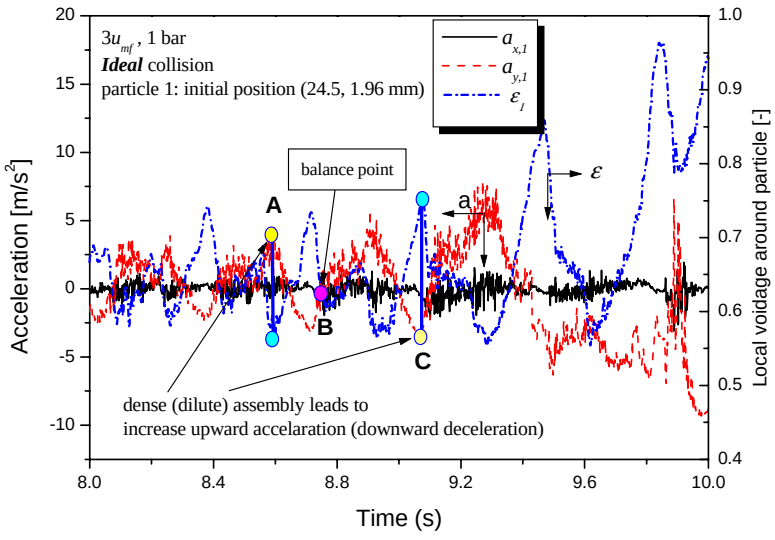

Figure 4.8: The motion of a single particle and its adjacent void fraction in a gas-fluidized bed. The particle inside a dense assembly is accelerated while particle in a dilute assembly is decelerated leading to a "phase separation" phenomenon induced by non-linear gas drag. See Figure 4.9 for the specific positions in the bed.

It is surprisingly found that there exists a close correspondence between the particle motion and the solids volume fraction in the vicinity of the particle under consideration, indicating that the

particle is accelerated while it resides inside the dense cluster, but decelerated while it is enveloped by the dilute gas! This demonstrates that the particles present in the emulsion or dilute phase are exposed to ***non-equal*** drag forces, large drag acting on the particles in the emulsion phase (or cluster) but small drag acting on the particles in the dilute phase. Acceleration in a local dense region can induce enhanced particle collision during particle lifting whereas the deceleration in the local dilute region speeds up downward particle motion to yield a "vacuum" bubble, Therefore, once a transient local non-uniform structure originates and the system can not destroy it, the non-linear drag plays the role of expediting the "phase" separation. In such a way, the so-called "bubble/emulsion" two-phase flow structure with a clear-cut boundary, develops.

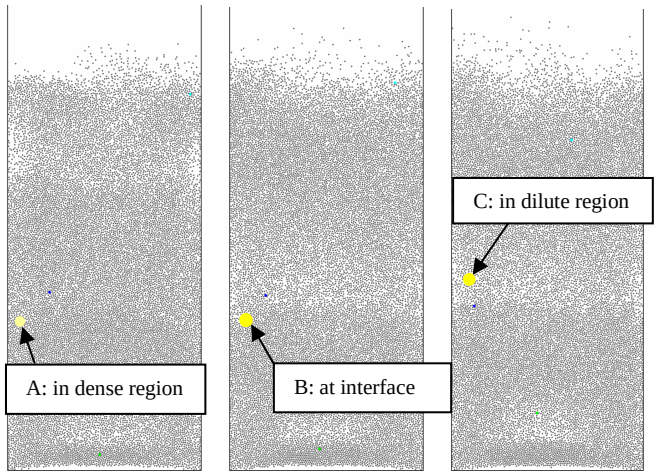

Figure 4.9: The positions of a single particle (light color) in gas-fluidized beds with *ideal collisional particles* at t = 8.57 s (left, in dense region), 8.75 s (middle, at interface) and 9.07 s (right, in dilute region). Superficial gas velocity: $3u_{mf}$, d_p = 0.947 mm, ρ_p = 1170 kg/m^3. The corresponding dynamic behaviors are shown in Figure 4.8.

Figure 4.9 shows the particle positions, corresponding to positions at A, B and C in Figure 4.8, in the gas-fluidized bed. Clearly, the accelerated particle at A is in the emulsion phase and the decelerated particle at C in the dilute phase. Particularly, it is noted that the particle residing near the boundary region maintains its equilibrium state (B in Figure 4.8).

In addition, a correlation analysis between the particle vertical acceleration and void fraction has been carried out to confirm the universality of the above mentioned conclusion. For the traced particle, the Pearson correlation coefficient of -0.602 is obtained with significance at the level of 0.01. The values for the other two particles are -0.724 and -0.682 respectively. Since the voidage values taken are based on the cell voidage, these values are suited to confirm the existence of the correspondence between the force acting on the particle and the particle environmental condition.

This “phase separation” capacity of nonlinear drag can be understood directly by examining the dependence of drag force on void fraction, or, the drag correlation. According to the Wen and Yu correlation, the drag correlation function leads to the following properties: 1) a denser packing results in a larger gas drag and 2) increasing the exponent of the voidage function can enlarge the drag difference between the dilute and dense phases. Combing the structure evolution with the voidage function exponent in Figure 4.1, we can conclude that it is this uneven drag force distribution experienced by the particles at different locations that triggers the heterogeneous flow structure formation and transforms the initial disturbances into a permanent “phase” separation. As the uneven drag distribution results from the non-linearity dependency of drag on voidage, Therefore, the non-linearity of drag force is the fundamental that underlying the pattern formation in dense gas-fluidized beds.

In retrospect to the flow structure obtained from the modified Happel equation, we could now easily understand why the slight increase of drag force in dilute region can produce a more homogeneous flow structure with a higher bed height since the uneven drag distribution between the dilute and dense regions is improved. On the opposite, the flow structure obtained from the modified Happel model validates our above proposed bubble formation mechanism.

3.4 Contribution due to particle collisional dissipation

A set of simulations for systems with non-ideal particle collision has also been carried out to identify the contribution of particle collisional dissipation to pattern formation. Figure 4.10 shows the effect of the voidage function exponent α on the bed pressure drop fluctuations. The corresponding flow structures are presented in Figure 4.11.

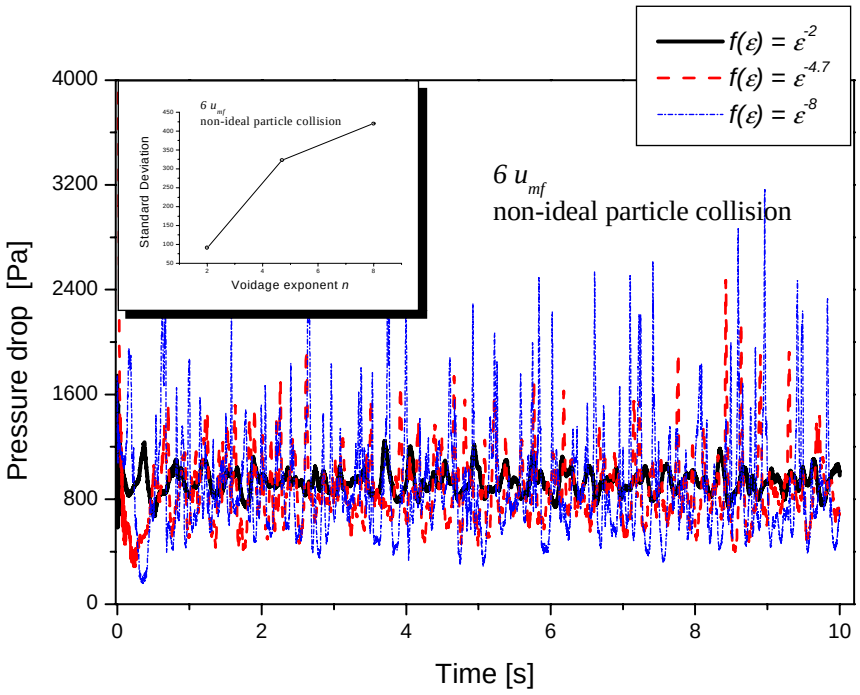

Figure 4.10: Variation of flow heterogeneity with voidage function exponent α expressed by pressure drop fluctuation in a gas-fluidized bed with non-ideal collision.

The heterogeneity in all these flows is much more pronounced than the heterogeneity observed for the ideal collisional systems. This demonstrates that particle collision, through inducing energy dissipation, enhances particle aggregation.

The flow structures computed by using the various drag correlations listed in table 4.1 are shown in Figure 4.11. It can be seen that the flow structures obtained by using these correlations differ only slightly when compared to the ideal collisional systems. Heterogeneity reduces from left to right in Figure 4.11, indicating that enhanced gas drag can improve homogeneous fluidization.

In Figure 4.12 the bed pressure drop and its fluctuation and the vertical position of bed mass center and its fluctuation are shown computed by using different drag correlations. It can be

seen that the differences produced by the various drag correlations are quite small generally when compared to the ideal collision system. Again, the simulations using the original and the modified Happel's correlations produce higher bed mass centers indicating that the increased drag in the dilute region can lead to incorrect prediction of flow structure (more homogeneity). This supports the pattern formation mechanism proposed previously.

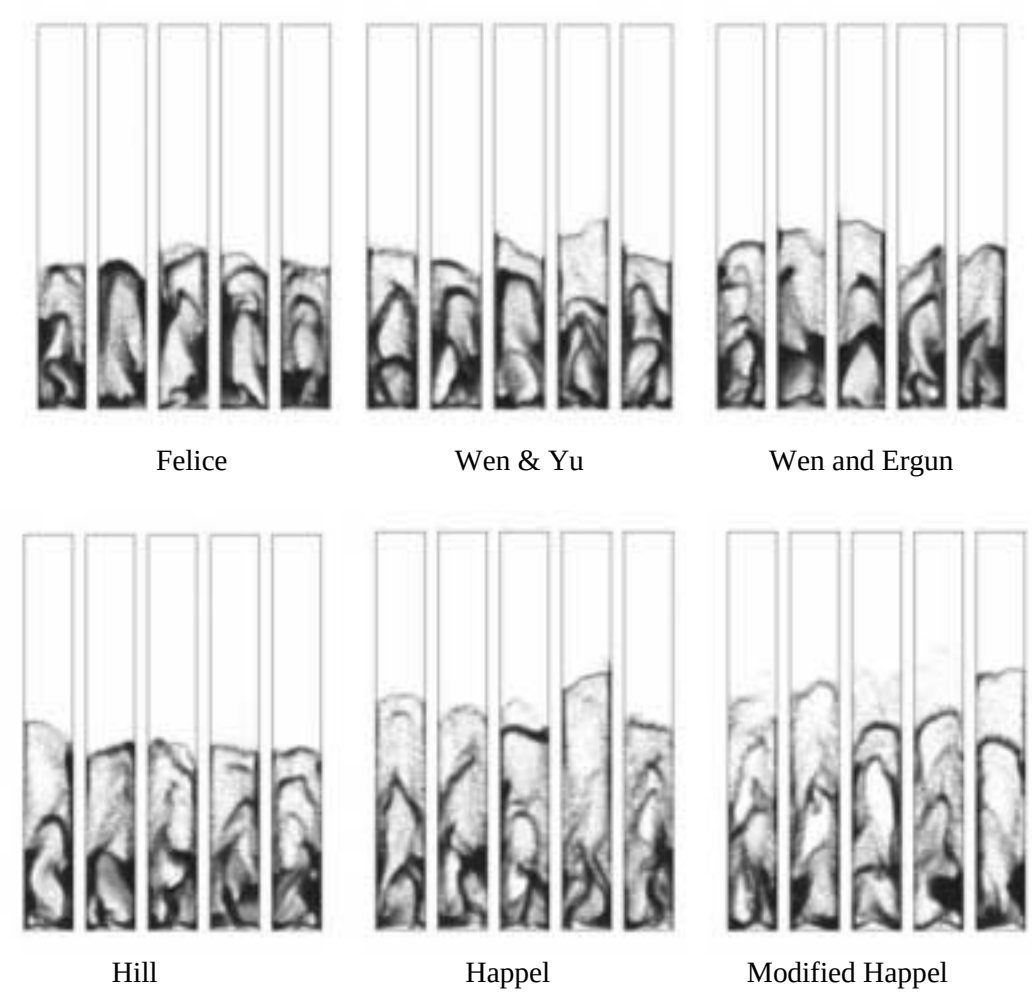

Figure 4.11: Snapshots of flow structures obtained for u_g = 1.8 m/s, non-ideal particle collision in a bed with 10 mm width and 80 mm height. The drag correlations for particles in assembly due to Wen and Yu, Felice, the combined Wen and Ergun, Hill et al., Happel and modified Happel are employed.

Particle motion analysis for non-ideal collisional systems has also been carried out. Figure 4.13 shows the time-series of the particle acceleration and void fraction in the vicinity of three types of reference particles. The positions of the particles in the bed are displayed in Figure 4.14.

Clearly, similar phenomena have been found in gas-fluidized beds with ideal particle-particle collisions: the particle in the emulsion phase is accelerated while the particle in the dilute phase is decelerated. Meanwhile, the particle at the boundary maintains steady motion (zero

acceleration). In contrast to the ideal collisional system, a clear-cut border between the emulsion phase and bubble phase prevails in non-ideal systems. This motion mode not only triggers bubbling, but also keeps this flow structure stable. Particularly, particle steady motion around the bubble boundary would assist to form a shell separating bubble gas and outer emulsion phase. From the perspective of particle motion, this could explain why a bubble remains stable

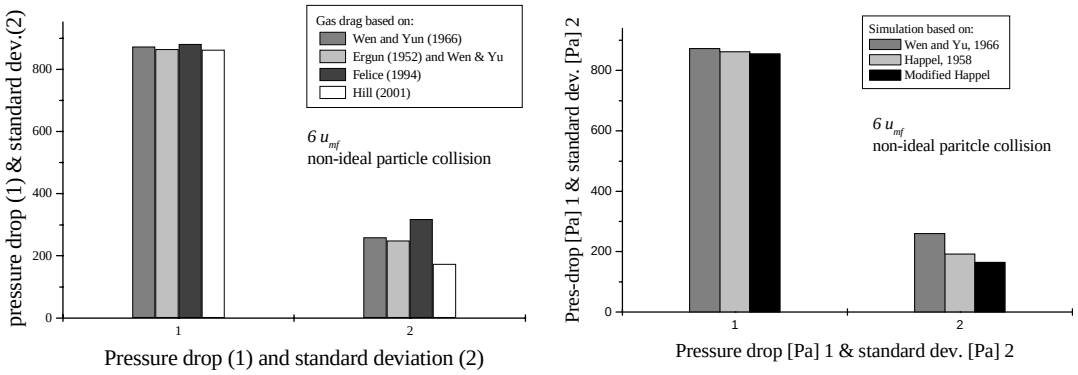

a) pressure drop

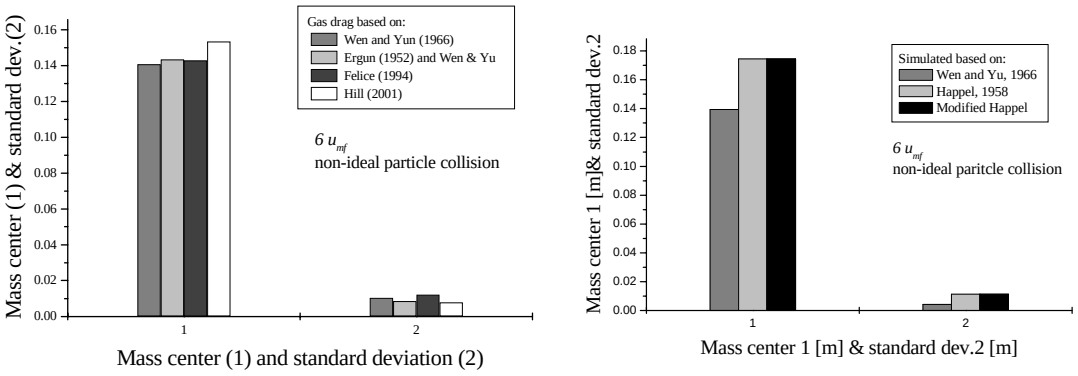

b) Bed mass center

Figure 4.12: Bed pressure drop and its fluctuation a) and vertical position of bed mass center and its fluctuation b) computed by using different drag correlations.

in a gas-fluidized bed. It would be interesting to examine the full picture of flow around a single bubble with respects to both particle motion and gas flow and connect the findings to Davidson's Bubble Theory.

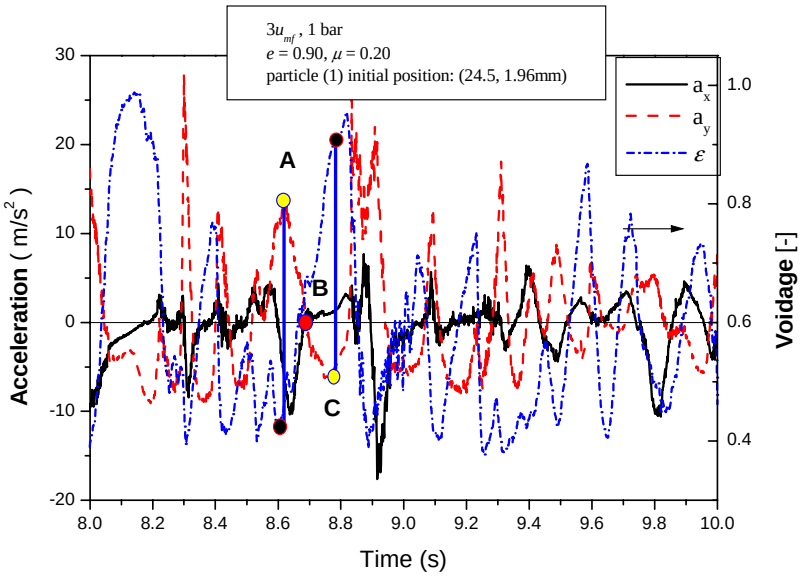

Figure 4.13: Acceleration of a single particle and its adjacent void fraction in a gas-fluidized bed with non-ideal collisional particles. The particle in the dense region is accelerated while particle in the dilute region is decelerated, leading to a "***phase separation***" phenomenon induced by non-linear gas drag.

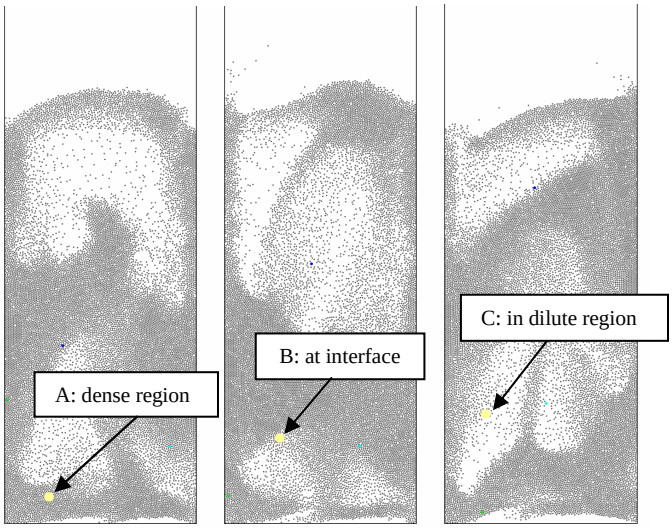

Figure 4.14: Positions of a single particle (light color) in the bed with non-ideal collisional particles (e = 0.9, μ = 0.30) at time 8.57 s (left, in dense region), 8.75 s (middle, at interface) and 9.07 s (right, in dilute region). Superficial gas velocity: 3u_{mf}, d_p = 0.947 mm, ρ_p = 1170 kg/m^3.

3.5 Conditions leading to homogeneous flows

Up to now, it has demonstrated that a heterogeneous flow structure in gas-fluidized bed is triggered by non-linear drag force and enhanced by dissipative particle-particle collisions. Also, the heterogeneity in ideal collisional systems has been clarified to be caused purely by non-linear drag. However, there indeed exist some systems, or at least some flow regimes, where particle collision is non-ideal but the flow structure is really homogeneous, such as fluidized Geldart group A powders at $u_{mf}<u_g<u_{mb}$, as well as liquid-fluidized beds. Why can a homogeneous flow structure prevail in these systems?

For Geldart group A powders attractive forces between the particles (Van der Waals forces) could lead to a kind of mechanical network of particles which to a certain extent can suppress disturbances (in voidage) and mountain stability of the system. In liquid-fluidized beds the fluid-particle interaction is very strong and the force balance (equilibrium) holds at the particle level with a very strong tendency to dampen any disturbance (due to non-ideal collisions) completely and maintain again system stability. These two structures root from different bases: the former results from particle controlling but the latter from fluid controlling.

According to the energy budget analysis for the homogenous flow regime for Geldart group B powder at elevated pressure (see Chapter 5) we have found that a relatively small portion of energy is distributed to collisional dissipation. Therefore, for non-ideal collisional particles, both the force balance and energy balance condition are necessary to guarantee an equilibrium state and therefore permit the existence of a homogeneous flow. For ideal collisional particles, due to zero collisional dissipative in the system (energy balance), the force balance for the particles itself can decisively ensure the existence of a homogeneous flow.

So, it can be deduced that only those systems with either equilibrium-suspended particles (force balance) or systems with a limited particle collisional dissipation (energy balance) can maintain a homogeneous flow structure. Since our hard sphere model can not handle systems with multiple particle contacts, the detailed exploration of the homogeneous flow structure formed in Geldart group A powder will not carried out here. It is definitely an interesting research topic in future.

4 Conclusions

Gas drag, or gas-solid interaction, plays a very important role in the formation of heterogeneous flow structures in dense gas-fluidized beds in case of both ideal and non-ideal particle-particle collision systems. With respect to gas drag acting on particles in suspension flow structure evolves dramatically, ranging from the pattern of homogeneity and small bed expansion to the pattern of strong heterogeneity and high bed expansion. The stronger the non-linearity, the more heterogeneous flow structure develop.

Regarding the quantification of gas drag the correlations due to Wen and Yu, Felice , Ergun and Wen and Yu and Hill and Koch have a similar capacity, but produce increasing drag (in the order given) leading to a certain degree of flow pattern evolution. Hill's equation results from Lattice-Boltzmann simulations and provides a good predictive capacity and therefore could replace the Wen and Yu equation to predict gas drag in gas-fluidized beds.

Particularly, it is discovered that the non-linearity of gas drag has a "phase separation" function by accelerating particles in the dense phase and decelerating particles in the dilute phase to trigger the formation of non-homogeneous flow structures. Meanwhile, the force balance holds for the particle at the interface to keep the co-existence of the bubble and emulsion phase stable. Particle collisional dissipation dramatically intensifies the formation of heterogeneous flow structures after the system equilibrium breaks.

The force balance condition ensures the formation of a homogenous pattern for systems without collisional dissipation. For dissipative systems, homogeneous flows are only possible in case both the force balance and energy balance are obeyed. Clearly, an elaborate correlation of the local gas-solid interaction based on first principles is urgently needed to completely master the quantitative description of dense gas-solid two-phase hydrodynamics.

Notation

C_d	drag coefficient, [-]
C	particle fluctuation velocity, m/s
d_p	particle diameter, m
e	coefficient of restitution, [-]
E	energy, J
$\mathbf{F}$	force, N
Fr	Froude number, [-]
f_s	solids volume fraction, [-]
$f(\varepsilon)$	voidage function, [-]
$\boldsymbol{g}$	gravitational acceleration, m/s^2
h	bed height, m
M	molecular weight, kg/mol
m	particle mass, kg
N	particle number, [-]
n	voidage exponent in R-Z equation, [-]
p	pressure, Pa
R	gas constant, J/mol K
Re	Reynolds number, [-]
R_p	particle radius, m
s	standard deviation of pressure, Pa
$\boldsymbol{S}_p$	source term defined in Equation 4.4
T	temperature, K
t	time, s
$\boldsymbol{u}$	gas phase velocity, m/s
$\boldsymbol{v}$, $\boldsymbol{V}$	particle velocity, m/s
V	volume, m^3

Greek symbols

α	voidage function exponent, [-]
δ	δ function,
ρ	density, kg/m^3
θ	granular temperature, m^2/s^2
ε	void fraction, [-]
β	volumetric inter-phase momentum transfer coefficient, kg/(m^{3}s)
μ_g	gas shear viscosity, kg/(ms)
μ	friction coefficient, [-]
$\boldsymbol{\tau}$	gas phase stress tensor, kg/ms^2

Subscripts

av	average
buoy	buoyancy
drg	drag
dsp	dissipated
f	fluid
g	gas phase
kin	kinetic
p, part	particle
s	single
t	terminal
x	x-component
y	y-component

References

Agarwal, P. K and O'neill, B. K. 1988 Transfer phenomena in multi-particle systems. *Chem. Eng. Sci*., **43**, 2487.

Ergun, S. 1952 Fluid flow through packed columns. *Chem. Eng. Prog*., **48**, 89.

Felice, R. D. 1994 The voidage function for fluid-particle interaction systems. *Int. J. of Multiphase Flows*, **20**, 153.

Happel, J. 1958 Viscous flow in multi-particle systems: slow motion of fluids relative to beds of spherical particles. *AIChE J.*, **4**, 197.

Helland, E., Occelli, R. and Tadrist, L. 2000 Numerical study of cluster formation in a gas-particle circulating fluidized bed. *Powder Tech.*, **110**, 210.

Hill, R. 2001 *The Effects of Fluid Inertia on Flow in Porous Media.* Ph.D. dissertation, Cornell University.

Hoomans, B. P. B., Kuipers, J. A. M., Briels, W. J. and van Swaaij, W. P. M. 1996 Discrete particle simulation of bubble and slug formation in a two-dimensional gas-fluidized beds: a hard sphere approach. *Chem. Eng. Sci.*, **51**, 99.

Li, J. and Kuipers, J. A. M. 2001 Effect of pressure on flow behaviors in dense gas-fluidized beds: a discrete particle simulation, *Fluidization* X, M. Kwauk, J. Li and W.-C. Yang eds., Beijing: Engineering Foundation, p.389.

Jaeger, H. M., Nagel, S. R. and Behringer, R. P. 1996 Granular solids, liquids and gases. *Rev. Mod. Phys*., **68**, 1259.

Jean, R. H. and Fan, L. S. 1992 On the model-equations of Gibilaro and Foscolo with corrected buoyancy force. *Powder Tech*., **72**, 201.

Choi, H. G. and Joseph, D. D., 2001 Fluidization by lift of 300 circular particles in plane Poiseuille flow by direct numerical simulation. *J. Fluid Mech*., **438**, 101.

Koch, D. L. and Hill, R. J. 2001 Inertial effects in suspension and porous-media flows. *Annu. Rev. Fluid Mech*., **33**, 619.

Koch, D. L. and Sangani, A. S. 1999 Particle pressure and marginal stability limits for a homogeneous mono-disperse gas fluidized bed: kinetic theory and numerical simulations. *J. Fluid Mech*., **400**, 229.

Morgan, J. P., Taylor, R. W. and Booth F. L. 1970/1971 The value of the exponent *n* in the Richard and Zaki equation, for fine solid fluidized with gases under pressure. *Powder Tech..*, **4**, 286.

Richardson, J. F. 1971 Chapter 2 in *Fluidization*, J. F. Davidson and D. Harrison eds., Academic Press, New York.

Rowe, P. N. 1987 A convenient empirical equation for estimation of Richard-Zaki exponent. *Chem. Eng. Sci.*, **42**, 2795.

Wen, C. Y. and Yu Y. H. 1966 Mechanics of fluidization. *AIChE Series*, **62**, 100.

Wylie, J. J. and Koch D. L. 2000 Particle clustering due to hydrodynamic interactions. *Physics of Fluids*, **12**, 964.

Zhang, J., Fan, L-S., Zhu, C., Pfeffer R. and Qi, D. 1999 Dynamic behavior of collision of elastic spheres in viscous fluids. *Powder Tech*., **106**, 98.

Chapter 5

PARTICLE COLLISION IN GAS-FLUIDIZED BEDS

Abstract

Particle collision, or particle-particle interaction, plays an important role in pattern formation through dissipating particle suspension energy. This chapter is devoted to understanding this role in a variety of flow phenomena in dense gas-fluidized beds, with focus on bubbling and jetting flows, regime transition and pressurized homogeneous flows.

It is shown that each bubble feeds back to the emulsion phase an extremely strong collisional dissipation. The most pronounced random motion of particles occurs in the wakes of bubbles and at two wings below the bubbles. Gas jets introduce pronounced spatial variation of particle-particle collisional interaction characterized by a "Gauss" or "M" type distribution. The granular temperature distribution is highly non-uniform in the bed with a maximum value in the jet region of up to 6 ~ 7 times the average value.

The simulation also demonstrates that at elevated pressure the incipient fluidization velocity decreases, whereas the uniform fluidization regime widens leading to a quick transition to the turbulent regime. Particularly, it is found that high pressure, through enhancing gas-solid interaction and reducing the particle collision frequency, efficiently suppresses formation of large bubbles. As a consequence, more uniform gas-solid flow structures are produced leading to particulate fluidization.

Additionally, it is interestingly found that particle collisional dissipation directly corresponds to the regime transition from homogeneous flow to the bubbling flow. In the homogeneous flow regime, less energy budget is distributed to dissipative collisions. With increasing gas velocity, a bigger portion of energy is consumed by particle collisions and gas suspension therefore gradually gives the way to particle collision. The transition to bubbling flow is realized when the collision dissipation arrives at its maximum.

High fluid density leads to an earlier transition to turbulent fluidization where particle-particle interaction is further intensified. Meanwhile, there exists the strongest particle

collision in the annular region in turbulent fluidized beds and at the bed surface in bubbling fluidized beds.

1. Introduction

Particle-particle interaction plays a very important role in a variety of industrial processes employing particulate solids, such as fluidized beds, spray dryers, blenders, to name just a few. Due to the complexity of the particle motion in (dense) gas-solid flows, it has, however, been treated in a simple way, if not neglected. Up to now, there is still very limited knowledge available to clarify its role in flow phenomena, such as bubble and cluster formation and regime transition. This seriously prevents our understanding of particulate flows and the development of efficient processes involving particulate solids.

In many fluidization studies the particulate phase is assumed to constitute a continuous medium without internal interactions (Davidson, 1963; Jackson 1963). The bubble/emulsion two-phase model is widely applied to explain the various phenomena in gas-fluidized beds. Hoomans (2000) found that particle collisional properties seriously affect the bubble formation. It has also been demonstrated (see Chapter 3) that bubble size increases with intensified particle collisional dissipation. Apparently, besides the gas-solid interaction as clarified in Chapter 3, particle collision also plays an essential role in the formation of the heterogeneous flow structure.

The effect of the particle-particle collisional dissipation itself is definitely important for flow structure formation and evolution, as evidenced in Chapter 3 and Hoomans' work (1996, 2000). However, once a bubble or jet is formed, it feeds back to the particulate phase its influence. Also system pressure will have great impact on hydrodynamics since it changes gas-solid and solid-solid interactions. In this study, we aim to explore the role of particle-particle interaction in some typical phenomena encountered in particulate flows. Particularly, we are interested in the following questions: 1) why do bubbles prevail in a strong particle collisional system? 2) What role does the collisional dissipation play in the regime transition? 3) How does elevated pressure affect fluidization quality?

Particle collision in the vicinity of bubbles and jets will first be examined to understand what they feed back to the system. Then, results of two parallel sets of simulations conducted at atmospheric and elevated pressure will be reported to elucidate the effect of pressure on flow structure, gas bubble behavior and flow regime transition. Particularly, the associated energy budget analysis is used to obtain insight into the G-S-S interactions in gas-fluidized beds and clarifying why elevated pressure produces a more homogeneous flow. Finally, the fluid density influence will be highlighted.

2. Simulations

The simulation conditions for the bubbling regime and the related parameters are listed in Table 5.1. To examine the jet influence, a nozzle positioned at the center of the gas distributor is used whereas the remaining part of the bed is kept at incipient fluidization conditions. The other conditions for the bed with a jet are the same as those for the bubbling bed simulation. The computational grid is employed as the reference volume to calculate the average particle velocities and then to evaluate the granular temperature.

Table 5.1: Simulation conditions for bubbling and jetting fluidized beds.

Parameter	Value(s)
Bed geometry	2-D
Width (cm)	9
Height (cm)	25
Nozzle diameter (mm)	9, at center of the bed
Particles	Polystyrene
Diameter (mm), Number	1.545, 3400
Density (kg/m^3)	1170
Incipient fluid. vel.(m/s)	0.472
Simulation	
Grid	20×40
Total time (s), time step (s)	15 (bubble) and 5 (jet) ; 1×10^{-4}
Restitution Coef. Norm. (p-wall & p-p)	0.90
Shear	0
Friction Coef. Norm. (p-wall & p-p)	0.25
Shear	0
Gas velocity (m/s)	
Fluidization	0.9 ($1.9\ u_{mf}$)
Jet	Run 1: 11.8 ($25u_{mf}$, permanent jet)
	Run 2: 5.90 ($12.5u_{mf}$, bubbling string)

The simulation conditions to examine the pressure influence are summarized in Table 5.2. A series of simulations has been performed using different superficial gas velocities. Higher bed heights were employed to accommodate the bed expansion in the turbulent fluidization regime.

Table 5.2: Simulation conditions to examine the pressure influence in gas-fluidized beds.

Bed geometry	2-D
Width (cm) × Height (cm)	$10 \times 40 \sim 80$
Particles	
Diameter (mm), Density (kg/m^3)	0.949, 1170
Number [-]	16,000
Incipient fluid. vel.(m/s)	0.301 (for 1 bar), 0.105 (for 21 bar)
Simulation	
Grid	20×40 or 80 cells
Total time (s) & Time step (s)	10, 1×10^{-4}
Restitution Coef.: Norm. (p-w & p-p)	0.95 or 0.00 (ideal)
Shear	0
Friction Coef.: Norm. (p-w & p-p)	0.30 or 0.00 (ideal)
Shear	0
Operation conditions	
Superficial gas vel. (m/s)	For 1 bar: *0.05 ~ 3.0* For 21 bar: *0.05 ~ 1.0*
Static bed height (m)	0.15
Porosity at incipient fluidization [-]	0.4
Pressure (bar)	1, 21

3. Results and Discussion

3.1 Bubble and jet influences

3.2.1 GAS BUBBLE-INDUCED PARTICLE COLLISION

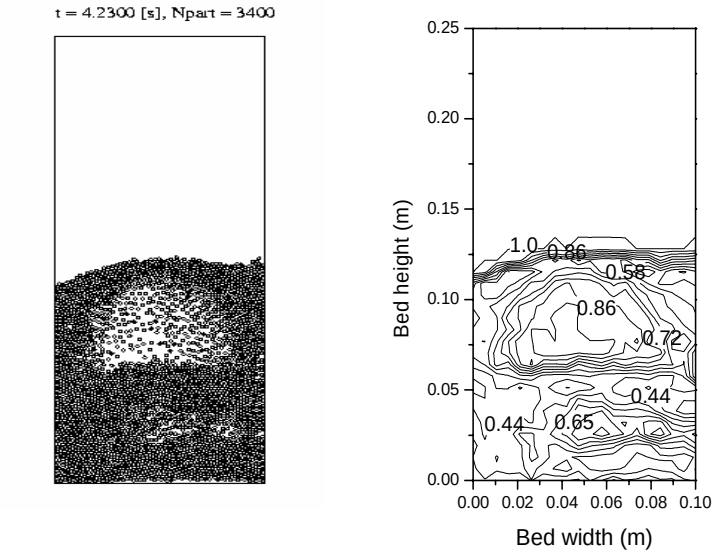

Figure 5.1: Two-phase structure (left) in snapshot and (right) in voidage distribution in a bubbling fluidized bed.

To explore the feedback effect of bubbles to the emulsion phase, two kinds of information are required: flow structure and granular temperature distribution. Figure 5.1 shows the typical simulation result of flow structure in terms of a snapshot of particle configuration and the

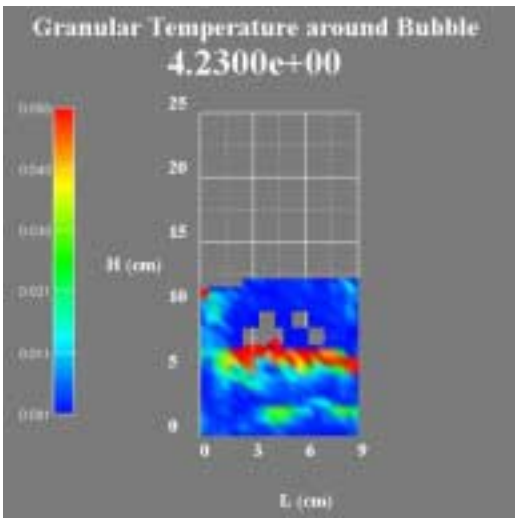

Figure 5.2: Granular temperature distribution around a single bubble in a gas-fluidized bed.

corresponding voidage distribution. Figure 5.2 presents the corresponding granular temperature distribution around bubble compiled by AVS/Express graphical display technology.

Clearly, just below the bubble in the wake region, there exists an extremely high granular temperature, indicating the strong particle-particle collisional interaction. The granular temperature distribution as shown in Figure 5.3, indicates that the bubble actually induces three zones of increased random granular motion. One is located at the center of the bubble wake whereas the other two are located at the left and right of the bubble base.

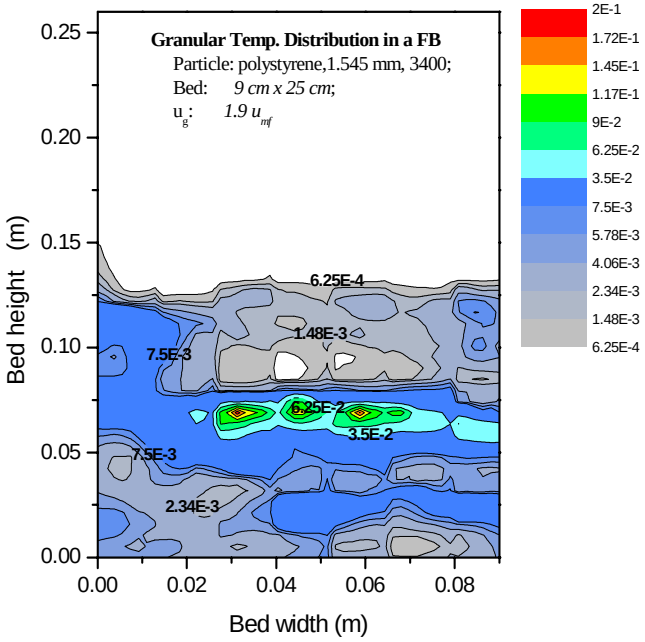

Figure 5.3: The detailed granular temperature distribution around a single bubble in gas-fluidized beds: *three hot spots*.

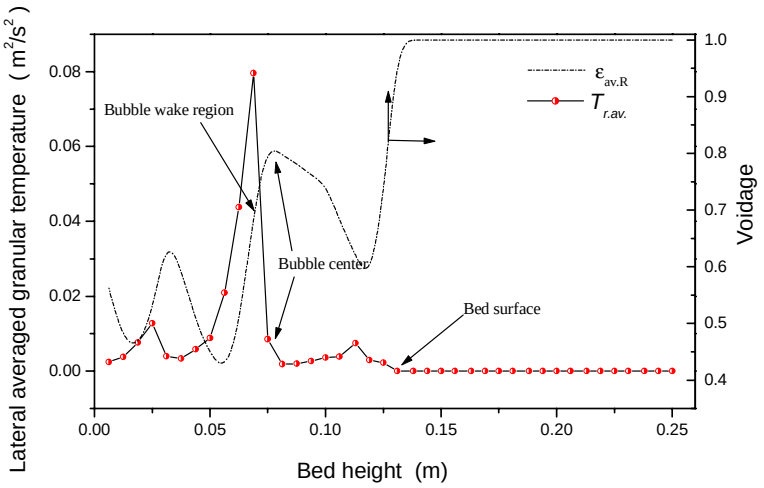

Figure 5.4: Granular temperature as a function of bed height

In order to locate the exact position of the intensive particle-particle interaction region, the lateral-averaged granular temperature and corresponding voidage distribution along the bed height are also plotted, as shown in Figure 5.4. Clearly the bubble introduces an extremely strong particle-particle interaction in the wake region of the bubble.

Figure 5.5 shows the lateral granular temperature distribution at several axial positions in the bed. We can see that most granular temperatures at the bed height of 6.25 cm exceed 0.03 m^2/s^2 with a maximum value of $0.11 m^2/s^2$, which is $6 \sim 22$ times as high compared to those at an elevation of 3.75 cm. Again, we notice the strong feedback effect of the bubble to the emulsion phase.

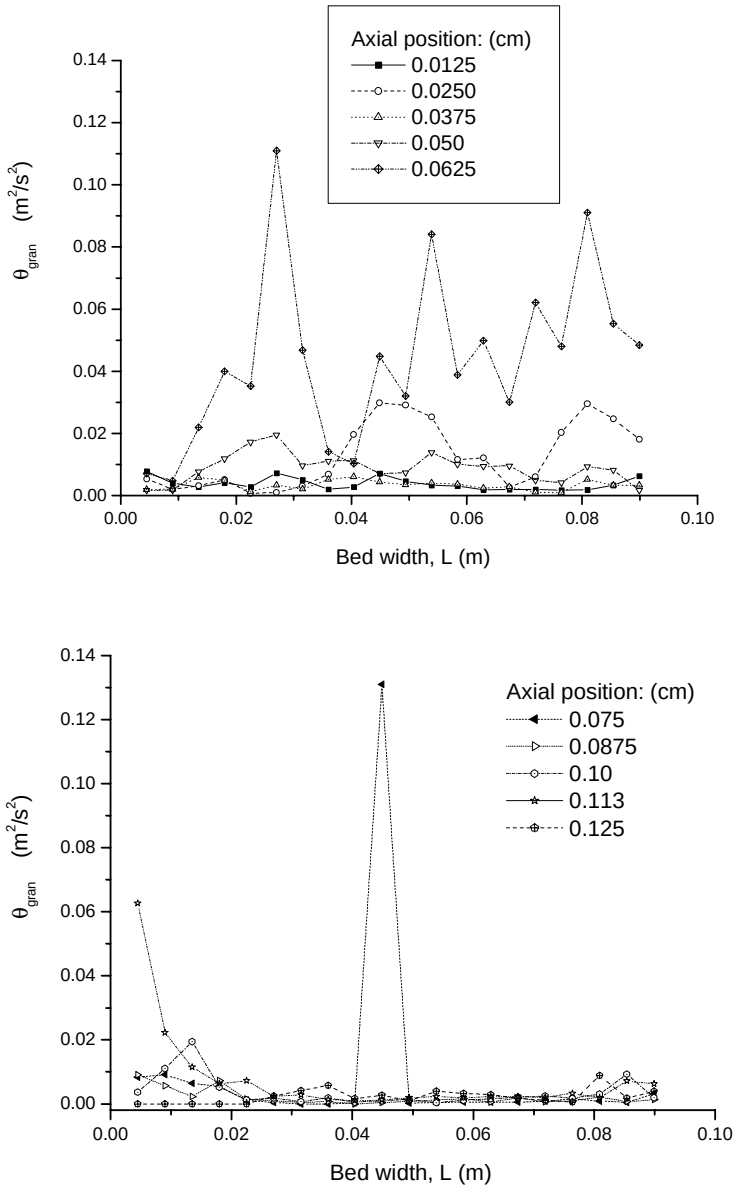

Figure 5.5: Lateral granular temperature distribution in a bubbling fluidized bed at several axial positions in the bed.

The simulation results for glass beads (bed of 15 mm in width and 50 mm in height, glass beads with density of 2600 kg/m^3, 1.8u_{mf}) exhibit the same trends as the case described previously, but with even stronger particle collisional dissipation. The granular temperature distribution, at t ≈ 14 s is shown in Figure 5.6. A fifteen-second movie of the granular temperature distribution indicated the universal nature of this phenomenon in dense bubbling beds.

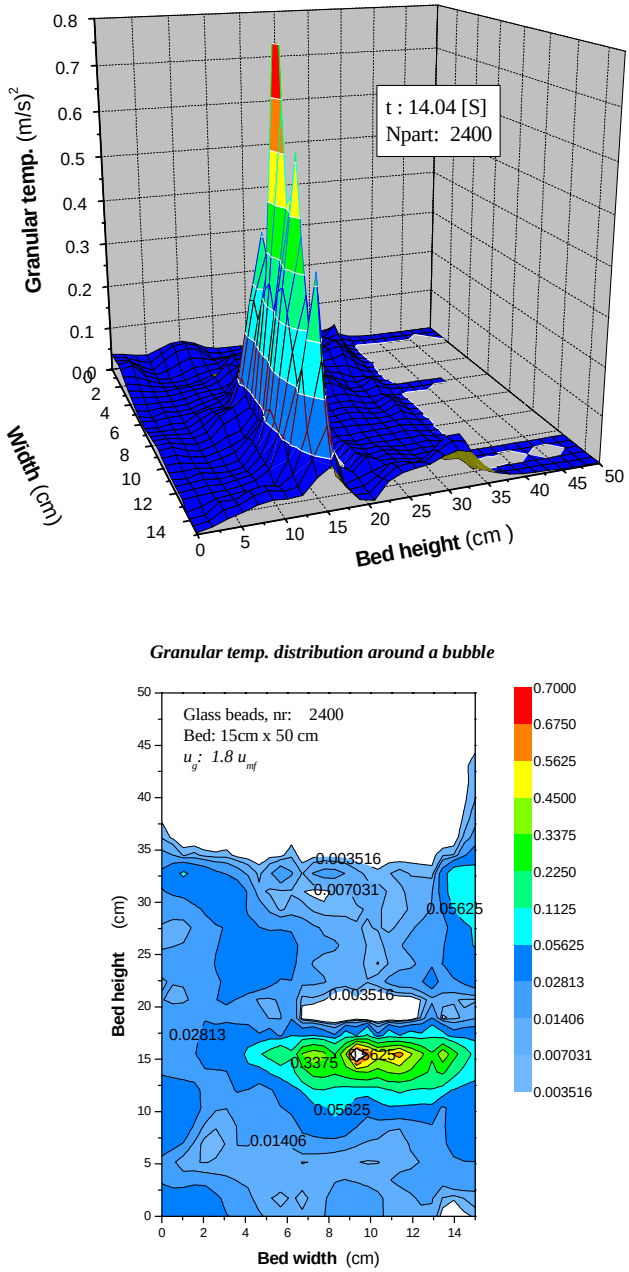

Figure 5.6: Granular temperature distribution around a single bubble in a gas-fluidized bed. (2-D bed with 15 cm in width and 50 cm in height, glass beads, 1.8u_{mf})

A high granular temperature implies a strong fluctuating motion, intensive particle-particle collisions and associated mixing of particles. The special granular temperature pattern around a bubble demonstrates that a pronounced difference of particle–particle interaction exists

between the upper and bottom boundaries of the bubble. Near the upper boundary, particles are in near equilibrium (see chapter 4) and therefore the fluctuating motion is suppressed. Due to the very small drag inside a bubble (dilute), the upper boundary is not influenced by particles present inside the bubble.

On the contrary, the bottom boundary experiences a different gas-particle and particle-particle interaction. The under pressure sucks a certain amount of particles into bubble (Davidson, 1971). However, the solid fraction inside bubble is not large enough to produce enough drag to carry the particles and consequently they fall down. When encountering the upward moving particles, strong collisional interaction occurs. When the descending solids flows around the bubble they encounter upward moving wake solids and consequently intensive collisional interaction prevails producing two zones of high granular temperature.

3.2.2 GAS JET-INDUCED PARTICLE-PARTICLE COLLISION

In many gas-fluidized beds gas is introduced via jets and therefore gas-jet-induced particle-particle interaction has also been studied. When the gas injection velocity is slow, the gas passes through the bed in a series of subsequent bubbles. As the injection velocity is increased a string of bubble is produced. At very high gas velocities a permanent jet is formed.

3.2.2.1 Permanent jet (fountain) regime

Figure 5.7 shows a snapshot of the particle configuration at t ≈ 1.3s and the corresponding time-averaged granular temperature distribution (5 s of averaging). It can clearly be seen that the highest granular temperature is obtained near the surface of the emulsion phase contacting the spout. (i.e. gas core)

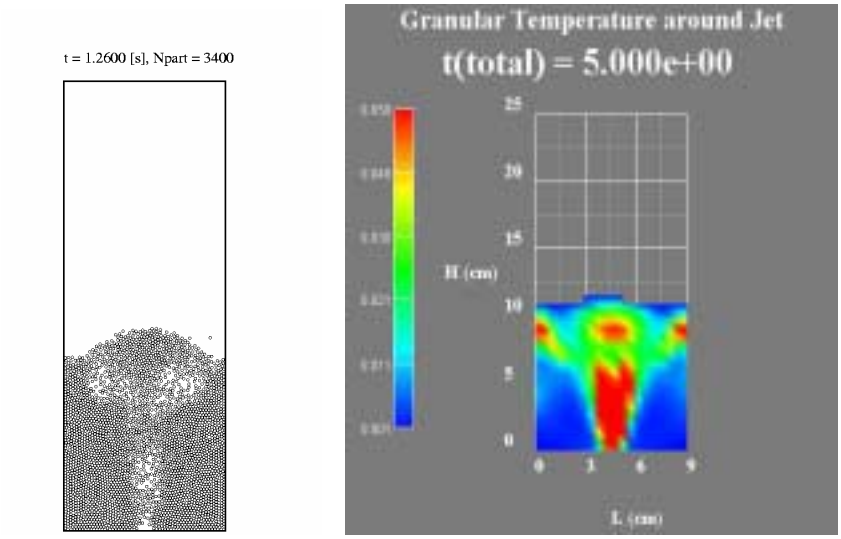

Figure 5.7: Fluidized bed with a permanent jet flow: (left) particle configuration, (right) time-averaged granular temperature distribution in a fluidized bed. (25 u_{mf})

The lateral, granular temperature distribution displays a Gaussian shape. This distribution transforms into an "M" distribution (see Figure 5.8) at higher elevation in the bed. This distribution remains present until the bed surface where two streams of circulating particles with relative slow velocities re-cycle back into the jet. Upward further along the jet center line, the fountain zone with relative large velocity difference is encountered producing a second zone with high granular temperature.

Clearly, permanent jet operation also induces an extremely intensive particle-particle collisional interaction inside a gas-fluidized bed.

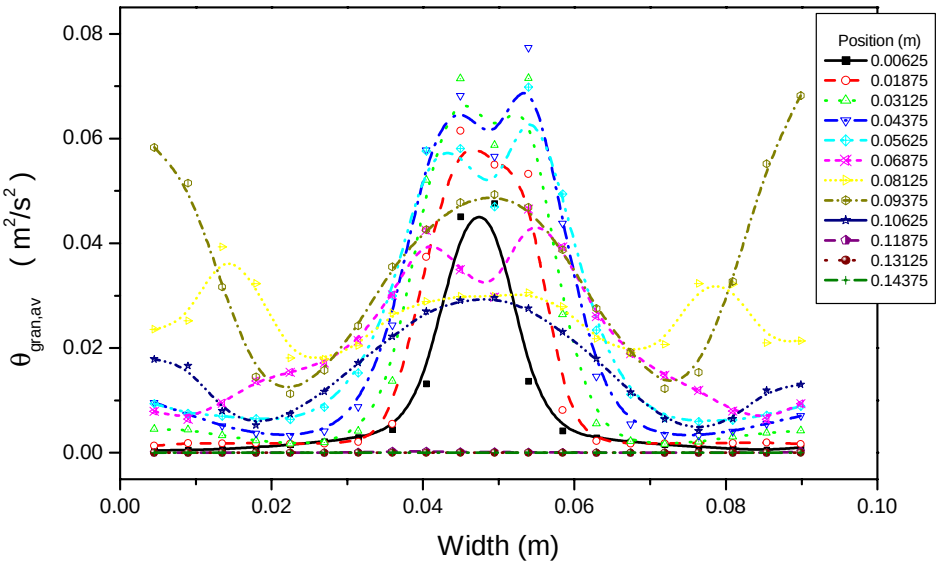

Figure 5.8: Time-averaged lateral granular temperature distribution in a jet fluidized bed ($25\ u_{mf}$)

3.2.2.2 Bubble string flow regime

Figure 5.9 shows a snapshot of particle configuration and associated time-averaged granular temperature distribution for the bubble string flow regime. The lateral granular temperature distribution shows the same trend as those in the bed with a permanent jet, although the granular temperature is lower. In Figure 5.10 the evolution of the time-averaged lateral granular temperature distribution is shown as a function of the axial position. Once again, it is evident that in this flow regime also intensive particle-particle collisional interaction prevails, despite the fact that the gas velocity is not so high.

To alleviate any initial effects, an additional simulation with 10 s of jet operation was performed. The time-averaged granular temperature distribution, as shown in Appendix Figure A5.5, compares very well with the previous images. It is therefore concluded that the reported results are not sensitive with respect to the duration of the simulation.

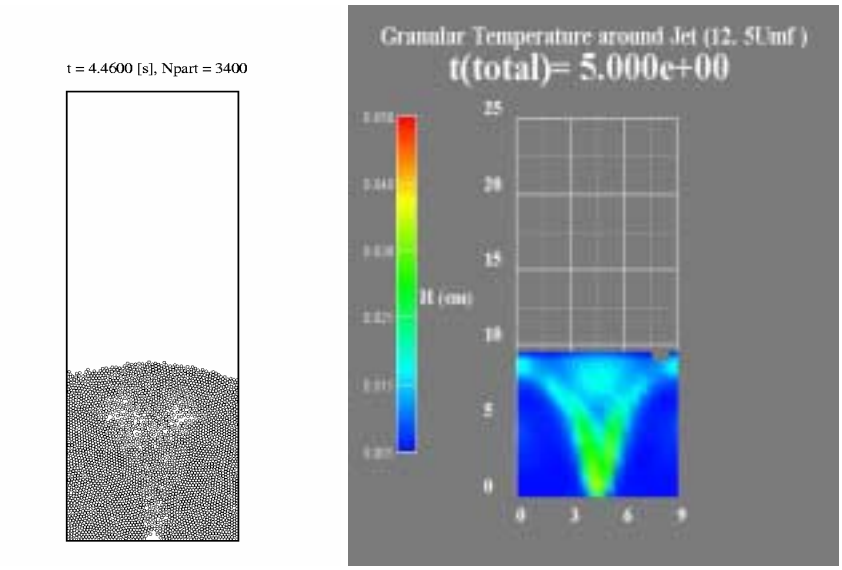

(a) (b)

Figure 5.9: Snapshot of fluidized bed in bubble string flow regime: (a) particle configuration, (b) time-averaged granular temperature distribution.

Because gas jets naturally form near distributors and produce strong collisional dissipation, this easily provides the necessary condition, namely voidage variation, to trigger flow instability. Therefore, the distributor (including the jets) should be designed with extreme care to avoid high-velocity jets if one desires to obtain a relatively homogeneous flow structure. It would be interesting to carry out further work to understand how jet behavior is related to the overall flow structure in fluidized beds.

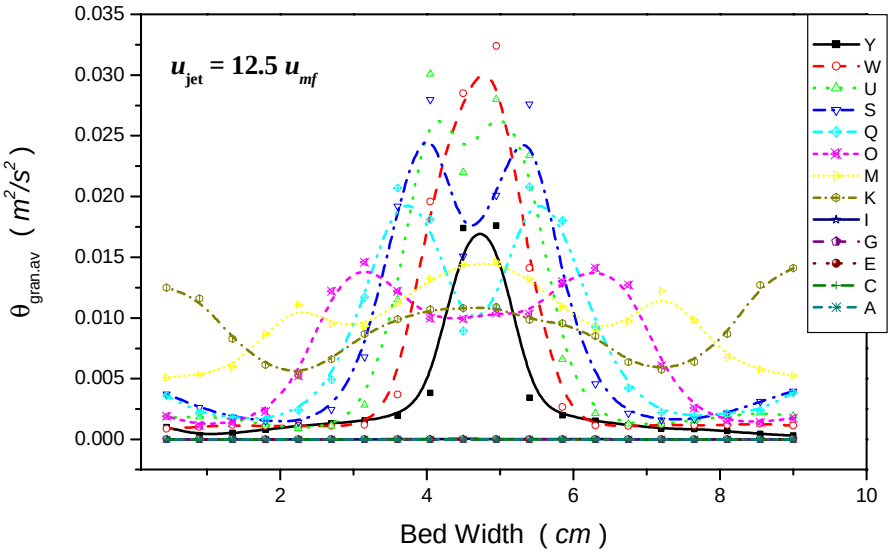

Figure 5.10: Time-averaged granular temperature distribution in a gas-fluidized bed with a bubbling string flow.

3.2 Pressure influence

3.2.1 EFFECT ON FLOW STRUCTURE

High pressure may change particle-particle and particle-fluid interactions, which would lead to the different flow patterns. These patterns, or alternatively heterogeneous structures, have a pronounced effect on gas-solid contacting. As a first step, the following simulations for the same flow regime but different pressure were carried out to understand this effect: 1) immediately above incipient fluidization point (homogeneous fluidization regime), 2) bubbling regimes and 3) near turbulent regimes.

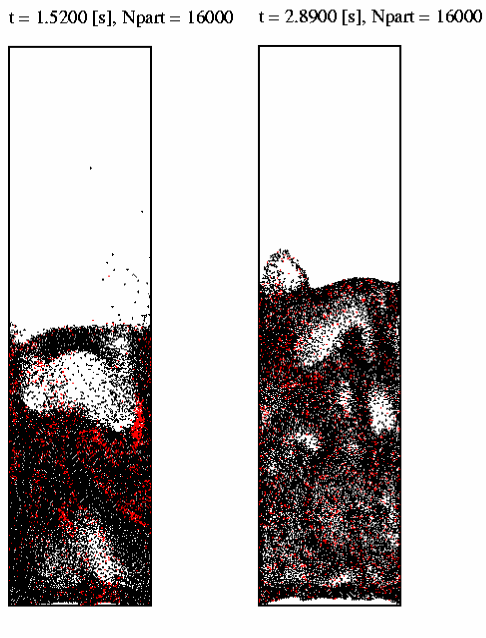

Figure 5.11: Typical flow structures computed in the bubbling regime: *pressure effect* (left: 1 bar, $2.7u_{mf}$; right: 21 bar, $3u_{mf}$).

Immediately above the incipient fluidization point there exists a homogeneous flow structure in the high-pressure case (21 bar) whereas on the contrary no homogeneous gas-solid patterns are found at atmospheric conditions (1 bar). In the latter case, occasional small bubbles or voids pass through the bed with a relatively lower bed height compared to the high pressure case.

Figure 5.11 shows the simulation results obtained in the bubbling regime at 1 bar and 21 bar. The heterogeneous gas-solid two-phase flow structures at atmosphere conditions, characterized by the presence of big bubbles, dominate the flow. On the contrary, at high pressure the voids are best described as swirling tongue-shaped masses containing gas and solids with no stable boundary, which corresponds to the experimental findings of Fan and

Danko (1984). Thus, at higher pressure the bubble growth is efficiently suppressed and as a consequence thereof a more uniform gas-solid flow structure is produced. Meanwhile, the bed height for the high pressure case is higher too, indicating availability of more free space for each individual particle.

Figures 5.12(a) and 5.12(b) show the simulation results near the turbulent regimes at 1 bar and 21 bar respectively. Once again the flow patterns for the high-pressure case display the uniform two-phase flow structures. Interestingly, bed pressure drop is characterized by a lower amplitude but higher frequency, indicating that there still exist heterogeneous local flow structures. However, they are much smaller compared to those obtained in the low

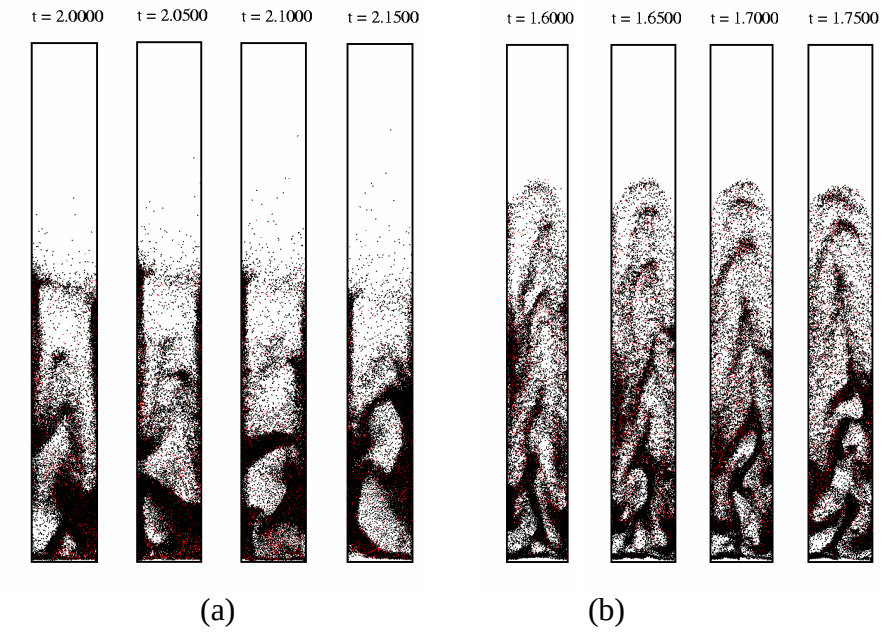

Figure 5.12: Flow structures near turbulent regime at (a) 1 bar, $8u_{mf}$ and (b) 21 bar, $8u_{mf}$.

pressure case and in the range of meso-scale size. Additionally the simulation shows that the particle-particle collision frequency for the high-pressure case is much less compared to the corresponding low-pressure case. This evidence once again elucidates that fewer particle-particle encounters prevail at elevated pressure.

3.2.2 EFFECT ON THE REGIME TRANSITIONS

Simulations at the various flow regimes were carried out by employing the hard-sphere model and the results of the variation of the bed pressure drop versus superficial velocity are shown in Figures 5.13(a) and 5.13(b) at 1 bar and 21 bar respectively. It should be stressed here that the gas phase turbulence was not taken into account in these simulations.

By comparing the flow regimes obtained at high pressure and atmospheric conditions, we can draw the following conclusions. 1) The standard deviation of the pressure drop signal at elevated pressure is higher than that for the atmospheric case demonstrating that elevated pressure produces a more homogeneous two-phase flow. 2) High pressure reduces the incipient fluidization velocity, at our simulation conditions from 0.3 m/s at 1 bar to 0.105 m/s at 21 bar. The incipient fluidization point in the elevated pressure case could be predicted satisfactorily.

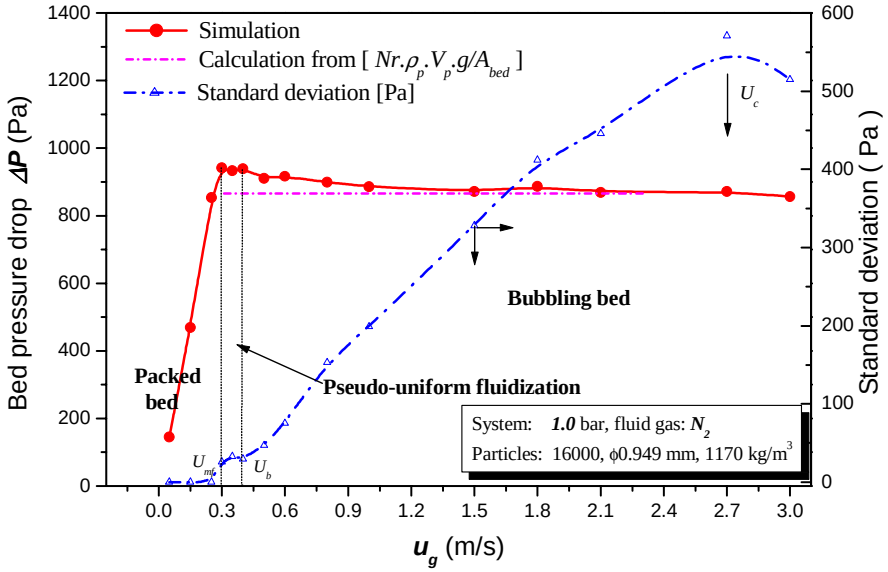

(a) 1 bar

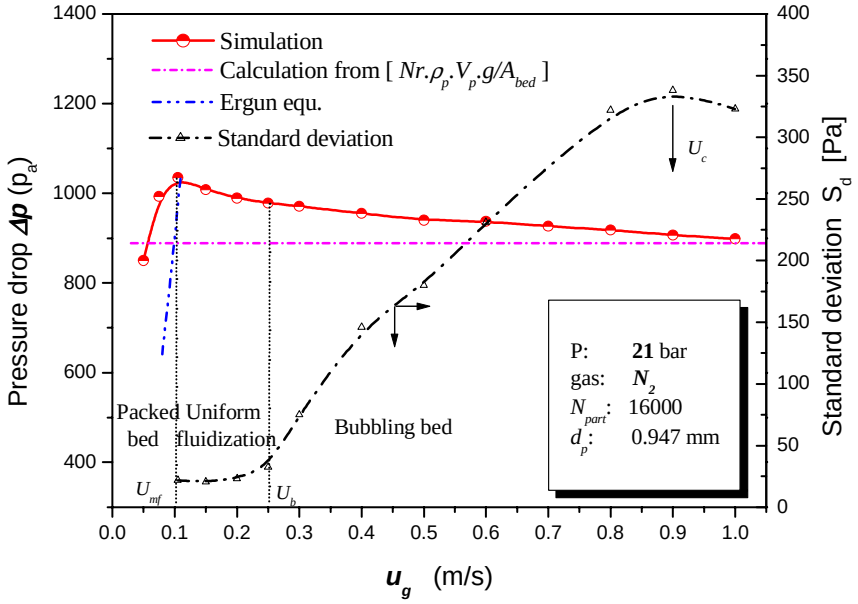

(b) 21 bar

Figure 5.13: Simulated flow regimes at different pressures: a) atmospheric and b) elevated.

3) There exists a wider homogeneous particulate-fluidization regime (0.105 ~ 0.25 m/s at 21 bar and 0.30 ~ 0.40 m/s (pseudo-homogeneous) at 1 bar) but a more narrow bubbling regime in the high pressure case compared to atmospheric conditions. 4) At elevated pressure increasing gas velocity more easily leads to the transition of the fluidization regime from bubbling to turbulent (0.9 m/s) indicating that high pressure shortens the bubbling regime, 5) The computed pressure drop agrees well with the theoretically predicted pressure drop. The deviations near the incipient fluidization point are owing to the contribution of gas phase and the friction loss between the fluid and the bed wall, which is more pronounced in the high pressure case.

3.2.3 EFFECT ON FLUID-PARTICLE-PARTICLE INTERACTIONS

The results mentioned above demonstrate that elevated pressure significantly affects the hydrodynamics of the gas-solid two-phase flows both from the macro-scale and from the meso-scale point of view and tends to form the particulate fluidization. Then, why and how does it introduce such a remarkable change? As we know, there are three kinds of interactions in dense gas-particle flows: internal interactions in both the solid phase and the gas phase and particle-fluid interactions. Therefore, detailed examination of these interactions from a micro-scale point of view at the different operation conditions would help us to understand the influencing mechanisms. For the gas-solid two-phase flow operating at low gas velocity, it is important to consider 1) particle-particle interactions and 2) particle–fluid interactions, which will subsequently be examined in more detail.

3.2.3.1 Effect on the particle-particle interaction

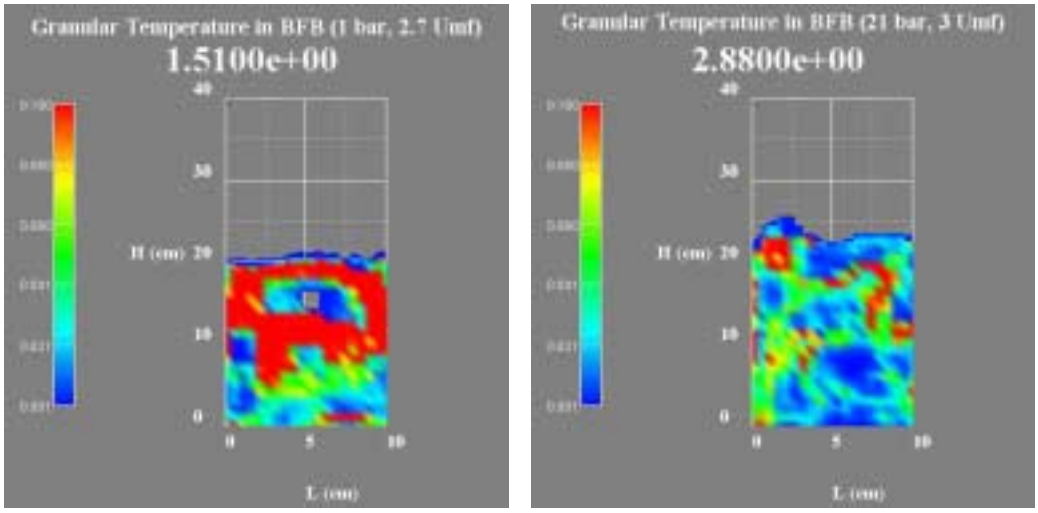

(a) (b)

Figure 5.14: Granular temperature distribution in fluidized beds operating at (a) 1 bar, $3u_{mf}$; (b) 21 bar, 2.7 u_{mf}

By employing the granular temperature, defined similarly as in kinetic theory of granular flow, we obtained the interaction distribution in the gas-fluidized beds. Figure 5.14 presents two snapshots of the granular temperature distribution in gas-fluidized beds corresponding to flow structures prevailing at 1 bar and 21 bar respectively. From the figures we can clearly see that elevated pressure produces a very uniform distribution with lower value, i.e. moderately intense particle-particle collisions. On the contrary at atmospheric pressure a pronounced non-homogeneous distribution is obtained indicating intense interactions between the particles. Particularly, the most intensive particle collisions prevail in the regions around the bubbles where the granular temperature can be eight times higher than that of the surrounding emulsion phase.

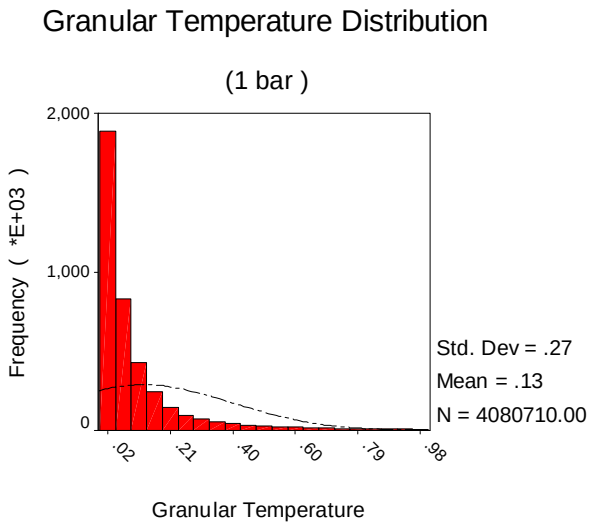

Figure 5.15: The frequency distribution of local granular temperature (m^2/s^2) in a gas-fluidized bed at 1 bar. (10 seconds).

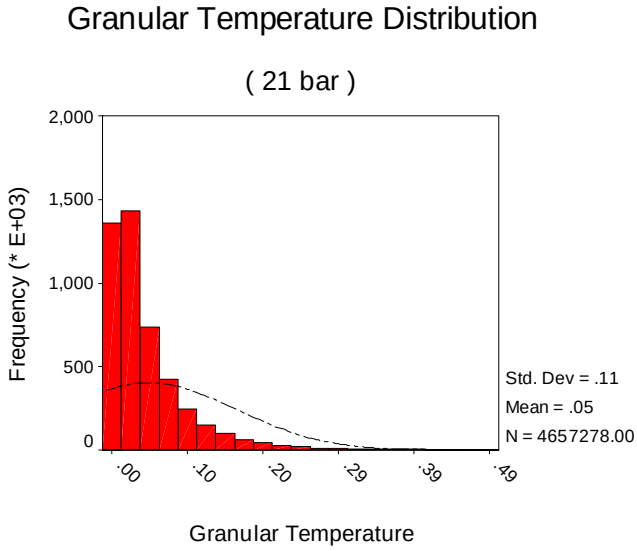

Figure 5.16: The frequency distribution of local granular temperature (m^2/s^2) in a gas-fluidized bed at 21 bar (10 seconds).

Additionally, statistics analyses of granular temperature data in time/spatial domains are also carried out to quantitatively understand the effect of pressure on particle-particle interaction. The zero value is skipped during the statistical analysis (zero in granular temperature means that the region either is occupied by gas only or packed with static particles). Figures 5.15 ~16 show the results for both cases respectively. Compared to the case at 1 bar, the spatial-averaged granular temperature at 21 bars is much lower, demonstrating that elevated pressure effectively reduces particle-particle collisions.

The other important parameter in the statistics is the "standard deviation", which represents the extent of the collisional intensity variation. Clearly, from the figures we can see that the granular temperature distribution at 1 bar is broader than that at 21 bars, indicating that there exists a stronger heterogeneity in time/space domains at 1 bar. In other words, high pressure yields in a more uniform flow structure.

3.2.3.2 Effect on particle-fluid interaction and energy distribution

Since the particle-fluid interaction accounted for in our model is based on a semi-empirical formula as used by Hoomans (2000), it is impossible at this stage to directly obtain insight on this issue from the simulation. However, by comparing the two kinds of energy dissipated due to particle-particle interaction and fluid-particle interaction we can understand indirectly this interaction from the macro-scale because both sources of energy dissipation can be easily obtained from our model. Additionally, the pressure influence on the gas-solid two-phase flows can be elucidated.

Figure 5.17 presents the results of the energy analysis obtained at pressures of 1 bar and 21 bars. Here, f represents the ratio of one kind of particle energy to the particle total energy, drawing from gas phase by drag force and the initial particle energy. Three main kinds of energy distributions are displayed in Figure 5.17, including kinetic, potential, dissipation energy due to particle collisions. Apparently, there are very remarkable differences for the energy distribution for particle collisional dissipation and suspension at two substantially different system pressures. The suspension energy at 21 bars is up to 90% of the total energy input in 10 seconds, against 40% for the corresponding value at 1 bar. Meanwhile, at the high-pressure case most of energy was distributed on increasing the particle potential energy, i.e. increasing bed height. Additionally, the particle kinetic energy is increased, although not so pronounced. This finding demonstrates that the higher pressure enhances the gas-solid interaction and suppresses the particle-particle interactions. Since more energy is spent on particle suspension at elevated pressure it results in higher bed heights.

Although a high operating pressure does not directly change the particle-particle interaction (due to the rigidity of the particles), through increasing gas density, the gas-particle interaction (buoyancy and drag force) increases. This intensification promotes the particles to obtain more energy to suspend themselves in the gas flow and to provide themselves more

movement space, which consequently efficiently reduces the chance for particle-particle collision. The larger the particle the more pronounced this effect becomes. Meanwhile, a denser gas depresses the originally freely moving particles (as increasing drag force and buoyancy can result in a strictly obeyed force balance for each individual particle), which furthermore leads to less particle collisions. In this way, the elevated pressure successfully changes the role of the particle-particle inelastic collision and particle-fluid interaction in their competition process. As a result, it leads to a relative homogeneous flow structure. However, owing to the existence of non-ideal collisions small bubbles still appear but they are much smaller than those in the atmospheric case. It is also observed from the computed particle configuration that the solid mixing in the high pressure case is not so intensive compared to the atmospheric case which is due to the different gas bubble behavior.

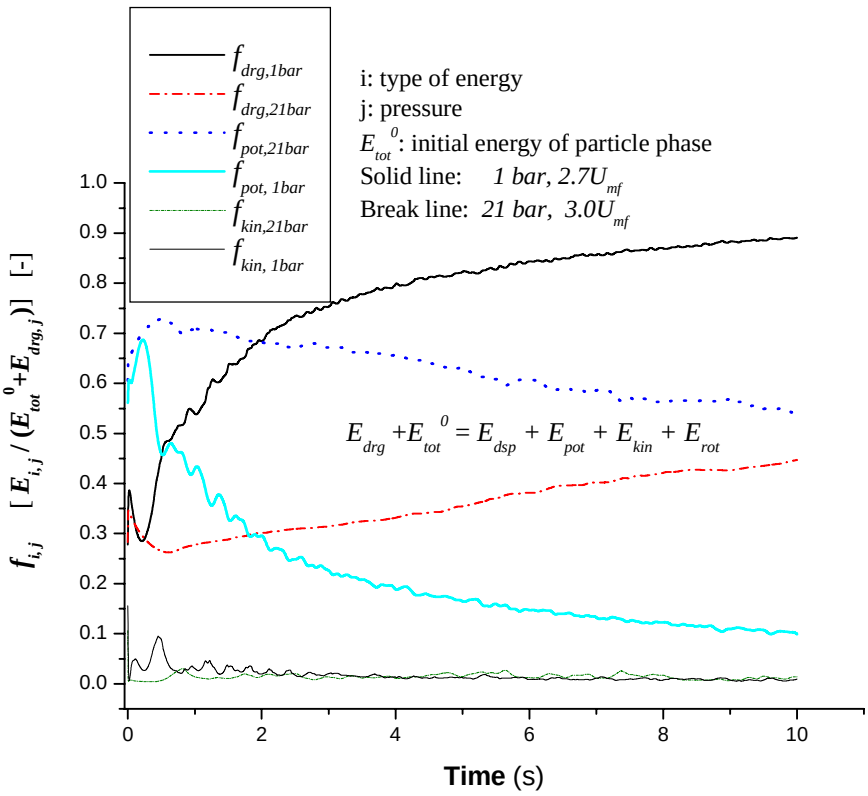

Figure 5.17: Energy analysis in gas-fluidized beds: *elevated pressure efficiently suppresses the particle collisional dissipation.*

Based on the above understanding, it is inferred that the normal fluidized beds operated at atmosphere pressure are very suitable to achieve efficient particle mixing. On the other hands, fluidized beds operated at elevated pressure would offer advantages for systems requiring good gas-solid contacting, such as FCC regeneration.

3.2.4 THE ROLE OF PARTICLE COLLISION IN THE REGIME TRANSITION

It is well known that there are several flow regimes for gas-solid two-phase flows ranging from the packed bed to the dilute transportation regime. Accordingly, it is expected that the role of gas/particle and particle/particle interactions on the flow patterns and their evolution for the different regimes will differ substantially. Energy analyses are therefore carried out, up to the turbulent regime, to clarify this issue. The results are displayed in Figure 5.18 and 5.19 respectively for the atmospheric condition and the elevated pressure situation.

As expected the energy distributions depend to a large extent on the flow regimes. In the (pseudo-) uniform regime the energy portion for particle collisional dissipation is very low and most of the energy is distributed to increase particle potential energy, indicating that the particle-fluid interaction dominates the system even if the system is relatively dense.

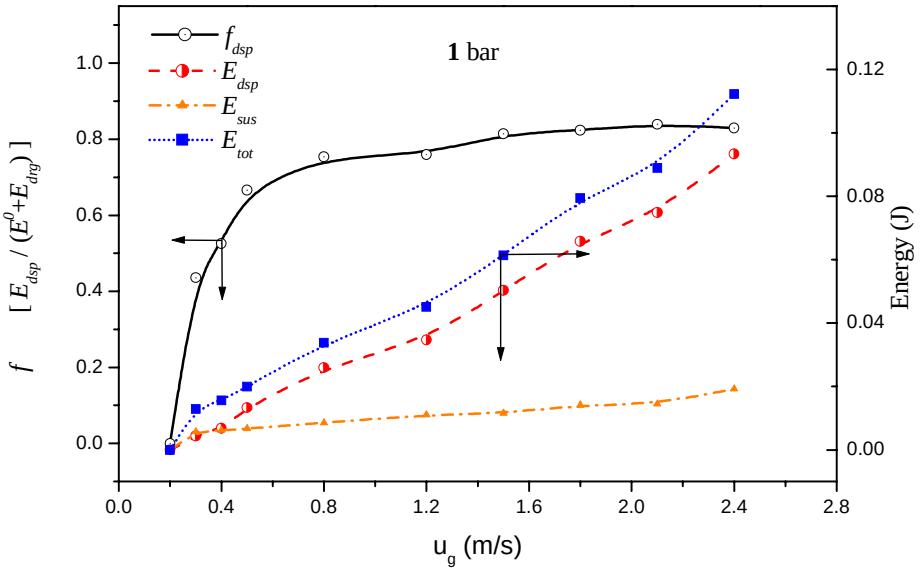

Figure 5.18: Energy distributions in gas-fluidized beds at 1 bar, when the bed is fluidized, particle collisional dissipation rapidly increases.

On the contrary, if the superficial gas velocity exceeds the bubbling point and enters the bubbling regime (which is determined by the standard deviation of pressure-drop fluctuation), it is found that the energy fraction partitioned to collisional dissipation becomes extremely high and a relatively small portion of energy is available to increase particle suspension energy, indicating that particle-particle collision dominates the system in this regime.

This also demonstrates that the region transition from the uniform regime to the bubbling regime is actually caused by the changing role of gas suspension and particle collision. This agrees well with the findings reported in Chapter 3: **a dissipation-dominated system shows a distinct two-phase structure**.

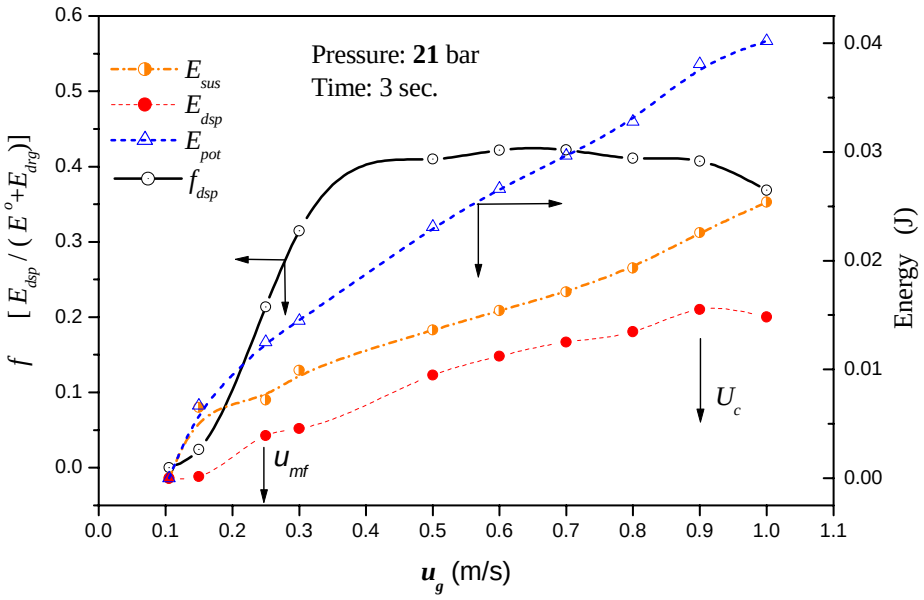

Figure 5.19: Energy distribution of the particle phase in a gas-fluidized bed at 21 bar. Regime transition depends on the competition between particle collision and gas suspension: less dissipation in uniform regime but more dissipation in the bubbling regime.

From Chapter 3, we have already know that more pronounced the energy dissipation due on particle collision leads to the development of more heterogeneous flow structures. From this point of view, the regime transition point from uniform to bubbling is actually the critical point where the two kinds of actions are compromising. After this point, the gas-solid suspension gives its way to particle collision. Apparently, this point is related to solids and fluid properties (influencing collision and suspension).

After entering the turbulent fluidization regime, the collisional dissipation rate decreases compared to the bubbling regime but it is still higher than that in the uniform regime. This indicates that the roles of the P-P and the F-P interactions are equivalent and neither is able to control the system. Consequently, in the bed there will be the void/cluster structures, such as those observed near the wall and at the bottom region, which is induced by intensive particle collision. Meanwhile, there are also some uniform structures of gas-solid suspension due to the good gas suspension, such as those present in the bed center and at the top region.

3.3 Fluid density effect

Two runs have been performed at the same superficial velocity but different gas densities of 1.18 and 24.75 kg/m^3 to examine the effect of fluid density on particle-particle interaction. The simulation conditions are summarized in Table 5.3. Figure 5.20 shows the two snapshots for the particle configuration in the bed.

Table 5.3: Simulation conditions for gas density influence in gas-fluidized beds.

Bed geometry		2-D
Width (cm)		10
Height (cm)		40
Static bed height (cm)		15
Particles		Polystyrene
Diameter (mm)		0.949
Density (kg/m3)		1102
Number (-)		16000
Simulation		
Grid		20×40
Total time (s) , time step (s)		5, 1x10-4
Restitution coef. Norm. (p-wall & p-p)		0.90
Shear		0
Friction coef. Norm. (p-wall & p-p)		0.25
Shear		0
Gas velocity (m/s)		0.50
Fluid density (kg/m^3)	Run 1	***1.180***
	Run 2	***24.75***

Apparently, under the given condition, the system with the high gas density has already entered the turbulent regime. This implies that the high density gas can provide more energy to the particulate phase. But we do obtain a higher granular temperature in the high gas density system as shown in Figure 5.21. This is reasonable since from the absolute value point of view turbulent bed yields stronger particle collision. Also, it shows that intensive particle-particle collisional interaction occurs along the wall in the turbulent regime. This could be induced by the "core-annulus" flow structure. The contour, in Figure 5.22, provides the detailed granular temperature profile to highlight the spatial distribution of zones of intense collisional interaction in the two systems: around and mainly below bubbles for the bubbling regime and in clusters near the wall for the turbulent regime.

Additionally, the time-averaged granular temperature distributions across the bed for both cases are displayed in Figure 5.23 respectively. Figures 5.24 ~ 25 show the detailed plots for the corresponding radial and axial distributions of the granular temperature.

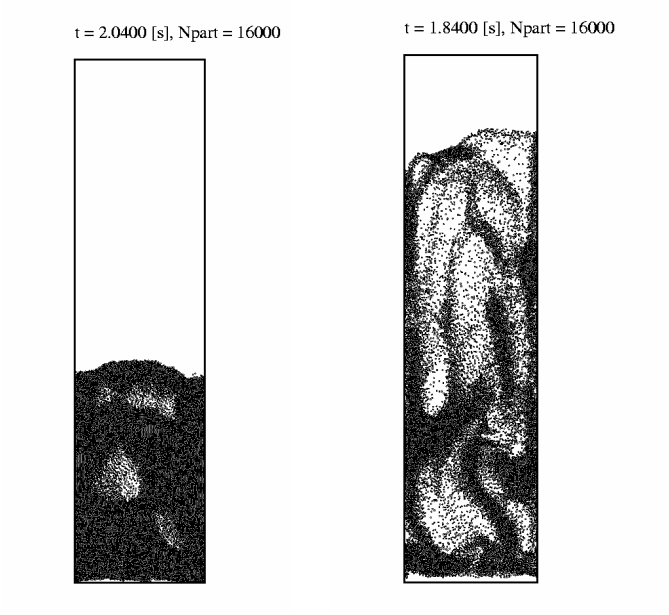

(a) (b)

Figure 5.20: Snapshots for particle configuration in gas-fluidized beds operating at u_g = 0.5 m/s and gas density of a) 1.18 kg/m^3 and b) 24.75 kg/m^3.

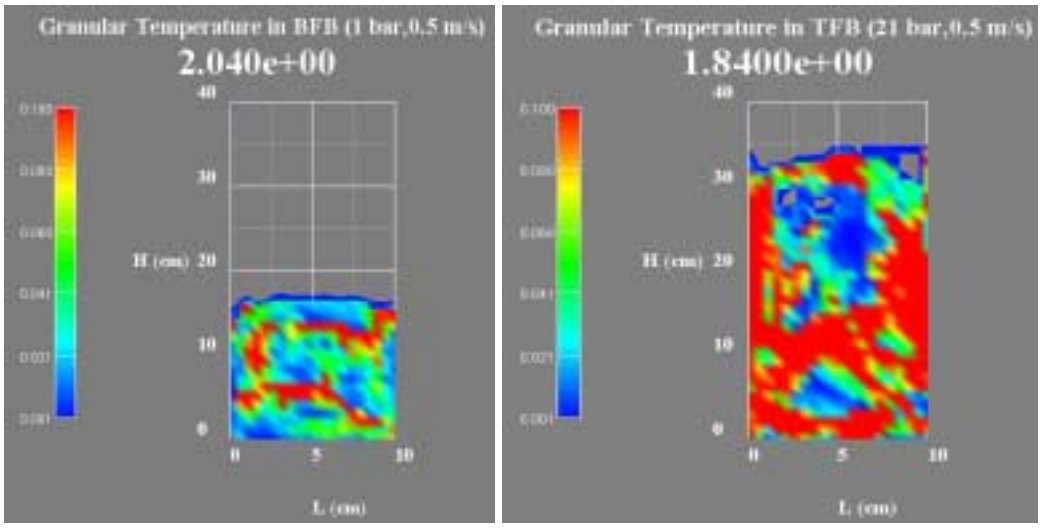

(a) (b)

Figure 21: Snapshots for granular temperature distributions in gas-fluidized beds operating at u_g = 0.5 m/s and gas density of a) 1.18 kg/m^3 and b) 24.75 kg/m^3.

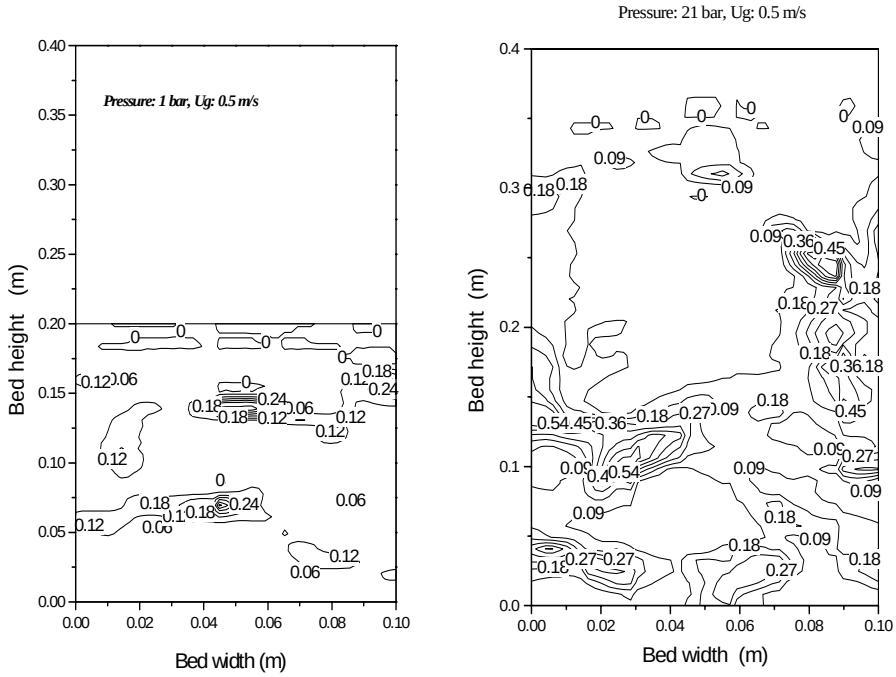

Figure 5.22: Granular temperature distribution in bubbling gas-fluidized beds operating *at* u_g = 0.5 m/s with gas density of a) 1.18 kg/m^3 and b) 24.75 kg/m^3.

It is interestingly noticed that the radial distributions of the granular temperature for the two cases show opposite trends: higher in the bed center for the bubbling regime but higher near the wall for the turbulent regime. This can be explained by the different modes (mechanisms)

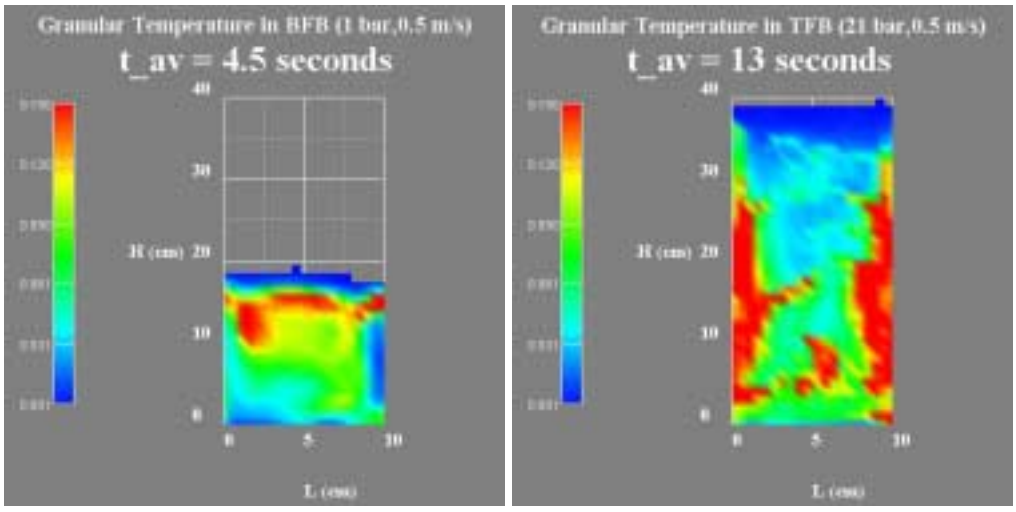

(a) (b)

Figure 5.23: Time averaged granular distributions in gas-fluidized beds operating at u_g = 0.5 m/s and gas density of a) 1.18 kg/m^3 and b) 24.75 kg/m^3.

causing particle interaction. For the low density case the most intensive particle-particle collision is caused by the bubbles, which always ascend from the center of the bed. On the contrary, the intensive shear action between the gas and particles occurs near the wall.

Particularly, it shows that the highest granular temperature is located at the position of nearly 80% of the bed radius, which corresponds very well to a maximum slip velocity as experimentally demonstrated by Yang et al. (1992) in the high-velocity gas-fluidized beds.

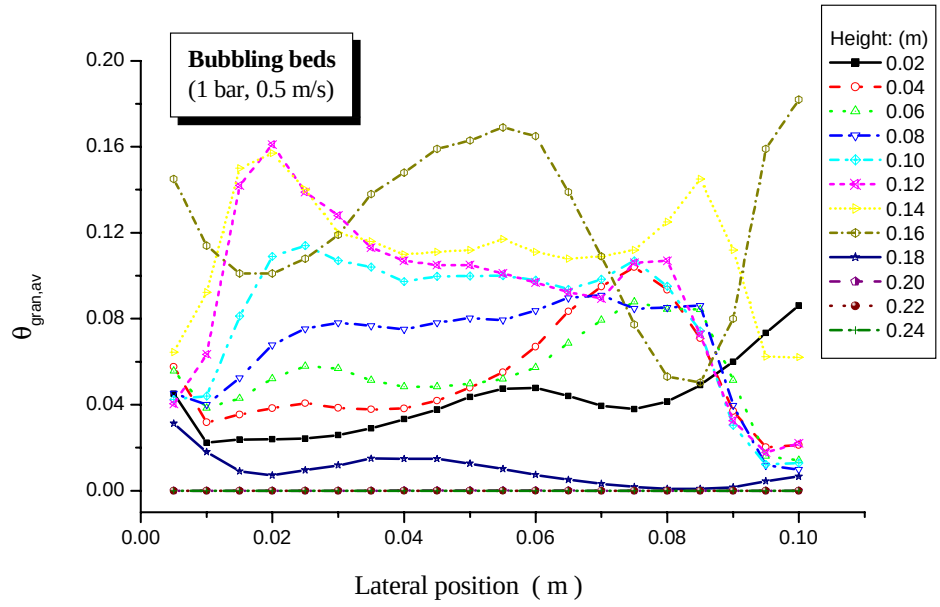

(a)

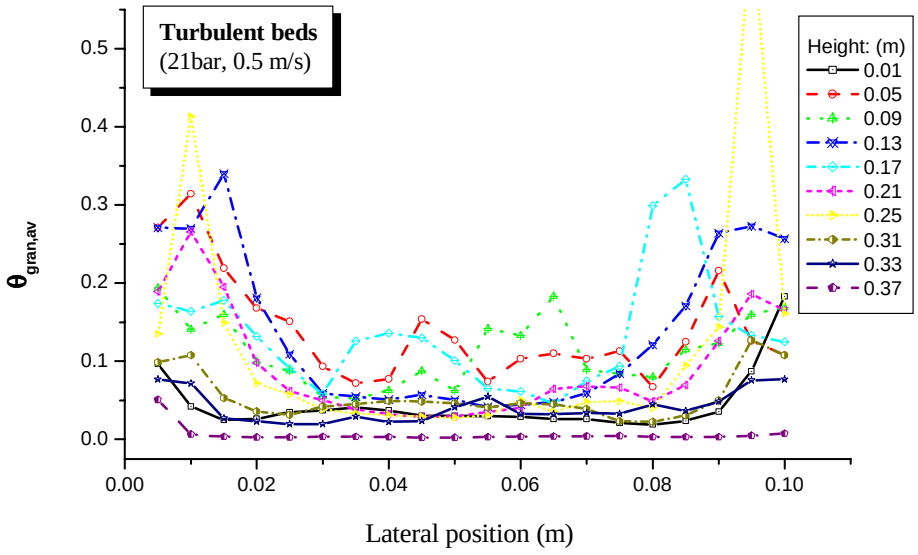

(b)

Figure 24: Granular temperature distributions in radial direction in gas-fluidized beds operating at 0.5 m/s and gas density of a) 1.18 kg/m^3 and b) 24.75 kg/m^3.

Along the axial direction, the granular temperature increases and reaches its maximum value just below the bed surface in the bubbling bed since the bubbles become larger and larger and finally erupt at the bed surface. However, for turbulent beds the granular temperature decreases because of less particles being available in the free board.

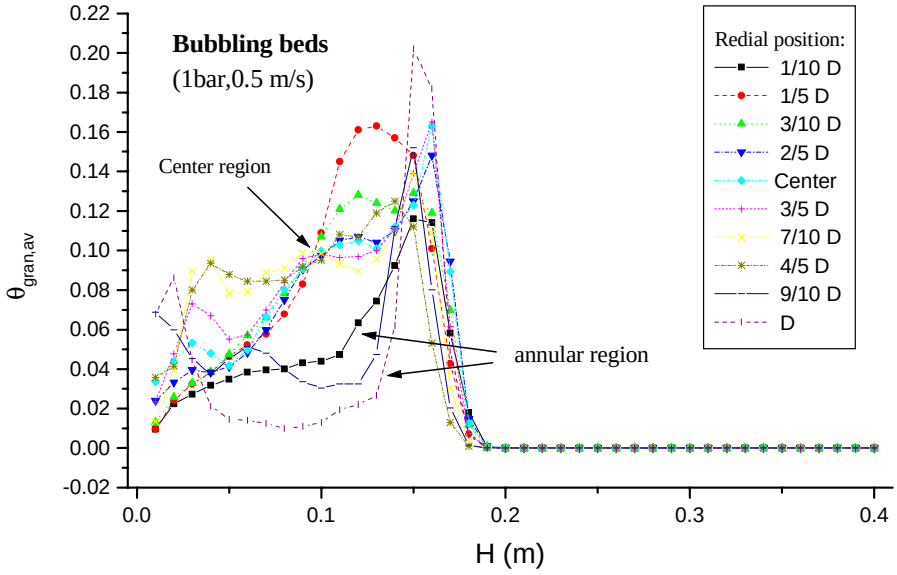

(a)

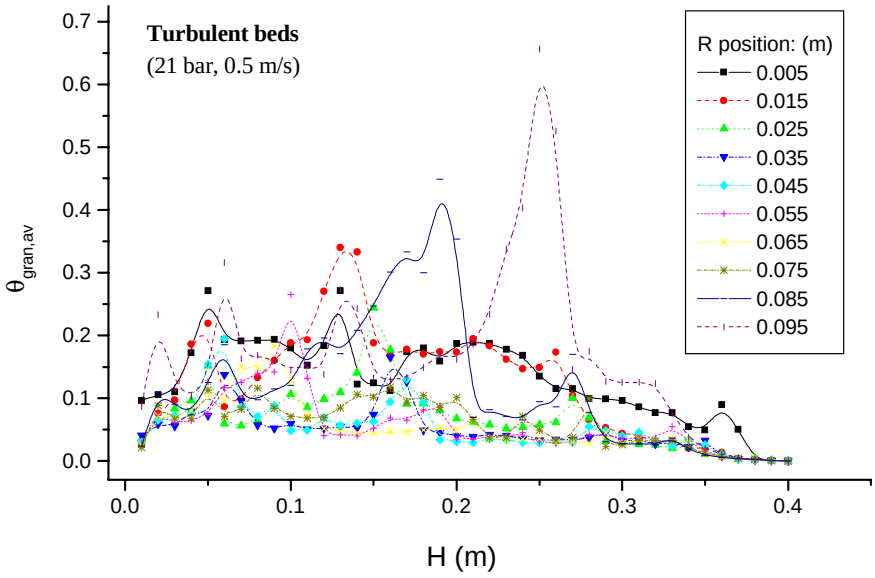

(b)

Figure 5.25: Granular temperature distributions in axial direction in gas-fluidized beds operating at 0.5 m/s and gas density of a) 1.18 kg/m^3 and b) 24.75 kg/m^3.

4. Conclusion remarks

By employing the discrete particle simulation method it is possible to explore the role of particle-particle interaction in dense particulate flows. It is demonstrated that particle-particle interaction plays an important role in many key phenomena observed in gas-fluidized beds.

Bubbles and jets feed back to the emulsion phase the extremely strong particle-particle collisional interaction. There exist three zones around rising bubbles where intensive particle-particle interaction prevails: one in the bubble wake and two others at the left and right part of the bubble base. Along a gas jet boundary, including both permanent jets and jets producing a string of bubbles, there exist very intensive particle-particle interactions.

It is also demonstrates that elevated pressure reduces the incipient fluidization velocity, widens the uniform fluidization regime and leads to a quick transition to the turbulent regime. Particularly it is has been found that high pressure, through enhancing gas-solid interaction and reducing the particle collision frequency, efficiently suppresses formation of large bubbles. As a consequence, thereof more uniform gas-solid flow structures are produced leading to particulate fluidization.

Particle collisional dissipation plays an important role in the regime transition from homogeneous flow to the bubbling flow. In the homogeneous flow regime, a smaller portion of the energy budget is distributed to dissipative collisions. With increasing gas velocity, an increased portion of energy is dissipated during particle collisions and gas suspension is gradually dominated by particle collision. The transition to bubbling flow is realized when the collisional dissipation arrives at its maximum value.

A high-density gas provides more energy to particles and shifts the regime transition point ahead when compared to the low density gas whereas local particle-particle interaction is intensified (gas velocity is kept the same). Along the vertical coordinate in the bed, particle-particle interaction increases and reaches its highest value at the surface in the bubbling bed. Across the bed, relatively weak particle interaction prevails near the wall. On the contrary, in the turbulent bed, particle-particle interaction shows a core/annular distribution with maximum intensity at 80% of the redial position from the center. In the vertical direction strong particle interaction prevails in the bottom zone.

REFERENCES

Davidson, J. F. and Harrison, D. 1963 *Fluidized Particles*, Cambridge, University Press.

Davidson, J. F. and Harrison, D. 1971 *Fluidization*, Academic Press, UK.

Fan, L-S. and Danko, J. 1984 Characteristics of fluidization at high pressure. *Chem. Eng. Sci.*, **39**, 253.

Hoomans, B. P. B. 2000 Granular dynamics in gas-solids two-phase flows. *Ph.D. dissertation*, Twente University, The Netherlands

Hoomans, B. P. B., Kuipers, J. A. M. Briels, W. J. and van Swaaij, W. P. M. 1996 Discrete particle simulation of bubble and slug formation in a two-dimensional gas-fluidized bed: a hard-sphere approach. *Chem. Eng. Sci*., **51**, 99.

Jackson, R. 1963 The mechanics of Fluidized beds. I: The stability of the state of uniform Fluidization. *Trans. Inst. Chem. Eng*., **41**, 13-21.

Yang, Y., Jin, Y. and Yu, Z. 1992 Investigation of slip velocity distribution in the riser of dilute circulating fluidized bed. *Powder Technol*., **73**, 67-73

Appendix

Table A1. Simulation conditions for granular temperature in bubbling fluidized beds with glass beads

Bed geometry		2-D
	Width (cm)	15
	Height (cm)	50
Particles		Glass beads
	Diameter (mm)	4.0
	Density (kg/m^3)	2700
	Number (-)	2400
	Incipient fluid. vel.(m/s)	1.77
Simulation		
	Grid	30 x 50
	Total time (s)	10
	Time step (s)	$1x10^{-4}$
	Restitution Coef. Norm. (p-wall & p-p)	0.97
	Shear	0
	Friction Coef. Norm. (p-wall & p-p)	0.15
	Shear	0
Superficial gas velocity (m/s)		3.2 ($1.8\ u_{mf}$)

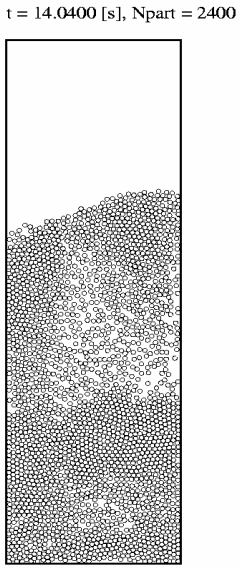

Figure A5.1: Snapshot for particle position in bubbling bed.

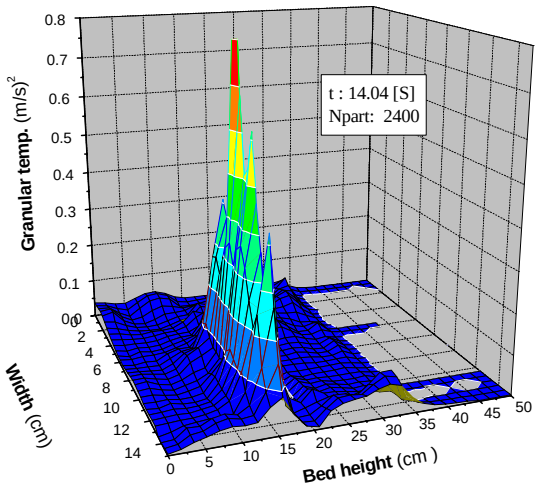

Figure A5.2: Granular temperature in the distribution bubble wake.

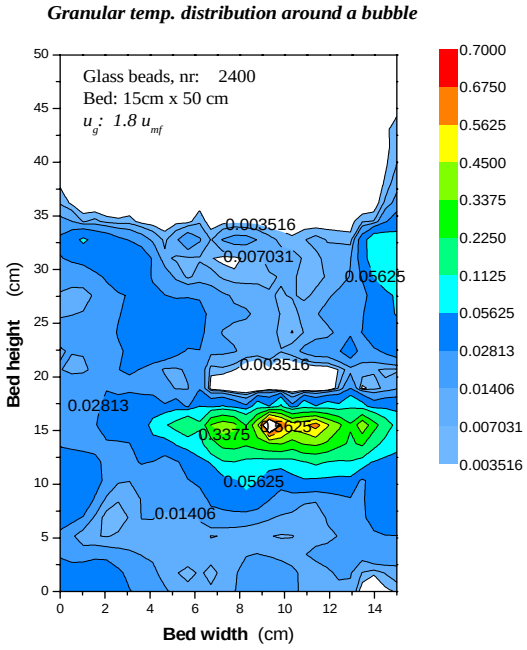

Figure A5.3: Granular temperature distribution in the bubble wake (contour).

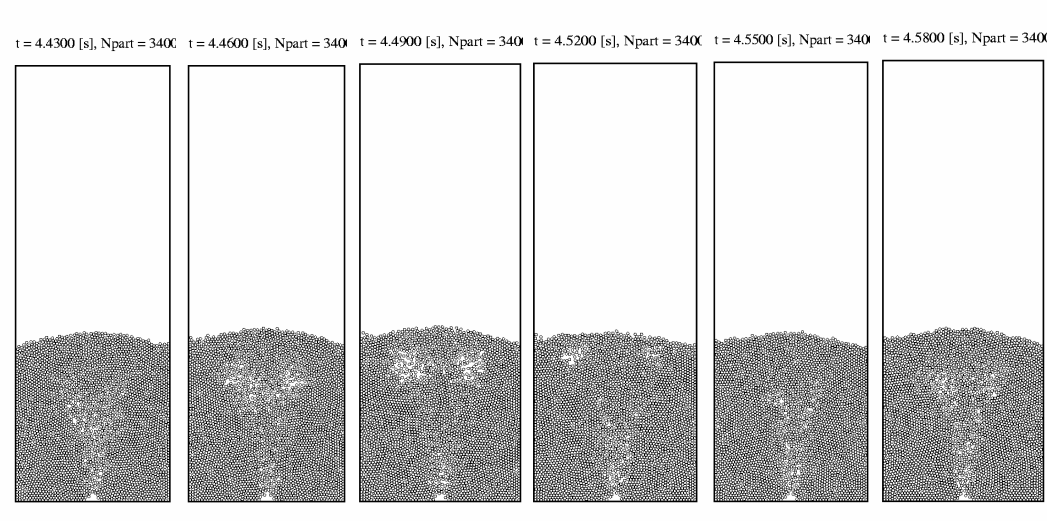

Figure A5.4: Snapshots for bubbling string flow (center jet, $12.5u_{mf}$).

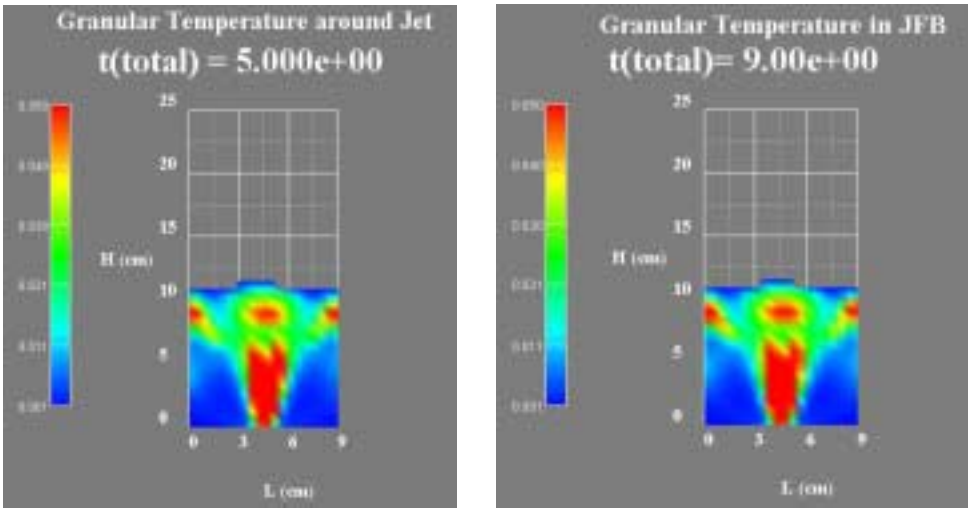

Figure A5.5: Comparison of time-averaged granular temperature distributions: (left: 5 seconds, right: 10 seconds).

Chapter 6

FLOW STRUCTURE FORMATION IN CIRCULATING GAS-FLUIDIZED BEDS

Abstract

The occurrence of heterogeneous flow structures in gas-particle flows seriously affects the gas–solid contacting and transport processes in high-velocity gas-fluidized beds. Particles do not disperse uniformly in the flow but pass through the bed in a swarm of clusters. The so-called "core-annulus" structure in the radial direction and "S" shaped axial distribution of solids concentration distribution characterize the typical flow structure in the system.

A computational study, using the discrete particle approach based on Molecular Dynamics techniques, has been carried out to explore the mechanisms underlying the cluster and the core/annulus structure formation. Based on energy budget analysis including work done by the drag force, kinetic energy, rotational energy, potential energy, and energy dissipation due to particle-particle and particle-wall collisions, the role of 1) *gas-solid interaction and* 2) *inelastic collisions between the particles are elucidated.*

It is concluded that the competition between gas-solid interaction and particle-particle interaction determines the pattern formation in high-velocity gas-solid flows: if the gas-solid interaction (*elevated pressure*) *dominates, most of particle energy obtained by drag from the gas phase is partitioned such that particle potential energy is raised leading to a uniform flow structure. Otherwise, a heterogeneous pattern exists, which could be induced by both particle-particle collisions and gas-solid interaction. Although both factors could cause the flow instability, the non-linear drag force is demonstrated to be the necessary condition to trigger heterogeneous flow structure formation.*

The core-annular structure is initialized by the non-uniform distribution of gas flow in gas-fluidized beds and is intensified by particle collisional dissipation. As gas velocity goes beyond a

critical value, the fluid-particle interaction suppresses particle collisional dissipation and as a consequence a more homogeneous flow regime is formed.

1. Introduction

The occurrence of heterogeneous flow structures in gas-particle flows seriously affects the quality of gas–solid contacting and transport processes in high-velocity gas-fluidized beds. Therefore, it has attracted interest of physicists and engineers from many application fields all over the world. In the last decade, significant efforts have been made to understand this heterogeneous structure, including formation of the clusters and the core-annulus structure. Useful information on cluster shapes, size, internal structure and core region size etc. has been collected (Li et al., 1980; Horio, 1994; Sharma et al., 2000; Lackermeier et al., 2001). Particularly, it has been found that the system instability is closely related to the properties of the fluid-particle system. Systems with large fluid-solid density difference tend to more easily form clusters (Grace and Tuot, 1979).

However, owing to the complex and transient properties of dense gas-solid flows, the mechanisms underlying the origin and evolution of the heterogeneous flow pattern have not been completely elucidated. Some researchers supposed that the core-annulus structure results from the wall effect, which slows down the gas phase and forms a swarm of particle clusters. However, there are indications (Hoomans, et al. 2000) that non-ideal particle-particle collisions cause formation of particle agglomerates and consequently lead to formation of a core-annulus flow structure. Furthermore, by employing discrete element simulation Helland et al. (2000) demonstrated that non-linear drag also leads to a heterogeneous flow structure.

In this chapter, a computational study has been carried out to explore the mechanisms which control the cluster/dilute pattern formation by employing a discrete particle method (a “hard-sphere model” based on Molecular Dynamics). Particular attention was paid to the effect of 1) gas-solid interaction and 2) inelastic collisions between particles on pattern formation in high velocity gas-solid two-phase flows by employing a simple but powerful tool, namely energy budget analysis, to understand how the flow structures are related to these two phenomena. First, simulations will be performed using different particle collisional properties to quantitatively understand collisional dissipation induced instability. Then, simulations with different gas phase properties (drag force), but zero collisional dissipation will be carried out to explore the effect of gas-particle interaction on flow pattern formation. In addition, a system with strong collisional dissipation and enhanced gas-solid interaction (elevated pressure system) will be studied to highlight whether there exists a necessary condition between those two instability- inducing factors by which the heterogeneous flow structure is initialized. Moreover, the time-averaged voidage distribution across the bed for an ideal collisional system with strong gas-solid interaction is investigated to understand the wall effect on the macro-scale flow structure. Finally, the evolution of flow structure with flow rate to the dilute transportation regime will be examined.

2. Theoretical background

In our discrete particle model the gas phase is described by the volume-averaged Navier-Stokes equation, whereas the particles are described by the Newtonian equations of motion while taking particle-particle and particle-wall collisions into account. The original computer codes for solving these sets of equations were developed by Kuipers (1992) for the gas phase and Hoomans (1999) for the granular dynamics including both 2D and 3D geometries. Additional codes were developed in this study to enable energy budget analysis.

2.1 Gas phase model

Continuity equation gas phase:

$$\frac{\partial(\varepsilon\rho_g)}{\partial t} + (\nabla \cdot \varepsilon\rho_g \boldsymbol{u}) = 0 \tag{6.1}$$

Momentum equation gas phase:

$$\frac{\partial(\varepsilon\rho_g \boldsymbol{u})}{\partial t} + (\nabla \cdot \varepsilon\rho_g \boldsymbol{u}\boldsymbol{u}) = -\varepsilon\nabla p - \boldsymbol{S_p} - (\nabla \cdot \varepsilon\overline{\boldsymbol{\tau}_g}) + \varepsilon\rho_g \boldsymbol{g} \tag{6.2}$$

where the source term S_p [N·m^{-3}] represents the reaction force to the drag force exerted on a particle per unit of volume suspension which is fed back to gas phase. In this work transient, two-dimensional, isothermal flow of air at atmospheric and elevated pressure conditions is considered.

2.2 Granular dynamics model

Force balance for a single particle:

$$m_p \frac{d\boldsymbol{V}}{dt} = m_p \boldsymbol{g} + \frac{V_p \beta}{1-\varepsilon}(\boldsymbol{u} - \boldsymbol{V}) - V_p \nabla p \tag{6.3}$$

In equation (6.3) the third term represents the force due to the pressure gradient. The second term is due to the drag force where β represents the interphase momentum exchange coefficient similar to the one encountered in two-fluid models. The following well-known expression (Wen and Yu,

1966) has been used with n = 2.7. Other values of n will also be used to examine the particle group effect in the simulation.

$$\beta = \tfrac{3}{4} C_d \frac{\varepsilon(1-\varepsilon)}{d_p} \rho_g \left|\boldsymbol{u}-\boldsymbol{V}\right| \varepsilon^{-n} \tag{6.4}$$

The drag coefficient C_d is a function of the particle Reynolds number Re_p and is given by:

$$C_d = \begin{cases} \dfrac{24}{\mathrm{Re}_p}(1+0.15\,\mathrm{Re}_p{}^{0.687}) & \mathrm{Re}_p < 1000 \\ 0.44 & \mathrm{Re}_p \geq 1000 \end{cases} \tag{6.5}$$

where Re_p is defined as:

$$Re_p = \frac{\varepsilon \rho_g \left|\boldsymbol{u}-\boldsymbol{V}\right| d_p}{\mu_g} \tag{6.6}$$

2.3 Simulation technology

The hard sphere model is used to describe a binary, instantaneous, inelastic collision with friction. The key parameters of the model are 1) the coefficient of restitution ($0 < e < 1$) and 2) the coefficient of friction ($\mu > 0$). In this approach a sequence of binary collisions is processed. This implies that a collision list is compiled in which for each particle a collision partner and a corresponding collision time is stored. A constant time step is used to take the external forces into account and within this time step the prevailing collisions are processed sequentially. In order to reduce the required CPU time neighbour lists and cell lists are used. For each particle a list of neighboring particles is stored and only for the particles contained in this list a check for possible collision partners is performed. The simulations are carried out only for the central part of the riser section without considering inlet and exit effects. A certain amount of particles was fed at the bottom at a specified velocity according to a prescribed solid mass flux. When particles approach the top they are removed from the system. The simulation conditions are listed in Table 6.1. Effects due to particle size distribution are not included in this research, but can be found in Hoomans et al. (2000, 2001).

2.4 Energy analysis

In fluid-particle systems, there exist two types of interactions: fluid-particle interaction due to drag and particle-particle interaction due to collisions. Our hard sphere based DPM model accounts for these two interactions in great detail and particularly allows for computing the various work terms and energy types during the process. Thereby it is possible to study the underlying mechanisms which control flow pattern formation.

The particle phase energy analysis includes 1) energy input (work) to the particulate phase, which is composed of a) the work done by the drag force, b) system initial energy, c) energy introduced by newly fed particles; 2) energy budget distribution in the particulate phase, including kinetic, rotational, potential energies and collisional dissipation. For circulating fluidized beds, the energy carried by outgoing particles should also be taken into account. According to the energy conservation principle for the particulate phase, the relationship between work done by drag and these energies is as follows:

$$W_{drg} = E_{dsp} + \Delta E_{pot} + \Delta E_{kin} + \Delta E_{rot} \tag{6.7}$$

For a circulating fluidized bed, we have:

$$W_{drg} = E_{dsp} + (E_{pot} + E_{pot,out}) + (E_{kin} + E_{kin,out}) + (E_{rot} + E_{rot,out}) - E_{inp,tot} - E_{tot}^{0} \tag{6.8}$$

where E_{tot}^{0} is the initial energy of the particulate phase and $E_{inp,tot}$ is the energy added by the feeding of particles at the inlet. In addition to the absolute energy, a parameter of the energy partition fraction was defined to characterize the fractional energy budget:

$$f_i = \frac{E_i}{W_{drg} + E_{tot}^{0} + E_{inp,tot}} \tag{6.9}$$

where the subscript *i* refers to either total particle collisional dissipation, kinetic, rotational and potential energies respectively.

Table 6.1: Simulation conditions for base case: run 1.

System	Bed height (m)	2	Width (m)	0.08
Particles	Density (kg/m^3)	2600	Diameter (μm)	500
	Solids flux (kg/m^{2}s)	25	Restitution coef.	0.95
	Inlet velocity (m/s)	0.4	Friction coef. (μ)	0.30
Gas	Velocity (m/s)	5 (23u_{mf})	Pressure (bar)	1.20
Simulation	Grid	20 ×100	*dt* (ms)	0.1
	Voidage exponent (n)	4.7		

Conditions for run 2: same as run 1 except: e = 1.0, μ = 0; (run 2b: G_s = 75 kg/m^{2}s).
run 3: same as run 2 except: voidage exponent n = 0.
run 4: same as run 1 except: pressure 50 bar, U_g = 1.68 m/s (23 u_{mf}, 50 bar).
Refer to Legends for other conditions

3. Results and discussions

3.1 Collisional dissipation induced instability

Figure 6.1(a) shows the snapshot of the flow patterns for e = 0.95, μ = 0.30. Compared to the flow pattern under conditions of ideal collisions (see Figure 6.1b), the case with non-ideal collisions produces a flow structure containing (dense) clusters. Also, the particle hold-up in the non-ideal case is higher than with ideal collisions. The energy budget analysis presented in Figure 6.2 clearly demonstrates that a higher fractional component of energy is consumed due to collisional dissipation, which greatly reduces both the particle potential and kinetic energy. This

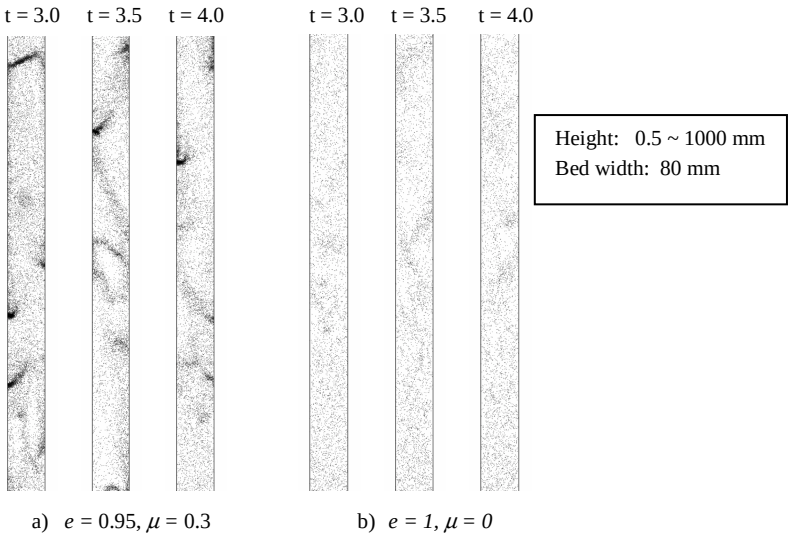

Figure 6.1: Flow structures in a CFB: *effect of collisional dissipation*.

conclusion is similar to that drawn from a previous study on bubbling fluidized beds (Li and Kuipers, 2001). Once non-ideal particle-particle collisions prevail, a certain amount of energy is consumed due to the collisional dissipation. Particles obtain less energy to suspend themselves freely in space (raising potential energy). When new particles are encountered, additional dissipation occurs and the process repeats itself. If fluid-solid interaction is not strong enough to prevent the particles to approach each other, eventually a “particle cluster” is formed.

However, unlike the situation in dense gas-fluidized beds where particle clusters form as a continuous phase, all initial particle clusters in circulating fluidized beds can not connect each other to form a continuous emulsion phase, but only exist as individual separated “particle islands”. This stems from the much stronger gas-solid interaction in a CFB (potential energy

fraction up to 80%, in Figure 6.2) compared to that in dense bubbling beds (only 20%, Li and Kuipers, 2001). In other words, although collisional dissipation results in flow instability in both cases, owning to the fundamental change of particle-particle controlled interaction giving way to gas-solid controlled interaction, local heterogeneity is displayed in a circulating fluidized bed.

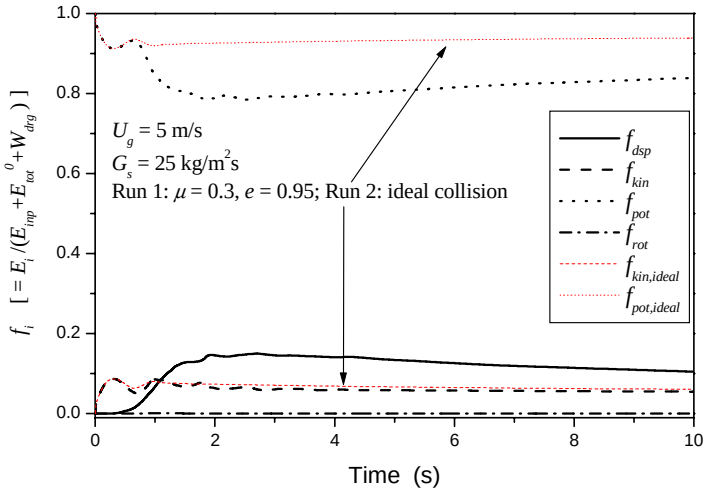

Figure 6.2: Energy analysis in a circulating fluidized bed: effect of *collisional dissipation*.

For this mode of cluster formation mechanism, two conditions are necessary: one is the collision actually to occur and the other one is that the collisions should be companied with energy dissipation. Should one of them not be fulfilled, a dissipation induced heterogeneous structure would be impossible. However, it should be noted that in Figure 6.1(b) some degree of flow heterogeneity still exists. What causes this heterogeneity then?

3.2 Non-linear gas drag induced instability

Many researchers have found from experiments that fluidization quality is closely related to the voidage exponent (2.35 ~ 4.7) in the well-known Richardson-Zaki (referred to as "R-Z" subsequently) equation: small values correspond to good fluidization quality or a uniform flow pattern. Unfortunately, a theoretical formulation to fully predict the drag force for such a dynamic system is still not available. Based on the R-Z correlation, Wen and Yu derived a drag correlation for a group of particles immersed in a fluid. In this well-known correlation a voidage exponent of 4.7 is employed. However, this fixed value is only valid in the high and low Reynolds number regime (Felice, 1994).

Figure 6.3 shows snapshots taken from the simulations with ideal collisions using the voidage exponents of 0 and 4.7 in the drag formulation respectively. Note that a value of n equal to 0

implies no effect of neighbour particles on the drag. Since this particle group effect on drag force is insensitive at low solid fraction, a higher solids flux of 75 kg/m^2.s has been employed in these simulations. In addition, the domain-averaged mean square solid volume fraction fluctuation, defined below, was used to quantitatively characterize and compare the flow structures.

$$< f_s^{'2} >= \frac{1}{NR \cdot NZ} \sum_{i=1}^{NR} \sum_{j=1}^{NZ} (f_{s,i,j} - \overline{f}_s)^2 \qquad (6.10)$$

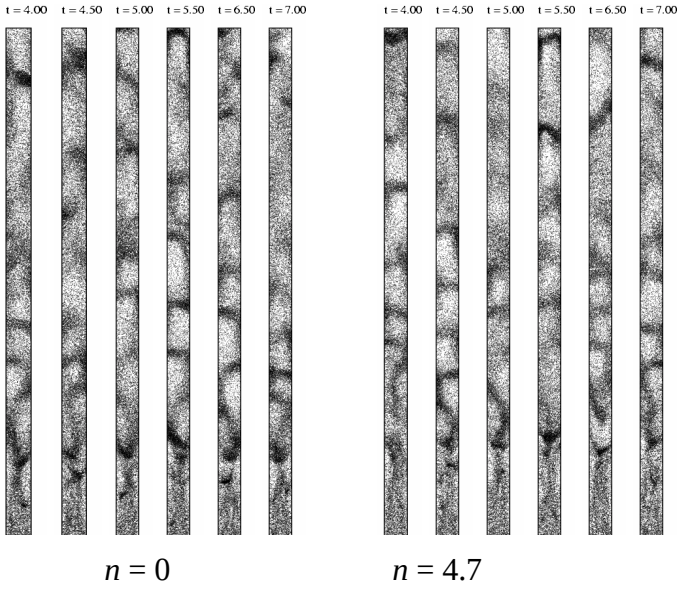

Figure 6.3: Flow structures in a CFB: *effect of non-linear drag* (*ideal collisions*, $C_d = C_{d,single} . \varepsilon^{-n}$).

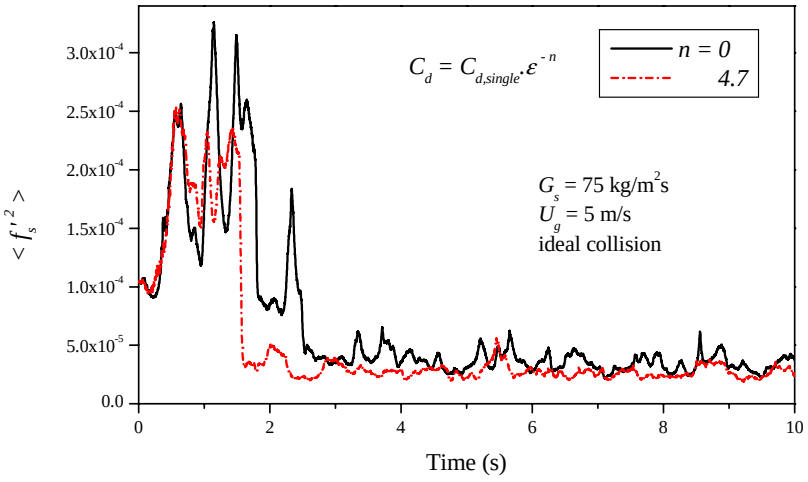

Figure 6.4: Domain-averaged mean square solids volume fraction fluctuation: *effect of exponent n in drag equation.*

where NR, NZ are the number of computational cells in respectively the radial and axial direction and $f_{s,i,j}$ is the solids volume fraction in cell (i, j). The bar represents the domain-averaged value. The results are shown in Figure 6.4. Clearly, particle clusters still exist in the system with ideal particle collisions. Our results indicate that a large voidage exponent produces a more uniform flow structure.

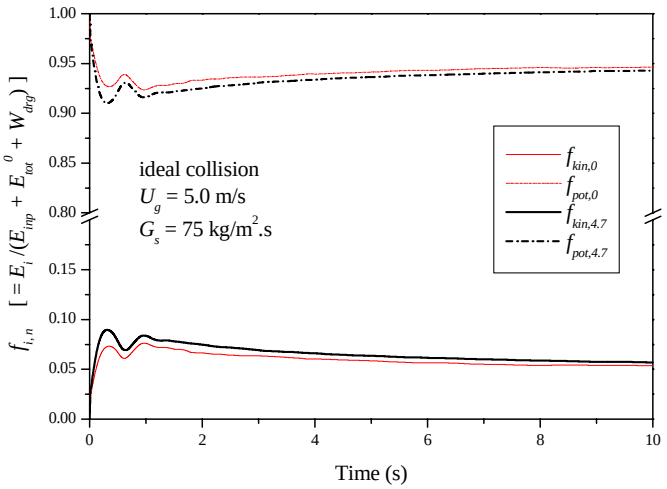

Figure 6.5: Energy analysis in circulating fluidized beds: *effect of non-linear drag*.

A comparison of the energy budget analysis for n = 0 and n = 4.7 focusing on the kinetic and potential energies (no dissipation and rotation due to ideal collision) is shown in Figure 6.5 indicating that the dominant drag force distributes a greater portion of the energy to particle kinetic energy.

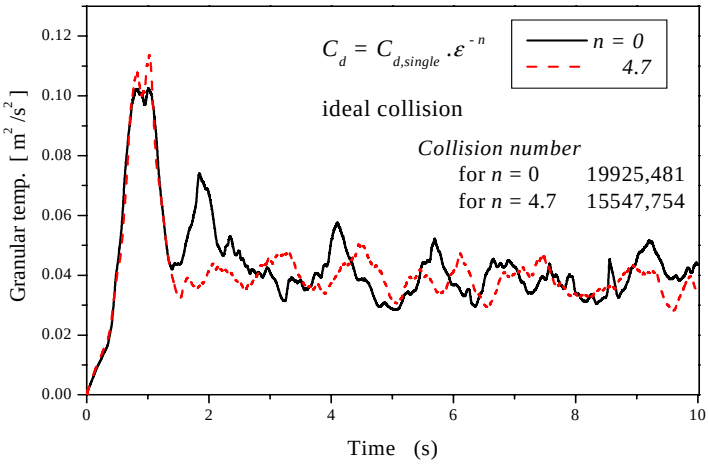

Figure 6.6: Granular temperature in CFB: *effect of non-linearity of drag or group effect.*

In addition, the domain-averaged granular temperature is shown in Figure 6.6 indicating that a bigger voidage exponent results in fewer collisions of particles. This means that a stronger group effect reduces the particle fluctuation motion and therefore the collision tendency. As a result, it results in a more homogeneous flow structure in circulating fluidized beds.

3.3 Combined effect of particle collision and gas drag

As shown above, both non-ideal particle-particle collision and non-linear drag could produce heterogeneous flow structures. However, the respective conditions and their induced cluster structures are different and therefore also a case was studied in which the combined effect of non-ideal particle-particle collision and a strong gas-solid interaction was considered.

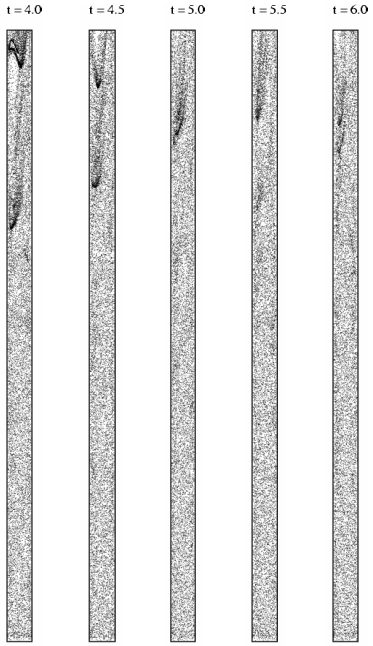

Figure 6.7: Flow structure in a CFB at elevated pressure (run 4): *homogeneous flow structure*.

Figure 6.7 shows the simulation results of run 4 with non-ideal particles at an elevated pressure of 50 bar and superficial gas velocity of 1.68 m/s (= $23u_{mf}$), a strong "fluid-controlled" system. Interestingly, we obtain a homogeneous flow structure. This demonstrates that collisional dissipation can only play a role in case collisions can actually occur. In other words, it is not the necessary condition for heterogeneous flow structure formation. This could also be employed to explain the homogeneous flow patterns observed in most of the liquid/solid systems.

Corresponding energy analysis, shown in Figure 6.8, indicates that nearly all energy is employed to suspend particles in such a case, implying that particles are always in an equilibrium state.

Different from cluster formation driven by collisional dissipation, the non-linear drag-induced cluster formation mechanism, which depends on the flow regime, material properties (viscosity, density and particle size), always plays a role if the drag force in the system has the non-linear

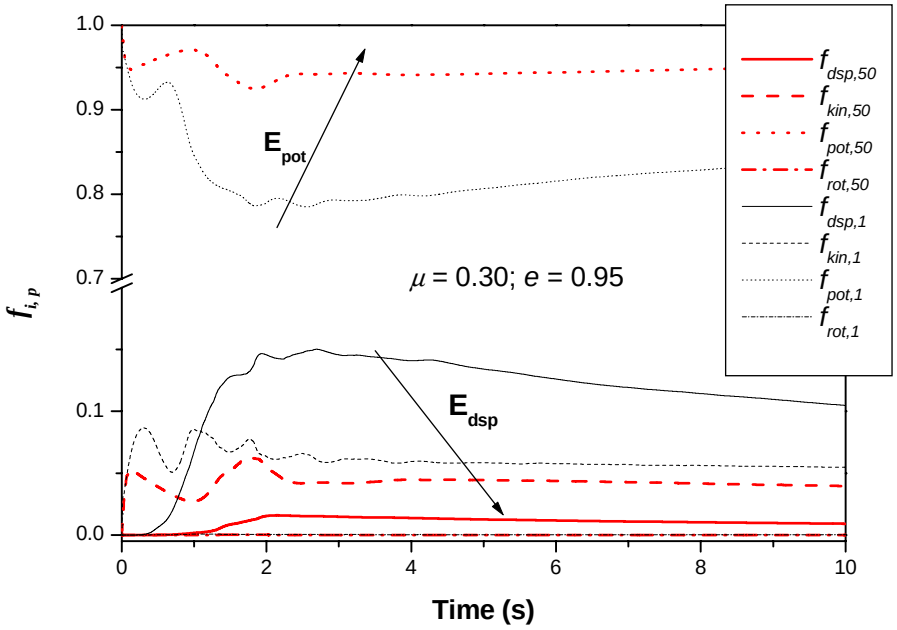

Figure 6.8: Comparison of energy budget analysis for the dissipation suppressed system at elevated pressure and the normal system at atmosphere pressure.

voidage-dependent property. For circulating gas-fluidized beds operating at atmospheric conditions, owing to the large density difference, the non-linearity of the drag force always exists or particles are always in a non-equilibrium motion. Therefore, it is the fundamental source leading to particle agglomerate. Non-linear drag force has a “phase separation” function, which definitely enhances particle-particle collision. If the drag-force-induced particle collisions are non-ideal, it furthermore intensifies particle agglomeration.

3.4 Particle motion in circulating fluidized beds

Compared to the influence of the non-linear drag on flow structure in bubbling fluidized beds, the influence of non-linear drag on flow structure in circulating fluidized beds shows the opposite trend: the system with stronger voidage dependence tends to form a more heterogeneous flow structure in bubbling flow, but a more homogeneous flow structure in circulating fluidized beds. How can this finding be explained?

To answer this question and obtain an insight in local cluster formation, it is necessary to know how the particles move inside and outside of the cluster. Keeping this question in mind, single particle motion and its aggregating status including its neighbor particle number will be monitored focusing on position, velocity and acceleration in a circulating fluidized bed with both ideal collision and non-ideal collision. When the particle being monitored leaves the system, a new fresh particle is monitored again. The analysis is specific to particles which are located in the central region in the riser.

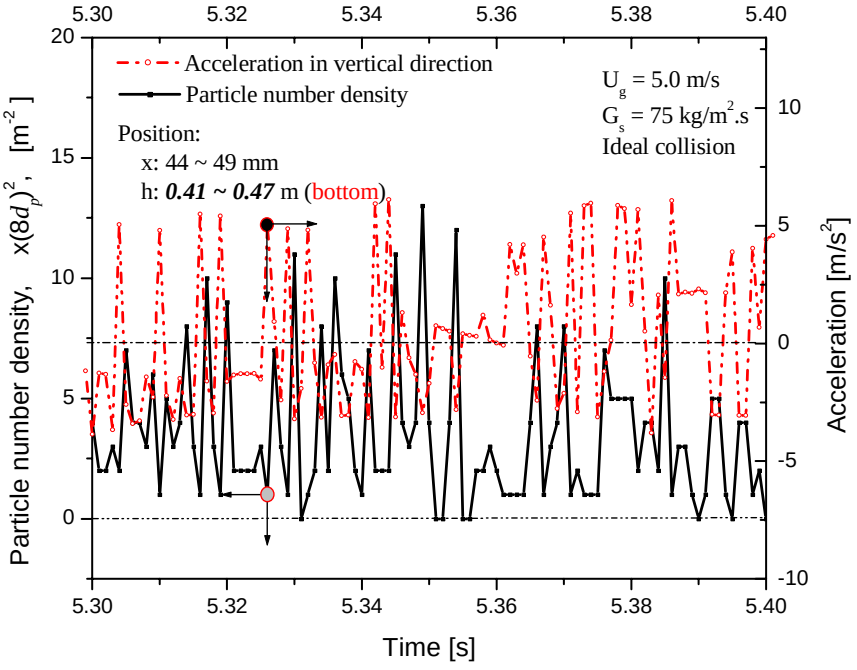

Figure 6.9: Influence of particle group effect on particle motion in a circulating fluidized bed at the bottom region: suppressing the otherwise accelerated individual particles. Where, *x*, *h* represent respectively the radial and axial position.

From the circulating fluidized bed simulations, **two types** of particle group effects can be identified: one greatly suppresses the otherwise accelerating motion of the particles. This effect is prevailing in the bottom and in the annular regions of the circulating fluidized bed, or collectively in the dense particle region. Figure 6.9 and 6.10 show these cases respectively. The flow typically displays the presence of clusters with relatively small acceleration and individual particles which experience considerable acceleration.

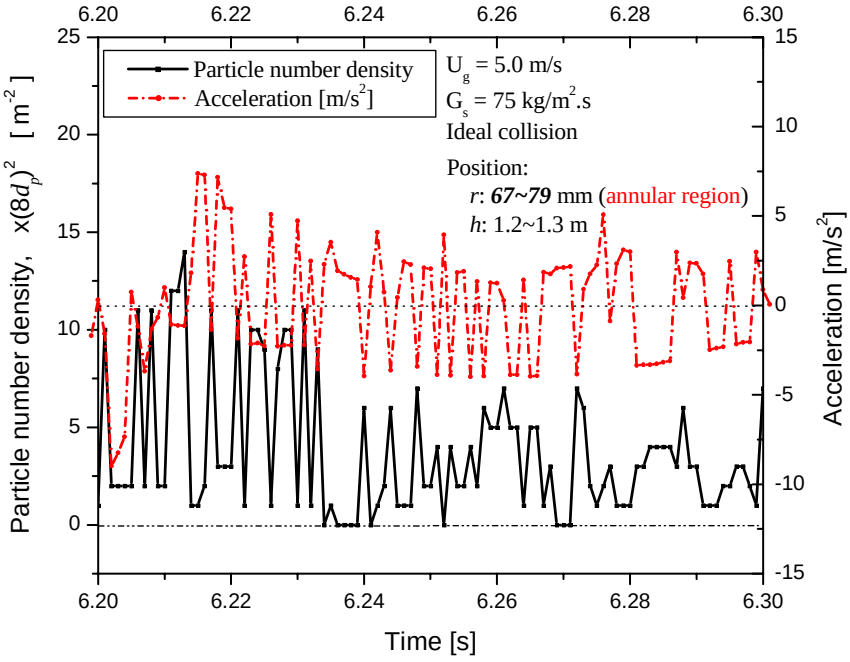

Figure 6.10: Influence of particle group effect on particle motion in a circulating fluidized bed in the annular region: suppressing the otherwise accelerated individual particles. Where, *x*, *h* represent respectively the radial and axial position.

The other effect maintains a high particle shifting velocity otherwise the individual particle tends to decelerate, as demonstrated in Figure 6.11. This phenomenon is prevailing in the middle section and near the bed center. When the particle runs outside of cluster, it decelerates. Similar results are found in circulating fluidized beds with non-ideal collisional particles (See Figure 6.12).

The fundamental difference between the effects originates from the difference of flow state of the cluster: a cluster moves slowly in the dense region but fast in the fully developed region. Therefore, the particle group effect leads to two opposite results depending on the local hydrodynamics. Since the extent of clustering is naturally determined by system properties, reflected by the voidage function, systems with a strong group effect (large voidage function

exponent) suppress the heterogeneous flow structure in dense regions by reducing the difference in force acting on particles inside and outside of a cluster. Unfortunately, it meanwhile enlarges the difference in the dilute region, which deteriorates the homogeneity and results in a more pronounced heterogeneous local flow structure.

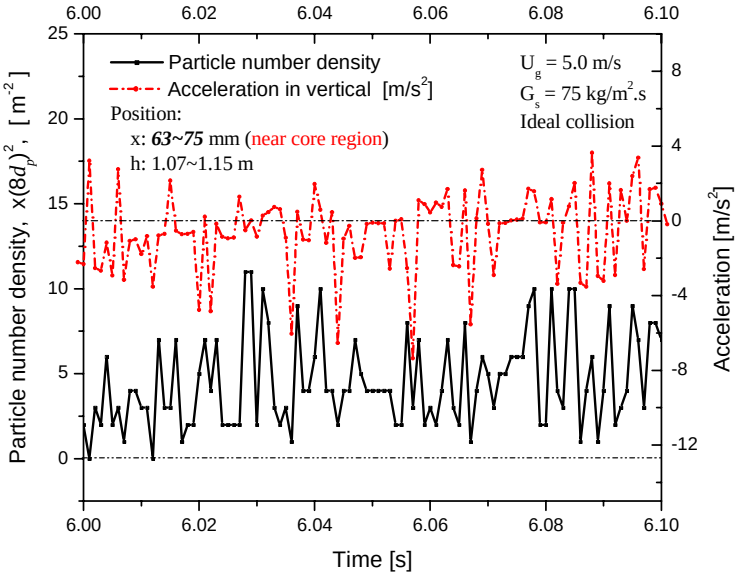

Figure 6.11: Influence of particle group effect on particle motion in a circulating fluidized bed near core region: promoting the otherwise decelerated individual particles, where *x* and *h* represent respectively the radial and axial position.

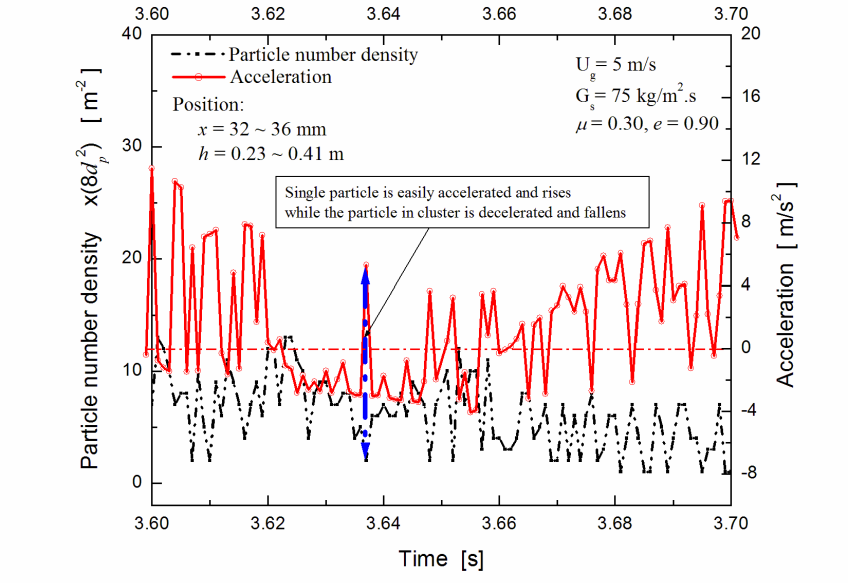

Figure 6.12: Comparison of particle motions inside and outside of cluster in a circulating gas-fluidized bed with non-ideal collisional particle (bottom region): group effect suppresses the accelerated individual particle motion. Voidage exponent equals 4.7 where *x* and *h* represent respectively the radial and axial position.

3.5 Regime transition to dilute flow

Regime transition to dilute transportation has also been simulated to understand the flow structure evolution. In the simulations, the rate of circulating solids is fixed whereas the gas velocity is increased to observe the regime transition. Since bed experiences an unstable process in the initial period of simulation, which should be excluded during the time-averaged calculation to obtain the flow structure profiles, time-averaged mass flux is monitored against the input solids flux.

Figure 6.14 presents time-averaged solids flux as a function of time. Clearly, after a certain period of operation, the systems gradually become stable: the output flux equals the input flux. For high gas velocity this period is quite short (1 s in case of 9 m/s) whereas it is a little longer for low gas velocity (3 s in case of 5 m/s). To compare the flow structures on the same base, the initial 3 seconds for all runs will be excluded accordingly.

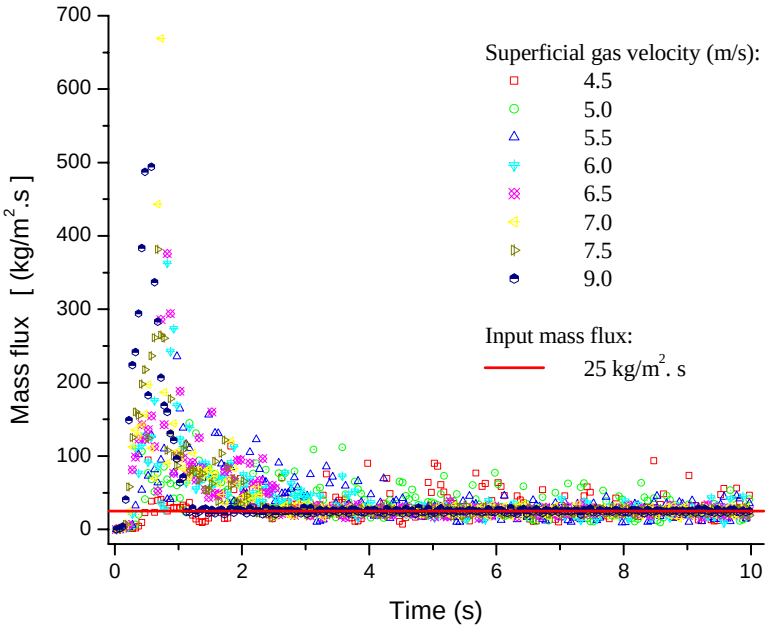

Figure 6.14: Variation of the time-averaged mass flux of output particles with time: *effect of superficial gas velocity*. All systems become stable approximately at 3 second.

Interestingly, it is also observed that the fluctuation of the time-averaged mass flux of output solids is significantly reduced with increasing gas velocity as shown in Figure 6.15 (same values as in Figure 6.14 but with large scale). This demonstrates that the system transfers from a heterogeneous flow structure to a homogeneous one.

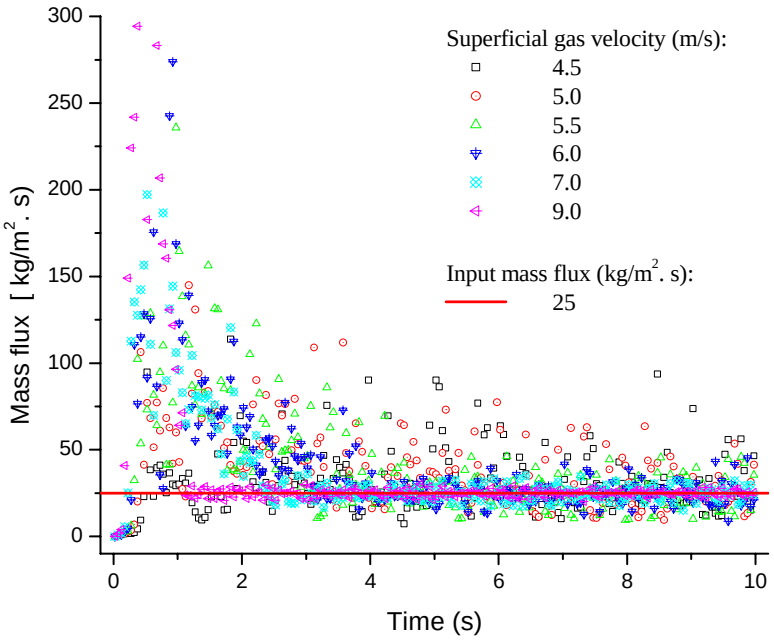

Figure 6.15: Variation of the time-averaged mass flux of output particles with time: *effect of superficial gas velocity*. *Increasing gas velocity damps the fluctuation of solids circulating flux* (color is required for this figure).

The variation of flow structures with gas velocity in terms of the time-averaged radial and axial solids volume fraction are presented in Figures 6.16 and 6.17 respectively. Figure 18 shows snapshots of the flow structures.

As expected, with increasing gas velocity the flow structure becomes more homogeneous both at the micro-scale and the macro-scale. When the gas velocity exceeds a critical value (5.5 m/s in this case) the system suddenly enters the dilute transportation mode: the dense bottom zone disappears and, instead, a homogeneous flow structure prevails in the system. Both in radial and axial direction a relatively flat time-averaged distribution of solid volume fraction is obtained.

Although the solids volume fraction profiles are flat, small spatial variations can still be recognized. In case the gas velocity exceeds 5.0 m/s the solids volume fraction across the bed exhibits a profile which is opposite to the normal profile corresponding to the “core-annulus” structure: low solid concentration near the wall. This suggests that the gas phase completely controls the particle (shifting) motion and consequently a second uniform flow regime (against the uniform regime after initial fluidization) is obtained.

Keeping in mind the nature of non-ideal particle interaction and non-linear gas drag for these systems, we can deduce that system equilibrium can uniquely determine the flow structure

formation since it controls solids spatial distribution and thereof induced particle dissipative collisions.

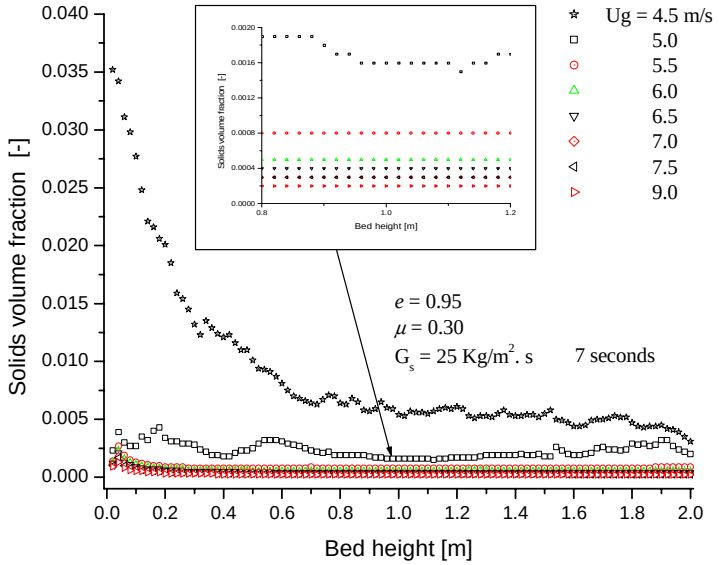

Figure 6.16: Evolution of flow structure with gas velocity in a circulating fluidized bed: regime transition to dilute transportation, *time-averaged solids volume fraction versus height is plotted. Flow structures both at micro and macro scales tend to homogeneity.*

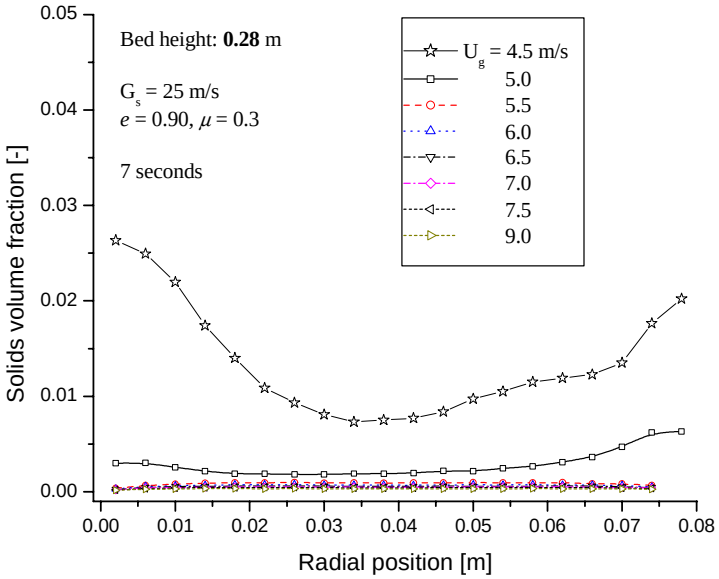

Figure 6.17 (a): Evolution of flow structure with gas velocity in a circulating fluidized bed and transition to dilute transportation: the time-averaged radial solids volume fraction distribution *at the bottom.*

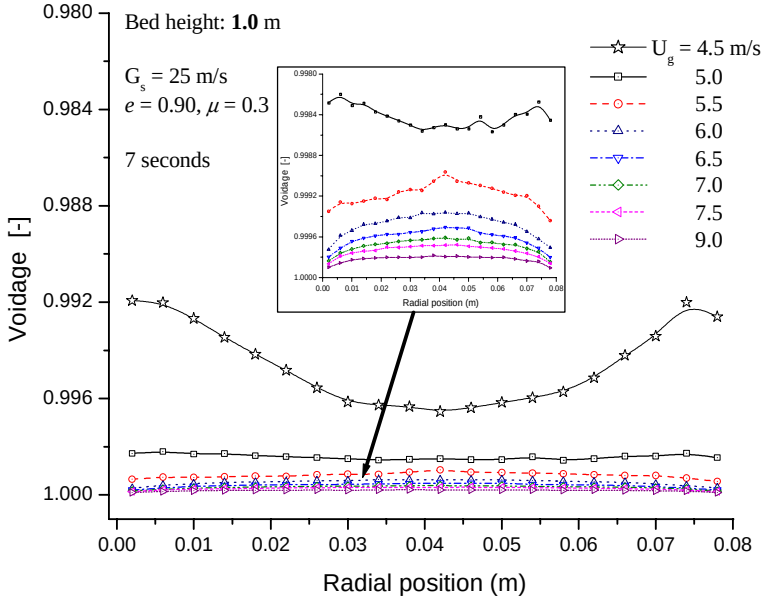

Figure 6.17 (b): Evolution of flow structure with gas velocity in a circulating fluidized bed and transition to dilute transportation: the time-averaged radial solids volume fraction distribution *in the middle.*

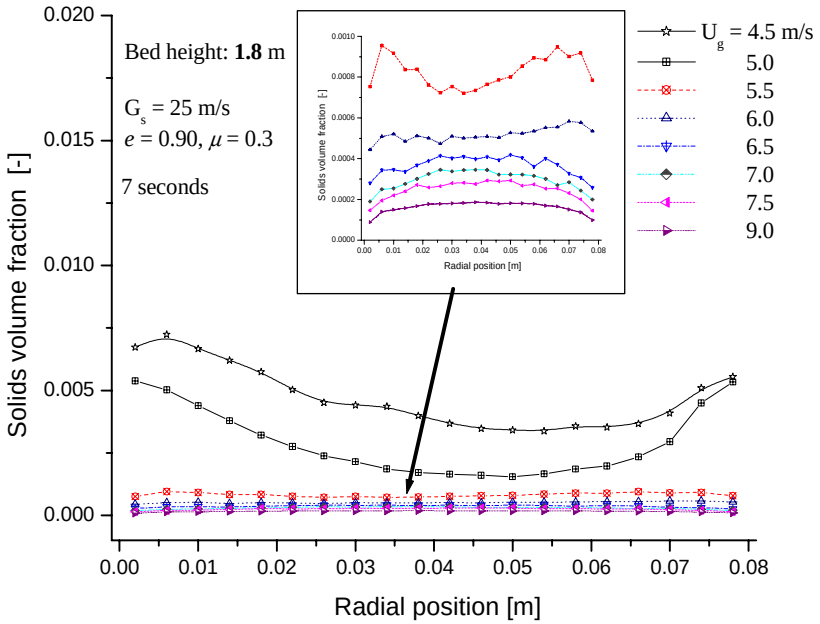

Figure 6.17 (c): Evolution of flow structure with gas velocity in a circulating fluidized bed and transition to dilute transportation: the time-averaged radial solids volume fraction distribution *on the top.*

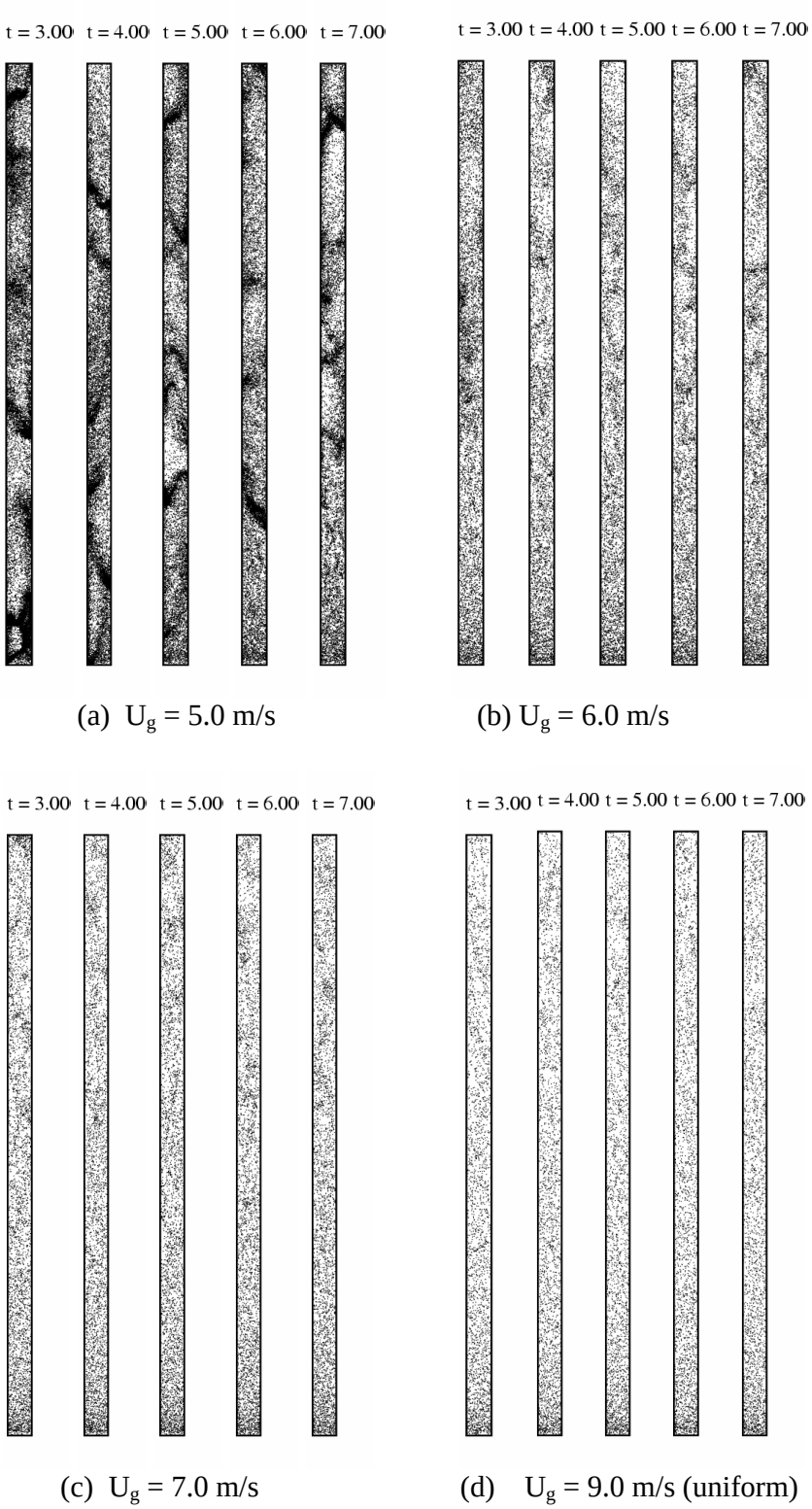

(a) U_g = 5.0 m/s (b) U_g = 6.0 m/s

(c) U_g = 7.0 m/s (d) U_g = 9.0 m/s (uniform)

Figure 6.18: Evolution of flow structure with gas velocity in a circulating fluidized bed and transition to dilute transportation: snap shots of the flow structure: -systems become uniform (non-ideal collisional particle) and produce a uniform flow regime.

4. Conclusions

Heterogeneous flow structures in circulating fluidized beds are induced by two kinds of mechanisms: non-linearity of gas drag force and particle collisional dissipation. These two factors determine the internal local flow structure of the system.

For the simulated CFB system, a smaller group effect in the drag correlation produces a more pronounced heterogeneous flow pattern where the inter-particle collisional dissipation consumes the particle energy, drawn from the gas phase, up to 20%. Of these two mechanisms, the non-linear drag force or gas-solid interaction is the key one to initialize the heterogeneous flow structure formation. Particle group effect has two opposite functions in circulating fluidized beds: 1) suppressing the otherwise accelerated individual particles in dense regions, and 2) promoting the otherwise decelerated individual particles in dilute regions. When both the non-linear drag and non-ideal particle collision take effect, a denser cluster/dilute flow structure is formed.

The wall effect, due to the non-slip condition, does exist in high-velocity gas-fluidized beds, even though the system is a perfectly homogeneous flow. This factor originates from macro-scale heterogeneity, the core/annulus structure, in gas circulating fluidized beds.

As gas flow rates exceed a certain critical value, the flow suddenly transforms to the uniform dilute transportation regime. To achieve a fully homogeneous flow structure controlled by gas suspension all over the bed, it is necessary to operate at even higher gas velocity.

Notation

C_d	drag coefficient, [-]
d_p	particle diameter, m
e	coefficient of restitution, [-]
E	energy, J
$\mathbf{F}$	force, N
G_s	solids circulating rate, kg/m^2.s
f_s	solids volume fraction, [-]
f	energy fraction, [-]
$\boldsymbol{g}$	gravitational acceleration, m/s^2
h, r	horizontal position, m
m_p	particle mass, kg
NR	grid number in horizontal direction, [-]
NZ	grid number in vertical direction, [-]
p	pressure, Pa
Re_p	particle Reynolds number, [-]
$\boldsymbol{S}_p$	source term defined in equation 6.2
t	time, s
$\boldsymbol{u}$	gas phase velocity, m/s
U_g	superficial gas velocity, m/s
$\boldsymbol{v}$	velocity, m/s
V	volume, m^3
w	work, J

Greek symbols

ρ	density, kg/m^3
θ	granular temperature, [m^2/s^2]
ε	void fraction, [-]
β	volumetric inter-phase momentum transfer coefficient, kg/(m^3.s)
μ_g	gas shear viscosity, kg/(ms)
$\boldsymbol{\tau}$	gas phase stress tensor, kg/m.s^2

Subscripts

0	initial condition
buoy	buoyancy
drg	drag
dsp	dissipated

g	gas phase
inp	input
kin	kinetic
out	output
p	particle
pot	potential
rot	rotational
s	solid
tot	total

Superscripts

0	initial state

References

Felice R. D. 1994 The voidage function for fluid-particle interaction systems. *Int. J. of Multiphase Flow*, **20**, 153-159.

Grace, J. R. and J. Tuot 1979 A theory for cluster formation in vertically conveyed suspensions of intermediate density. *Trans. Inst. Chem. Eng*., **57**, 49-54.

Helland, E., R. Occelli and L. Tadrist 2000 Numerical study of cluster formation in a gas-particle circulating fluidized bed. *Powder Technology*, **110**, 210-221.

Hoomans, B. P. B., J. A. M. Kuipers and W. M. P. van Swaaij 1999 Discrete particle simulation of cluster formation in dense riser flow. In *CFB-VI*, J. Werther, Ed., Wurzburg, pp. 255-260.

Hoomans, B. P. B., J. A. M. Kuipers and W. P. M. van Swaaij 2000 Granular Dynamics Simulation of Segregation Phenomena in Bubbling Gas-Fluidized Beds. *Powder Technology*, **109**, 41-48.

Hoomans, B. P. B., J. A. M. Kuipers, M. A. M. Salleh, M. Stein and J. P. K. Seville 2001 Experimental validation of granular dynamics simulations of gas-fluidised beds with homogenous in-flow conditions using positron emission particle tracking. *Powder Technology*, **116**, 166-177.

Horio, M. and H. Kuroki 1994 Three dimension flow visualization of dilutely dispersed solids in bubbling and circulating fluidized bed. *Chem. Eng. Sci*., **49**, 2413-2421.

Kuipers, J. A. M., K. J. van Duin, F. P. H. van Beckum, and W. P. M. van Swaaij 1992 A numerical model of gas-fluidized beds. *Chem. Eng. Sci*., **47**, 1913-1924.

Lackermeier, U., C. Rudnick, J. Werther, B. Bredebusch, and H. Burkhardt 2001 Visualization of flow structures inside a circulating fluidized bed by means of laser sheet and image processing. *Powder Technology*, **114**, 71-83.

Li, J. and J. A. M. Kuipers 2001 Effect of pressure on flow behaviors in dense gas-fluidized beds: A discrete particle simulation study. *Fluidization X*, M. Kwauk, J. Li and W.-C. Yang, Eds., Engineering Foundation, Beijing, pp. 389-396.

Li, Y. and M. Kwauk 1980 The dynamics of fast Fluidization". In *Fluidization-III*, J. R. Grace and J. M. Matsen, Eds., Plenum Press, pp. 537-544.

Sharma, A. K., K. Tuzla, J. Matsen and J. C. Chen 2000 Parametric effects of particle size and gas velocity on cluster characteristics in fast fluidized beds. *Powder Technology*, **111**, 114–122.

Wen, C.Y. and Y. H. Yu 1966 Mechanics of fluidization. *Chem. Eng. Prog. Symp. Ser*., **62**, 100-111.

Publications

Jie Li and Kuipers J. A. M. 2001 Effect of Pressure on Flow Behaviors in Dense Gas-fluidized Beds: A Discrete Particle Simulation Study. *Fluidization X*, Kwauk, M., Li, J. and Yang, W.-C. (eds), Engineering Foundation, Beijing, p.389-396.

Jie Li and Kuipers, J. A. M. 2002 Flow Pattern Formation in High Velocity Gas-fluidized Beds. *Proceedings of the 7th International Conference on Circulating Fuidized Beds.* Grace, J. R., Zhu, J and de Lasa, H. (Eds), Canada Society of Chem. Eng., Niagra Fall, p.419-427.

Jie Li and Kuipers J. A. M. 2002 Effect of Pressure on Flow Behaviors in Dense Gas-fluidized Beds: A Discrete Particle Simulation Study (extended version). *Powder Technology*, **127**(2), 173-184.

Jie Li and Kuipers, J. A. M. 2002 Gas-Particle Interactions in Dense Gas-Fluidized Beds. *Oral presentation at The 17th Int. Symp. on Chem. Reaction Eng.* and accepted for publication by *Chem. Eng. Sci.*, October 25-28, HongKong, P. R. China.

Jie Li and Kuipers J. A. M. 2002 Flow Structure Formation in Dense Gas-Fluidized Beds. *Oral presentation at The 6th Int. Conf. on Fluid-Particle Interaction*, October 25-30, Barga, Italy.

Jie Li and Kuipers, J. A. M., 2002 Pattern Formation and Evolution in Dense Gas-Solid Two-Phase Flows. *Oral presentation at Ann. Meeting of Amer. Phys. Soc.*, March, Indianapolis, USA.

Jie Li, and J. A. M. Kuipers, Particle-Particle Interactions in Dense Gas-Fluidized Beds: A Discrete Particle Simulation Study, to be published.

Jie Li, and J. A. M. Kuipers, Energy Dissipation in Dense Gas-Fluidized Beds: A Discrete Particle Simulation Study, to be published.

Acknowledgement

Hydrodynamics, among transport and reaction processes, acts as a foundation of chemical reaction engineering science. The hydrodynamics of particulate flows provide the basis to study the formation and evolution of heterogeneous flow structures which has a significant impact on the reactor design and scale-up. Therefore, it attracts great interest from both scientists and engineers. A couple of theories have been proposed but the dispute prevails intensively in this field. At the early 80's while I was an undergraduate student, I had a dream to attempt to tackle this problem by using first principles. However, this dream had not been realized until I joined the Twente Group. Using the discrete particle method, a powerful tool oringinating from the joint efforts in this group, especially due to Dr. Hans Kuipers and Dr. Bob Hoomans, I could finally explore the fascinating world of heterogeneous flow structure formation in dense gas-solid flows. Hopefully, as reported in the previous chapters, our work begins to shed a light on this problem although there is still a lot of work to do to finalize the quantification.

From Feb. 1999 I joined the Chem. Eng. Sci. group as a postdoctoral fellow and spent nearly three years at Twente University. During this period, I received lots of support in many respects which allowed me to fully devote myself to my study. With my family, I experienced a truly happy time in the Netherlands. I cherish very much such a rich property and good memory. Herewith, I wish to express my great gratitude to all who provided their kindness and friendship!

In particularly, I would like to thank Professor Hans Kuipers, my promotor. He offered me the precious opportunities of a two-year postdoctoral position firstly, for me to establish the

framework of this research, and then a one-year extension, to complete the high velocity flow simulation (collaboration with Princeton University) and to produce this booklet. It was during this time that I could be involved in the fascinating world of Computational Fluid Dynamics based simulation of particulate flows, which permitted me to take a significant step toward my dream of understanding engineering problems from the science base. Professor Kuipers himself is a great resource in this respect. He has great knowledge and experience on fluidization and multiphase flows, especially on the numerical simulation. Under his direction, I, a fresh man in CFD, could quickly step on the right track: compiling CFD codes and developing various simulation and post-processing tools. During three years, we had lots of stimulating discussions on a wide range of interesting topics, which not only enriched my knowledge on various aspects of fluidization but also expanded my confidence in using fundamental tools (CFD) to solve engineering problems. Particularly, I am convinced that his multi-scale simulation idea would be the most appropriate way to study multiphase flows (an extremely complex system) in depth. I also appreciate his art of the leadership! He always gave me and other students a great freedom and encouraged us to test our new ideas, but meanwhile alerted us timely in case of diverting to an aberrant track. Therefore, many new ideas could be developed in this group, as exemplified by the "hard sphere method" and "energy budget analysis". In such a way, we fortunately could reduce the chance to hit the "hidden island", which would otherwise have lead to "chaos". From him I learned the excellent spirits for a scientist: dedicated, strict and creative. I benefit from him and owe him a lot !

I was especially grateful to have the honor of receiving Professor van Swaaij's kind encouragement at several events, which firmed my belief to go forward with my study. Particularly, I wish to express my gratitude to Dr. Bob Hoomans who has spent a considerable amount of time to help me with my simulations. He laid the foundation for the "pogo" code on basis of the two-fluid model, developed by Dr. Hans Kuipers some years ago, and therefore knew every detail. As a beginner, I posed a lot of questions to him, especially at

the early stage. He was so kind to answer all of these questions even though he was extremely busy in writing his Ph.D. thesis during that time. Without his kind support, I would probably have still explored in dark and been busy with the codes. Sincerely, I appreciate his assistance and friendship! Along this line, I want to thank all the crew working on the discrete particle method who helped me in some respect. They are: Dr. Mathijs Goldschmidt, Mr. Pranay Darda, Ms. Renske Beetstra, Mr. Jeroen Link, Dr. Mao Ye, and Mr. Albert Bokkers. Best wishes to them all a successful future.

Thanks also to Dr. Martin van Sint Annaland, Mr. Michiel Gunsing and Dr. Martin van der Hoef for their essential assistances both on academic and non-academic aspects. I can not forget my collaboration with Martin to compile the CFD simulation software. Through co-operation with Michiel, a computer expert, I could develop the very beautiful AVS/Express movie. Dr. Martin van der Hoef was so kind to present on my behalf a paper at the 6th International Conference on Fluid-Particle Interaction in Barga Italy. Indeed, his great spirit of responsibility to make clear every detail is highly appreciated. Hereby, I just mention a few to cherish the good memories we share.

I am also indebted to Mr. Rik Akse, Mrs. Ria Stegehuis, Mrs. Ria Hofs Winkelman and Mrs. Nicole Haitjema. Their excellent secretarial and administration skills provided us a good working environment. From them I not only got the daily support but also learned a lot: Dutch language, history, customs, living style, etc. ……. Without Rik's help, I would have had to spent much longer time to settle down. Nicole works in an exceptionally efficient way, which has definitely speeded up the appearance of this booklet. The assistance received from Robert Meijer, Wim Leppink and Gerrit Schorfhaar is also appreciated. Special thank goes to Mrs. Liesbeth Kuipers. She has been so kind to organize so many wonderful social activities, which provided us a great environment allowing for work comfortable, mutual communication, relaxing and enjoying life. I treasure the good time thereof created: - the tropic-

forest-like green office, the attractive barbecue smell, the stimulating skiing in a chilly wind at Valfrejus (France), the exciting Karaoke evening …… What a peaceful and enjoying life! It seems that everything just happened yesterday.

The various assistances received from other colleagues from this group, Mr. Ulrich Kűrten, Mr. Dhaneshwar Patil, Ms. Esther van den Hengel and Mr. Salim Deshmukh and from the OOIP group, Dr. Wim Brilman, Dr. Arnound Higler, Dr. Senthil Kumar, Mr. Toine Cents, Mr. Sousa Tarazi and Mr. Vishwas Dindore as well as from the IPP group, Dr. Wolter Prins and Mr. Xiaoquan Wang is also highly appreciated.

Special thanks also goes to Dr. Mark Gilbertson, from the University of Bristol, Dr. Reghan Hill, Professor Donald Koch from Cornell University and Professor Sankaran Sundaresan from Princeton University. With Mark, we have collaborated for a short period of time on validation of DPM by studying gas-fluidized beds at elevated pressures. Although the validation result is not so ideal owing to the limitation of our 2-D code, this cooperation sparked the idea to examine the effect of intensified gas-solid interaction on flow structure by employing elevated pressure, as reported in Chapter 3 and 5. This plays an important role in understanding the relationship between system stability and gas suspension and identifying the fundamental role underlying the heterogeneous flow structure formation. Dr. Hill had kindly sent me his Ph. D dissertation before his papers appeared in JFM, which enabled a comprehensive comparison of flow structures simulated by using various drag correlations, as reported in chapter 4. Promisingly, it was noticed that their drag correlation based on the Lattice Boltzmann method produced reasonably good results. This, therefore, highlights the future research direction for the gas-solid two-phase flow simulation on the micro-scale. With Professor Sundaresan, we aimed to understand the cluster behaviors in CFB's, extended our code further to include periodical boundary conditions and the calculation of various statistical quantities. Due to time limitations, these results have not been included in this booklet.

Of course, I would like to thank the Dutch National Foundation (NWO) and Twente University for their financial support!

Last but not at least, I want to express my gratitude to my parents Yanqing Li and Qinglian Han for their never changed encouragement and my wife, Hua Zhu, and son, Erluo Li, for their understanding and support.

Again, thank you all !

Jie Li

About the author

Born in Shaanxi on September 4th 1964, Jie obtained his Bachelor of Sciences degree on Chemical Engineering from Northwest University, Xi'an, P. R. China in 1985. Continuing his study as a Master candidate and working on drying kinetics of droplets in a spray dryer he graduated from the same university in June 29th, 1988. Thereafter, he joined the Institute of Applied Chemistry, Shaanxi Province as a Process Engineer, being actively involved in a variety of R & D projects with focus on particulate flows.

In September 4th 1994, he returned to academia as a Ph.D. candidate at the Institute of Chemical Metallurgy, Chinese Academy of Sciences, Beijing and worked on gas-solid mass transfer in circulating fluidized beds to explore the influence of the heterogeneous flow structure until 1998. After finishing his Ph.D., he moved to Twente University, the Netherlands as a postdoctoral researcher with research focus on formation and evolution of heterogeneous flow structure in dense gas-solid flows by employing discrete particle simulation technique.

In 2002, he has been continuing his scientific journey at Argonne National Laboratory, USA working on self-assembly pattern formation in a shallow gas-fluidized bed using oscillating flow to develop a new type of gas-solid contacting technique.

Gas-solid two-phase flow is a ubiquitous phenomenon in nature and also widely applied in process industries. However, its extraordinary complexity of dynamic behaviors and flow structure hinders the theoretical prediction and as a sequence thereof many important aspects of hydrodynamics of the fluidized system are still poorly understood. By using the discrete particle method, this work aims at exploring the fundamental phenomena prevailing in dense particle laden flows.

In our model the gas phase is described by the volume-averaged Navier-Stokes equation, whereas the particles are described by the Newtonian equations of motion while taking particle-particle and particle-wall collisions into account. Different from the traditional “two-fluid” model, this approach offers the advantage that both particle-fluid and particle-particle interactions can be precisely accounted for.

The results show that the competition between particle-particle collisional dissipation and fluid-particle interaction fully determines the flow pattern formation and evolution. Dominant fluid-particle interaction results in a uniform flow. On the contrary, intensification of particle-particle and particle-wall collisions increase the energy dissipation and leads to a heterogeneous flow structure. The flow regime transition is actually the expression of the altering role of particle-particle interaction and fluid-particle interaction.

The heterogeneous flow structure also exist in systems with ideal particle collisions. This heterogeneity is purely caused by non-linearity of the drag: the stronger the dependence of drag on voidage, the more heterogeneous flow structures prevail and the shorter the homogeneous flow regime. Particularly, it is clarified that the non-linear drag force has the “phase separation” function by means of accelerating the particles in the dense phase and decelerating the particles in the dilute phase thereby triggering non-homogeneous flow structure formation. Particle collisional dissipation further prevents the formation of a homogeneous flow structure.

The influences of other factors including the feedback of bubble and jet, elevated pressure and fluid density are numerically examined in detail and their impacts on the flow structure formation and evolution are also highlighted.

Finally, the understanding concerning with the pattern formation and evolution in high-velocity gas-solid flows is also presented.

ISBN: 90 365 1860 1

PrintPartners Ipskam